Characterising immunoglobulin-polysorbate interactions

by

Ruairidh Gair Couston

A Thesis submitted to the University of Strathclyde in fulfilment of the requirement for degree of Doctor of Philosophy

March 2013

Declaration of Authenticity and Author's Rights

'This thesis is the result of the author's original research. It has been composed by the author and has not been previously submitted for examination which has led to the award of a degree.'

Signed:

Date:

Acknowledgements

I would like to first thank Doctor Chris van der Walle for the opportunity to carry out this work and for all of his help, time and valuable insight throughout the duration of this PhD. I would also like to thank Professor Clive Wilson for welcoming me into his research group and for his guidance and advice.

I am very grateful to Doctor Maximilian Skoda of ISIS, Rutherford Appleton Laboratory and Sarah Grasso of MedImmune, Cambridge for their help and with NR and DSC. Many thanks to MedImmune, Cambridge for funding this project and to Doctor Shahid Uddin, MedImmune for his input during the course of this research.

From the University of Strathclyde I would like to thank Doctor Dimitrios Lamprou for his help with AFM and Doctor Eva Gonzalez for her help. I would also like to thank the workshop staff for designing and producing the rotating cell holder.

Thank you to my fellow PhD students and friends Gemma, Shonagh, Jen, Michelle and Stewart with a special thanks to Lisa, Joe, Gracie and Munerah for their kind listening from the start. I would also like to thank Doctor Jenifer Mains of Encap, Livingston for her advice and time. To my friends Mark, Kez, Laura, Kathleen, Martin, Neil and Jen, thank you for offering a welcome distraction at times of need.

I would like to thank my family especially my parents for all of your support with every decision I have made and for making me the person I am today. Your love and belief in me means a lot and I could not have done it without you. To my siblings, you drive me on to do the best I can. Finally, a very special thank you to Laura for all of your patience, support and understanding throughout my PhD. Your love inspires me each day to do better and to make you proud.

Contents

Abbreviations

AFM - Atomic force microscopy

ANS - 8-anilino-1-naphthalene sulphonic acid

APTES - (3-Aminopropyl)triethoxysilane

APTMS - (3-aminopropyl)trimethoxysilane

BSA - Bovine serum albumin

CAC - Critical aggregation concentration

CAG - Contact angle goniometry

CMC - Critical micelle concentration

CD - Circular dichroism

DMF - N,N-dimethylformamide

DMSO - Dimethyl sulphoxide

DSC - Differential Scanning Calorimetry

EPO - Erythropoietin

F_{ab} - Fragment antigen binding

F_{ad} - Force of adhesion

F_c - Fragment constant

F_{des} - Force of desorption

FITC - Fluoroscein isothiocyanate I

FTIR - Fourier transform infrared

Fv – hypervariable region

GPTMS - (3-glycidyloxypropyl)trimethoxysilane

GST - Gluthathion S-transferase

hCG – human chorionic gonadotropin

HEWL - Hen egg white lysozyme

hGH - Human growth hormone

HLB - Hydrophilic-lipophilic balance

HSA - Human serum albumin

Ig - Immunoglobulin

ITC - Isothermal titration calorimetry

mAb - Monoclonal antibody

mPEG-silane - Methoxy-polyethylene glycol-silane

NMR - Nuclear magnetic resonance

NR - Neutron reflectivity

Nrmsd – normalized root mean square deviation

OTS - octadecyltrichlorosilane

OVA - Hen egg ovalbumin

PEG/PEO - Polyethyene glycol

PFTOS - 1H,1H,2H,2H-perfluorooctyltriethoxysilane

PPO - Polypropylene glycol

rhGH - Recombinant human growth hormone

rhIFN-γ - Recombinant human interferon-γ

rIL-2 - Recombinant human interleukin-2

SAM - Self-assembled monolayer

SCF - Supercritical fluid

SDS-PAGE - Sodium dodecyl sulphate polyacrylamide gel electrophoresis

SLD - Scattering length density

SPM - Scanning probe microscopy

STM - Scanning tunnelling microscopy

TCDS - trichloro(dodecyl)silane

TCMS - trichloro(methyl)silane

TCOS - trichloro(octyl)silane

TCPS - trichloro(propyl)silane

TDOCA - Taurodeoxycholeate

Tg - Glass transition temperature

TIRF - Total internal reflection fluorescence

T_m - Thermal transition midpoint

Abstract

Therapeutic proteins, such as immunoglobulins, are typically formulated with polysorbates as stabilisers. However, the nature of the immunoglobulin-polysorbate interaction, particularly at the solid-liquid interface, is poorly characterised. This thesis presents an investigation of immunoglobulin (mAb-1)-surfactant interaction in bulk solution with particular focus on the interaction at the solid-liquid interface.

It was first established using isothermal titration calorimetry that no specific binding interaction between mAb-1 and surfactant in solution takes place. Furthermore, circular dichroism and differential scanning calorimetry showed surfactant inclusion had no effect on mAb-1 native structure or thermal stability.

The adsorption/desorption of mAb-1 and the effect of polysorbate was quantified in real-time by total internal reflection fluorescence. MAb-1 desorption was dependent on polysorbate concentration, fatty acid tail group and point of injection relative to mAb-1. MAb-1 adsorption to a hydrophobic surface was significantly less than to a hydrophilic surface. Concomitant conformational changes to mAb-1 were not apparent upon adsorption to a hydrophilic surface but a varying degree of β-sheet loss was observed upon adsorption to hydrophobic surfaces. This was corroborated by neutron reflectivity (NR) data which modelled a bilayer for mAb-1 adsorbed to a hydrophilic surface and a monolayer for mAb-1 adsorbed to a hydrophobic surface. These NR data suggested a range of mAb-1 orientations were adopted.

This combination of orthogonal surface analytical techniques can build up a detailed molecular-level image of the adsorbed protein layer enabling rapid characterisation of protein surface adsorption which will improve bioprocess design and formulation.

Chapter 1. Introduction

Therapeutic proteins are used to treat a wide range of conditions including cancers and autoimmune disorders. To achieve a therapeutic dose at a small volume, a high concentration formulation is necessary. Proteins formulated at high concentration are susceptible to aggregation (Ripple and Dimitrova, 2012) and loss of structure due to surface adsorption-desorption (Pinholt et al., 2011). To reduce aggregation, thereby increasing protein stability, excipients such as non-ionic surfactants are included in formulations. However, although their use is common and widespread, the interaction between non-ionic surfactants such as the polysorbates and monoclonal antibodies is, to date, poorly characterised particularly at solid/liquid interfaces.

1.1 Protein Structure

Proteins are composed of primary and secondary structures which together form the tertiary structure. A protein quaternary structure is formed by the coming together of a number of individual protein subunits to form one protein with multiple subunits (Figure 1-1). The tertiary and quaternary structures of a protein can be highly complicated and adopt a wide range of conformations. In this study proteins will be considered as being over one hundred amino acids in length and have a defined 3-D folded structure, polypeptides will be regarded as approximately sixty to one hundred amino acids in length and peptides defined as below sixty amino acids in length.

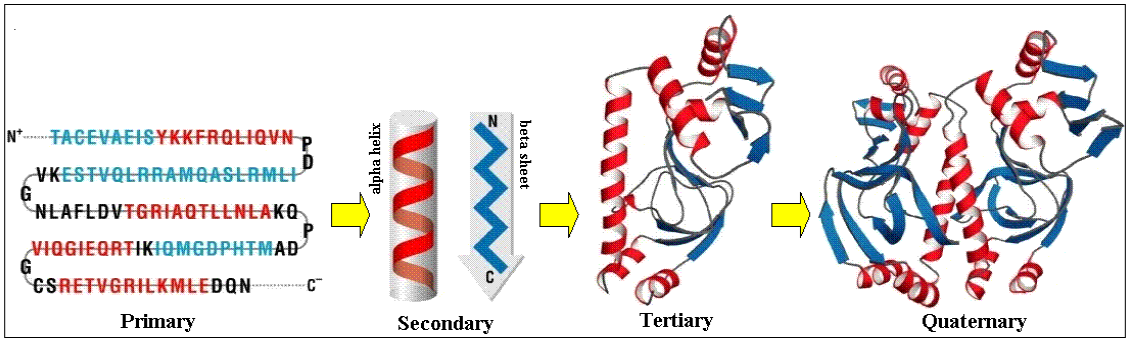

Figure 1-1 Diagram showing protein structure (Adapted from G.L. Kerr 2009)

The amino acids (as shown in Figure 1-2), which are the primary structure of a protein, form chains through the formation of peptide bonds (-COOH + H_2N- → C(O)NH + H_2O) between adjacent residues. The amino acid sequence will determine the secondary structural conformation of the protein in its native state.

The secondary structure of a protein is a regular structure which is repeated and stabilised via hydrogen bonds between carboxyl and amino groups of amino acids on the secondary structural motifs. The main types of motif which form the secondary structure of a protein are alpha (α)-helices, beta (β)-sheets and beta (β)-turns each of which are highly regular (i.e. the motif has a regular repeating sequence and structure). These secondary structures mentioned are regular which suggests a high degree of order within the protein; however, proteins can also have an irregular structure such as a random coil. The secondary structure of a protein is localised and thus different regions of the same protein may have a different secondary structure.

The tertiary structure of a protein is created as a result of the secondary structure(s) present and this forms the overall shape. It is common for this structure to be stabilised through the presence of nonlocal interactions, for example salt bridges (which most commonly take place between aspartic acid/glutamic acid and lysine/arginine) or disulphide bonds (between cysteine residues). Folded proteins

have a hydrophobic core which contains the hydrophobic residues and is stabilised by the packing of amino acid side chains. The charged or polar side chains of the amino acids occupy the exposed surface of the protein and interact with water or solvents in the surrounding environment.

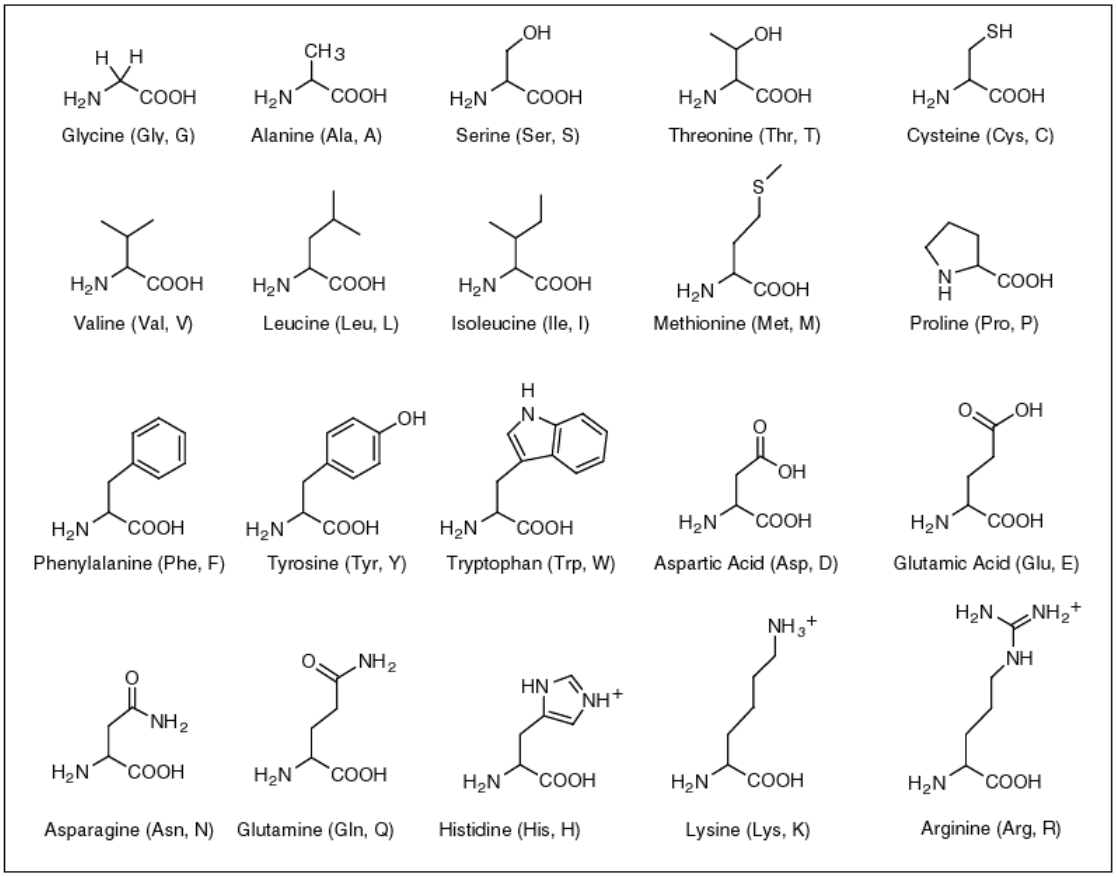

Figure 1-2 Amino acids - form the primary structure of proteins (Adapted from http://www.neb.com/nebecomm/tech_reference/general_data/amino_acid_structures.asp).

A number of analytical techniques exist to identify the structure of a protein, some of which are capable of investigating changes in protein structure in solution or at a surface. For example, 'liquid state' circular dichroism can be used to determine the native secondary structure of a protein in solution (Kelly and Price, 2000, Kelly et al., 2005) while 'solid state' circular dichroism is able to investigate structural changes upon adsorption to a surface (Ganesan et al., 2006). Circular dichroism can

also be used to monitor structural changes which take place due to heat induced denaturation which is important when considering storage and manufacture of therapeutic protein formulations. Both 'liquid' and 'solid state' circular dichroism are used in this study and so they are discussed in greater detail in section 2.1.3 and 3.1.3.

The structures of a large number and range of proteins have been elucidated with two techniques being commonly used, X-ray crystallography (Yang et al., 2012) and nuclear magnetic resonance (NMR) spectroscopy (Sengupta et al., 2012) . These techniques have a high resolution and they produce information on the arrangement of the atoms forming the protein. In X-ray crystallography an X-ray beam is directed at the protein, as the beam strikes the protein it will be diffracted into numerous directions. From the angle and intensity of the diffracted beam the 3-D structure of the protein can be established. NMR spectroscopy produces information on the structure of a protein but also on physical, chemical and electronic aspects. It can be used to determine the structure of a molecule in solution or in a solid state. The protein is placed in a magnetic field and the nuclei of the molecules composing the protein will have a resonance which has a specific frequency, energy of absorption and intensity of signal. These features are directly related to the force of the magnetic field and when the data is analysed the structure of the protein can be resolved.

1.2 Bioprocessing

The bioprocessing of proteins is a large subject area and so will only be discussed briefly here; a more detailed review of protein bioprocessing is available in the

literature (Elvin et al., 2013). Recombinant proteins are produced through expression in a mammalian cell line with a number of different cell lines available for this purpose. The choice of cell line depends on the protein of interest, but options include Chinese Hamster Ovary (CHO) cells which have been used for erythropoietin (EPO) and Pulmozyme, and Human Embryonic Kidney (HEK) or CHO cells for monoclonal antibodies (mAbs). Plants cells have also been investigated for their ability to express immunoglobulins (Benvenuto et al., 1991, Vine et al., 2001) with a review discussing the area in greater detail published by De Muynck et al., (2010). The growth media and bioreactor used must be selected to maximise cell growth and the quantity of protein produced. Methods including multivariate data analysis (Kirdar et al., 2008) and a parallel high throughput micro-scale bioreactor (Legmann et al., 2009) have been suggested as ways in which optimal growth and expression conditions can be investigated.

The host cell must be altered to incorporate the protein-coding DNA sequence. A suitable plasmid DNA expression vector, the plasmid chosen is dependent upon the sequence to be inserted, and the protein-coding DNA sequences are cut using the same restriction enzyme (a restriction enzyme recognises a specific sequence of nucleotides in the DNA strand before cutting the strands). This process results in complimentary nucleotide sequences being available on the two components which can then be annealed to reform the plasmid. The protein-coding DNA sequence is then incorporated into the plasmid and the protein expression vector is subsequently inserted into a cell line for production of the protein. One problem with the use of expression vectors is undesired or uncontrolled post translational modification of the protein, which includes glycosylation, galactosylation and deamidation (Jenkins,

2007). For example, the glycosylation of cetuximab via the linkage of galactose-α-1,3-galactose has been linked to an immunogenic response (Chung et al., 2008). It is therefore important that any post translational modifications which occur are consistent and controlled. It has been shown that the degree of antibody F_c galactosylation can be controlled, in part by the inclusion of different constituents in the culture medium (Gramer et al., 2011).

The protein of interest must be purified from the cell lysate and then concentrated through the removal of liquid. The protein is first extracted from the cells, a process which is carried out via lysis - methods such as repeated freeze-thaw cycles and sonication can also be used - before purification. It is common for a molecular tag, for example a hexahistidine tag (His-tag) (da Silva et al., 2012) or a glutathione S-transferase (GST)-tag (Xiong et al., 2012), attached to a protein to be used for purification via affinity chromatography. A high throughput high-yield affinity chromatography method has been developed for protein purification using a completely automated system involving a robotic arm and the option to use up to 9 different solutions to extract and purify the protein (Steen et al., 2006). An alternative technique to affinity chromatography is the use of poly(ethylene glycol) to precipitate the protein from the culture media as has been shown for an IgG4 (Knevelman et al., 2010). However, the main method for the removal of recombinant antibodies from culture media in the pharmaceutical industry is via the use of Staphylococcal protein A affinity (Hober et al., 2007). Once the protein has been successfully purified from the host cell proteins it is necessary for it to be concentrated (i.e. removal of excess liquid). Concentration of the protein can be achieved using lyophilisation or ultrafiltration (which is also used for purification).

The protein can be lyophilised (dried), if it is the only soluble component of a solution, which concentrates the protein solution through removal of liquid during the freezing process and removal of water (through a decrease in pressure causing the liquid to go directly from the solid to gas phase). The freezing process can however affect protein stability (Kueltzo et al., 2008). Ultrafiltration brings about the concentration of a protein from a solution through the use of selectively permeable membranes (Baruah et al., 2006). A selectively permeable membrane is mounted in a tube (e.g. a centrifuge tube depending on the quantity of protein being concentrated) and a buffer is forced through which results in the protein being deposited on the membrane surface. During the concentrating period, a degree of the protein in solution can be lost, as with the during purification step.

During bioprocessing, proteins are susceptible to aggregation and surface adsorption. As an example, the effect of shear on aggregation of an IgG4 has been investigated using computational fluid dynamics (CFD). During processing the predicted shear rates proteins are expected to be exposed to is up to 20,000 s^{-1}. A reduction in the monomer content of an IgG4 was detected when using shear rates up to 34,000 s^{-1} at a low antibody concentration (Biddlecombe et al., 2007). The pH of the solution and nanometre-scale roughness of the surface were identified as important factors in the aggregation detected in a further study by the authors. It was also found that the inclusion of polysorbate 20 below its critical micelle concentration reduced loss of monomer content (Biddlecombe et al., 2009). Protein formulation is discussed in section 1.5 along with the use of excipients to reduce aggregation and surface adsorption.

1.3 Immunoglobulins

Immunoglobulins (Ig), which are commonly known as antibodies, are proteins around 140 kDa in weight and are found within the body including the serum and mucosae. They are produced by the plasma cells (a specific type of white blood cell) and form an integral part of the immune system. Immunoglobulins identify foreign objects, for example bacteria and viruses, through the specificity of the antigen binding domain. The presence of immunoglobulin on the surface can signal to other components of the immune system to attack the foreign body preventing it carrying out its function or directly binding to the foreign body which prevents it from acting.

Five different immunoglobulin isotypes exist in mammals: IgA, IgD, IgE, IgG and IgM which are shown in Table 1-1 along with the number of sub-classes and a brief description of their location within the body and their function. The heavy chain of the immunoglobulin determines the isotype class and the name is derived from the Greek letters α (alpha), δ (delta), ε (epsilon), γ (gamma), and μ (mu). There are two forms of immunoglobulin which are considered to exist: a surface immunoglobulin which is bound to the membrane of white blood cells (specifically the plasma cells) and antibodies which are secreted into the bloodstream.

The crystal structures of a monomeric IgG and a pentameric IgM are shown in Figure 1-3 along with a simplified diagram of the structure in Figure 1-4 to illustrate the different domains. The crystalline dimensions of a human IgG1 range between 142 x 85 x 38 Å (Silverton et al., 1977) and 146 x 135 x 69 Å (Harris et al., 1998). The dimensions of each immunoglobulin isotype will differ. The basic structure of human immunoglobulins is very similar, with each immunoglobulin monomer being composed of two heavy and two light chains (Figure 1-4).

Immunoglobulin isotype	Number of subclasses	Location and function
IgA (dimer)	2	Found in mucosal areas (e.g. gut, respiratory tract. Prevents the colonisation of the body by pathogens
IgD (monomer)	1	Antigen receptor on B cells not previously exposed to antigen. Activates immune cells (basophils, mast cells).
IgE (monomer)	1	Triggers the release of histamine from basophils and mast cells. Involved in the allergic response system.
IgG (monomer)	4	Found on the surface of B cells and in solution. Provides immunoglobulin-based immunity against pathogens.
IgM (pentamer)	1	Elimination of pathogens prior to the presence of sufficient IgG during early B cell mediated immunity.

Table 1-1. The different types of immunoglobulin name, number of types and function(s).

The fragment antigen binding (F_{ab}) region is responsible for antigen binding. It is composed of one constant and one variable domain of the heavy and light chains. Immunoglobulins have been shown to have a large level of interdomain flexibility which allows the accommodation of a variety of F_{ab} region conformations (Saphire et al., 2002). The F_{ab} region of the immunoglobulin is differentiated by the variable domain which enables recognition of a wide range of antigens. This area at the tip of the F_{ab} region is highly variable and thus is known as the hypervariable region (Fv region). As there are two F_{ab} regions (Figure 1-4) each immunoglobulin can theoretically bind to two antigens at once. The variability of this region enables the existence of innumerable immunoglobulins, and so the immune system, with the

ability to recognise a great number of antigens. Immunoglobulins recognise a characteristic part of the antigen called the epitope which is unique to each antigen. The binding between an immunoglobulin and an antigen is specific allowing each to recognise a single antigen. Techniques including atomic force microscopy (Hinterdorfer et al., 1996, Li et al., 2002) and the immobilisation of antibody on the surface of a chip (Saleh and Sohn, 2003) have been used to investigate antibody-antigen binding. The F_c (fragment constant) region of the immunoglobulin activates the defence mechanism of the host leading to an immune response. This region binds to F_c receptors on the host cell triggering phosphorylation within the cell and activation of kinases which leads to endocytotic and phagocytotic events (Daeron, 1997).

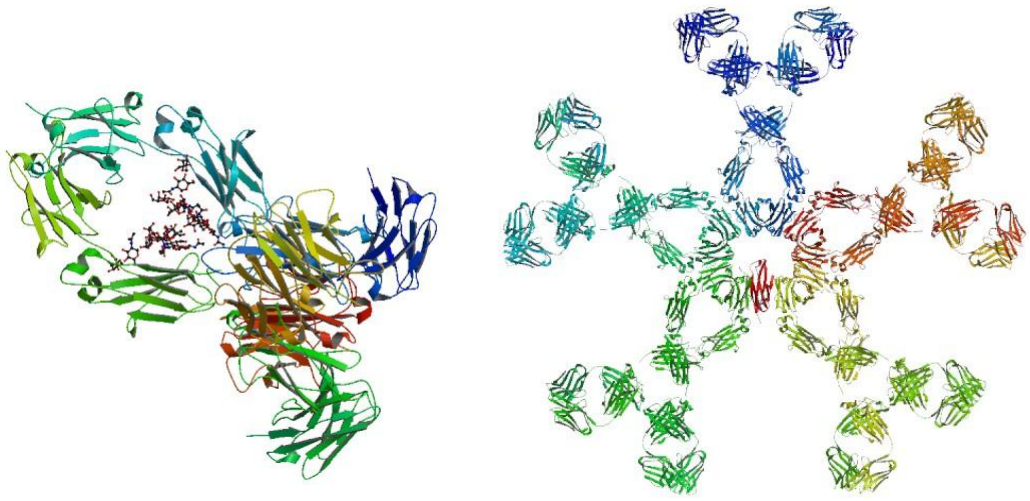

Figure 1-3. Examples of (left) an IgG (Saphire et al., 2001) and (right) an IgM structure (Perkins et al., 1991) (images used with permission from Protein Data Bank).

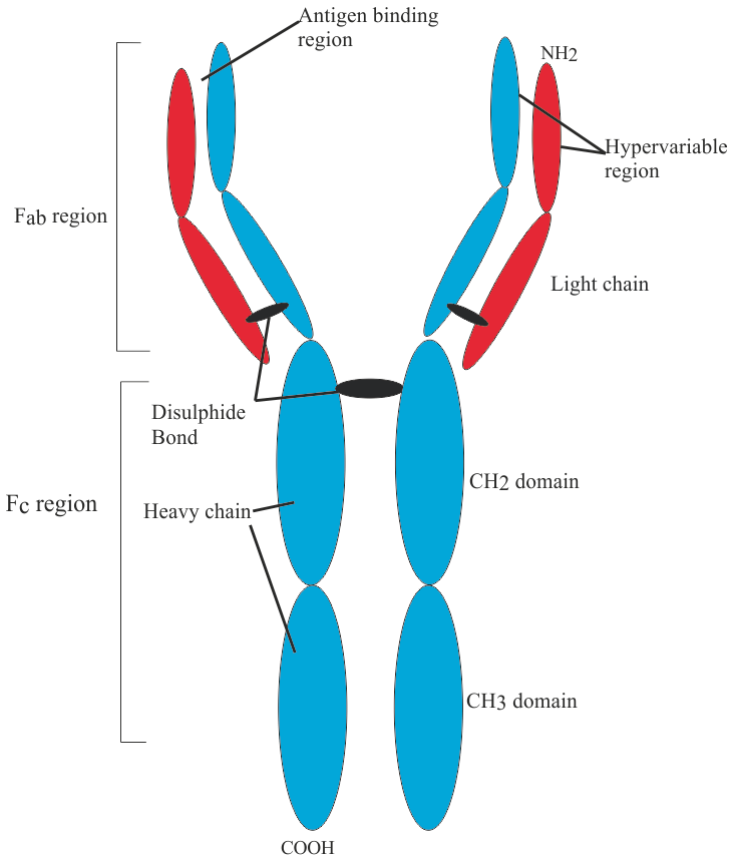

Figure 1-4. A simplified diagram of an immunoglobulin structure to illustrate the different component domains.

Therapeutic antibodies were initially derived from murine (mice and rat) sequences, however, due to problems with immunogenicity (Hwang and Foote, 2005) and efficacy, a number of different formats have been developed. The different types of antibody and their origin together with examples are shown in Table 1-2. Each antibody is designed to interact with a specific target which will increase efficacy, thereby reducing the dose required and potential side effects. In addition to the whole antibody formats in Table 1-2, antibody fragments and conjugates are also available which include Ranibizumab a F_{ab} fragment (for treatment of macular degeneration) and the conjugate tositumomab-iodine 131 (for the treatment of Non-Hodgkin's lymphoma).

Format	Origin	Suffix	Examples
Murine	Fully murine	n/a	Muromonab-CD3
Chimeric	Murine variable region	-ximab	Rituximab, cetuximab
Humanised	Murine complementary determining region (CDR)	-zumab	Palivizumab, trastuzumab
Human	Human sequences	-umab	Adalimumab

Table 1-2. Therapeutic antibody formats, their origin and available drug examples.

In addition to the use of immunoglobulins to treat various conditions, they are also immobilised on surfaces in protein assay kits designed to detect the presence of an antigen. A high-throughput screening method exists to test for recognition of an antigen by recombinant antibodies (de Wildt et al., 2000) which could be used prior to the selection of an antibody for an assay. Some examples of assay kits are the detection of serum proteins (Rissin 2010) and to test for HIV (Pavie 2010, Lee 2011). In the studies mentioned, the ability of the immunoglobulin to detect an antigen will be dependent on the orientation adopted on the surface. One method for achieving a specific immunoglobulin orientation on the surface is generation of a membrane protein array which has been shown to enable binding of a polyclonal IgG in a specific orientation (Le Brun et al., 2011). Through determination of the layer thickness during each step of the array construction the thickness of the polyclonal IgG layer was established which enabled determination of the likely surface orientation. Antigen binding capability was identified by an increase in the layer thickness (Le Brun et al., 2011).

1.4 Proteins available on the market

A large number of monoclonal antibodies are available on the market to treat a range of conditions, with the two most common targets by percentage of sales being cancer and autoimmune/inflammatory diseases (Table 1-3). A study published in 2005 suggested that by 2008 five antibodies would together make up a 68% share of the market - Rituximab (Rituxan®) (for treatment of cancers including Non Hodgkins lymphoma), infliximab (Remicade®) (which is used to treat conditions including Crohn's disease and ulcerative colitis), trastuzumab (Herceptin®) (treatment of breast cancer), adalimumab (Humira®) (its uses include treatment of rheumatoid arthritis and Crohn's disease) and palivizumab (Synagis®) (for treatment of respiratory syncytial virus) (Pavlou and Belsey, 2005). The suggestions made by Pavlou and Belsey (2005) are in general confirmed by a more recent study which reported the mAb therapeutic market in 2010 to be worth $43 billion with 75 % of the sum generated by five mAbs (four of which were reported in the previous studies mentioned): bevacizumab (Avastin®); rituximab (Rituxan®); adalimumab (Humira®); infliximab (Remicade®); and trastuzumab (Herceptin®) (Elvin et al., 2013). The exception is that sales of palivizumab (Synagis®) were not as high as anticipated by Pavlou and Belsey (2005). A full review of the therapeutic antibody market including the different mAbs on the market and their targets has recently been published (Elvin et al., 2013).

Target area	Percentage of sales in 2010 (%)
Oncology	50.8
Autoimmune/inflammatory	37.8
Neovascular (eye)	7.1
Infectious disease	2.4
Haemostasis	1.7
Rejection	0.1

Table 1-3. Monoclonal antibody sales by target area in 2010 (Elvin et al., 2013).

Protein therapeutics are typically injected subcutaneously at a high concentration in order to achieve a therapeutic dose (Dani et al., 2007) which avoids enzymatic degradation, and increases the reproducibility of the dose. A notable exception to this route is nebulised Pulmozyme for local delivery to the lungs for the treatment of cystic fibrosis patients (Quan et al., 2001). However, proteins are susceptible to the formation of aggregates at high concentrations used in therapeutic formulations (Treuheit et al., 2002). Additionally, proteins can adsorb to surfaces including that of a syringe, a needle (Bee et al., 2010) or an intravenous drip (Burke et al., 1992) which would lead to a reduction in the concentration. In addition to the loss of protein concentration due to adsorption on surfaces encountered during storage and delivery, it has been shown that antibody secreted by cells during bioprocessing can also be lost due to surface adsorption. The concentration of a mouse monoclonal IgG1 in solution was found to decrease when added to sterile plant culture containing no biomass or proteases (Doran, 2006). To reduce this loss of concentration due to surface adsorption, and to also increase stability, proteins are formulated with excipients which will now be discussed.

1.5 Protein Formulations

Proteins are generally more physically stable when stored in their solid form than in solution. This is because when they are stored in a humid environment or in solution their main chain flexibility increases which has been shown to result in unfolding (Mukherjee et al., 2011). This leads to a dramatic decrease in the conformational stability of the protein and may result in the formation of aggregates through an interaction between denatured/partially denatured protein chains (Fields et al., 1992) (a detailed review of the stability of protein pharmaceutics was undertaken by Manning et al., (2010)). Upon aggregation the structure of the protein may be altered and thus potentially cause an unfavourable immune response (Hermeling et al., 2004). Protein aggregation as a result of solution instability (resulting in unfolding) is one of the main problems encountered in therapeutic protein formulations, although it is by no means the only cause with freeze-thawing and exposure to container surfaces also being shown to cause mAb aggregation (Kueltzo et al., 2008). The prevention of aggregation is essential for generation of an effective therapeutic protein and to ensure product quality. The manufacturing processes used during the production of protein formulations can also cause aggregation and precipitation, with shear strain placed upon an IgG4 being shown to result in aggregate formation (Biddlecombe et al., 2007, Biddlecombe et al., 2009). Agitation has also been found to result in the aggregation of an IgG2 with exposure to an air/liquid interface being shown to be a potentiating factor (Brych et al., 2010). Due to this, stabilisers are added to protein formulations to maintain long-term stability and protein function include non-ionic surfactants, tri-block co-polymers and non-reducing sugars.

1.5.1 Entropy, enthalpy and free energy

Before the effect of excipients on protein formulations can be discussed, it is necessary to first give an overview of the thermodynamics involved - entropy, enthalpy and free energy.

Entropy is a measurement of the number of different potential conformations a system can be arranged in. It is frequently considered to be a measure of the level of "disorder": the higher the entropy of a system the higher the level of "disorder". The second law of thermodynamics, as stated by Smith (Basic Chemical Thermodynamics, 4th edition, Chapter 3 p.21-35), says "*Spontaneous changes are those which, if carried out under the proper conditions, can be made to work. If carried out reversibly they yield a maximum amount of work. In natural processes the maximum work is never obtained."* The entropy of an isolated system not in equilibrium will increase over time during a chemical process and will reach a maximum value at equilibrium, although this value is unlikely to be the theoretical maximum. The entropy change (ΔS) of a system which is going through an infinitesimal reversible process was first introduced by the Clausius equation (Equation 1-1):

$$\delta q_{rev}/T = \Delta S \qquad \text{Equation 1-1}$$

where, δq is the heat supplied to the system and T is the absolute temperature of the system as a whole.

ΔS will remain the same during the transition from one state (A) to another state (B) if the change is reversible (a change is considered to be reversible when the system is at equilibrium).

The thermodynamic property enthalpy can be used to calculate the internal energy of a system at a constant pressure. This is equivalent to the heat transfer which takes place during the chemical process. However, the change in enthalpy (ΔH) is more commonly used. ΔH is the change in the energy of the system which is the heat absorbed or released by a chemical reaction. A chemical reaction which absorbs energy is referred to as an endothermic reaction and one which releases energy is known as an exothermic reaction. It is not possible to measure the total enthalpy of a reaction so the change in enthalpy is measured; it is calculated using the following equation (Equation 1-2):

$$\Delta H = H_{\text{final}} - H_{\text{initial}} \qquad \textbf{Equation 1-2}$$

The Gibbs free energy is the maximum quantity of work which can be obtained from a closed system at a constant pressure and temperature during a process which is fully reversible (at equilibrium). The change which takes place in a system from an initial state to a defined final state is referred to as the change in the Gibbs free energy (ΔG). The value for Gibbs free energy when a system is at equilibrium, and so is not capable of doing work, is zero. The maximum Gibbs free energy will be obtained when a system is at a constant temperature and pressure but is yet to reach equilibrium. The ΔG is calculated using the change in entropy (ΔS) and the change in enthalpy (ΔH) using the equation (Equation 1-3):

$$\boldsymbol{\Delta G = \Delta H - T\,\Delta S} \qquad \textbf{Equation 1-3}$$

where, T is temperature (°K).

As equation 1-3 shows, the ΔG of a system is calculated from the values for the entropy and enthalpy of the system. A number of weak interactions characteristically take place within a system including hydrogen bonding, van der Waals interactions and hydrophobic interactions. Depending on the circumstances, the contribution of each of these can be endothermic or exothermic. The contribution of entropy (ΔS) and enthalpy (ΔH) can vary widely which could result in a smaller ΔG value. This is known as entropy-enthalpy compensation and can lead to difficulties in understanding the thermodynamics of a macromolecular interaction (Cooper et al., 2001). It was also observed by the authors that there was a correlation between ΔS and ΔH of binding between different chemical species. It was noted that a pair of ΔS and ΔH values appeared likely to fall along a common line. This finding was attributed to be a result of the limited Gibbs 'free energy window' of experimental techniques (Cooper et al., 2001).

For example when considering water, it is most stable in its gaseous state at high temperatures, in intermediate regions it will form a liquid and at low temperatures it is most stable as a solid.

The equilibrium which forms between the different states of a surfactant; whether it remains as a single alkyl chain, a self-assembled monolayer (SAM) or forms a micelle; is determined by the free energy value for each phase. The phase which has the lowest energy under the conditions will be the most stable and therefore will be the one adopted. Studies have been carried out into the effect of alkyl chain length on the formation of SAMs and their critical micelle concentration (CMC). The interaction between the carboxylic end groups was found to induce a degree of conformational stability of the alkyl chains (Schmitt et al., 1998). Alkyl chains are

ordered when at low temperature but become disordered when the increase in temperature is sufficient to surmount the stabilising effects of inter-chain van der Waals interactions.

With respect to proteins, the ΔG refers to the conformation the protein adopts in solution or when present at an interface. The protein will adopt a conformation in which the ΔG value is at its lowest. In an unfolded state, the hydrophobic residues of a protein are exposed to the aqueous environment which results in water molecules ordering around these regions in hydration shells. Upon folding of the protein, the hydrophobic regions become buried in the centre of the structure forming the hydrophobic core which increases the entropy of the water molecules. The increase in entropy of the water molecules is greater than that of the entropy decrease resulting from protein folding and is thus favoured. The ΔS value is positive due to the formation of hydrogen bonds, ionic salt bridges and Van der Waals interactions within the protein. Through combining the values for each thermodynamic process, protein folding has a negative ΔG and therefore takes place spontaneously.

1.5.2 Non-ionic surfactants

Non-ionic surfactants which have been European Medicines Agency (EMEA) (http://www.ema.europa.eu/) or Food and Drug Administration (FDA) (http://www.fda.gov/) approved are commonly used to stabilise proteins formulated as liquid solutions as they have been found to protect against aggregation (Bam et al., 1998). Although they have been widely used, the method by which they protect proteins from aggregation or degradation is currently not fully understood.

Surfactants spontaneously form micelles as a result of their amphiphilic nature; they are composed of a hydrophilic fatty acid tail and a hydrophobic group such as poly(ethylene glycol (PEG). The concentration at which micelles spontaneously form is called the critical micelle concentration (CMC). The CMC for non-ionic surfactants, including Tween®, is reported in the literature with the solution typically being either pure water or a weak buffering solution. However, studies have shown that the binding of Tween to a protein or polymer can alter the CMC value calculated (Bam et al., 1995, Barreiro-Iglesias et al., 2003).

1.5.3 Hydrophilic-lipophilic balance (HLB)

A feature of non-ionic surfactants which is important when discussing their inclusion in protein formulations is the hydrophilic-lipophilic balance (HLB). The number of polar and non-polar groups present in the surfactant molecule will determine how lipophilic (oil loving) or hydrophilic (water loving) the surfactant is. A high HLB value signifies a hydrophilic surface-active molecule compared to a low HLB value which indicates that the surfactant is lipophilic. Oil will spread on the surface of water, or form droplets in suspension, because it contains a high proportion of polar groups such as –COOH and –OH and is therefore not hydrophilic. As stated in Martin's Physical Pharmacy (Martin et al., 2011) as the length of the carbon chain of an acid, such as oleic acid, increases the ratio of polar to non-polar groups will decrease. This will therefore increase its miscibility resulting in the molecule becoming more hydrophilic.

Specific molecules and ions when dispersed in liquid will move independently of other factors towards the interface; this can be a liquid-gas, liquid-liquid, or liquid-surface. This preferential partitioning is termed adsorption, this process is observed with surfactants adsorbing at interfaces due to their amphiphilic nature. The number of carbon atoms in the alkyl chain of straight-chain alcohols, amines and acids results in a transition from a mainly hydrophilic to a lipophilic substance; for example ethyl alcohol is fully miscible in water. The HLB values of a selection of amphiphilic substances are listed in Table 1-4.

Substance	**HLB value**
Oleic acid	1
Sorbitan monoleate (Span 80)	4.6
Sorbitan monolaurate (Span 20)	8.6
Methyl cellulose (Methocel 15 cps)	10.5
Polyoxyethylene sorbitan monooleate (Tween 80)	15.0
Polyoxyethylene sorbitan monolaurate (Tween 20)	16.7
Sodium lauryl sulphate (sodium dodecyl sulphate)	40

Table 1-4. The hydrophilic-lipophilic balance (HLB) values of surface-active agents (surfactants).

1.5.4 Polysorbates

Polysorbates have been suggested to have a protective mechanism by stabilising a protein through binding to its native state and increasing the free energy of unfolding (Chou et al., 2005). For this mechanism of stabilisation to take place, the strength of the polysorbate interaction with the native state of a protein must be greater than that of the denatured state. The free energy of the native state would therefore decrease and thus have a stabilising effect. The free energy of the denatured state would be increased and consequently the native fold of the protein would be energetically

favourable. An alternative protective mechanism against aggregation has been suggested which is via steric interference leading to a blocking of the hydrophobic sites (Bam et al., 1998) which are involved in protein-protein interactions (Tsai et al., 1997).

The unfolding of the protein Albutropin™ in the presence and absence of Tween was investigated using guanidine hydrochloride (Chou et al., 2005). It was found that the addition of Tween 20 and Tween 80 to a solution containing Albutropin™ at stoichiometric ratios of 10:1 and 9:1 resulted in a shift in the unfolding curves to higher guanidine hydrochloride concentrations (Figure 1-5) which indicates an increased stability (Chou et al., 2005).

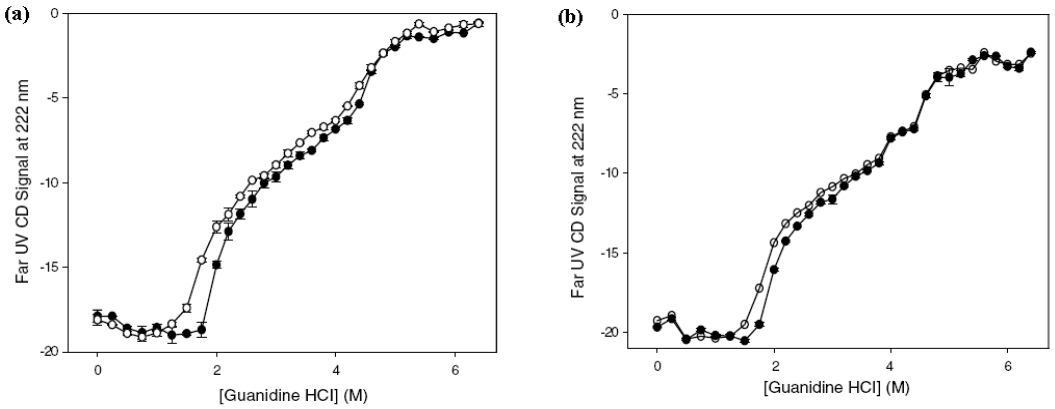

Figure 1-5 Effect of (a) Tween 20 (Tween 20 10:1 Albutropin™) and (b) Tween 80 (Tween 80 9:1 Albutropin™) on the unfolding curves of Albutropin™. Control, no Tween, shown by an open circle (○) and Tween included in the solution is shown by a filled circle (●) (Chou et al., 2005).

Recombinant human growth hormone (rhGH) has been shown to bind to Tween 20 and Tween 80 with the results indicating the binding to be hydrophobic in nature

(Bam et al., 1995). To confirm that hydrophobic binding was involved, recombinant human interferon-γ (rhIFN-γ) was used which is a highly hydrophobic protein. It was found using electron paramagnetic resonance (EPR) that a larger number of Tween 40 molecules bound to rhIFN-γ than rhGH, 6 molecules compared to between 2.5 and 3 (Bam et al., 1995). The blockage of hydrophobic binding sites via surfactant binding would decrease the likelihood of the protein aggregating as protein-protein interactions commonly take place via hydrophobic sites (Tsai et al., 1997).

An investigation by Hoffmann et al., (2009) found that both polysorbate 20 and 80 (the structures of which are shown in Figure 1-6) non-covalently bound bovine serum albumin (BSA) with a binding constant (K_a) of between 8 and 12 x 10^3 M^{-1} (Hoffmann et al., 2009a). Although an interaction between the polysorbates and BSA was evident, the interaction between the two polysorbates and both lysozyme and immunoglobulin (IgG1) was negligible. Thermal stability studies showed Tween inclusion did not affect the stability of either lysozyme or the IgG1 which suggests that a specific interaction between the protein and Tween would not be the cause of any changes in stability (Hoffmann et al., 2009a). A separate investigation into the binding of polysorbate 20 and 80 to Human Serum Albumin (HSA) and three immunoglobulins yielded similar results. The surfactants bound to HSA with a K_a value of 1600 ± 110 M^{-1} for polysorbate 20 with the authors stating a similar value to have been obtained for polysorbate 80, but their binding to the immunoglobulins studied was again negligible (Garidel et al., 2009).

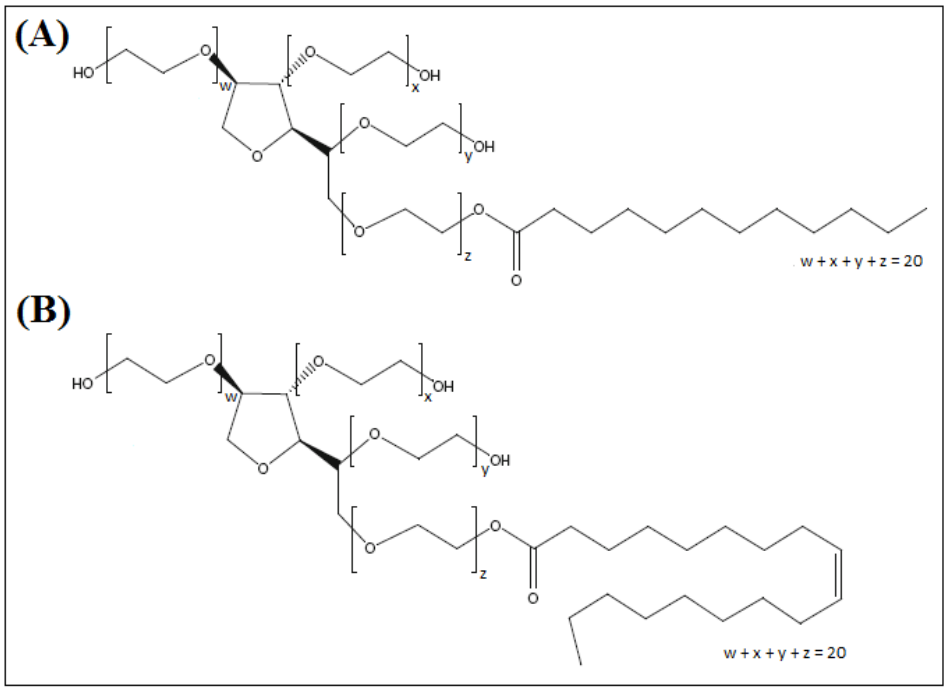

Figure 1-6 The structure of the (a) predominantly monolaurate ester Polysorbate 20 and (b) monooleate ester Polysorbate 80 (Adapted from Hoffmann *et al.*, 2009 (Hoffmann et al., 2009a)).

Tween 20 has been found to be effective at preventing the agitation-induced aggregation of recombinant human growth hormone (rhGH) (Bam et al., 1998). Studies on the effect of agitation, via shaking on a Glass-Col shaker at 120 shakes/min, showed that in the absence of Tween 20 nearly all of the monomeric rhGH protein was lost within ten hours (Bam et al., 1998). The half-life of the monomeric rhGH increased as the stoichiometric ratio of Tween 20:rhGH increased. The effect of Tween 20 and Tween 80 on the agitation-induced aggregation of Albutropin™ (a human growth hormone genetically fused to human albumin) was also been investigated (Chou et al., 2005). It was found that a stoichiometric ratio of

10:1 Tween 20:Albutropin prevented aggregation for up to 96 hours of agitation at room temperature. The use of a 5:1 ratio delayed, but did not prevent, the onset of aggregation with similar results being obtained for Tween 80 (Chou et al., 2005).

The inclusion of Tween in protein formulations has been shown to have a protective mechanism during the freeze-thaw process. The inclusion of Tween 80 in formulations at 0.02 and 0.1 % w/w decreased, but did not prevent, the formation of bovine IgG aggregates after freeze-thawing (Sarciaux et al., 1999). Tween 80 has also been shown to protect lactate dehydrogenase freeze-thaw induced aggregation (Hillgren et al., 2002). A similar finding has been observed for recombinant human factor XIII as evidenced by the presence of Tween 20 at concentrations of 60 and 120 µM reducing the percentage of insoluble aggregates (Kreilgaard et al., 1998). This protective effect of Tween has been observed for a number of other proteins including interleukin-1 receptor antagonist and tumour necrosis factor binding protein (Chang et al., 1996). The protective mechanism of Tween was suggested to be as a result of competition with the protein for surface binding sites.

Proteins adsorb to interfaces such as the air/liquid interface, where it has been suggested that immunoglobulins orientate with the F_c region (which is hydrophobic) toward the interface and the F_{ab} region (which is hydrophilic) facing the aqueous layer (Baszkin et al., 2001). Polysorbates are included, in addition to increasing protein stability, to reduce protein adsorption at interfaces (e.g. solid/liquid and air/liquid). Tween 80 has been shown to reduce IgG adsorption to surface including nylon and cellulose acetate (Mahler et al., 2010). The quantity of two mAbs one of which was hydrophilic and one was hydrophobic, adsorbed to bare silica in the presence of Tween 80 at 0.01 % or 0.02 % was decreased from ~ 5 and 10 mg/m^2 to

~2 mg/m^2 and negligible respectively (Oom et al., 2012). The inclusion of Tween 80 in protein solution has also been found to reduce lysozyme adsorption to a hydrophobic surface (Joshi and McGuire, 2009) and recombinant factor VIII to a hydrophilic surface (Joshi et al., 2008).

In addition to increasing protein stability and reducing surface adsorption, polysorbates have been found to reduce the reconstitution time of proteins in spray dried formulations. The reconstitution time of an immunoglobulin-trehalose formulation decreased from between five and six minutes to approximately three minutes when 0.002% w/v Tween 20 was included. This was hypothesised to be due to Tween 20 increasing the wettability of the powder (Dani et al., 2007). The inclusion of Tween in reconstitution media also reduces the formation of aggregates in the protein solution. The presence of 0.1 % Tween 80 in the reconstitution medium for a 1 mg/mL interleuikin-1 receptor antagonist reduced aggregate formation from 50 to 23 % (Chang et al., 1996).

Although the presence of Tween has been shown to decrease protein aggregation and surface adsorption, the surfactant itself can adsorb to filter surfaces used during processing which could result in a reduced final surfactant concentration in the formulation. For example, it has been shown that Tween 80 adsorbed to a polyethersulfone filter membrane (Mahler et al., 2010) and it has also been found that Tween 20 adsorbs to both polyvinylidene fluoride and polyethersulfone filter membranes (Zhou et al., 2008).

1.5.5 Tri-block co-polymers

Tri-block co-polymers are a group of non-ionic polymers commonly used in protein therapeutic formulations. They are composed of a central hydrophobic chain and two hydrophilic chains. There is a diverse number of such block co-polymers, which can be custom synthesised, but as regards protein formulation the poloxamers (or Pluronic® made by BASF Gmbh.) are generally considered. These are tri-block co-polymers consisting of a poly(ethylene glycol)-poly(propylene glycol)-poly(ethylene glycol) (PEO-PPO-PEO) chain (Figure 1-7). The length of the polymer chains can be customised and so a wide range of poloxamers exist with differing properties. A detailed review on the use of Pluronics in drug delivery is available in the literature (Kabanov et al., 2002).

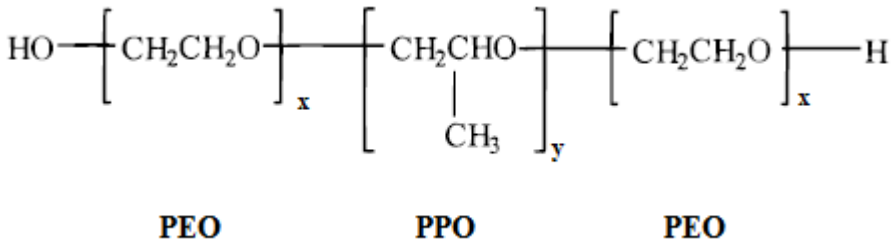

Figure 1-7. Structure of the Pluronic triblock copolymer surfactants: x – number of PEO repeating units; y – number of PPO repeating units.

Poloxamers are amphiphilic in nature and so are used in industry to increase the water solubility of hydrophobic substances (Sek et al., 2006). For example, an investigation into the effects of a number of Pluronics on the precipitation of a poorly water soluble compound (molecular weight 676.77 g/mol) in simulated gastric fluid and simulated intestinal fluid has been carried out (Dai et al., 2008). It was found that Pluronic F-127 and Pluronic F108 prevented the precipitation of the compound in

aqueous media, with F108 yielding a solution concentration of 36.4 µg/mL, compared to ≤ 10 µg/mL for the other surfactants studied (Dai et al., 2008).

An investigation by Croy and Kwon (2004) centred on the role of Pluronics in preventing aggregation of the antifungal drug nystatin through increasing its solubility. They found that the Pluronics F98, P105 and F127 increased the critical aggregation concentration (CAC) of nystatin from 20 µM to greater than 350 µM (Figure 1-8) (Croy and Kwon, 2004).

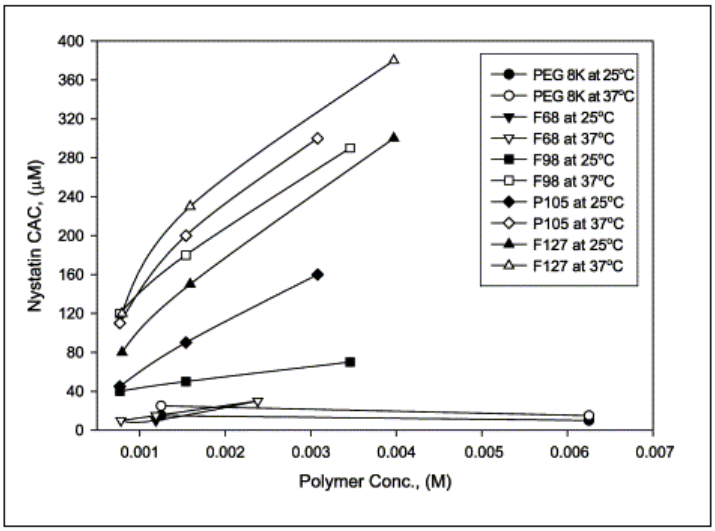

Figure 1-8. Effect of polymer concentration (Pluronic F68, F98, P105 and F127 and poly(ethylene glycol) (PEG 8K)) and temperature on the critical aggregation concentration (CAC) of nystatin as determined by dynamic light scattering (Croy and Kwon, 2004).

The ability to solubilise nystatin was strongly dependent on the nature of the Pluronic under study and similar relationships can be expected when studying non-covalent protein-Pluronic interactions (Croy and Kwon, 2004). Given that there are many different Pluronics, it would be inefficient to test all in a series of protein formulation studies. Fortunately, the generic function of the Pluronics is reasonably well known

by the manufacturers and some Pluronics can be excluded from protein formulation studies due to undesirable characteristics such as foaming or poor water solubility. Pluronic inclusion in formulations can also increase protein stability through the PPO segment interacting with exposed hydrophobic patches on the protein preventing the formation of protein-protein interactions and the PEO segment providing added steric hindrance. Pluronics have been shown to interact with the hydrophobic patches on proteins which are exposed when unfolded (Lee et al., 1992, Marks et al., 2001). Pluronic F-127 has been observed to reduce the degree of insulin aggregation when included at a concentration of 2 mg/mL (Taluja and Bae, 2007). The authors suggested that the decreased insulin aggregation in the presence of Pluronic F127 may be due to an interaction between the PPO component of the Pluronic, which is hydrophobic, and the insulin itself (also hydrophobic) thereby sterically preventing insulin-insulin interaction (Taluja and Bae, 2007). In addition to the decrease in protein aggregation, Pluronic F-127, at 2 mg/mL, has also been shown to increase the stability of insulin at pH 5.5, as evidenced by 42 % of the native structure being retained compared to 0 % in its absence.

In addition to increasing solubility and stability of compounds, Pluronic surfactants have been shown to reduce protein surface adsorption. The molecular weight and Pluronic chain length determine the reduction in protein adsorption with higher molecular weight and chain length Pluronics found to be more effective (McGurk et al., 1999, Amiji and Park, 1992). A further study has also shown that the PEO chain length of the Pluronic surfactant determined its ability to reduce or repel protein adsorption (Kiss et al., 2008). Adsorption of collagen to hydrophobic surfaces when co-dissolved with Pluronic F68 reduced adsorption by between approximately 50 and

80 % depending on the concentration of Pluronic included (Dewez et al., 1997). Co-dissolved Pluronic PE6800 has also been shown to decrease the level of collagen surface adsorption by more than 50 % (De Cupere et al., 2003). It is possible that the reduction in protein adsorption observed in the studies mentioned could be due to incorporation of the protein into the core of Pluronic micelles. The incorporation of drugs within Pluronic micelles has been shown previously (Sugin et al., 2006, Sahu et al., 2011) with the capacity of the micellar core determining the quantity of drug encapsulated. The PPO segment forms the core of the micelle and the PEO segment the outer shell and the capacity of the core will be determined by the length of the PPO segment.

It is believed that Pluronics, like Tween, protect proteins from aggregation through preventing exposure to interfaces – for example, a range of Pluronics have been shown to adsorb to a silanised surface (Lee et al., 2004) and reduce protein adsorption (Amiji and Park, 1992). Pluronic surfactants have been shown to be present at air/liquid interfaces, exposure to which is a source of protein aggregation. Through the use of a vibrational spectroscopy technique, peaks corresponding to the C-H backbone and the CH_3 side-chain of the PPO were detected establishing that the PPO component was dominant at the interface (Chen et al., 2003). In the vibrational spectroscopy technique, two laser beams are shone onto a surface and mix producing an output beam with a frequency. Analysis of the data allows the investigation of co-polymer orientation at an interface. The PPO segments are ordered at the interface with the PEO segments adopting random orientations in the aqueous layer below. At low concentrations the PPO block still dominates as studies using a low concentration of PEG alone, which has a similar surface behaviour to PEO, produced

a weak signal (Chen et al., 2003). At high Pluronic concentrations the methyl groups adopt a highly ordered orientation. This is not the case at low concentrations however, as the PPO backbone is stretched leading to the orientation of the methyl groups becoming less ordered. The PPO:PEO ratio does not affect the structure formed by the Pluronic surfactants at the air/liquid interface (Chen et al., 2003).

Adsorption of an IgG to a polystyrene surface (hydrophobic) coated with Pluronic F68, which has a PPO chain length of 30 (Huang et al., 2002), was reduced by ~20 % (Torcello-Gomez et al., 2011) corroborating the suggestion by Amiji and Park (1992). An alternative hypothesis for reduced protein adsorption to Pluronic coated surfaces is that the length of the PEO chain determines the ability of the Pluronic to repel protein adsorption. This is illustrated by adsorption of the protein fibrinogen to a hydrophobic surface coated with Pluronic F108 (PEO chain length of 129 monomers) being inhibited compared to adsorption observed on surfaces coated with Pluronic F88, F68 and P105 (PEO monomers numbers reported as 104, 76 and 37) (Li and Caldwell, 1996). As for Pluronic F68 co-dissolved with protein in solution, coating of a surface with Pluronic F68 has also been shown to decrease protein adsorption. A nanoparticulate surface coated with Pluronic F68 reduced adsorption of an IgG by approximately 1 mg/m^2 (Torcello-Gomez et al., 2011). The concentration of Pluronic F68 used to coat a surface prior to exposure of a monoclonal IgG1 was shown to affect the concentration remaining in solution. The percentage of protein in solution increased from 26-42 % when the surface was coated with 0.1 to 10 mg L^{-1} Pluronic F68 to approximately 93% in solution from a tube coated with 0.01 mg mL^{-1} Pluronic F68 (Doran, 2006). At the air/liquid interface protein adsorption has also been found to be decreased by Pluronic F68.

The Pluronic was not displaced by the IgG over time (as the surface pressure does not become equal to pure IgG) but it is likely that the protein penetrated the Pluronic layer to a degree forming a mixed layer (Torcello-Gomez et al., 2011).

1.5.6 Non-reducing sugars

Non-reducing sugars such as trehalose and sucrose (Figure 1-9 and Figure 1-10) are incorporated into protein formulations to protect proteins. A non-reducing sugar is one which does not contain either an aldehyde, RC(=O)H, or a ketone, RC(=O)R', group. In order for a sugar to act as a reducing agent, for example in the Maillard reaction, it must have an open-chain structure in addition to the presence of an aldehyde or ketone group. The Maillard reaction takes place between a reducing sugar and an amino acid – specifically between the carbonyl group of the reducing sugar and the nucleophilic amino group (e.g. NH_3) of an amino acid. As shown in Figure 1-9 and Figure 1-10 trehalose and sucrose do not have an open chain or contain aldehyde or ketone groups. The inclusion of non-reducing sugars was not investigated in this study but as will be discussed here they are an important class of excipient used in protein formulations.

Trehalose (Figure 1-9) is a non-reducing natural disaccharide found throughout nature and is used during the process of lyophilisation. It has been found to protect organisms against stresses such as drying and freezing (Crowe et al., 1996, Crowe et al., 2005). It has a high thermostability (ability to resist irreversible changes due to high temperature), is stable across a wide pH range and is non-reducing (Higashiyama, 2002). These properties make trehalose an effective stabiliser in preventing protein denaturation.

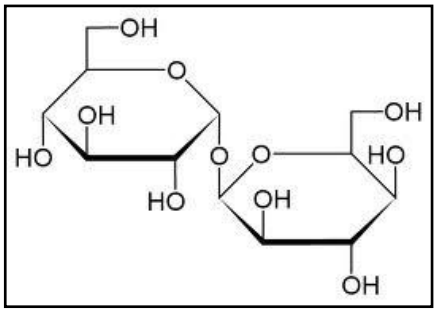

Figure 1-9. Structure of trehalose.

Trehalose has been used as a stabiliser in monoclonal immunoglobulin formulations such as ranibizumab (marketed as Lucentis®, Genetech and Novartis). Trehalose has a high glass transition temperature (T_g), 388.5K (116ºC) (Elias and Elias, 1999), which is desired as it will be physically stable at higher temperature and thus will continue to protect the product. This allows a pharmaceutical product containing trehalose within the formulation to be stored at room temperature and transported/shipped without cooling being essential (Simperler et al., 2007).

The monoclonal immunoglobulin immunoglobulin M (IgM) is susceptible to aggregation and loss of binding activity after being subjected to freeze-thaw cycles (Draber et al., 1995). An investigation into the effect of 0.25 M trehalose inclusion in an IgM formulation found it retained its binding efficiency after freeze-drying (Draber et al., 1995). The inclusion of trehalose in a solution of BSA has also been found to lead to a significant reduction in the percentage of BSA molecules aggregating (Jain and Roy, 2008). In the absence of trehalose, with a moisture level of 8 µl/10 mg BSA, approximately 50% of the BSA aggregated. The inclusion of trehalose at a 1:1 (w/w) ratio decreased the percentage of aggregation to a level at which it was no longer observed by analytical electrophoresis and tryptophan intrinsic fluorescence (Jain and Roy, 2008).

Inclusion of trehalose in a spray-dried recombinant humanised anti-IgE monoclonal immunoglobulin formulation reduced aggregation from 5-6 % to ≤ 1 % at ratios from 100:1 to 900:1 (trehalose: immunoglobulin) (Andya et al., 1999). The rate of aggregation of the formulation containing trehalose at a ratio of 100:1 (trehalose: immunoglobulin) decreased to half that of the formulation containing no excipient. The maximum stability of anti-IgE was found to occur with a molar ratio between 300:1 and 500:1 excipient:protein. However, trehalose molar ratios of above 200:1 increased the cohesiveness of the spray-dried particles resulting in undesired formulation characteristics of large particles and poor dispersion (Andya et al., 1999).

Sucrose is, like trehalose, a naturally occurring disaccharide which is only synthesised by plants (Figure 1-10). Sucrose stabilises a protein in aqueous solution as it is excluded from the protein surface. This favours a highly compact protein as the free energy will be lower and shift the equilibrium away from one favouring aggregation (Kendrick et al., 1997).

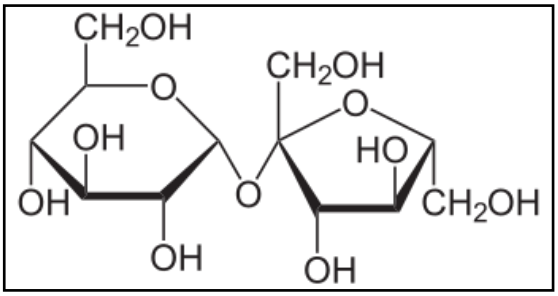

Figure 1-10. Structure of sucrose.

As is the case with trehalose, one of the reasons sucrose is chosen for protein formulations is that it has a high T_g. The T_g of sucrose is reported in the literature as being 343K (70ºC) (Orford et al., 1990). The high T_g enables physical stability at

higher temperatures and therefore also storage at room temperature and transport without the need for cooling.

Sun and Davidson (1998) investigated the effect of amorphous glucose/sucrose and glucose/trehalose (both 1:10, weight/weight) on the inactivation of the protein glucose-6-phosphate dehydrogenase. It was observed that the inclusion of trehalose with glucose increased enzyme activity for a longer duration than sucrose/glucose (Figure 1-11) (Sun and Davidson, 1998).

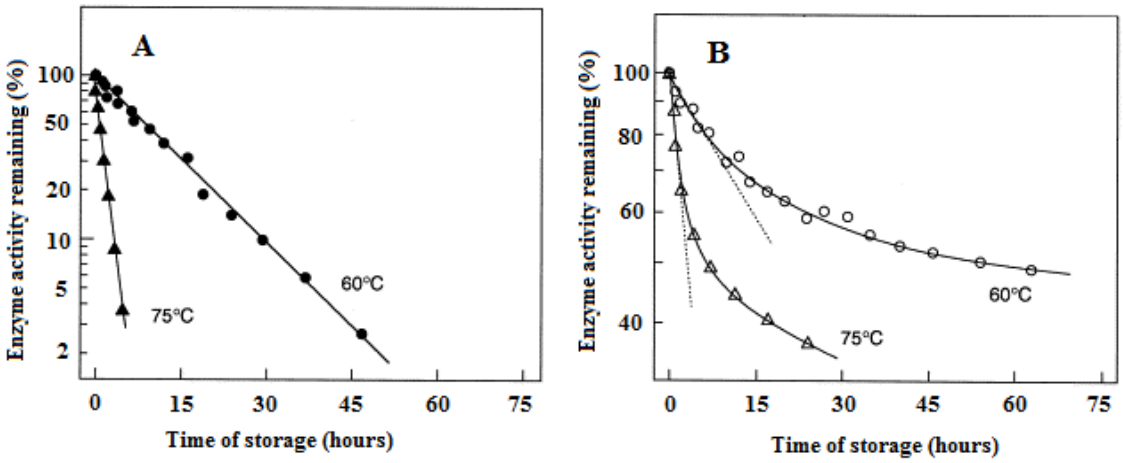

Figure 1-11. A) glucose/sucrose (1:10, w/w); B) glucose/trehalose (1:10, w/w) (Sun and Davidson, 1998).

The use of sucrose and trehalose in an IgG formulation which had been spray dried reduced the formation of soluble aggregates upon reconstitution at both low (5 mg/mL) and high (200 mg/mL) concentrations (Dani et al., 2007). The monomer concentration of the reconstituted IgG formulation at 200 mg/mL which did not contain sugar was 79.9 ± 0.1 % which was a decrease from the solution concentration prior to drying (91.1 ± 0.7 %). This is compared to a monomer concentration of 89.5 to 90.5 % from IgG formulated with a sugar (Dani et al., 2007).

Figure 1-12 shows that the features of the native secondary structure are retained upon reconstitution in formulations containing a disaccharide when investigated using Fourier transform infrared (FTIR) (Dani et al., 2007).

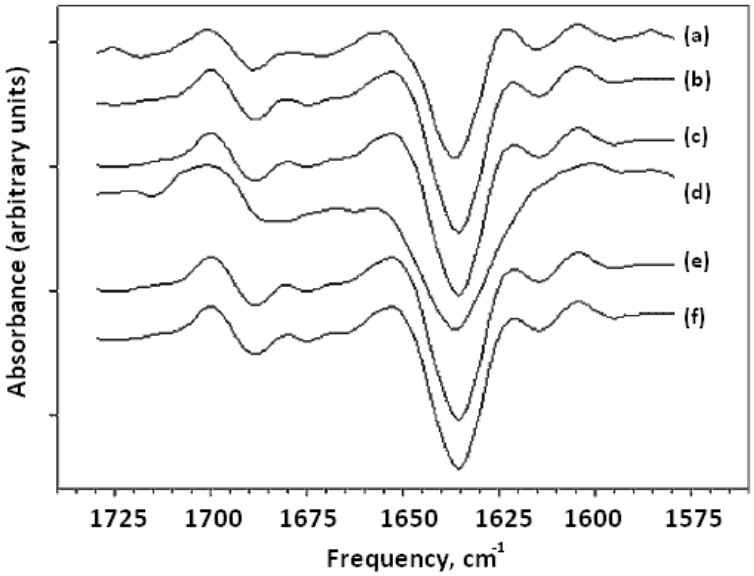

Figure 1-12 Fourier transform infrared (FTIR) spectra for: (a) native IgG (10 mg/mL); (b) spray-dried IgG-trehalose which had been reconstituted at 200 mg/mL; (c) spray-dried IgG-trehalose-Tween 20 which had been reconstituted at 200 mg/mL; (d) bulk IgG reconstituted at 200 mg/mL; (e) spray-dried IgG-trehalose poweder; and (f) spray-dried IgG-trehalose-Tween 20 powder (Dani et al., 2007).

1.6 Protein aggregation

Proteins formulated in a high concentration liquid form are susceptible to aggregation (Ripple and Dimitrova, 2012). Excipients such as polysorbates and Pluronics are included to reduce the occurrence of aggregation. The concentration of surfactant which is required to prevent aggregation is dependent on the protein and surfactant type. The inclusion of 0.1 % Tween 80 in a recombinant human interleukin-2 (rIL-2) solution significantly reduced the formation of aggregates after 24 hours of shaking at room temperature (Wang et al., 2008a). The rIL-2 protein will

orientate itself to maximise the interaction with the surface thus exposing the hydrophobic regions. Exposure of the hydrophobic regions within a protein would increase the chances of protein-protein interactions which could subsequently lead to an increase in the level of aggregation. Surfactants such as Tween compete with proteins to occupy the interfaces which prevent the protein coming into contact with the surface (Kreilgaard et al., 1998) and the subsequent reorientation and unfolding that would likely occur. Protein aggregates have been found to be present in an rIL-2 formulation containing 0.1 % Tween 80 stored at 40 °C for 2 months. These aggregates were not found in formulations in which Tween 80 was absent (Wang et al., 2008a). The formation of aggregates may be due to degradation of the Tween producing peroxides and destabilising the protein, which will be discussed further in section 1.8. Sodium dodecyl sulphate polyacrylamide gel electrophoresis (SDS-PAGE) experiments showed rIL-2 bands consistent with dimer, trimer and oligomer formation (Wang et al., 2008a). The aggregation index values did not indicate a significant change in the number of aggregates formed and suggests that the aggregates are mainly soluble. The same study showed that aggregates formed when stored at 5 °C for 22 months were not linked by disulphide bonds using SDS-PAGE (Wang et al., 2008a). A weak non-specific interaction between Tween 80 and the protein may take place during storage (regardless of the storage temperature and duration) which could reduce the free energy of the folded state making unfolding favourable. This interaction is likely to occur via exposed hydrophobic regions which are a source of protein-protein interaction and this in turn can lead to aggregation (Kumar et al., 2011).

The aggregation of Albutropin™ after agitation in the presence of both Tween 20 and 80, with which it is known to interact, is influenced by surfactant concentration. It was found that an Albutropin™: Tween 20 ratio of 5:1 delayed the onset of aggregation but did not prevent it. A stoichiometric ratio of 10:1 was, however, sufficient to prevent Albutropin™ aggregation from occurring. A 9:1 Albutropin™: Tween 80 stoichiometric ratio also inhibited agitation induced aggregation as did a concentration of Tween 80 which was just above its CMC (Chou et al., 2005).

Agitation of immunoglobulin has also been found to result in aggregate formation. Agitation of a fully human monoclonal IgG2 antibody for 72 hours in a vial with headspace, which allowed for an increase in the air-liquid interface, resulted in the formation of visible aggregates. Analysis revealed the aggregates to be insoluble (Brych et al., 2010). A Tween 20 concentration of 0.004 % (w/v) prevented the formation of IgG2 aggregates when agitated under the same conditions. Addition of soluble IgG2 aggregates to the formulation with 0.004 % (w/v) Tween 20 did not cause the formation of aggregates. Similarly, spiking of both soluble aggregates and 0.004 % (w/v) Tween 20 into the formulation, which did not previously contain Tween 20, did not result in aggregate formation (Brych et al., 2010). It was therefore concluded that the inclusion of Tween 20 at a concentration of 0.004 % (w/v) is sufficient to prevent the formation of IgG2 aggregates under these conditions. The effect of shaking and stirring stress on the aggregation of a chimeric mouse/human monoclonal IgG1 antibody is affected by the presence/absence of Tween 80. Sample vials were either shaken horizontally on a shaking plate or stirred using a Teflon coated stirring bar (Mahler et al., 2005). Teflon is a hydrophobic surface, which has been shown to cause protein unfolding (Vermeer et al., 1998), and so this may be an

additional source of aggregation in the authors' findings. Shaking and stirring caused the formation of IgG1 aggregates larger than 10 and 25 μm in diameter (these values correspond to the particle sizes analysed using laser light diffraction in both European and American pharmacopoeia) to a similar extent. The formulations containing Tween 80 at a concentration of 0.01 % w/v, aggregates greater than 10 and 25 μm were identified in the stirred vials, while aggregation was found to decrease in the vials that were shaken. Dynamic light scattering identified a second larger peak with a larger hydrodynamic diameter in the IgG1 samples which had been stirred but not in those which had been shaken. In formulations containing Tween 80 a second larger peak was observed in both stirred and shaken samples. An additional air/water interface may be generated between the stirring bar and sample which would accentuate IgG1 aggregation (Mahler et al., 2005). Although Tween 80 did not prevent the formation of the visible particles (10 and 25 μm in diameter) in the sample which had been shaken, sub-visible particle formation was inhibited (those with a diameter less than 10 and 25 μm). Tween 80 is capable of preventing the formation of aggregates of differing size depending on the stress to which the IgG1 is exposed to (Mahler et al., 2005). The presence of Tween 20 at 0.01 % has been shown to be adequate to prevent aggregation of a mAb after shaking. The concentration of Tween 80 required was found to be double that of Tween 20, 0.02 % (Kishore et al., 2011a).

Findings by Chang et al., (1996) demonstrated that protein denaturation during freeze-thawing was due to exposure of the protein to the ice-water interface. The addition of 0.01 % (w/v) Tween 80 to lactate dehydrogenase and glutamate dehydrogenase prevented freeze-thaw induced denaturation, while the catalytic

activity of lactate dehydrogenase was decreased as a result of freeze-thawing. The catalytic activity was however largely maintained in the presence of 0.01 % (w/v) Tween 80, with activity of 95 % compared to 23 % in the absence of Tween 80. The protective effect of Tween 80 from freeze-thaw-induced aggregation was also found for four other model proteins (phosphofructokinase, interkeukin-1 receptor antagonist, tumour necrosis factor binding protein, ciliary neurotropic factor) (Chang et al., 1996).

1.7 Surface adsorption as a mechanism of aggregation

Therapeutic proteins have been observed to adsorb to the surfaces of pharmaceutical containers (Burke et al., 1992) including the stainless steel needle and glass surfaces of prefilled syringes (Bee et al., 2010, Eu et al., 2011). Adsorption to a hydrophobic surface, such as plastic commonly encountered during processing, is generally accepted to result in unfolding (Norde et al., 1986) which has been shown by Vermeer et al., (2001). X-ray photoelectron spectroscopy has shown rituximab and a polyclonal human IgG to adsorb to a glass vial, the rubber cap liner of the vial and a syringe plunger tip while demonstrating adsorption to polyvinylchloride (PVC) did not take place (Zangmeister, 2012). Further studies by the author indicated unfolding to take place upon adsorption. Protein adsorption to interfaces is often irreversible and can lead to perturbations in native structure affecting stability resulting in aggregation (Pinholt et al., 2011) and which are potentially immunogenic (Johnson and Jiskoot, 2012). For example, aggregates of recombinant human interferon beta-1a (rhIFNβ-1a) formed as a result of adsorption to steel microparticles increased its immunogenicity (Van Beers et al., 2012). In addition to adsorption at interfaces, adsorption of proteins to particles in solution or leachables can also cause

aggregation and particle formation (reviewed by Bee et al., 2011). The detection of protein particles and determination of their size and number in pharmaceutical formulations with respect to their immunogenicity is, at present, poorly understood (Bee et al., 2012). The presence of particles can potentially cause immunogenicity but each factor during production from expression to the container can be involved in causing an immune response (Singh, 2011).

It has been observed that an IgG adsorbed to the surface of microparticles in solution produced from glass, cellulose, a glass syringe and a glass vial with a near native state structure of the IgG determined (Bee et al., 2009). The pH of the solution affects the quantity of IgG adsorbed to a glass surface as shown by Mathes et al., (2011). Adsorption was highest between pH 4-5 at ~ 5mg/m^2 with decreased adsorption observed at pH values either side of this. Ionic strength was also determined to influence adsorption with adsorption increasing with ionic strength at pH 4 and the opposite being the case at pH 7.2 and 8.6 (Mathes and Friess, 2011). Further studies found adsorption of three human mAbs to a glass microparticle surface did not result in unfolding. However, this was not an indication that aggregation would be absent (Hoehne et al., 2011). The native β-sheet secondary structure was retained as shown by FT-IR spectroscopy and minimal tertiary structural changes determined through measurement of intrinsic fluorescence. The mAbs were attracted to the negatively charged glass microparticles forming a monolayer on the surface with coverage of 2-4 mg/m^2 and reducing the zeta potential of the suspension causing destabilisation. The sedimentation rate of the microparticles with this quantity of mAb adsorbed would not be expected to alter significantly but this was not the case. The rate of particle settling (which is

proportional to the square of its size) was rapid in each buffer after protein addition. This suggested that nucleation of aggregates was taking place in the suspensions (Hoehne et al., 2011). Similar to the findings of Hoehne et al., (2011), it has also been observed that the presence of cellulose particles causes nucleation of aggregates through preferential adsorption of aggregated mAb. Additionally, adsorption of the mAb to stainless steel particles resulted in the formation of soluble aggregates (Bee et al., 2009).

1.8 Tween degradation and oxidation of proteins

The Tween surfactants are known to undergo degradation which can lead to peroxide formation. The degradation of both Tween 20 and 80 takes place via auto-oxidation, cleavage at the ethylene oxide subunits and hydrolysis of fatty acid ester bonds (Kerwin, 2008). This results in the formation of hydrogen peroxide and acids in the solution. The temperature at which the solution is stored influences the specific degradation pathway of Tween in a formulation. For example, hydrolysis of the fatty acid ester is favoured at 25 °C compared to auto-oxidation of the ethylene oxide subunit being favoured at higher temperatures (Kerwin, 2008). Thermal oxidation and a reduction in weight of Tween 20 and 80 takes place when exposed to an oxygen atmosphere (Kishore et al., 2011b). The beginning of the autooxidation process is signified by the presence of exothermic peaks at 120 and 240 °C observed in DSC and thermal gravimetric analysis (TGA) experiments. The first peak corresponds to the insertion of oxygen and the subsequent breakage of the ethylene oxide chain. The authors suggested the second peak could be linked to secondary degradation reactions which are likely to include hydrolysis of fatty acid ester bonds and the peroxide formation resulting from this (Kishore et al., 2011b).

In placebo therapeutic protein formulations, i.e. those not containing a protein, a high level of peroxide formation and degradation of polysorbate was detected after storage for 24 weeks at 40 °C. Polysorbate formulations stored for 5 weeks at 40 °C had a peroxide content of 150 µmol/L. In an IgG1 formulation the degradation of Tween 20 and 80 was monitored for 12 months at both 5 and 25 °C. The level of degradation at 5 °C was low for both surfactants compared to the significant degradation of Tween 80 detected after storage at 25 °C indicating the influence that temperature has on the degradation rate of these polysorbates (Kishore et al., 2011b). The formation of peroxide in 20 % Tween 80 aqueous solution under air is faster and the peak level of peroxides formed was approximately 10 times that of neat Tween 80 (Ha et al., 2002). The presence of oxygen is therefore a potentiating factor in peroxide formation in diluted Tween solutions. It was found that by removing oxygen from the environment the formation of peroxide in Tween 80 solutions could be inhibited. As in the investigation by Kishore et al., (2011), the degradation rate of Tween 80 was decreased at lower temperatures (Ha et al., 2002).

Oxidation of rIL-2 after storage at 40 °C takes place in a linear fashion in aqueous buffer containing histidine at pH 5.5. This was also the case for formulations which contained 0.1 % Tween 80. However, the oxidation rate was increased by between 1.3 and 4.5 times (Wang et al., 2008a) in the presence of Tween 80. This increase in oxidation rate of rIL-2 by Tween 80 was also observed after storage at 5 °C with the increase ranging from 15 to 253 times. The increase in rIL-2 oxidation in the presence of Tween 80 may be due to degradation of the surfactant during storage. The level of oxidised rIL-2 mutein increased from 2.8 to 5.4 % when stored for 30

days under nitrogen compared to an increase to 10.9 % when stored under air (Ha et al., 2002).

Exposure of a protein to oxygen is therefore an initiator of protein oxidation. Inclusion of a surfactant would prevent this exposure but could also in turn lead to peroxide-induced oxidation of the protein. The inclusion of 0.1 % Tween 80 which had not been stressed prior to addition into the protein solution, and therefore had a low peroxide content, did not induce oxidation of rIL-2 mutein. However, Tween 80 which had been stressed, and therefore had a high peroxide content, caused rapid oxidation showing that the presence of peroxides was critical in initiation of protein oxidation. This was found to be the case under both air and nitrogen which suggests that the oxidation was due to Tween 80 degradation and the subsequent peroxide formation (Ha et al., 2002). The oxidation of lyophilised rIL-2 mutein exposed to air was 5.5 % which is lower than that in the liquid state. The inclusion of low peroxide Tween 80 caused oxidation in the lyophilised state after incubation at 40 °C. High peroxide Tween 80 caused the formation of oxidised rIL-2 mutein during lyophilisation and during storage in the solid state. Inclusion of the antioxidant glutathione reduced rIL-2 mutein oxidation in the solid state when incubated but did not prevent it from taking place during the lyophilisation process. During lyophilisation, constituent parts of the formulation are concentrated down and so it is feasible that the peroxides become concentrated and react with the rIL-2 mutein in the solid cake. Oxidation of the protein was found to be greater under air than vacuum which suggested that the oxygen potentiated the rate of oxidation (Ha et al., 2002).

The concentration of Tween 20 and Tween 80 in a mAb formulation stored at 5 or 25 °C for 12 months has been found to decrease. From an initial concentration of 0.05 % this decreased to 0.006 and 0.001 % at 25 °C and 0.02 and 0.003 % at 5 °C for Tween 20 and Tween 80 respectively (Kishore et al., 2011a). An increase in the number of subvisible particles (those below 10 µm) to 4500 particles per mL was observed in the mAb formulation containing Tween 20 compared to less than 20 particles per mL for Tween 80. The presence of degraded Tween, as well as Tween which had not begun to break down, increased the quantity of insoluble aggregates in a mAb solution (Kishore et al., 2011a). The presence of only degraded Tween increased the level of soluble aggregates in the solution. The addition of 0.01 % degraded Tween 20 increased soluble aggregate concentration to 75 % compared to 60 % in a sample which had been shaken in the absence of Tween (Kishore et al., 2011a). A 30 % aggregate content was found upon spiking in of Tween 80 at the same concentration.

Lauric acid, a degradation product of Tween 20, present in a mAb formulation at a Tween 20 to Lauric acid ratio of 1.0:0.5 or greater resulted in a significant increase in aggregate formation (Kishore et al., 2011a). Free lauric acid was also found to have an adverse effect on mAb stability in samples which were shaken in the absence of Tween 20 but it also increased soluble aggregate formation when Tween 20 was included in the formulation (Kishore et al., 2011a).

1.9 Aims and objectives of the thesis

The keys aims of this project are as follows:

- To investigate the interaction in bulk solution between an immunoglobulin (mAb-1) and surfactants. Investigation of the interaction in bulk solution will enable determination of the driving force behind mAb-1 surface adsorption.
- To determine the effect of surfactant presence on mAb-1 secondary structure and thermal stability. Through investigating the effect of temperature and surfactant presence on mAb-1 stability, the structure of the mAb-1 in solution during the surface adsorption experiments will be determined.
- To determine the force of adhesion between mAb-1 and surfaces with a range of hydrophobicites to aid selection of surfaces which have the potential to reduce protein adsorption.
- Throughout the manufacturing process and storage, proteins are exposed to a variety of solid/liquid interfaces including glass, metals and plastics which can lead to aggregation. This study will investigate the effect of surface energy on the structure of adsorbed mAb-1.
- Proteins have been shown to adsorb to solid/liquid interfaces including those of plastic bags, intravenous lines (McLeod et al., 2000) and glass vials (Mathes and Friess, 2011). This adsorption would result in a decrease in the protein concentration of the formulation and so this study aims to investigate the effect of surface energy, pH and surfactant on mAb-1 surface adsorption under flow conditions using total internal reflection fluorescence (TIRF).
- To characterise mAb-1 surface adsorption at the molecular level in terms of the number of layers formed and the orientation which mAb-1 adopts.

Chapter 2. Investigation of immunoglobulin-polysorbate interaction in the bulk solution

2.1 Introduction

The aim of the first stage of this investigation was to characterise the interaction between the immunoglobulin and non-ionic (Tween) and tri-block co-polymer (Pluronic) surfactants in the bulk solution. Prior to investigating the effect of surfactant on protein surface adsorption it was first necessary to characterise the protein-surfactant interaction in bulk solution. This will enable conclusions to be drawn regarding immunoglobulin surface adsorption and the role surfactants play in this process. Isothermal titration calorimetry was used to determine if a specific binding interaction took place between the two different types of surfactant and the immunoglobulin. The effect of surfactant inclusion on the thermal stability of the immunoglobulin was studied using differential scanning calorimetry, and circular dichroism was used to investigate the effect of surfactant on the secondary structure of the immunoglobulin.

2.1.1 Isothermal Titration Calorimetry

Isothermal titration calorimetry (ITC) is a technique used to investigate the thermodynamics of a chemical interaction, most commonly the binding of a ligand/drug (or other small molecule) to a protein or DNA molecule (Pierce et al., 1999). ITC measures the thermodynamic interaction between two substances as a function of the heat given out or taken up when, for example, a ligand solution is titrated into a solution containing a protein. In a single ITC experiment, the binding

constants (K_a), reaction stoichiometry (n), enthalpy (ΔH) and entropy (ΔS) are generated. The cell containing the protein and a reference cell are maintained at a constant temperature by an electrical current with a feedback system (Figure 2-1). There are two feedback systems in place: ΔT_1, between the sample and reference cell, which maintains the sample cell at a constant temperature and provides information on the thermodynamics of the interaction; and ΔT_2, between the reference cell and the adiabatic jacket (a double layered surrounding which prevents heat loss), which maintains the reference cell at a set temperature.

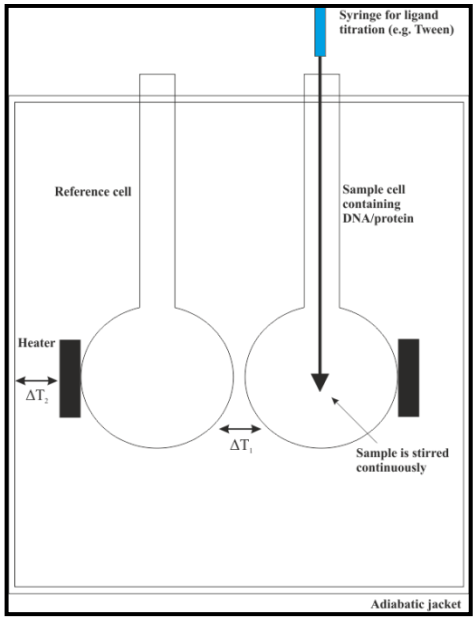

Figure 2-1. Isothermal titration calorimetry system set up. ΔT_1 is the sample cell feedback and ΔT_2 is the jacket feedback.

Upon the addition of a ligand into a protein solution the reaction which takes place can be either exothermic or endothermic. For example, the binding of distamycin A (a DNA minor groove binder) to DNA is exothermic (Pagano et al., 2008) while the interaction of a trisaccharide inhibitor (tri-N-acetyl-glucosamine) to hen egg white lysozyme is endothermic (Cooper et al., 2001). As a result of the feedback

mechanism the power to the reference cell is either increased or decreased to maintain a constant temperature; the power is increased if the reaction is endothermic and decreased if the reaction is exothermic (Figure 2-2). Analysis of the data enables calculation of the binding affinity constant (K_a), enthalpy changes (ΔH) and binding stoichiometry (n) of the interaction. The formation of a binary complex of DNA or S-adenosyl methionine (a co-repressor molecule) to *E.coli* methionine repressor is weakly exothermic, ~8 to 10 ΔH (kJ mol^{-1}). This is significantly less than the heat produced during the formation of a ternary complex, ~ 99 ΔH (kJ mol^{-1}) (Cooper et al., 1994). The entropy of the former complex is decreased in formation of the ternary complex which the authors suggested to be due to a decrease in the flexibility of the system. Therefore, the interaction of molecules can lead to different complex formations that affect the flexibility of the complex itself. This may in turn affect their ability to perform their function or triggering the interaction with encountered interfaces.

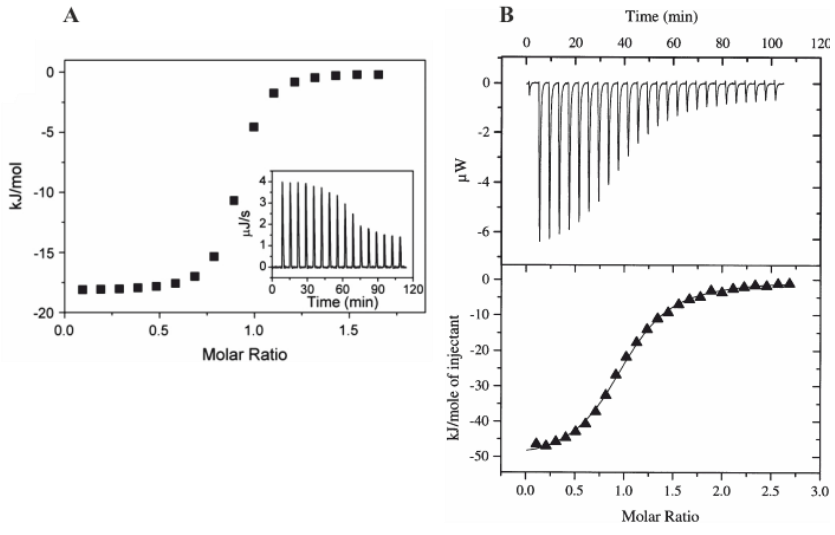

Figure 2-2. Examples of isothermal titration calorimetry (ITC) curves for (A) an endothermic reaction (Pagano et al., 2008) and (B) an exothermic reaction (Cooper et al., 2001).

ITC has been used to investigate the effect of the concentration of the chiral surfactant taurodeoxycholeate (TDOCA) on the formation of complexes with β-cyclodextrin. The results showed that at a TDOCA concentration below the critical micellar concentration (CMC), a 1:1 complex formed, compared to a 2:1 complex when a concentration above the CMC was used (Cooper et al., 1998). The binding stoichiometry of other surfactant-protein complexes may also be affected in a similar manner. Tween has been found to first bind to high affinity sites on Albutropin™ (a recombinant fusion protein composed of human growth hormone (hGH) genetically fused to HSA) followed by binding to the low affinity sites (Chou et al., 2005). In this scenario, at a low surfactant concentration the high affinity sites will be occupied first, and only once they become saturated will the surfactant bind to the low affinity sites. The binding stoichiometry would therefore change depending on the concentration of surfactant used.

The binding affinity of the non-ionic surfactants Tween 20 and Tween 80 for proteins varies depending on the protein type. It has been shown to be highest for Albutropin™, followed by HSA, and finally hGH to which only a weak interaction occurred. The Tween:hGH interaction was found to be too weak to allow the calculation of the thermodynamic binding parameters using ITC (Cooper et al., 2001, Chou et al., 2005). The interaction of Tween 20 and 80 with a recombinant human immunoglobulin IgG has also been investigated. The binding affinity of Tween 20 was shown to be lower for the immunoglobulin studied than for BSA, Figure 2-3 (Hoffmann et al., 2009a). A similar result was found for the affinity of Tween 80 for the immunoglobulin.

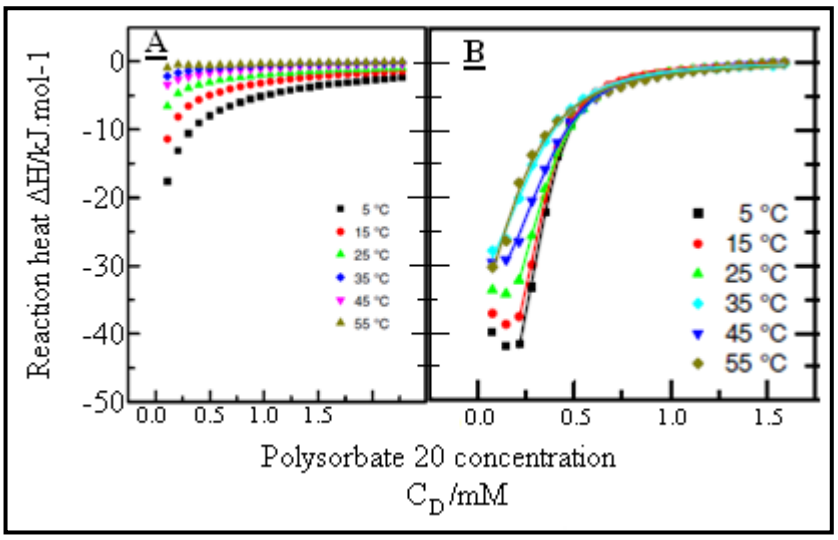

Figure 2-3. Binding isotherms for (A) Tween 20 to an immunoglobulin and (B) Tween 20 to bovine serum albumin (BSA) at temperatures varying from 5 to 55 ºC (Hoffmann et al., 2009a).

2.1.2 Differential Scanning Calorimetry

Differential scanning calorimetry (DSC) is used to study the phase transitions of a sample. In addition to the detection of melting, the transition from a solid to a liquid, and crystallisation, the formation of a crystal due to precipitation from solution, DSC can detect the more subtle changes which take place during glass transition of an amorphous material. Glass transition is a reversible process during which a solid material becomes molten or rubber-like. DSC can be used to study both solid and liquid state samples. The sample is heated linearly as a function of time and any change in the energy or heat capacity is detected. In the DSC set up, the reference and sample cells are maintained at a constant temperature throughout the duration of the experiment. As a sample undergoes a transition, the heat required to maintain the sample and reference cells at the same temperature will change. For proteins, the enthalpy (ΔH) of unfolding due to temperature denaturation is measured in conjunction with the thermal transition midpoint (T_m) and the change in the heat

capacity of denaturation (ΔC_P). T_m is the temperature at which 50 % of the molecule remains in its native state and 50 % is denatured. ΔC_P is the change in heat capacity between the native and unfolded state(s) of the molecule. Higher values for T_m and ΔH are generally suggestive of higher protein stability. DSC can be used for high throughput analysis of potential formulations to investigate the thermal stability of proteins in different solutions.

In this scenario, DSC has been used to study the unfolding of the monoclonal IgG1 immunoglobulin Rituximab. It was found to have three transitions during the unfolding process. As can be seen from Figure 2-4 the T_m values for the three transitions are approximately 71, 74 and 83 °C with the steps being assigned to the unfolding of the C_H2 domain, the F_{ab} region and the C_H3 domain respectively (Andersen et al., 2010).

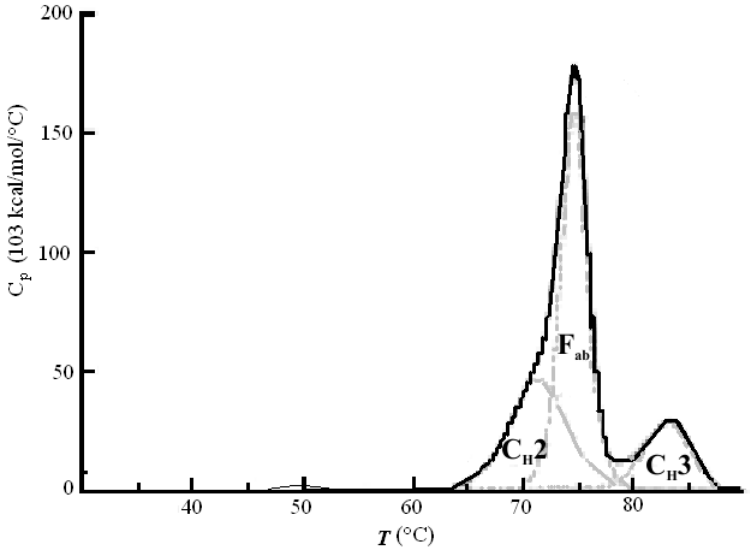

Figure 2-4. Three stage unfolding of the monoclonal IgG1 immunoglobulin Rituximab. The unfolding curve produced using differential scanning calorimetry (DSC) is shown by the solid (black) line with the dashed (grey) lines indicating the domain unfolding involved (Andersen et al., 2010).

The effect of surfactant inclusion in protein formulations on T_m has been studied using DSC. Bam *et al.,* (1998) found that the melting transition of rhGH decreased from 79.2 °C to approximately 77 °C in the presence of Tween 20, 40 and 80 (Bam et al., 1998). The melting temperature of the tobacco mosaic virus is also decreased by surfactant inclusion. In this case, Triton X-100 at 460 x 10^{-6} M decreased the melting temperature from 40.4 to 37.5 °C (Panyukov et al., 2008). The presence of Tween 20 and Tween 80 have been found to have little effect upon the heat capacity curves of a recombinant human immunoglobulin IgG (Hoffmann et al., 2009a). On the other hand, the thermal stability of BSA (which is known to interact with Tween 20 and 80 increased by 1.4 K in the presence of Tween at 2 mM (Hoffmann et al., 2009a).

2.1.3 Liquid-state Circular Dichroism

In circular dichroism (CD), circularly polarised light is used to investigate the structure of molecules such as proteins in solution. CD spectra are generated as a result of chromophores (the component of a molecule which confers colour) absorbing the left and right circularly polarised radiation to a different degree (Figure 2-5). The level of this absorption of the left and right components is dependent on the chirality of the chromophore. The sample will absorb a quantity of the light from both fields which are combined to produce a CD spectrum. This differential absorption is measured as a function of wavelength.

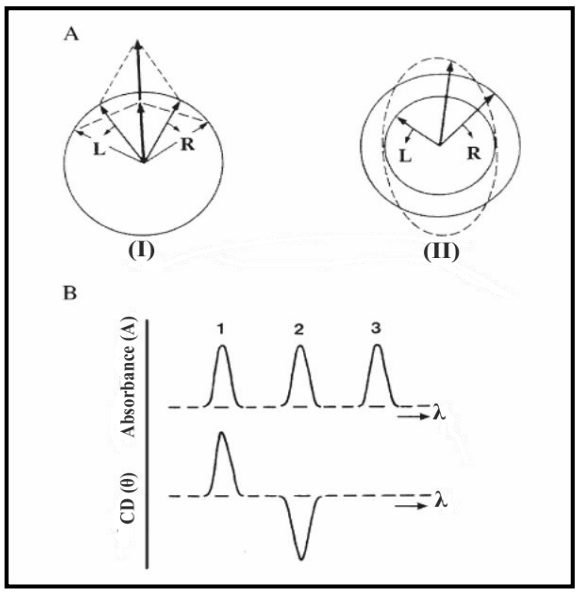

Figure 2-5. **(A)**: Plane polarised radiation comprises left and right circularly polarised components. **(I)**: both left and right components are of equal amplitude, and plane polarised radiation is generated when they are combined. **(II)**: both components have different magnitudes, and produces elliptically polarised radiation. **(B)**: Showing the relationship existing between absorption and CD spectra. Band 1 shows a positive CD spectrum, with greater absorption in the L field compared to R; band 2 demonstrates a negative CD spectrum with greater R absorption than L; band 3 arises from an achiral chromophore (Kelly et al., 2005).

Protein CD spectra can be measured in both the far and near UV regions, 180-260 nm and 260-320 nm respectively. The CD spectrum in the far UV region can show the main secondary structural features of the protein, for example α-helices and β-sheets as shown in (Figure 2-6). However, it should be noted that the spectrum is produced by the whole molecule and therefore does not indicate structural type in specific regions of the protein. The spectrum in the near UV region gives information on the environment (this refers to the degree of hydrogen bonding, polarity, dipole-dipole interactions and their potential to become polarised) within which the aromatic amino acid side chains and disulphide bonds exist and also the protein's tertiary structure (Kelly and Price, 2000).

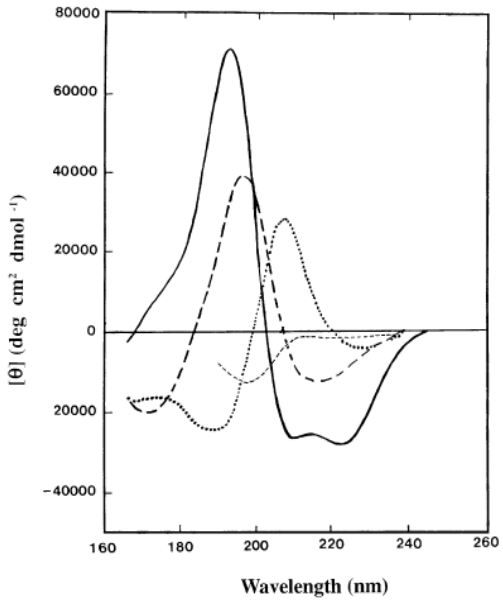

Figure 2-6. Far UV (160 to 250 nm) CD spectra associated with the different types of protein secondary structure. Solid line indicates α-helix; long dashed line indicates an anti-parallel β-sheet; dotted line indicates a type I β-turn; short dashed line indicates an irregular structure (Adapted from Kelly et al. 2005 (Kelly et al., 2005)).

2.2 Materials

L-Histidine, L-Histidine monohydrochloride monohydrate, D-(+)-Trehalose dehydrate, polysorbate 20 (Tween 20), polysorbate 80 (Tween 80), bovine serum albumin (BSA), sodium chloride, potassium chloride, and potassium phosphate monobasic were purchased from Sigma Aldrich (UK). Sodium phosphate monobasic was obtained from Melford Laboratories Ltd (UK). Water was purified to > 14 MΩ.cm with a BioSelect, Purite, UK. Pluronic L43, Pluronic L61, Pluronic P103 and Pluronic P123 were a generous gift from BASF (UK). The immunoglobulin (mAb-1) was kindly provided by MedImmune Ltd, Cambridge, UK.

2.3 Methods

2.3.1 Isothermal Titration Calorimetry

Prior to ITC analysis, the two proteins investigated, mAb-1 and BSA, were dialysed using a Slide-a-Lyzer® dialysis cassette 10,000 Dalton MWCO (Pierce, Thermo Scientific, UK) overnight in 10 mM phosphate buffer pH 7.4. BSA was used as a reference protein as it is known to interact with Tween 20 and Tween 80 (Hoffmann et al., 2009) and so was selected as a comparison for the enthalpogram of surfactant titration into mAb-1 solution. To ensure an exact buffer match the dialysed buffer was then used to prepare the Tween 20, Tween 80, Pluronic P103, Pluronic P123, Pluronic L43 and Pluronic L61 solutions. The structures of Tween 20 and 80 are shown in Figure 1-6. The structures of the Pluronic surfactants selected and their properties are displayed in Figure 1-7 and Table 2-1.

A VP-ITC from MicroCal™ Inc. (MicroCal, Buckinghamshire, UK) was used to carry out the calorimetric titration experiments. The titration experiments were undertaken at 25 °C. Prior to each experiment, the reaction cell and syringe were washed with 10 % Decon 90 followed by distilled water and finally 10 mM phosphate buffer. The reference cell was filled with degassed buffer. The reaction cell (volume 1.4 mL) was filled with the protein solution at a concentration of 14.4 mg/mL (0.24 mM) for both BSA and mAb-1. The injection syringe, with a volume of 300 µL, was filled with surfactant solution in 10 mM phosphate buffer.

The time delay prior to the first injection was 60 s. The reference power was set to 10 µcal/s and the filter to 2 s. Each titration experiment consisted of one injection of 1 µL followed by 25 injections with a volume of 10 µL. An injection speed of 0.5 µL/s

was used for all injections with a spacing of 300 s in between them. The time spacing between injections was set to a duration sufficient to allow the heat signal to return to the baseline. The paddle at the tip of the syringe was rotated at 300 rpm throughout the experiments. Control (blank) experiments of surfactant into buffer were undertaken in order to negate any contribution from the surfactant titration alone to the enthalpograms. Titration experiments of surfactant into protein solution and control experiments of surfactant into buffer were carried out using the parameters above.

The titration curves were analysed using the ORIGIN® MicroCal™ LLC ITC software supplied with the calorimeter instrument. Data for the control titration experiments of surfactant into buffer were subtracted from the titration of surfactant into protein solution data prior to fitting of the binding model. A one-site binding model was used to fit the data. The first injection, of 1 µL, was discarded from the data analysis as its only function was to ensure that the subsequent injection volumes were accurate by expelling any air present in the syringe.

Pluronic	**PEO:PPO:PEO**	**CMC (M)**
P103	17:60:17	6.1×10^{-6}
P123	20:70:20	4.4×10^{-6}
L43	6:22:6	2.2×10^{-3}
L61	3:30:3	1.1×10^{-4}

Table 2-1. Properties of the Pluronic tri-block copolymers selected (Kabanov et al., 2002).

2.3.2 Differential scanning calorimetry

DSC experiments to investigate the effect of surfactant inclusion on mAb-1 stability during thermal denaturation were carried out using a VP-DSC Differential Scanning Calorimeter (MicroCal, Buckinghamshire, UK) with assistance from Sarah Grasso at

MedImmune Ltd, Cambridge. The surfactants investigated using ITC were also studied with respect to their effect on mAb-1 thermal stability: Tween 20, Tween 80, Pluronic P103, Pluronic P123, Pluronic L43, and Pluronic L61. The concentration of mAb-1 used was 5 mg/mL with the solution containing surfactant at a concentration above or below its CMC/CAC (critical aggregation concentration) as shown in Table 2-2. The calorimetric traces were obtained from 25 to 100 °C with a scan rate of 95 °C per hour. A sample volume of 500 µL was used. Each sample was set up as a pair, one well containing mAb-1 plus surfactant (sample capillary) and one containing surfactant in buffer. The corresponding reference scan was subtracted from the sample scan to obtain the thermodynamic values for mAb-1 in each surfactant solution. The ΔH of unfolding, T_m and ΔCp were determined using the in-built Origin® software. Due to the DSC equipment being located off-site and the accuracy of the technique a single sample run was carried out for each surfactant and concentration.

Surfactant	**Concentration below CMC/CAC (mM)**	**Concentration above CMC/CAC (mM)**
Tween 20	0.05	1
Tween 80	0.005	1
Pluronic P103	0.005	1
Pluronic P123	0.001	0.1
Pluronic L43	1	5
Pluronic L61	0.05	0.5

Table 2-2. Concentrations of the surfactants used in the DSC experiments below and above their CMC/CAC.

2.3.3 Liquid-state Circular Dichroism

An Applied Photophysics Chirascan CD spectrometer (Applied Photophysics Ltd, Leatherhead, UK) with a static peltier was used to obtain CD spectra of pure mAb-1 and mAb-1 in the presence of surfactant with the aim of investigating possible changes in the secondary structure of the protein after surfactant inclusion. Additionally, the thermal unfolding of mAb-1 and mAb-1 in the presence of surfactant was studied in the far UV region.

2.3.3.1 **MAb-1 secondary and tertiary structure**

A quartz cuvette (Hellma, UK) with 0.02 mm pathlength was used and spectra were acquired at 20 °C with 4 repeat scans. A mAb-1 concentration of 100 μg/mL, a bandwidth of 0.5 nm and a time of 3 s per wavelength were used during the investigation of mAb-1 secondary structure in the far UV (180 to 260 nm). Investigation of mAb-1 tertiary structure in the near UV region (260 to 320 nm) was carried out using a cell pathlength of 1 mm and a concentration of 5 mg/mL. A bandwidth of 0.5 nm and a time of 1 s per point were used during spectra acquisition.

2.3.3.2 Far UV (180-260 nm) temperature ramping

The effect of temperature on mAb-1 secondary structure was investigated in the far UV (180-260 nm) using a quartz cuvette (Hellma, UK) with a 0.2 mm pathlength and an mAb-1 concentration of 100 μg/mL. Spectra were acquired at a temperature range from 20 to 80 °C. The initial temperatures at which spectra were obtained were 20, 40, 50 °C followed by step increases of 2 °C over the temperature range at which unfolding took place (as identified from DSC data) up to 80 °C. The sample was cooled down from 80 to 20 °C and a final spectrum taken to determine the refolding

capability of mAb-1. An equilibration time of 180 seconds was imposed at each temperature before a reading was taken. A 0.2 nm wavelength step was used during recording of the data, with a time of 1 s per point and 4 repeat scans being undertaken at each temperature.

2.3.3.3 Effect of Tween inclusion on mAb-1 structure during temperature ramping

The secondary structure of mAb-1 in the presence of Tween was investigated in the far UV (180-260 nm). A quartz cuvette (Hellma, UK) with a 0.2 mm pathlength was used and a mAb-1 concentration of 100 μg/mL. Spectra on the effect of Tween on thermal stability were acquired from 50 °C to 80 °C with 5 °C increments. All other parameters were as for pure mAb-1. A mAb-1 concentration of 100 μg/mL was used with surfactant concentrations of 0.05 and 1 mM Tween 20 and 5 μM and 1 mM Tween 80.

2.3.4 Dichroweb Analysis

The online CD secondary structure analysis server Dichroweb was used to make a quantitative interpretation of the CD data obtained for mAb-1 in solution (Whitmore and Wallace, 2004). The CONTIN algorithm (van Stokkum et al., 1990) with reference set SP175 (Lees et al., 2006) was used to reconstruct the data sets. The normalised root mean square deviation (nrmsd) with the experimental data was reported, with a value of ≤ 0.2 being within the acceptable range for this 'goodness of fit' parameter (Whitmore and Wallace, 2004).

2.4 Results

2.4.1 Isothermal Titration Calorimetry

ITC was used to investigate the presence or absence of an interaction between the surfactants studied (Tween and Pluronic) and mAb-1 in the bulk solution. The BSA as a reference protein enabled conclusions to be made regarding mAb-1-surfactant interaction, as its binding interaction with Tween has been characterised previously (Ruiz-Pena et al., 2010, Hoffmann et al., 2009b, Hoffmann et al., 2009a).

2.4.1.1 Titration of 1 mM Tween 20/80 into 0.24 mM (14.4 mg/mL) BSA and 14.4 mg/mL mAb-1.

The enthalpograms for the titration of 1 mM Tween 20 and 80 into phosphate buffer are shown in Figure 2-7 and Figure 2-8 to demonstrate the change in enthalpy upon each injection. These values were subtracted from the titration of Tween 20/80 in to the protein solutions.

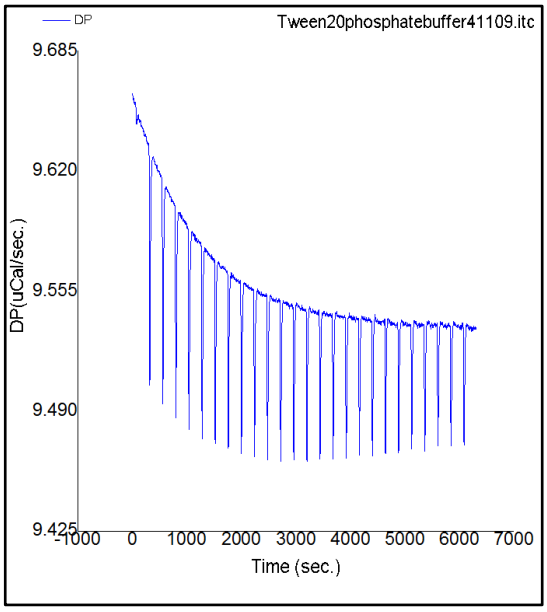

Figure 2-7. Enthalpogram of the titration of 1 mM Tween 20 into Phosphate buffer.

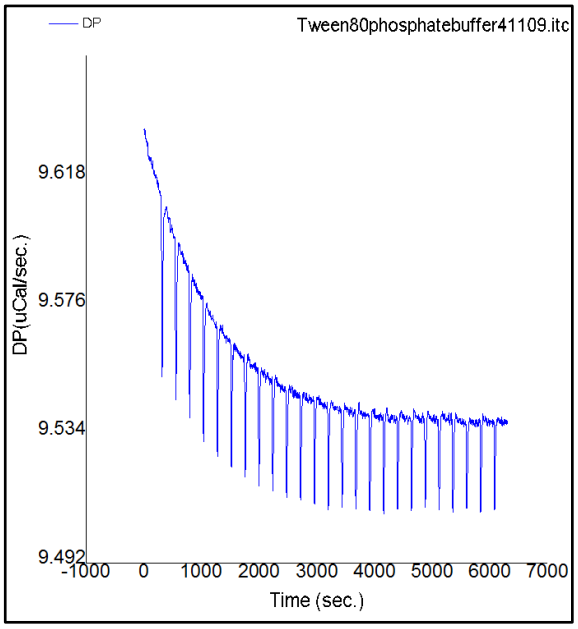

Figure 2-8. Enthalpogram of the titration of 10 mM Tween 80 into Phosphate buffer.

The enthalpogram, Figure 2-9, for the titration of 1 mM Tween 20 into 0.24 mM (14.4 mg/mL) BSA indicates an exothermic event takes place upon injection of Tween 20. The amplitude of the exothermic peak decreased with increasing Tween 20 concentration in the sample cell which is consistent with the binding sites on the BSA becoming saturated. Tween 20 was found to bind to BSA in a manner fitting a one binding site model after analysis of the enthalpogram using ORIGIN® MicroCal™ ITC LLC.

An exothermic event also occurred after each injection of 10 mM Tween 80 into a 0.24 mM BSA solution (Figure 2-10). Analysis of the titration of Tween 80 into BSA resulted in the fitting of the data to a one binding site model as for Tween 20. The thermodynamic parameters of the interaction between BSA and Tween 20 and 80 calculated from the fitting of the ITC data are shown in Table 2-3. The K_a for Tween 20 and Tween 80 into BSA were (4.02 ± 0.565) x 10^3 M and (1.32 ± 78.9) x 10^2 M respectively. The concentration of Tween 80 used in the ITC experiment was ten

times higher than that of Tween 20, however, this difference was necessary in order to obtain a decrease in the exothermic peaks and saturation of the BSA binding sites as observed for Tween 20.

Parameter	**BSA-Tween 20**	**BSA-Tween 80**
Binding constant (K_a)	$4.02 \pm 565 \times 10^3$ M	$1.32 \pm 78.9 \times 10^2$ M
Enthalpy (ΔH) (J)	$-3.272 \pm 121.4 \times 10^4$	$-2.436 \pm 3652 \times 10^3$
Entropy (ΔS) (J/K)	-88.6	-67.4

Table 2-3. Thermodynamic parameters determined using ITC for the interaction between bovine serum albumin (BSA) and Tween 20 and Tween 80.

Titration experiments of Tween 20 and 80, using the same concentrations as for BSA, into a 14.4 mg/mL mAb-1 were undertaken to determine if a specific binding event took place between mAb-1 and Tween. It is evident from the enthalpograms that neither Tween 20 nor Tween 80 bound in a specific manner to mAb-1 when compared to the enthalpograms obtained for BSA under the same conditions (Figure 2-9 and Figure 2-10).

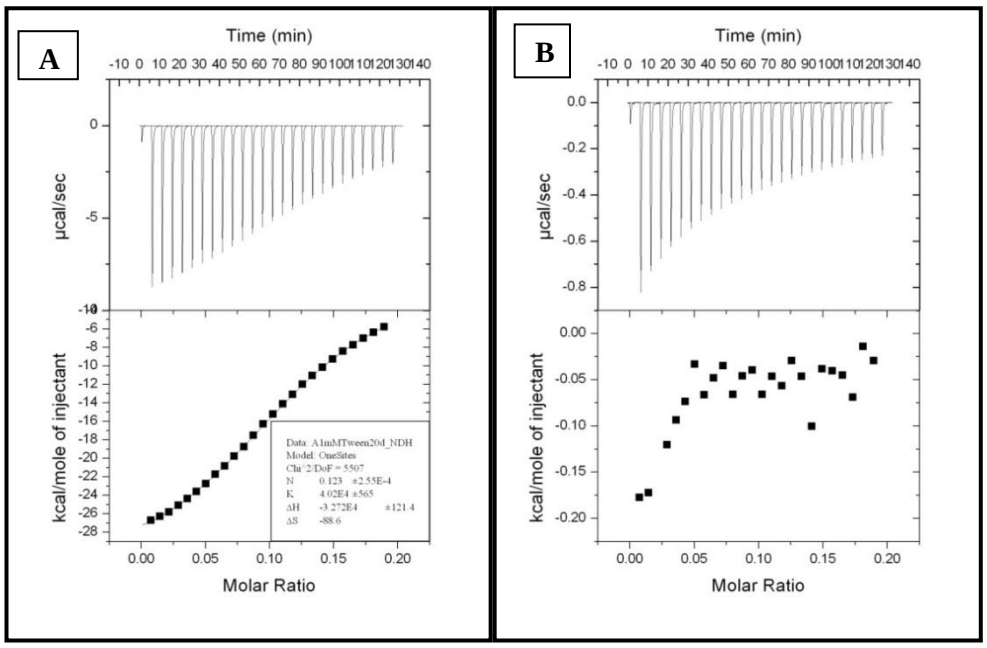

Figure 2-9. Enthalpograms for the titration of (A) 1 mM Tween 20 into 0.24 mM (14.4 mg/mL) bovine serum albumin (BSA) and (B) 1 mM Tween 20 into 14.4 mg/mL mAb-1.

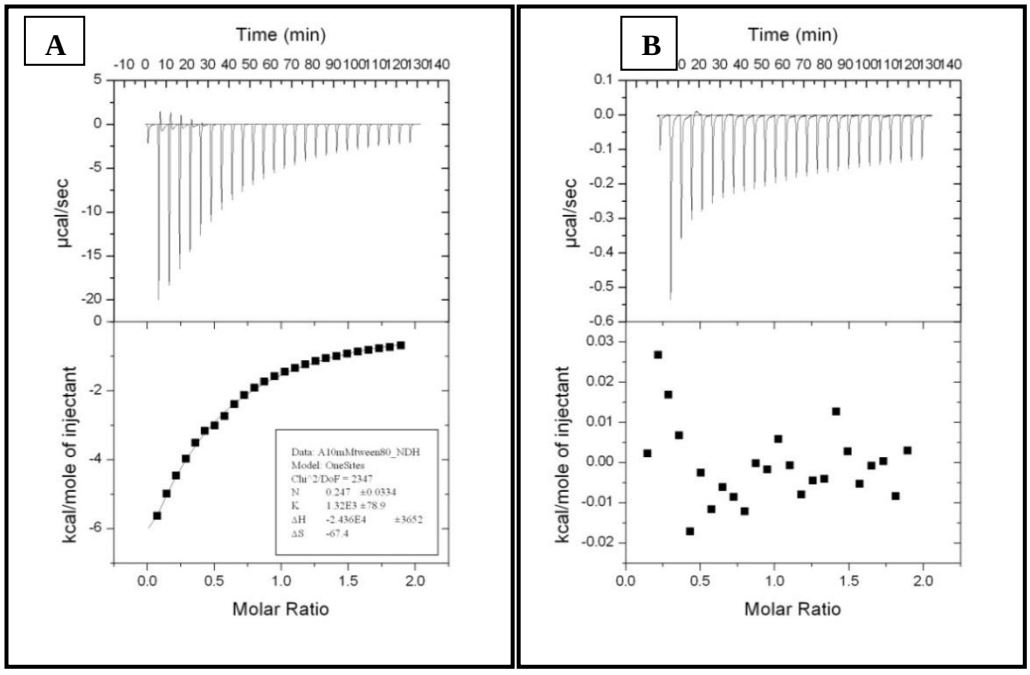

Figure 2-10. Enthalpograms for the titration of (A) 10 mM Tween 80 into 0.24 mM (14.4 mg/mL) bovine serum albumin (BSA) and (B) 10 mM Tween 80 into 14.4 mg/mL mAb-1.

Tween 20 and 80 are non-ionic surfactants and so it was important to investigate if an interaction took place between mAb-1 and an alternative class of surfactants. To investigate this, four triblock copolymers were selected which were Pluronic P103, P123, L43 and L61. These Pluronics were chosen based on specific properties determined from BASF data sheets avoiding those which foamed, formed a gel and were not soluble in water.

2.4.1.2 Titration of Pluronic P123 into 0.24 mM (14.4 mg/mL) BSA

The titration of 0.1 mM and 1 mM Pluronic P123 into 0.24 mM (14.4 mg/mL) BSA was carried out using the same parameters as for the titration of Tween 20 and 80 (2.3.1). A typical example of the titration of Pluronic into phosphate buffer is shown in Figure 2-11 for 0.1 mM Pluronic P123. The events upon each injection are representative of those observed for Pluronic P103, L43 and L61.

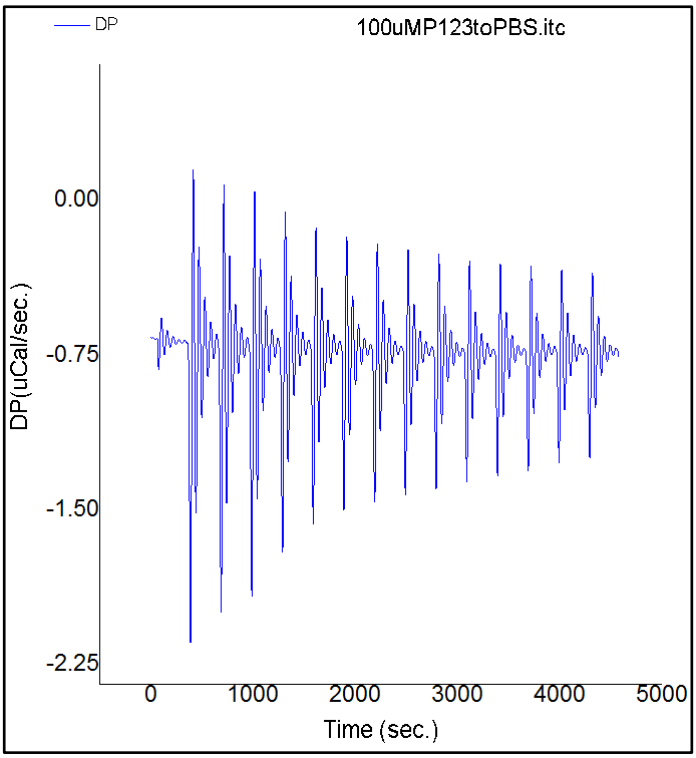

Figure 2-11. Titration of 0.1 mM Pluronic P123 into Phosphate buffer.

The events that took place upon titration of 0.1 mM or 1 mM Pluronic P123 into a 0.24 mM (14.4 mg/mL) BSA solution differed from those observed during the titration of Tween 20 and 80. The enthalpogram for the titration of 0.1 mM Pluronic P123 (Figure 2-12) into the BSA solution showed multiple endothermic and exothermic peaks occurred after each injection which decreased in amplitude. As the injection number increased, the size of the endothermic and exothermic (1.5.1) peaks decreased but the number of events which took place after each individual injection was not affected. The multiple events which occurred were in contrast to the single endothermic and exothermic event after each injection of Tween 20/80 into the BSA solution. The multiple events indicate that the interaction between BSA and the Pluronic occurs in a more complex manner than that observed for either Tween 20 or 80.

A specific binding model for this interaction was not determined after analysis of these data using ORIGIN® MicroCal LLC, ITC contrary to the one site binding model identified for the interaction between BSA and both Tween 20 and 80.

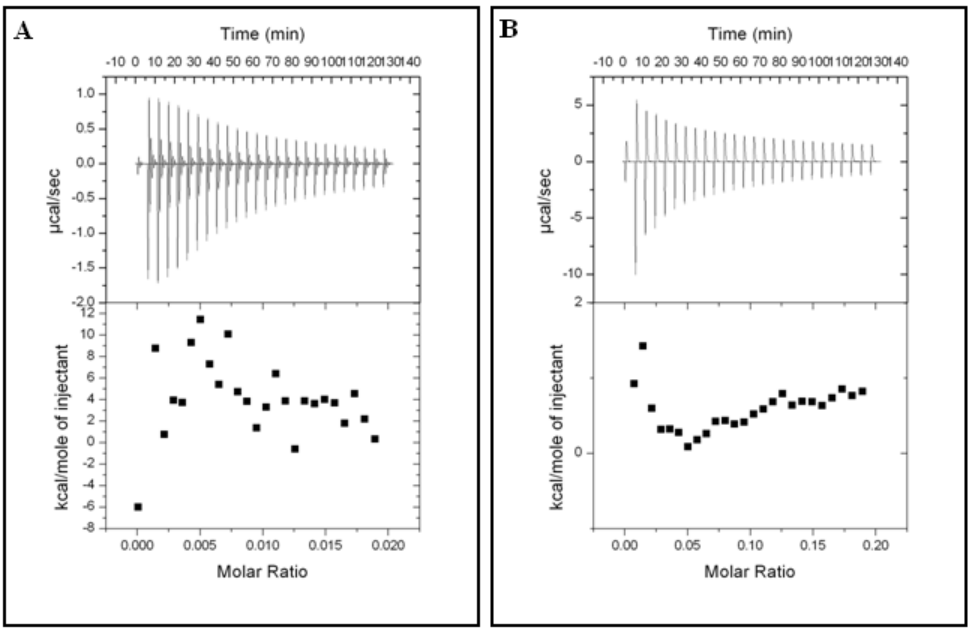

Figure 2-12. Enthalpograms showing the titration of Pluronic P123 into 0.24 mM (14.4 mg/mL) Bovine Serum Albumin (BSA): **(A)** 0.1 mM and; **(B)** 1 mM.

2.4.1.3 Titration of Pluronic P123, Pluronic P103, Pluronic L43 and Pluronic L61 into 14.4 mg/mL mAb-1.

The existence of an interaction between the Pluronic tri-block co-polymers and mAb-1 was investigated using an mAb-1 concentration of 14.4 mg/mL and Pluronic concentrations of 10 mM for P103 and 1 mM for the remaining 3 investigated - P123, L43 and L61.

Titration of 1 mM Pluronic P123 into a 14.4 mg/mL mAb-1 solution resulted in a single endothermic and exothermic peak. The amplitude of each event decreased as the concentration of Pluronic P123 in the sample cell increased (Figure 2-13).

The titration of 10 mM Pluronic P103 into mAb-1 solution resulted in the occurrence of both endothermic and exothermic events after each injection as observed for the

titration of Pluronic P123. The size of the peaks decreased as the concentration of Pluronic P103 increased in the sample cell (Figure 2-13).

The titration of the two remaining Pluronics, L43 and L61, led to a single exothermic event taking place upon their injection into mAb-1 solution, Figure 2-14. However, the baseline was particularly noisy for Pluronic L61 indicating a large degree of fluctuation in the electrical current required to maintain a constant temperature in the reference cell.

Analysis of the enthalpograms did not show a specific binding interaction to take place between mAb-1 and the four Pluronics under study - Figure 2-13 and Figure 2-14.

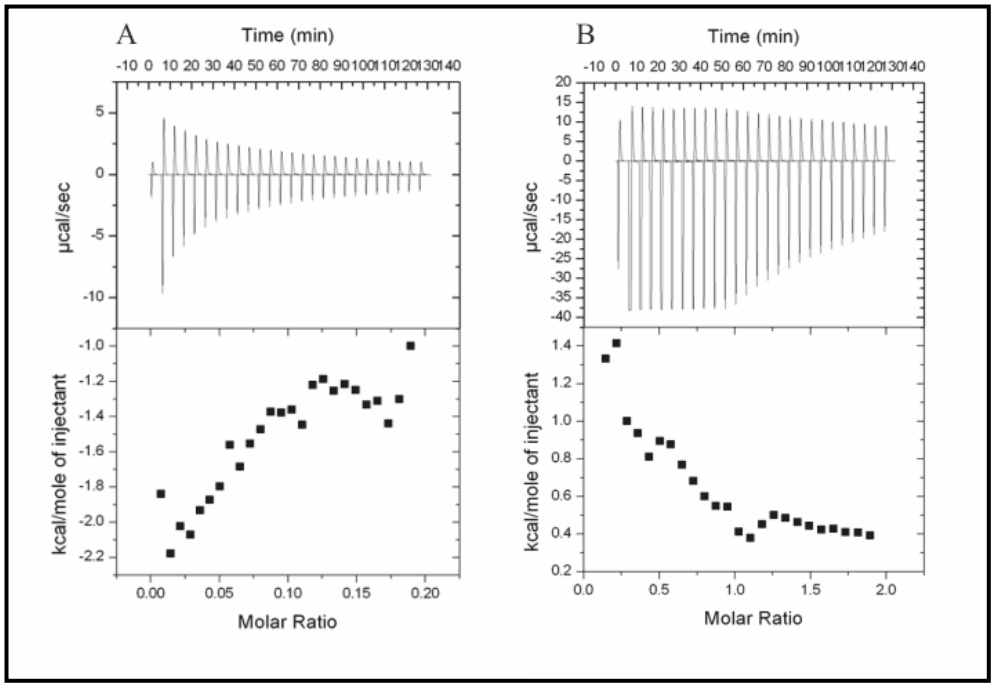

Figure 2-13. Enthalpograms for the titration of Pluronic into 14.4 mg/mL mAb-1: **(A)** Pluronic P123; and **(B)** Pluronic P103.

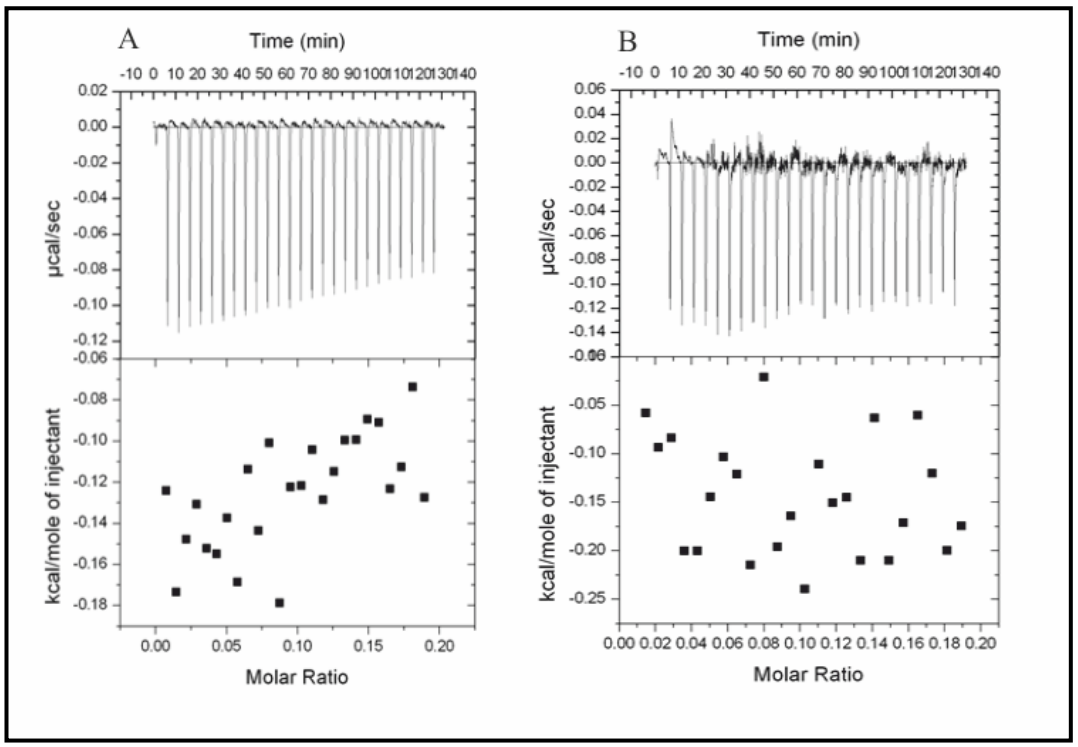

Figure 2-14. Enthalpograms for the titration of Pluronic into 14.4 mg/mL mAb-1: **(A)** Pluronic L43; and **(B)** Pluronic L61.

2.4.2 Differential Scanning Calorimetry

Using DSC, the temperature at which each mAb-1 domain unfolded was identified and the effect of surfactant inclusion at concentrations below and above their CMC/CAC investigated. The unfolding of mAb-1 was identified as being a three step process with thermal transition midpoints of 67.2, 71.2 and 76.1 °C (Figure 2-15 and Table 2-4). The inclusion of surfactant in the protein solution did not affect mAb-1 unfolding steps regardless of surfactant class or concentration as shown in Table 2-4. The thermograms for each surfactant are shown in Appendix A Figure 8-1 to Figure 8-6.

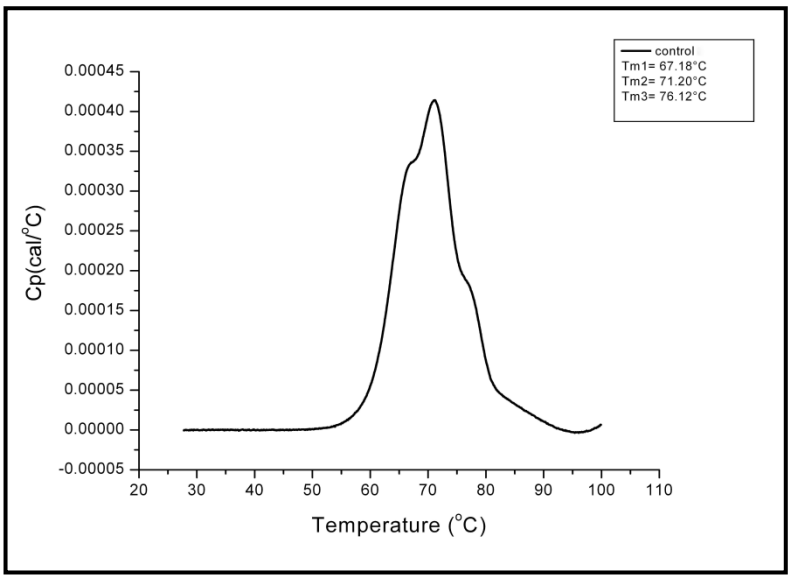

Figure 2-15. Thermogram of mAb-1 control solution (histidine buffer, pH 5.5 containing no surfactant).

[Surfactant]	T_m1 (°C)	T_m2 (°C)	T_m3 (°C)
No surfactant	67.2	71.2	76.1
0.05 mM Tween 20	67.1	71.0	76.2
1 mM Tween 20	67.2	70.8	76.1
5 µM Tween 80	67.3	71.1	76.3
1 mM Tween 80	67.4	71.0	75.6
5 µM Pluronic P103	67.4	71.1	76.1
1 mM Pluronic P103	67.4	71.0	76.0
1 µM Pluronic P123	67.1	71.1	76.1
0.1 mM Pluronic P123	67.5	71.1	76.2
1 mM Pluronic L43	67.4	71.0	75.6
5 mM Pluronic L43	66.9	70.7	75.8
0.05 mM Pluronic L61	67.4	71.0	76.1
0.5 mM Pluronic L61	67.2	71.1	76.2

Table 2-4. Differential scanning calorimetry (DSC) data for the thermal denaturation of mAb-1 in the presence of surfactant at a concentration above and below the critical micelle concentration (CMC).

2.4.3 Liquid-state Circular Dichroism

CD was used to determine the secondary structure of mAb-1 in solution and to establish the effect of thermal denaturation and surfactant inclusion on the native structure. CD complements the DSC data through generation of spectra demonstrating changes in the secondary structure as a result of unfolding. DSC produces a numerical value demonstrating the effect of surfactant on thermal stability whereas CD generates spectra which show any changes in native structure which occur as a result of surfactant presence. In addition, any differences in unfolding due to thermal denaturation spectra as a result of surfactant inclusion would be observed.

2.4.3.1 Far (180-260 nm) and Near UV (260-320 nm) CD spectra of mAb-1 in low salt buffer

The far UV (180-260 nm) spectrum indicated that mAb-1 indicated contains a large proportion of β-sheet as characterised by a positive maximum at c.a. 200 nm and a negative maximum at 218 nm (Figure 2-16).

The near UV (260-320 nm) spectrum of mAb-1, which provides information regarding the tertiary structure, showed a strong contribution from tryptophan residues as indicated by the peak at approximately 290 nm with some contribution from disulphides (the peak at 265 nm) (Figure 2-18).

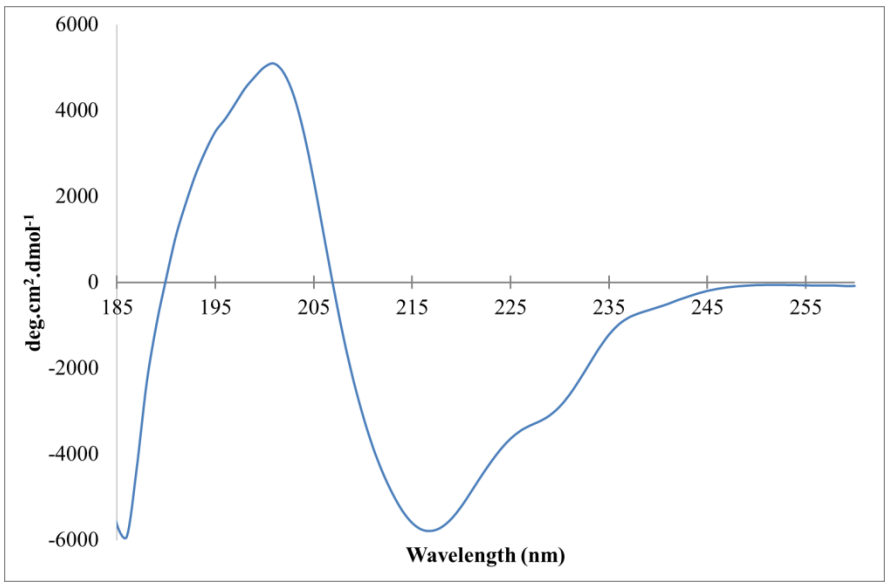

Figure 2-16. Far UV (180 to 260 nm) spectra of mAb-1 in solution at a concentration of 100 µg/mL using a 0.2 mm cell pathlength and a bandwidth of 0.5 nm.

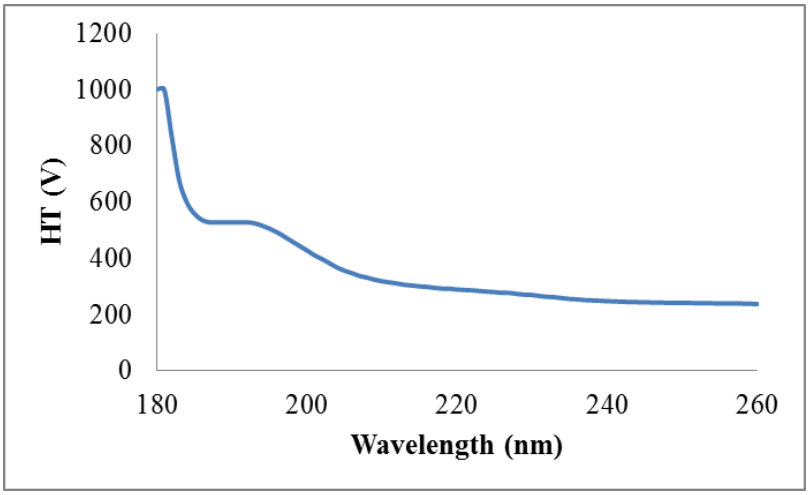

Figure 2-17. High tension (HT) signal for the far UV (180 to 260 nm) spectra of mAb-1 in solution at a concentration of 100 µg/mL using a 0.2 mm cell pathlength and a bandwidth of 0.5 nm.

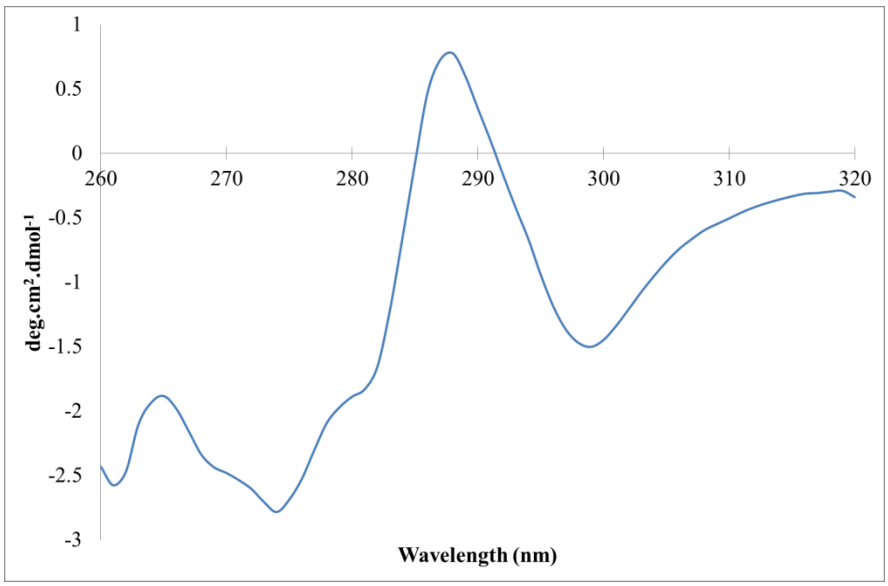

Figure 2-18. Near UV (260 to 320 nm) spectra of mAb-1 in solution at a concentration of 5 mg/mL using a 1 mm cell pathlength and a bandwidth of 0.5 nm.

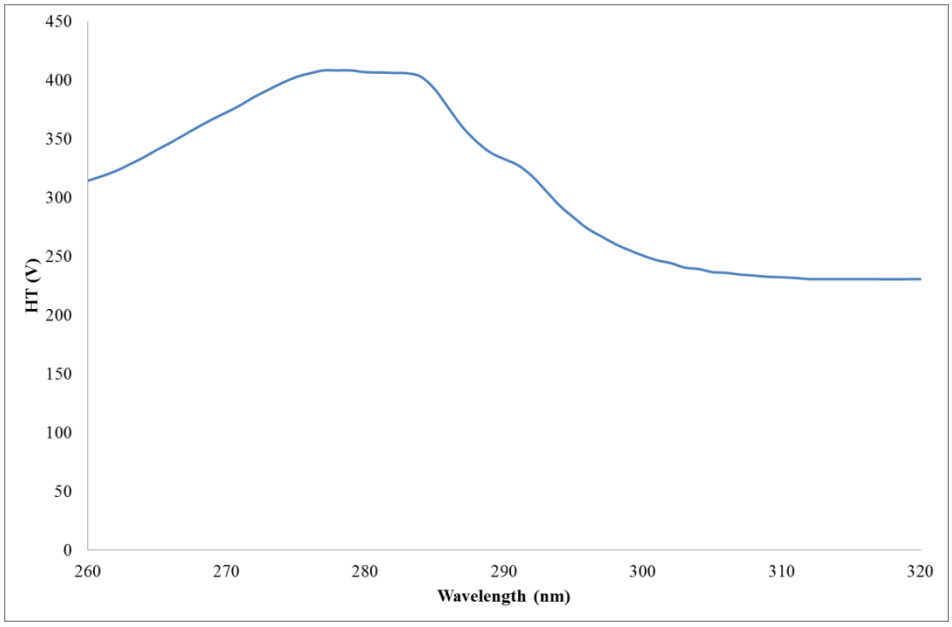

Figure 2-19. High tension (HT) near UV (260 to 320 nm) signal of mAb-1 in solution at a concentration of 5 mg/mL using a 1 mm cell pathlength and a bandwidth of 0.5 nm.

2.4.3.2 Far (180-260 nm) UV CD spectra of mAb-1 in low salt buffer containing surfactant

Figure 2-20 showed that the β-sheet structure of mAb-1 remained in the presence of Tween 20 and 80 below the CMC. However, the contribution to the native spectrum is weaker as evidenced by the decreased peak and trough ellipticity values. There is an apparent perturbation in mAb-1 structure below 205 nm in the presence of Tween 20 below its CMC. Above the CMC of Tween 20 and 80 a transition to negative ellipticity occurred which indicates a change in structure (Figure 2-21). The four Pluronic surfactants were also co-dissolved with mAb-1 in solution to study their effect on secondary structure. The CD spectra in Figure 2-22 to Figure 2-25 show that the β-sheet structure of mAb-1 remained except of in the presence of Pluronic L61 in which a loss of structure was evident. As was the situation with Tween 20 and 80, the contribution of β-sheet to the ellipticity values was decreased.

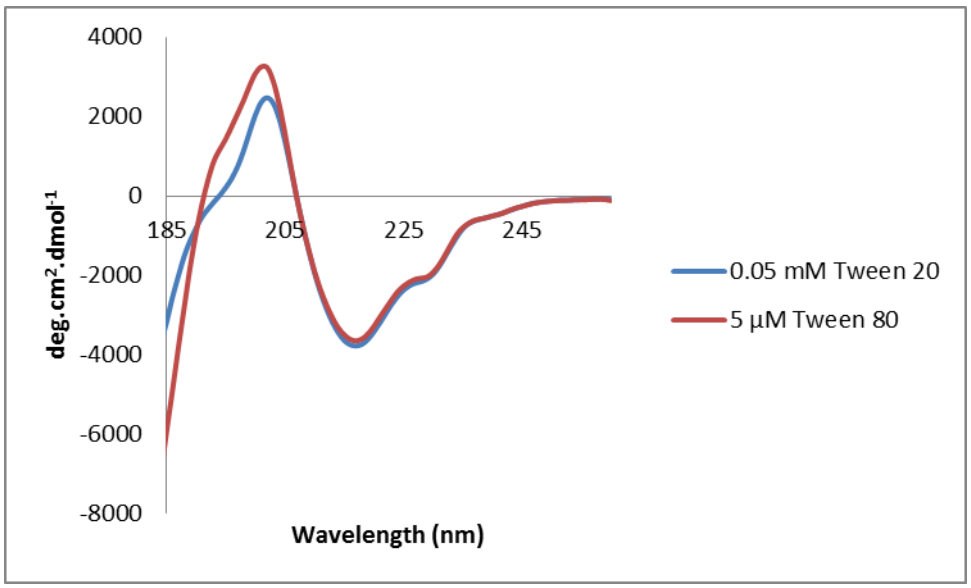

Figure 2-20. Addition of both Tween 20 and 80 below their CMC to a solution of mAb-1 did not affect its secondary structure. A cell pathlength of 0.2 mm was used together with a mAb-1 concentration of 100 µg/mL and a bandwidth of 0.5 nm.

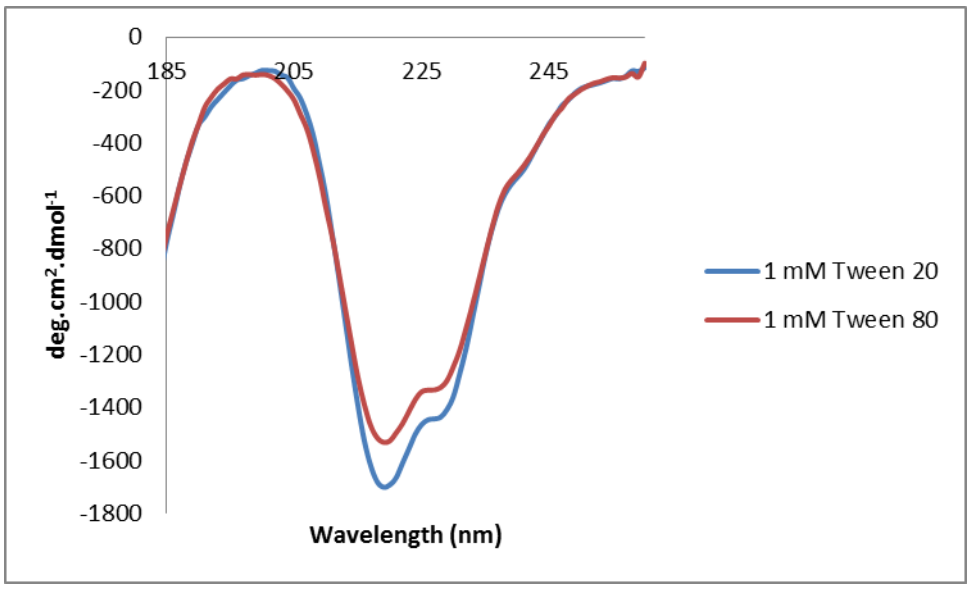

Figure 2-21. Addition of Tween 20 and 80 above their CMC to a solution of mAb-1 resulted in the ellipticity becoming negative. A cell pathlength of 0.2 mm was used together with an mAb-1 concentration of 100 µg/mL and a bandwidth of 0.5 nm.

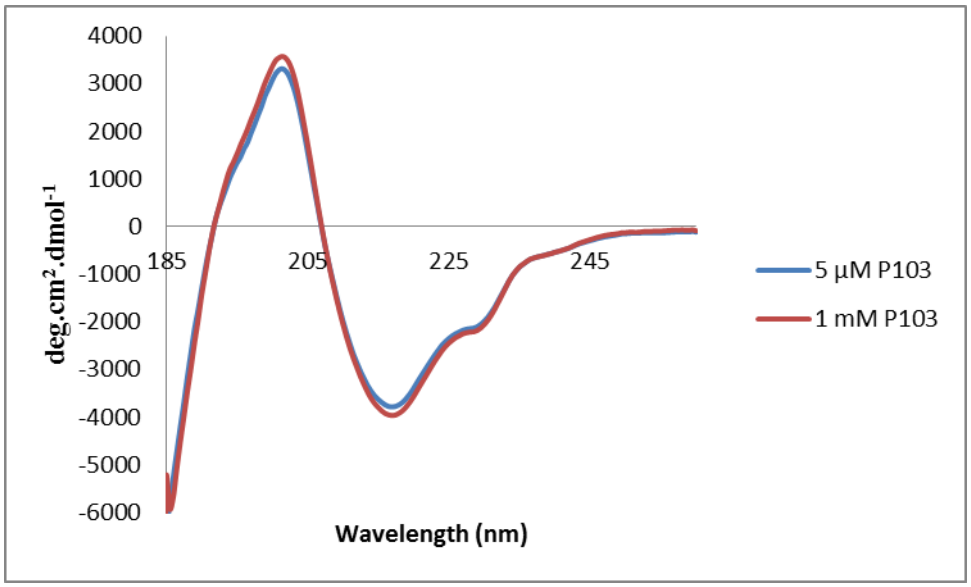

Figure 2-22. Addition of Pluronic P103 does not affect the secondary structure of mAb-1. A cell pathlength of 0.2 mm was used together with an mAb-1 concentration of 100 µg/mL and a bandwidth of 0.5 nm.

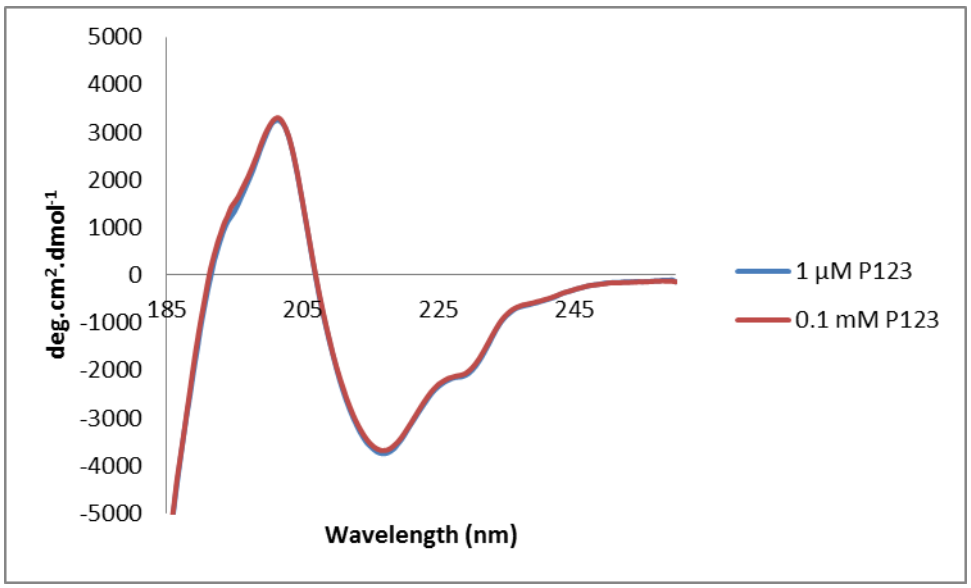

Figure 2-23. Addition of Pluronic P123 does not affect the secondary structure of mAb-1. A cell pathlength of 0.2 mm was used together with an mAb-1 concentration of 100 µg/mL and a bandwidth of 0.5 nm.

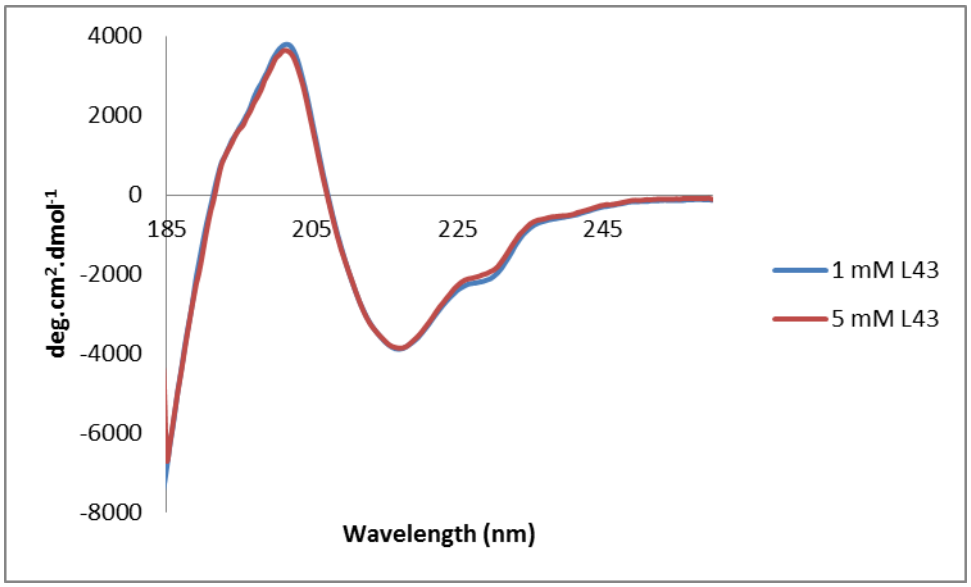

Figure 2-24. Addition of Pluronic L43 does not affect the secondary structure of mAb-1. A cell pathlength of 0.2 mm was used together with an mAb-1 concentration of 100 µg/mL and a bandwidth of 0.5 nm.

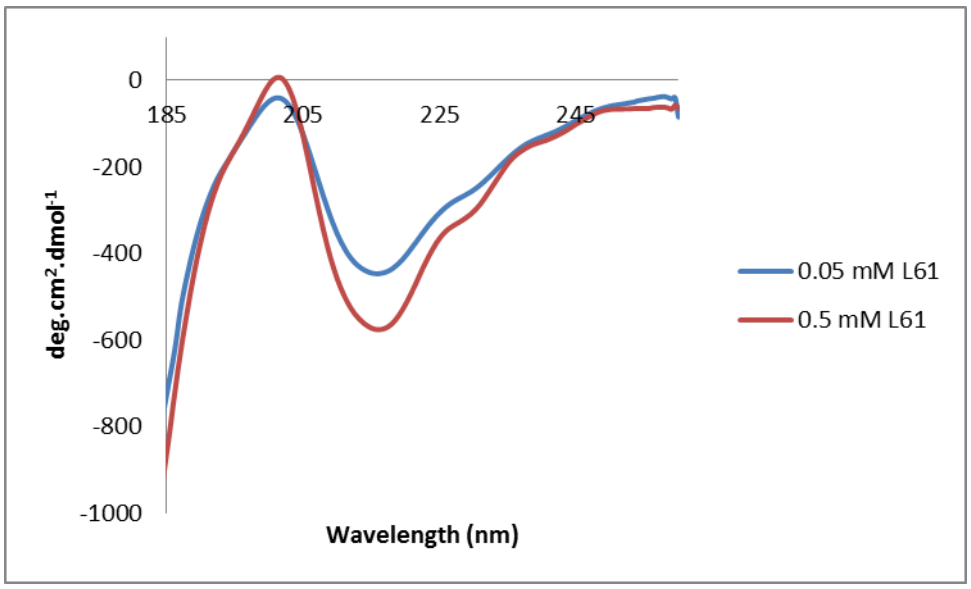

Figure 2-25. Addition of Pluronic L61 led to a loss of mAb-1secondary structure of mAb-1. A cell pathlength of 0.2 mm was used together with mAb-1 concentration of 100 µg/mL and a bandwidth of 0.5 nm.

2.4.3.3 Effect of temperature on mAb-1 secondary structure in low salt buffer in the absence and presence of surfactant

The next CD experiment carried out was investigation of the thermal denaturation of mAb-1 in aqueous solution (Figure 2-26 and Figure 2-27) and in the presence of Tween (Figure 2-28 to Figure 2-31). The initial study showed mAb-1 peptide backbone to be conformationally stable up to 60 °C in aqueous buffer, above which unfolding took place with no refolding observed upon cooling (Figure 2-26). Further spectra were acquired with smaller temperature increments to obtain a more detailed picture of the thermal unfolding undergone by mAb-1. It is evident from plots of ellipticity at 225 nm against temperature in Figure 2-27 that there is a change in mAb-1 secondary structure above 60 °C indicating that unfolding is taking place. Although an accurate T_m value cannot be determined from the CD spectra, the data show this value to be between 60-65 °C. Figure 2-28 to Figure 2-31 indicate that the

thermal denaturation undergone by mAb-1 in the presence of Tween did not differ from that observed in the absence of surfactant from the solution.

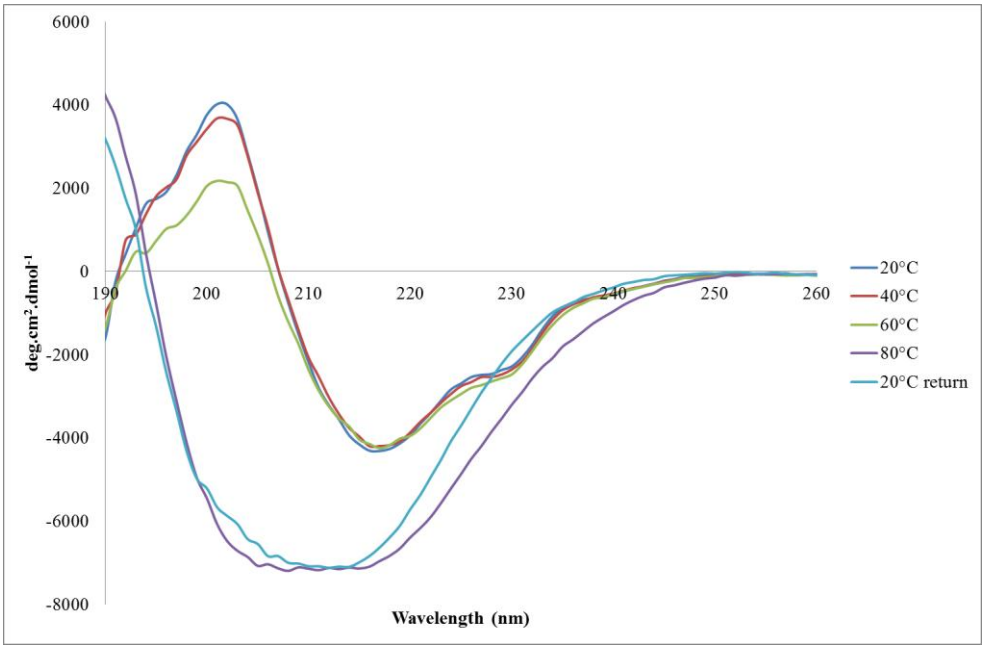

Figure 2-26. MAb-1 peptide backbone is conformationally stable up to 60 °C in aqueous buffer, above which unfolding occurs, without refolding on cooling. A cell pathlength of 0.2 mm, mAb-1 concentration of 100 ug/mL and a bandwidth of 0.5 nm were used during acquisition of the spectra.

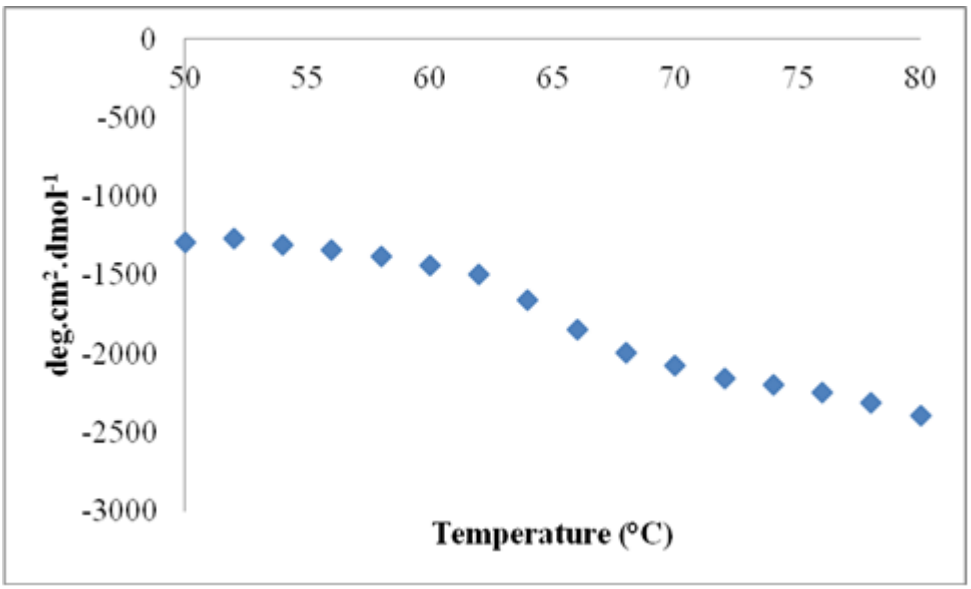

Figure 2-27. Unfolding of mAb-1 at 225 nm observed using circular dichroism. A cell pathlength of 0.2 mm, mAb-1 concentration of 100 ug/mL and a bandwidth of 0.5 nm were used during acquisition of the spectra.

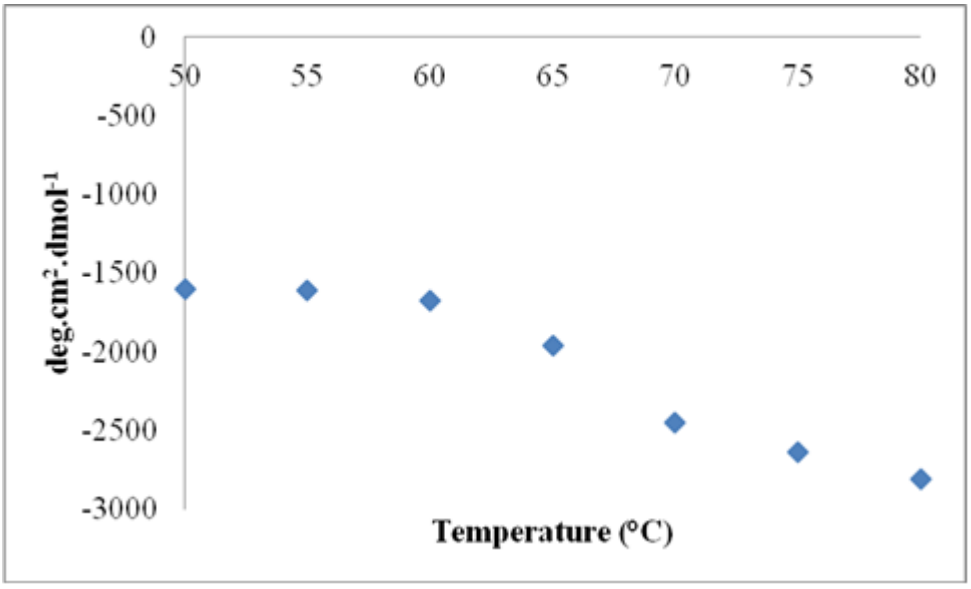

Figure 2-28. Unfolding of mAb-1 at 225 nm observed using circular dichroism in the presence of 0.05 mM Tween 20. During acquisition of the spectra, a cell pathlength of 0.2 mm, mAb-1 concentration of 100 ug/mL and a bandwidth of 0.5 nm were used.

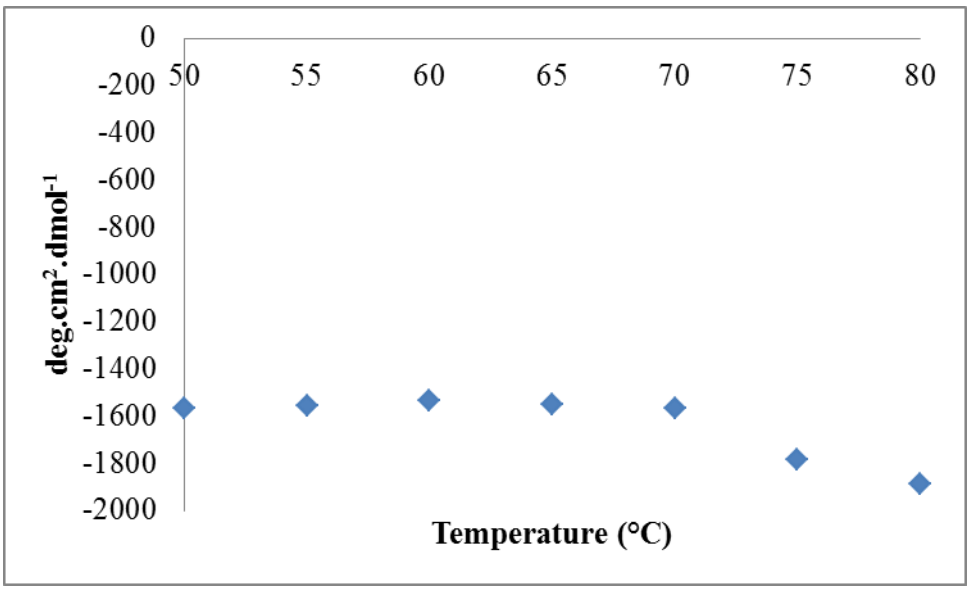

Figure 2-29. Unfolding of mAb-1 at 225 nm observed using circular dichroism in the presence of 1 mM Tween 20. The spectra were obtained using a cell pathlength of 0.2 mm, mAb-1 concentration of 100 ug/mL and a bandwidth of 0.5 nm.

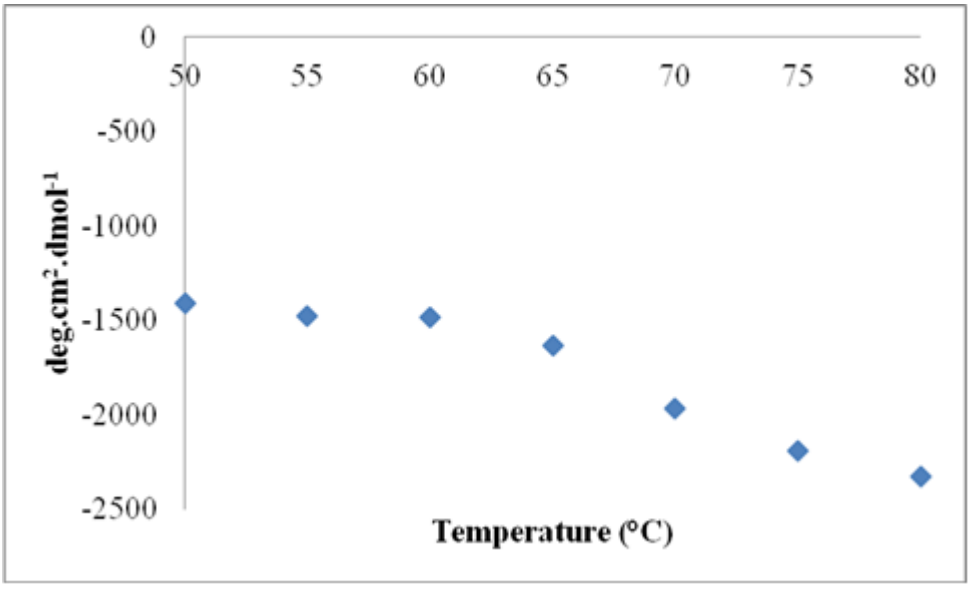

Figure 2-30. Unfolding of mAb-1 at 225 nm observed using circular dichroism in the presence of 5 µM Tween 80. MAb-1 spectra were acquired using a cell pathlength of 0.2 mm, a mAb-1 concentration of 100 ug/mL and a bandwidth of 0.5 nm.

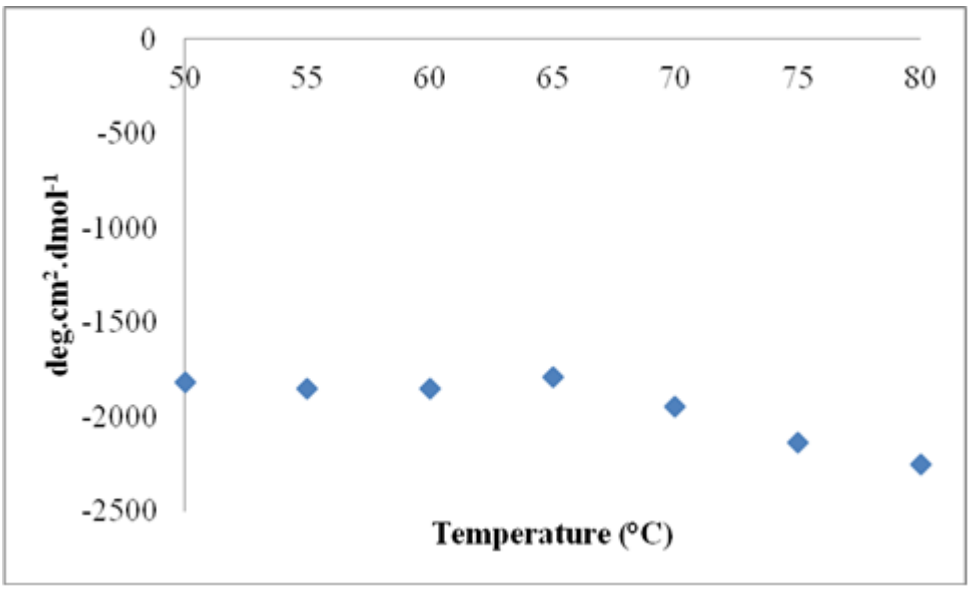

Figure 2-31. Unfolding of mAb-1 at 225 nm observed using circular dichroism in the presence of 1 mM Tween 80. A cell pathlength of 0.2 mm, mAb-1 concentration of 100 ug/mL and a bandwidth of 0.5 nm were used during acquisition of the spectra.

2.4.4 Dichroweb analysis

The Dichroweb analysis of mAb-1 in aqueous solution is consistent with a protein containing a high content of the β-sheet motif. The percentage of β-sheet is 51 % and the data showed that mAb-1 did not contain any α-helices (Table 2-5). However, the Dichroweb database is largely comprised of globular proteins based on α-helices or structures which are composed of an α-helix-β-sheet mixture. As mAb-1 is composed of a β-sheet scaffold the data were therefore compared to a database for different protein types and structures.

	α-helix	β-sheet	β-turn	random coil	nrmsd
MAb-1 in aq. solution	0.00	0.51	0.10	0.37[a]	0.068

Table 2-5. Fraction of secondary structure elements for mAb-1 in solution calculated using the Dichroweb online server. [a]Dichroweb does not necessarily generate a total value of 1.

2.5 Discussion

2.5.1 Tween-protein interaction

It is well known that surfactants can stabilise proteins in solution through a direct interaction with the protein, thereby decreasing the level of aggregation. For example, both Tween 20 and 80 have been found to bind to the HSA component of Albutropin™ and reduce the formation of aggregates (Chou et al., 2005). They have also been shown to increase the stability of HSA as demonstrated by an increase in the thermal denaturation temperature (Chou et al., 2005, Garidel et al., 2009). The two Tween surfactants have also been observed to interact with BSA (Hoffmann et al., 2009a), the binding affinity of Tween 20 for both HSA and BSA was found to be stronger than Tween 80 (Chou et al., 2005, Hoffmann et al., 2009a).

The ITC enthalpograms in this study also identified a binding interaction took place between BSA and both Tween 20 and 80 (Figure 2-9 and Figure 2-10). The affinity of Tween 80 for BSA was less than that observed for Tween 20 as shown by the binding constants of (1.32 ± 78.9) x 10^3 M and (4.02 ±565) x 10^3 M for Tween 80 and 20 respectively displayed in Table 2-3. This difference was also observed by Hoffmann et al., (2009). The interaction identified in this study between BSA and the two Tweens was found to be exothermic with the data fitting well to a one binding site model as observed previously by Hoffmann et al., (2009).

In contrast to the interaction of Tween with albumin proteins the ITC data in this investigation did not show a specific binding event between mAb-1 and either Tween 20 or Tween 80. This has also been found to be the case for the interaction of a recombinant human immunoglobulin IgG and the same two Tween surfactants

studied here (Hoffmann et al., 2009a). The binding of Tween 20 and Tween 80 to three immunoglobulins of the subtypes IgG1, IgG2 and IgG4 has similarly been found to be negligible as shown by binding constants in the region of 10^2 to 10^3 M^{-1} (Garidel et al., 2009). The lack of a specific binding site for Tween on immunoglobulins or the surfactant-surfactant interaction being stronger than protein-surfactant, in which case the formation of surfactant aggregates would be preferred (Bam et al., 1995), could have led to the results in this study and those mentioned.

The interaction between Tween and BSA, as identified in this study, has also been shown through monitoring of 8-anilino-1-naphthalene sulfonic acid (ANS) fluorescence changes. The fluorescent signal produced by ANS is increased when it is present in the hydrophobic region of a protein and fluoresces highly when bound to the hydrophobic patch on BSA (Ruiz-Pena et al., 2010). This fluorescence decreased to a small degree when Tween 20 or 80 below their CMC was included in solution but to a much greater level when the surfactants were present at concentrations well above their CMC (Ruiz-Pena et al., 2010). Surfactant binding would prevent the interaction of the ANS with the hydrophobic patches on the BSA.

2.5.2 Pluronic interaction

As was determined to be the case for Tween 20 and 80, the four Pluronic surfactants selected did not interact with mAb-1 via a specific binding interaction. A specific binding interaction was similarly not observed between Pluronic P123 and BSA. Although a specific binding interaction between mAb-1 and the four Pluronics was not identified, it is possible that a transient interaction could take place. A transient interaction would likely be one in which a weak non-specific interaction between the surfactant and the surface of the protein formed before the interaction was broken

allowing a different surfactant molecule to then interact. Collagen, like mAb-1 and BSA in this study, has been found not to interact with a Pluronic surfactant (PE6800) (De Cupere et al., 2003). In contrast to the findings in this study and that of De Cupere et al., (2003), the Pluronics P84, P103 and F127 have been shown to interact with a different protein (growth hormone releasing peptide-g (GHRP-6) acetate) (Jia et al., 2012).

In contrast to the enthalpograms for Tween 20 and 80, those of the Pluronic solutions showed multiple events occurred during titration indicating a more complex situation than that for the two Tweens. Pluronics form micelle-like aggregates in solution which may be taking place upon titration of the Pluronics into the mAb-1 solution in this study. The micelles formed can be spherical, rod-like or lamellar depending on the length of the PPO and PEO blocks as suggested by Nagarajan (1999). The lengths of these blocks differed between the Pluronics used in this study (Table 2-1) which may be a cause of the differences observed in the ITC enthalpograms. The fluctuation in electrical current required to maintain the two cells at the same temperature suggests that an equilibrium developed between the Pluronic complexes and single free Pluronic molecules present in the solution.

At a temperature above 37 °C, titration of Pluronic L64 into water above its CAC (Table 2-1) results in break down into individual monomers of the polymer. Once the concentration in the water increases above the CAC of Pluronic L64, further injections will result in a transition towards micellar formation (Roques et al., 2009). The CAC of Pluronic L64 was found to decrease as the temperature was increased, with micelles not found below 42 °C (Roques et al., 2009). As Roques et al., (2009) showed micelles of Pluronic L64 did not form below 42 °C which would suggest that

Pluronic L64 did not form micelles during the ITC experiments at 25 °C in this study. Temperature has also been shown to have an effect upon the micellisation of other Pluronic surfactants. An increase in temperature from 28 to 31 °C led to a reduction in the concentration at which Pluronic F127 micelles formed, from 0.197 to 0.079 mM (Bouchemal et al., 2009). In addition to the effect of temperature, the inclusion of excipients and the presence of protein (Bam et al., 1995) in a formulation also affect the concentration at which micelles are formed. For example, the inclusion of propylene glycol (which is used in pharmaceutical formulations) at a concentration of 3.7 % w/v decreased the critical aggregation concentration (CAC) of Pluronic F127 by 0.029 mM, from 0.095 ± 0.005 mM to 0.066 ± 0.004 mM (Bouchemal et al., 2009).

2.5.3 MAb-1 structure and thermal stability

The CD spectrum of mAb-1 was dominated by contributions from β-sheet (Figure 2-16). This was expected based on existing data of immunoglobulin secondary structure (Vermeer et al., 2001). The secondary structures of four IgGs of different classes and subclasses (IgG1, IgG2a, IgG2b, IgG3) have been found to be highly similar with ordered β-sheet and β-turns being the main features comprising approximately 40 % and 20 % of the structure respectively (Janda and Casadevall, 2010). The α-helical content of the four IgGs was low, being 3 % or less of the secondary structure. The secondary structure of mAb-1 studied here was, like those investigated by Janda and Casadevall (2010), mainly composed of β-sheet (51 %) and β-turns (10 %). However, in contrast to the findings of Janda and Casadevall (2010), analysis of the CD spectra using Dichroweb showed the α-helical content to be zero (Table 2-5). It is interesting to note that while the secondary structure of

immunoglobulins is highly similar, the F_{ab} fragments of three monoclonal IgG antibodies have been found to differ. The presence of a peak at 223 nm and a clear shoulder at 195 nm are two of the most evident differences (Tetin et al., 2003). A second small peak was apparent in the CD spectrum of mAb-1 in this study which may be due to the F_{ab} fragment as shown by Tetin et al., (2003) and the contribution of aromatic residues to the far UV spectra (Khan et al., 1989).

As surfactants are typically included in protein formulations it was important to determine the effect of their inclusion on the secondary structure of mAb-1 investigated here. A specific binding interaction between the surfactants and mAb-1 was not observed and so it was anticipated that mAb-1 native secondary structure would not be affected. This was largely found to be the case as demonstrated by mAb-1 CD spectra in the presence of Tween and Pluronic surfactants, with the exception of Pluronic L61, not being different to that of mAb-1 alone. This has also been shown for the proteins recombinant factor VIII and lysozyme in the presence of Tween 80 (Joshi and McGuire, 2009). Additionally, as the ITC data did indicate a specific binding interaction between mAb-1 and the surfactants it was therefore expected that the mAb-1 unfolding pathway would not differ. The CD spectra of mAb-1 during thermal denaturation in the presence of surfactant confirmed this expectation with no differences observed. In this investigation, the CD spectra showed mAb-1 unfolding took place above 60 °C in the absence and presence of surfactant. CD spectra of an IgG has previously shown the F_{ab} fragment to be stable up to 40 °C and the F_c fragment up to 60 °C (Vermeer et al., 2001, Vermeer et al., 2000). MAb-1 unfolding was found to be irreversible in this study which has also been observed for a monoclonal mouse anti-rat antibody of the subtype 2b (IgG2b)

(Vermeer et al., 2000), an IgG2 (Van Buren et al., 2009) and a human IgG (Ahrer et al., 2006). CD is an informative technique for studying protein secondary structure, thermal denaturation temperatures are more accurately investigated using DSC.

To obtain accurate thermal unfolding temperatures, and thus supplement the CD data, DSC experiments were carried out. The DSC data produced in this investigation identified three transition temperatures for mAb-1 at temperatures of 67.2, 71.2 and 76.1 °C. This finding is similar to that observed for an IgG1, IgG2 and IgG4 (Garber and Demarest, 2007) but in contrast to the two denaturation temperatures, a T_{m1} of 61 °C and a T_{m2} of 71 °C, which have previously been found for an IgG (Vermeer and Norde, 2000). These values correlate with mAb-1 unfolding observed by CD (Figure 2-26). The transition temperatures can be attributed to the different domains of mAb-1. The three transitions evident from the DSC data at ~67, ~71 and ~76 °C (Table 2-4) can be assigned to the C_H2 domain of the F_c region, the F_{ab} region and the C_H3 domain of the F_c region respectively (Figure 1-4).

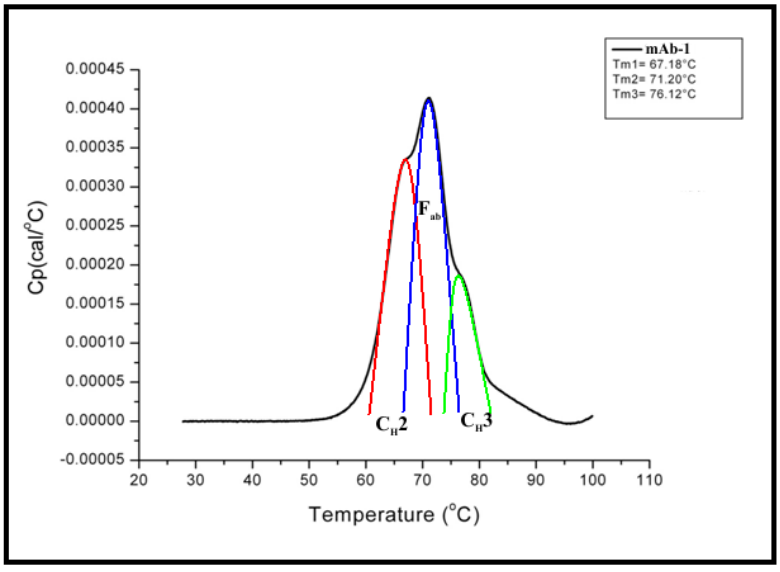

Figure 2-32. DSC thermogram of mAb-1 unfolding.

It has been shown that the transition temperatures of an IgG could be assigned to the F_c and F_{ab} fragments (Vermeer et al., 2000). The IgG was digested using papain and the F_c thermal transition temperature identified using DSC while the unfolding of an approximate F_{ab} region was studied using CD. T_{m1} was assigned to denaturation of the F_{ab} region and T_{m2} to the unfolding of the F_c region (Vermeer and Norde, 2000). The C_H2 domain of the F_c region is expected to unfold first, followed by the F_{ab} domain and finally the C_H3 domain of the F_c region. The unfolding of an IgG2 studied by Van Buren et al., (2009) was found to take place via three transition steps which were attributed to the C_H2 domain, the F_{ab} region and the C_H3 domain. The assignment of transition temperature to the individual regions of mAb-1 is in agreement with Garber and Demarest (2007) for three different immunoglobulin isotypes and other studies carried out previously and reported in the literature for different immunoglobulins (Maity et al., 2009, Ionescu et al., 2008).

The T_m values for mAb-1 studied here and those within the literature differ, however, this has been observed previously for different immunoglobulin isotypes (Garber and Demarest, 2007). The F_c domain of IgG1 was found to be the most stable while the F_c domain of IgG3 was shown to be the least stable as indicated by the T_m values for the C_H2 and C_H3 domains. IgGs of the same subclass have constant domains which are essentially identical but their stability differs. The T_m for the F_{ab} region ranged from 54.2 to 81.6 °C for 14 different IgG1s and 3 different IgG4s. This variability in stability between different subclasses of IgGs is due to differences in the Fv region. (Garber and Demarest, 2007). The thermal transition temperature of a protein can also be affected by the sensitivity of the protein, or domains of the protein, to pH changes. The C_H2 domain of two monoclonal IgG1 antibodies has been shown using

DSC to be more sensitive to pH than the other domains (He et al., 2010). This was in contrast to the unfolding transition of the F_{ab} region which did not change over the pH range of 4.0 to 8.0 used (He et al., 2010). The stability of an IgG2 when stored at 37 °C for 15 weeks was not disturbed at pH 5.0 or 6.0 and to only a small degree at pH 4.0 (Van Buren et al., 2009). The DSC and CD experiments for mAb-1 in this investigation were carried out at only a single pH although the surface adsorption studies using TIRF and NR (section Chapter 4) were undertaken at two pH values, pH 5.5 and 7.4. However, mAb-1 unfolding did not take place until above 60 °C and so the structure will be unaffected during the experiments undertaken at room temperature.

2.5.4 Effect of surfactant on mAb-1 thermal transition

The thermal transition temperatures of mAb-1 had been established in aqueous buffer and so the next step was to determine if surfactant inclusion affected thermal stability. As no interaction was identified using ITC and unfolding investigated using CD did not show a surfactant effect, it was anticipated that the inclusion of Tween would have no effect upon mAb-1 thermal denaturation investigated using DSC. Inclusion of Tween 20 and 80 at concentrations below and above their CMC, as expected, did not affect mAb-1 T_m. The CD and DSC data together show no protective effect of Tween on mAb-1 unfolding upon a temperature increase. This result is similar to a previous investigation using DSC which showed that Tween 20 and Tween 80 had no effect upon immunoglobulin T_m (Hoffmann et al., 2009a). An increase in the maximum heat capacity curve of the immunoglobulin of 0.2 K in the presence of Tween 20 at 2 mM was observed although this change was not significant, a similar result was also found for Tween 80 (Hoffmann et al., 2009a).

This has also been found to be the case for an IgG in the presence of Tween 20 with the exception of a small increase, of approximately 0.3 K, at the highest concentration investigated (2 mM) (Garidel et al., 2009). In contrast to the lack of Tween effect on the immunoglobulins mentioned, the T_m for HSA in the presence of Tween 20 and 80 has been found to increase by 2.3 K (Garidel et al., 2009). The surfactants are known to bind to HSA which increased its thermal stability due to the entropy favouring maintenance of the native state. However, a contrasting effect of Tween inclusion on rhGH thermal stability has also been observed. The melting temperature of rhGH was decreased by the presence of Tween 20, 40 and 80 in solution at molar ratio of 10:1 by 2 °C. CD spectra of the melting curves for rhGH corroborated the DSC data (Bam et al., 1998). The difference between the protein structures and interaction with Tween may be the cause of the differing surfactant effects.

As with the two Tween surfactants, DSC data showed that Pluronic inclusion in mAb-1 samples at concentrations below and above their CAC did not affect the T_m. This was expected as a specific interaction was not observed between the two during ITC experiments. Similar to the mAb-1 DSC data in this study, a concentration of 0.5 % w/w Pluronic F127 has been shown not to have an effect on the thermal stability of rIL-2 with its activity being 25% of initial after incubation at 50 °C (Wang and Johnston, 1993). The percentage of urease activity after incubation at 50 °C is greater when 1 % w/w Pluronic F127 is added to the phosphate buffer which was in contrast to the decreased activity level after the temperature was increased to 75 °C (Wang and Johnston, 1993). The Pluronic surfactants P108 and P188 and the multi-block copolymer Tetronic 1107 (T1107) have been found to affect the degree of

aggregation of BSA and hen egg white lysozyme (HEWL) after heat denaturation (Mustafi et al., 2008). T1107 (at a molar ratio of 2:1 polymer: HEWL) fully prevented the aggregation of heat denatured HEWL compared to Pluronic P108 and P188 which decreased aggregation but to a lesser extent. Pluronic P108 and P188 had very little effect on the aggregation of heat denatured BSA, while T1107 at a polymer: BSA molar ratio of 10:1 reduced aggregation by 50 % (Mustafi et al., 2008).

Surfactants can however destabilise proteins and cause their denaturation, as has been found to be the case for the mixed α-helical/β-sheet protein α-lactalbumin in the presence of four classes of surfactant: anionic, cationic, zwitterionic and non-ionic (Otzen et al., 2009). Investigation of α-lactalbumin using fluorescence intensity and CD showed that all four surfactant classes caused a loss of the protein's native structure (Otzen et al., 2009). The authors found the binding affinity of α-lactalbumin for surfactants to be general and not specific to one class, which would explain the denaturation effect of all types of surfactants in the study by Otzen et al., (2009). The surfactants used in this investigation did not, in contrast to α-lactalbumin, interact with of mAb-1 or, with the exception of Pluronic L61, affect the native secondary structure which would explain the lack of effect on mAb-1 stability.

2.6 Conclusions

A specific binding interaction between the surfactants and mAb-1 did not take place as shown by the ITC data. This was important in order for conclusions to be drawn regarding surface adsorption of mAb-1. As no interaction with the surfactant took place, it can be concluded that mAb-1 alone will be the driving force behind the surface adsorption of the protein, without the surfactants playing an important role in this matter. MAb-1 was shown to be stable at temperatures up to approximately 60 °C using both CD and DSC and so it is expected to retain its native structure during surface adsorption experiments, carried out at RT. Surfactant inclusion had a minimal effect on the structure of mAb-1 except for Pluronic L61 and therefore the protein will retain its native secondary structure when either the Tween or Pluronic surfactants are present in solution. The interaction of mAb-1 in solution with the surfactants has now been characterised along with their effect on the structure and stability of mAb-1. The next stage in this study was to investigate the interaction of mAb-1 with surfaces and the effect adsorption had on secondary structure.

Chapter 3. Interaction and destabilisation of mAb-1 with surfaces of varying functionality and hydrophobicity

3.1 Introduction

This chapter encompasses the work aimed to investigate the effect that different types of surfaces may have upon mAb-1 adhesion and secondary structural changes. The surfaces were first characterised using contact angle goniometry (CAG) to determine their hydrophobicity which was then used to calculate their surface energy using software developed in-house (Lamprou et al., 2010b, Lamprou et al., 2010c). The force of adhesion between mAb-1 and a range of surfaces was studied using atomic force microscopy (AFM) to determine the degree of attraction each surface has for mAb-1. The adhesion data was complimented with secondary structure analysis using 'solid-state' circular dichroism (CD), which is used to study the effect of adsorption on the structure of a protein. The surface characteristics and force of adhesion values were determined in order to investigate if a relationship between the loss of mAb-1 secondary structure and surface energy, or force of adhesion existed.

3.1.1 Contact angle goniometry (CAG) and surface energy

The surface energy (γ_s) of the silane, surfactant and protein coated surfaces was determined via contact angle measurements of liquid-on-solid prior to investigation of the surface effect on mAb-1 adhesion and structure. Contact angle goniometry (CAG) is an established technique for characterising surfaces (Lamprou et al., 2010a, Lamprou et al., 2010b, Lamprou et al., 2010c, Offord et al., 1994) allowing the measurement of the shape of a liquid droplet when in contact with a solid surface.

Contact angle is defined as the measurement of the angle that a liquid forms at the intersection between solid, liquid and gas (vapour (Zisman et al., 1964)) (Figure 3-1).

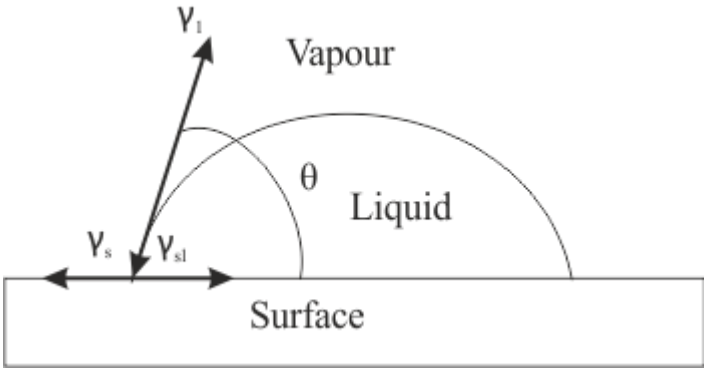

Figure 3-1. Contact angle - measurement of the angle of a droplet at the intersection between liquid, solid and gas.

The measurement of the excess of free energy derived from the polar and non-polar events taking place upon the interaction between a solid surface and the liquid droplet is known as surface energy (Zisman et al., 1964, Long et al., 2005), also known as the solid surface tension. In order to calculate the surface energy, the angle of drops of three solvents (for example filtered water, diiodomethane and 1,2-ethandiol (Lamprou et al., 2010a)) on solid surfaces is measured. The contact angle for a surface is investigated by placing small drops onto the surface and determining the angle between the drop and the surface. Each of the three solvents mentioned as examples has a different polarity and therefore will perform differently when in contact with the same surface. In addition to calculation of surface energy, the use of liquids such as diiodomethane enables determination of the lipophilicity of a surface.

Through calculation of surface energy and the contact angle of the three liquids, the hydrophobicity of a surface can be determined. The hydrophobicity of a surface is dependent upon the terminal group which is exposed to the air interface. For

example, a terminal amine (-NH_2) group will produce a hydrophilic surface compared to methyl (-CH_3) which will confer hydrophobicity (calculations for surface characterisation are detailed in 3.3.2).

3.1.2 Atomic Force Microscopy (AFM)

Scanning probe microscopy (SPM) is the name given to a range of related techniques that involve a combination of imaging and local physical property measurements by investigating physical or chemical interactions between a sharp proximal probe and a surface (Ros et al., 1998). The two primary forms of SPM are scanning tunnelling microscopy (STM) and atomic force microscopy (AFM). STM was first developed in 1982 at IBM in Zurich by Binnig et al., where atomic resolution images were first observed. The technique necessarily requires an electron-conductive material as a sample, which limits the materials that can be studied. In 1986, AFM was developed by Binnig with the important advantage of it being able to operate with insulating materials, such as ceramics, biological materials and polymers, in addition to conductors and semi-conductors. AFM can provide pseudo-three-dimensional images of surface topography in liquid or gaseous environments, over a range of temperatures (typically, ambient – 250 °C). In addition to high-resolution imaging, AFM is capable of measuring nano-mechanical surface properties, such as adhesion, compliance, friction, roughness, and the forces between a surface (which can be coated with a silane or protein) and an AFM probe. Additionally, the probe can also be functionalised with a protein or a silane for example. This section will focus on force of adhesion while briefly mentioning the method by which surface morphology is characterised using AFM. The investigation of forces is known as force *versus* distance curve acquisition and is used to measure the attraction or repulsion between

a cantilever tip and a surface. The force versus distance curve typically shows the deflection of the free end of the AFM cantilever as the fixed end of the cantilever is brought vertically towards and then away from the sample surface (Figure 3-2). In this study the force of adhesion between a functionalised AFM tip and surfaces with a range of surface energies was investigated.

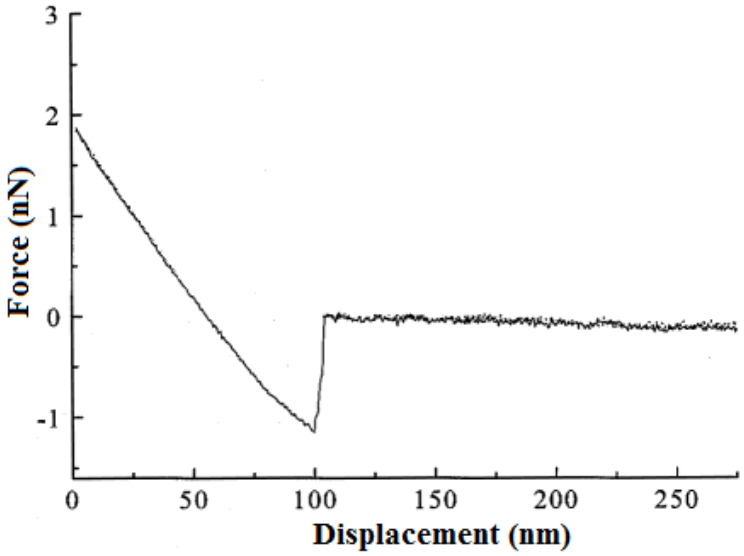

Figure 3-2. Example of a force versus distance curve (Adapted from (Lo et al., 2001)).

Figure 3-3 shows the set-up of the AFM: a laser is focused on the back of the cantilever (Figure 3-4) and a photodiode (detector) detects the intensity of light reflected. Deflection of the cantilever caused by forces between the tip and the surface are detected and through a feedback loop the cantilever is moved in the z-plane to maintain a constant deflection. The data produced is then plotted together with the x-y plane data to generate a 3-D image of the surface morphology.

To investigate the attraction or repulsion forces, the tip is lowered towards the surface until it comes within close proximity where attractive/repulsive forces act upon the tip. Deflection of the cantilever will take place if there is an attractive or

repulsive force exerted by the surface. The deflection of the cantilever will increase as it is moved closer to the surface before it is retracted. Adhesion forces can cause the tip to remain near the surface until the force being applied to remove it from the surface can overcome the adhesion force. The force applied is converted into a value of Newtons (N). It should be noted that AFM instruments are capable of measuring this interaction to the pico (10^{-12}) newton range (Wei and Latour, 2010). The relationship between the motion of a cantilever and the applied force is given by Hooke's Law (Equation): $F = kd$ where, F is the applied load (N), k is the force or spring constant (N m^{-1}), and d is the distance that the 'spring' has been stretched or compressed (m) from the equilibrium position.

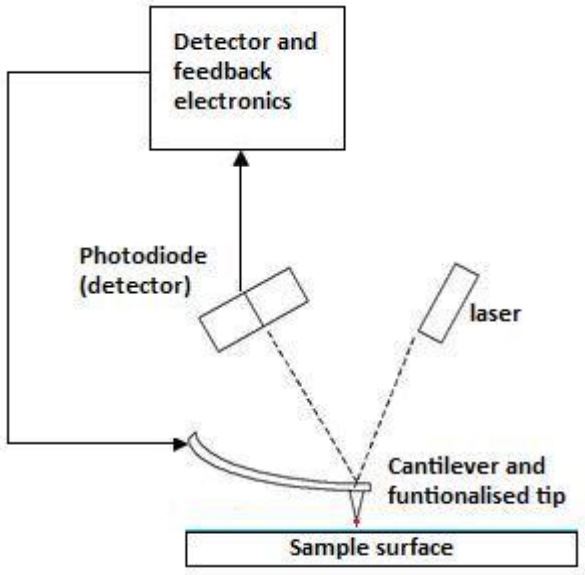

Figure 3-3. Main components of AFM (adapted from www.emt.uni-linz.ac.at).

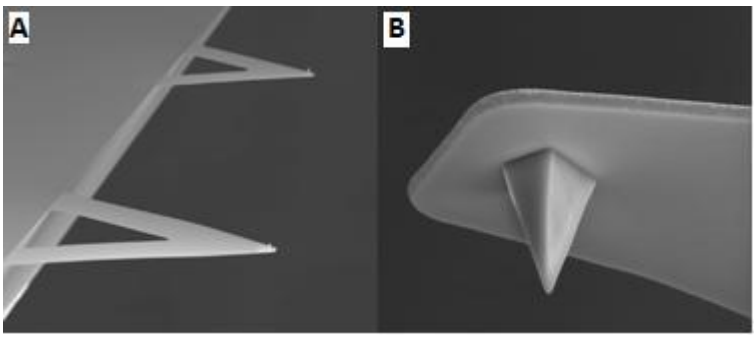

Figure 3-4. (A) NP-10 silicon nitride probe; (B) cantilever tip (http://www.brukerafmprobes.com/p-3370-np-10.aspx).

There are two modes of AFM operation: contact mode and tapping mode. In contact mode AFM, the probe is in constant contact with the sample surface and can be used to produce an image of the surface structure. During tapping mode, the probe taps the surface repeatedly and is commonly used to image surfaces which are soft, easily damaged or loosely adsorbed. Using tapping mode, the orientation of the mouse monoclonal antibody to the β unit of human chorionic gonadotropin has been determined using AFM in conjunction with neutron reflectometry (discussed in section 4.1.2). The height of the antibody was shown to be 30 Å which was in good agreement with published values for the short axial length (145 x 85 x 38) (Silverton et al., 1977). This showed that the antibody had adsorbed in a "flat-on" orientation and also that some deformation in structure had taken place due to the reduced height of 30 from 38 Å which was most likely due to compression of the layer by the cantilever tip (Xu et al., 2006.

The interaction between proteins and surfaces has similarly been investigated using AFM. The force of adhesion between albumin, fibrinogen and factor XII to surfaces which were established as having a high water contact angle, and were therefore hydrophobic, was stronger than to hydrophilic surfaces (Xu and Siedlecki, 2007b).

The force of adhesion (F_{ad}) between a protein and surface changes with time (Xu and Siedlecki, 2007b). A two-step interaction process was proposed for this finding which involved an initial stage in which quick perturbation of the protein structure took place upon contact with the surface. This was followed by relaxation and unfolding which resulted in the hydrophobic core of the protein becoming exposed to the surface. In addition to measuring the force of adhesion, AFM can also be used to investigate the force of desorption of a molecule from a surface. A cantilever tip is functionalized (e.g. with a peptide) and lowered onto a surface of interest, the tip is then retracted and the force required to pull the tip away from the surface is measured (Wei and Latour, 2010).

Only a small number of surfaces have been used in the studies mentioned and so a wider range and variety of surfaces was investigated in this study. The surfaces were selected to provide a greater understanding of the F_{ad} between mAb-1 and surfaces commonly encountered during manufacturing and processing. In addition, the interaction between surfactants (Tween and Pluronic) and HSA with mAb-1 was also studied as, their interaction with proteins is poorly characterised despite their common use in formulations to minimise surface adsorption of the protein.

3.1.3 'Solid-state' Circular Dichroism

'Solid state' CD was used to investigate the structure of mAb-1 adsorbed to surfaces with a range of surface energies. The principles and techniques for 'solid state' CD are the same as for studying a protein in solution using 'liquid-state' CD (section 2.1.3) (Kelly et al., 2005) but spectra are obtained for a protein film on a solid surface. The CD spectra produced have artefacts such as linear birefringence (the optical property of the material used) and linear dichroism (the ability of a material

to split a beam of light in two with the resulting beams having different wavelengths) which results in alterations to the spectra causing them to differ from that expected.

'Solid-state' CD has been used previously to determine the structure of subtilisin Carlsberg (Ganesan et al., 2006) and an IgG-like domain pair (Pereira et al., 2008) adsorbed to a silica surface. Hu et al. (2001) identified a change in the structure of some proteins upon the transition from bulk solution to a solid surface using 'solid-state' CD (Hu et al., 2001). This study found that the spectra of insulin, lysozyme and disulfide oxidoreductase (DsbA) protein were of a shape which could not be distinguished from that in solution. The ellipticities were different however, which was attributed to an unknown protein concentration and pathlength of the surface film formed (Hu et al., 2001). In contrast to this, the spectra of BSA and hen egg ovalbumin (OVA) did differ between solution and solid state. The spectra for these two proteins show that BSA contains a high α-helical content and ovalbumin contains a α/β mixture when in solution; this changes to a large proportion of β-sheet when both proteins are analysed attached to a solid surface (Hu et al., 2001). The 'solid-state' CD spectra of both insulin and BSA on a surface are shown in Figure 3-5.

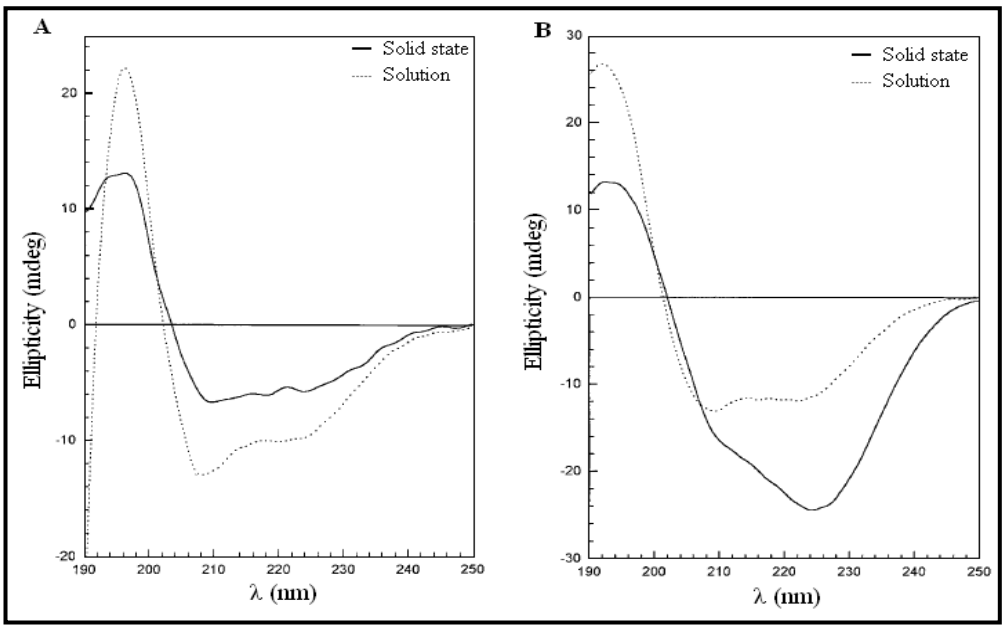

Figure 3-5. **(A)** Circular dichroism spectra of insulin; **(B)** circular dichroism spectra of bovine serum albumin (BSA). Adapted from (Hu et al., 2001).

A selection of proteins have been investigated previously, however, immunoglobulins were not among them. The free energy required to maintain a protein in its folded state, which influences the degree of unfolding upon adsorption to a surface, will differ between each one. Consequently, although a variety of proteins have been studied, it is necessary to investigate immunoglobulins as their secondary structure is different to those previously considered and therefore the effect of surface on unfolding of mAb-1 may differ.

The effect of surface on protein structure has been investigated on hydrophilic silica surfaces (Hoehne et al., 2011, Bee et al., 2009) and hydrophobic surfaces such as Teflon (Vermeer et al., 1998, Vermeer et al., 2001) or octadecyltrimethoxysilane (Pereira et al., 2008). In this study a range of silanised surfaces were investigated with the aim of studying the relationship, if any, between surface energy and changes in mAb-1 structure upon adsorption. Additionally mAb-1 secondary structural

changes on Tween coated surfaces was also investigated due to their common use in therapeutic proteins formulations. This will complement the previous study on the protein-surfactant interaction in the bulk of solution (section Chapter 2).

3.2 Materials

Bovine serum albumin (BSA), human serum albumin (HSA), concentrated sulphuric acid, hydrogen peroxide, toluene, N,N-dimethylformamide (DMF), diiodomethane, 1,2-ethanediol (ethylene glycol), Tween 20, Tween 80, and silica beads (pore size 60 Å, 230-400 mesh) were obtained from Sigma Aldrich (Dorset, UK). Silanes: (3-Aminopropyl)triethoxysilane (APTES), (3-aminopropyl)trimethoxysilane (APTMS), (3-glycidyloxypropyl)trimethoxysilane (GPTMS), trichloro(methyl)silane (TCMS), trichloro(propyl)silane (TCPS), trichloro(octyl)silane TCOS), trichloro(dodecyl)silane (TCDS), 1H,1H,2H,2H-perfluorooctyltriethoxysilane (PFTOS) and octadecyltrichlorosilane (OTS) were purchased from Sigma Aldrich. Methoxy-polyethylene glycol-silane (mPEG-silane; 1000 MW PEG group) was purchased from Creative PEGWorks, Winston Salem, USA. Pluronic P103, P123, L43 and L61 were a generous gift from BASF (UK). Water was purified to > 14 MΩ.cm with a BioSelect, Purite, UK. Mouse monoclonal secondary immunoglobulin to human IgG–Fc was obtained from Abcam, Cambridge, UK. The immunoglobulin (mAb-1) used throughout the surface conformation study was kindly provided by MedImmune Ltd., Cambridge, UK.

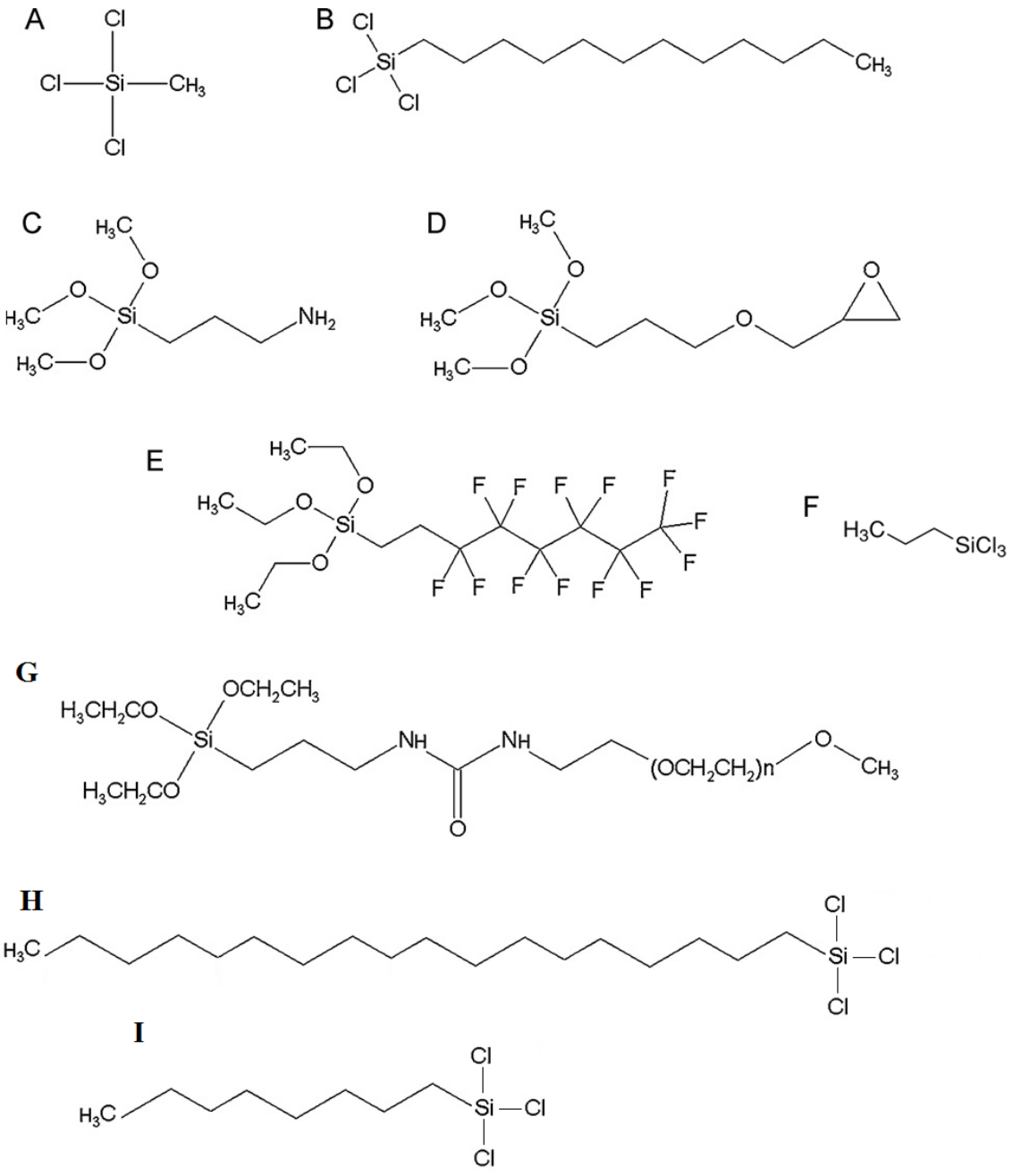

Figure 3-6 . The structure of the silanes used to prepare self-assembled monolayers (SAMs): (A) trichloro(methyl)silane (TCMS); (B) trichloro(dodecyl)silane (TCDS); (C) (3-aminopropyl)trimethoxysilane (APTMS); (D) (3-glycidyloxypropyl)trimethoxysilane (GPTMS); (E) 1H,1H,2H,2H-perfluorooctyltriethoxysilane (PFTOS); (F) trichloro(propyl)silane TCPS); (G) Methoxy-polyethylene glycol-silane (mPEG-Silane); (H) octadecyltrichlorosilane (OTS); (I) trichloro(octyl)silane (TCOS).

3.3 Methods

3.3.1 Self-assembled monolayer (SAM) preparation

Microscope cover slips (13 mm in diameter, VWR (UK)) were cleaned with Piranha solution (3:1 concentrated sulphuric acid: hydrogen peroxide) and deionised water before being dried under a nitrogen stream (Lamprou et al., 2010c). The contact angle of organosilanes has been shown to differ between approximately 10° between cleaned and not cleaned surfaces (Lamprou et al., 2010c). It is necessary to clean the slides to ensure there are no particles on the surface which would prevent a homogeneous SAM forming. The cover slips were immersed in 1 mM solutions of each of the 9 silanes (APTMS, GPTMS, TCMS, TCPS, TCOS, TCPS, TCDS, mPEG-Silane, PFTOS and OTS - Figure 3-6) for 16 hours at room temperature which has previously been shown to produce reproducible surface energy values (Lamprou et al., 2010c). The slides were then cleaned via sonication for 20 minutes in toluene, followed by the same procedure in DMF and deionised water before being finally dried under a nitrogen stream (Lamprou et al., 2010c). Surfaces coated with 0.05 and 1 mM Tween 20, 5 μM and 1 mM Tween 80, 1 μM and 1 mM Pluronic P103, 1 μM and 0.1 mM Pluronic P123, 1 and 5 mM Pluronic L43, 0.05 and 0.5 mM Pluronic L61 and, 2.5 and 12.5% HSA were prepared using the same method but washed with deionised water only. Polystyrene cover slips were used as purchased without further treatment.

3.3.2 Contact angle and surface energies

To probe liquid-surface interactions, contact angles of small drops of filtered water, diiodomethane (DIM) and 1,2-ethanediol (ethylene glycol, EG) placed on horizontal substrates were measured using a goniometer (Krüss DSA30B, Hamburg, Germany).

The ‘left’ and ‘right’ contact angles were taken after placement of the drops: five drops per substrate were measured and three individual substrates prepared for each surface giving a total of 15 drops to be measured for each liquid. Table 3-1 shows reported values found in the literature together with the values found in this study.

Surface energies of substrates (γ_s) were calculated from the contact angle and interfacial energy values of the three probe liquids (filtered water, diiodomethane and ethylene glycol) from Equation 3-1 to Equation 3-3, using a Visual Basic program (Lamprou et al., 2010c, Lamprou et al., 2010b). Through insertion of the values for the Lifshitz-van der Waals, Lewis acid and base together with the contact angles for the three probe liquids into the equations 3-1 to 3-3 the surface energy is determined.

Liquid	Surface tension (γ_L) (mN m^{-1}) at 18.8 °C	γ_L reported in the literature (mN m^{-1})
Filtered water (Millipore 18.2 MΩ cm)	73.4	73.05 (at 18 °C) [a]
Diiodomethane (DIM)> 99%	48.7	50.76 (at 20 °C) [a]
1,2-ethanediol (ethylene glycol, EG) > 99%	47.7	48.40 (at 20 °C) [a]

Table 3-1. Surface tension (γ_L) values of filtered water, diiodomethane and ethylene glycol [a](Kaye and Laby, 1995).

$$\gamma_s = \gamma_s^{LW} + \gamma_s^{AB} = \gamma_s^{LW} + 2\left(\gamma_s^+ \gamma_s^-\right)^{1/2} \quad \textbf{Equation 3-1}$$

$$\gamma_l = \gamma_l^{LW} + \gamma_l^{AB} = \gamma_l^{LW} + 2\left(\gamma_l^+ \gamma_l^-\right)^{1/2} \quad \textbf{Equation 3-2}$$

$$\gamma_l\left(1+\cos\theta\right) = 2\left[\left(\gamma_s^{LW}\gamma_l^{LW}\right)^{1/2} + \left(\gamma_s^+\gamma_l^-\right)^{1/2} + \left(\gamma_s^-\gamma_l^+\right)^{1/2}\right] \quad \textbf{Equation 3-3}$$

The superscripts denote the components of surface energy: Lifshitz-van der Waals = *LW*, acid-base = *AB*, Lewis acid γ^+ and Lewis base γ^-. (In mJ m^{-2}, deionized water:

$\gamma_l^{LW} = 21.8,\ \gamma_l^+ = \gamma_l^- = 25.5;$ diiodomethane: $\gamma_l^{LW} = 50.8,\ \gamma_l^+ = \gamma_l^- = 0;$ ethylene glycol: $\gamma_l^{LW} = 29,\ \gamma_l^+ = 1.92,\ \gamma_l^- = 47$ (Janczuk et al., 1999). For example, if the contact angles of the three liquids on a surface were each 40°, using the values denoted above and in Table 3-2 the calculated surface energy (γ) would be 42.43.

Liquid	γ_L	γ_L^{LW}	γ_L^+	γ_L^-
Filtered water	72.8	21.8	25.5	25.5
Diiodomethane (DIM)	50.8	50.8	0	0
1,2-ethanediol (ethylene glycol, EG)	48	29	1.92	47

Table 3-2. Example values of the surface energy components used in the Visual Basic program to determine the surface energy.

3.3.3 Atomic force microscopy (AFM)

A Bruker Multimode™ Scanning Probe Microscope (SPM) with Nanoscope IIID Controller (Digital Instruments, Santa Barbara, CA, USA; Bruker software Version 6.14r1) in tapping mode and V-shaped cantilever was used for AFM measurements in air under ambient conditions. Using a confocal microscope with a measuring function (DXR Raman Confocal Microscope, Thermo Scientific, UK) the length and width of the V-shaped cantilever were determined (Figure 3-7). The value for the thickness of the cantilever was taken from previously published data (Lamprou et al., 2010b).

The spring constant of the probes used was calculated using the following equation:

$$\boldsymbol{k = \frac{Ewt^3}{2l^3}} \qquad \textbf{Equation 3-4}$$

where l = length (μm), w = width (μm), t = thickness (μm) and E is Young's modulus = 175 GPa (Hazel and Tsukruk, 1999).

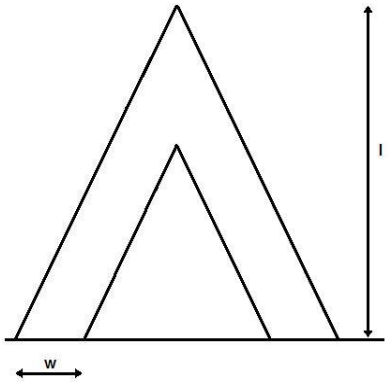

Figure 3-7. V-shaped atomic force microscopy (AFM) cantilever: length (l), width (w) as shown in **Figure 3-4**.

3.3.3.1 Functionalisation of AFM silicon nitride probe

AFM cantilevers are functionalised with proteins to determine the force of adhesion (F_{ad}) between the protein and various surfaces. Functionalisation of the AFM silicon nitride probe was carried out using a three step process (Figure 3-8). The NP-10 silicon nitride probe ('C' V-shaped cantilever, nominal length (l_{nom}) = 120 ± 5 µm, width (w_{nom}) = 20 ± 5 µm, resonant frequency (υ_{nom}) = 56 kHz and spring constant (k_{nom}) = 0.24 ± 0.018 N m^{-1}; Bruker Nano, Dourdan, France) was first amino-functionalised. This is commonly carried out using a silane such as APTES (Celik and Moy, 2012) or ethanolamine chloride (Wei and Latour, 2010). This is followed by the attachment of a PEG spacer molecule which has an end group which will interact with the protein or peptide of interest (McGurk et al., 1999, Wei and Latour, 2010). The amino-PEG functionalised tip is then immersed in the protein/peptide solution before being washed to remove any unbound protein/peptide. The amino-functionalization of the cantilever tips was also undertaken in this study but the second step differed. The primary antibody which was specific for the F_c fragment of human IgG2 (anti-F_c antibody) was non-specifically attached to the amino-functionalised cantilever with the interaction taking place between the carboxyl

groups of the anti-F_c antibody and the amine groups on the cantilever tip surface. The anti-F_c antibody will occupy a number of the amine groups on the surfaces although it is highly unlikely all of the amine groups will be occupied due to steric hindrance reducing the number of antibody molecules which can adsorb. The tip functionalised with APTES-anti-F_c antibody was then immersed in a solution of mAb-1 and washed. The anti-F_c antibody could adopt a number of orientations on the APTES surface but only those molecules oriented with the F_c binding domain facing away from the surface would be capable of interacting with mAb-1. The affinity of an antibody for its antigen is high and so mAb-1 will become attached to the tip. This high affinity and steric hindrance of the anti-F_c antibody will prevent mAb-1 from adsorbing in a non-specific orientation to the tip surface.

Non-specific attachment of mAb-1 was carried out through amino-functionalization of the tip followed by immersion in a solution of mAb-1. Although mAb-1 could be attached to the tip surface, accurate and reproducible F_{ad} measurements could not be achieved. This was due to mAb-1 being able to attach in a number of orientations and so the distance between the tip and surface at which adhesion took place was not uniform. The F_{ad} measurements were therefore carried out using mAb-1 attached to the tip in a specific orientation only.

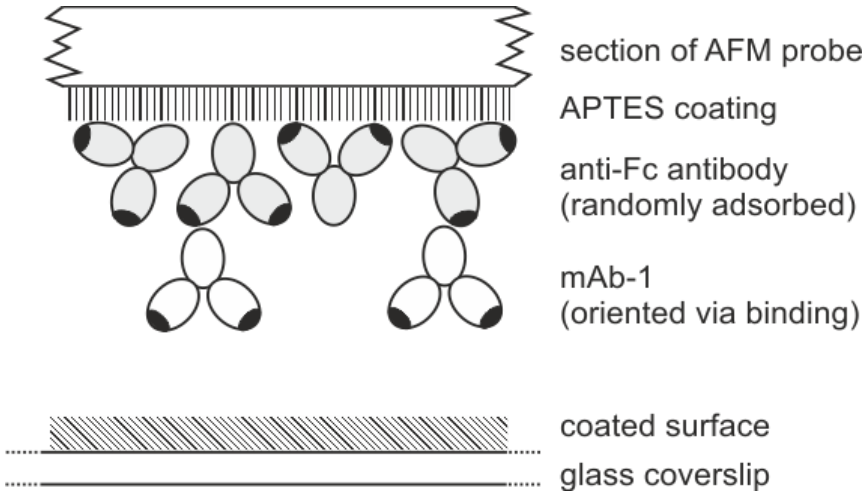

Figure 3-8. Functionalisation of AFM silicon nitride probe: three step process involving coating with APTES followed by attachment of a primary immunoglobulin and finally mAb-1.

3.3.3.2 Force vs. distance plots

Force versus distance plots were obtained for oriented monolayers of mAb-1 coming into contact with bare silica and coated silica surfaces using a functionalised silicon nitride probe and the J-scanner with assistance from Dr Dimitrios Lamprou (Uni. of Strathclyde). The laser alignment was unaltered during measurements (deflection sensitivity = 46 ± 3 nm/V) and arrays of 10 × 10 force-curves (lateral separation, 100 ± 5 nm; ramp size, 800 nm; scan rate, 1.03 Hz) were produced from two different areas (1000 nm × 1000 nm, separated by 1000 nm), on 2 surfaces of each sample in air (Lamprou et al., 2010a, Lamprou et al., 2010b). The F_{ad} was calculated using Hooke's Law (Cappella and Dietler, 1999) with the equation $f = k \,.\, d$, where f is the force of adhesion (F_{ad} / nN) collected using AFM, k is the accurate spring constant (N m^{-1}) and d is the distance (nm) at which the functionalised cantilever probe is retracted before the interaction with the surface breaks. Measurements were repeated

four times and F_{ad} values extracted from force curve data using a Visual Basic program (Lamprou et al., 2010b).

F_{ad} values for a non-functionalised AFM cantilever tip with the silane surfaces are available in the literature (Lamprou et al., 2010a) and so were not undertaken in this study. Additionally, it was not possible to orientate BSA in the same specific manner (as it does not contain a distinct domain equivalent to those in mAb-1) as mAb-1 and so F_{ad} measurements were not made between BSA and the investigated surfaces.

3.3.3.3 Statistical analysis

Statistical analysis of the contact angle data of the three probe liquids on the silanised silica surfaces, surfactant coated silica and HSA coated silica surfaces were undertaken using one-way ANOVA. A result was considered to be statistically significant at a 95 % confidence level. Statistical analysis of force of adhesion data for mAb-1 to the coated silica surfaces was performed using the same method as for contact angle and surface energy.

3.3.4 'Solid-state' circular dichroism

3.3.4.1 Preparation of silane-coated silica beads

Silica beads were immersed in 1 mM solutions of silane in anhydrous toluene, followed by end to end rotation for 4 hours and standing overnight at room temperature. The beads were sonicated for 20 minutes with toluene, DMF and deionised water in that order. Protein coated silica beads were prepared by incubating either 0.2 g of untreated or silane-coated silica beads with a 1 mg/mL mAb-1 or BSA solution at room temperature overnight on end-to-end rotation. The beads were then washed and centrifuged to harvest the beads (at 3000x g for 1 min) a minimum of

three times in phosphate buffered saline, pH 7.4. This was repeated until the value of the UV absorbance of the supernatant at 280 nm was zero.

3.3.4.2 Preparation of Tween coated silica beads

Silica beads were coated with Tween 20 and 80 at concentrations below and above their CMC (section 2.3.2, Table 2-2) to investigate mAb-1 secondary structure upon adsorption to surfactant coated surfaces. Silica beads were immersed in the respective Tween concentration dissolved in PBS overnight at room temperature while undergoing end to end rotation. The beads were washed and centrifuged as for mAb-1 adsorbed to silane coated beads. This was repeated until the UV absorbance value of the supernatant at 280 nm was zero.

3.3.4.3 Far UV (180-260 nm) spectra of mAb-1 adsorbed to silica and coated silica beads

The secondary structure of mAb-1 when adsorbed to the silica, silane-coated silica and Tween-coated silica beads was investigated using an Applied Photophysics Chirascan CD spectrometer (Applied Photophysics Ltd, Leatherhead, UK) as for the CD experiments in 2.3.3. The beads with mAb-1 adsorbed to the surface were inserted into a cylindrical quartz cuvette (Hellma, UK) with a pathlength of 0.02 cm. A rotating cell holder which was developed in-house was used (Figure 3-9) as it prevented sedimentation of the beads and enabled spectra to be acquired. The sample was rotated at 45 rpm for 5 minutes prior to insertion into the peltier to ensure a homogeneous distribution of beads throughout. Spectra for mAb-1 on each surface were obtained using the following parameters: 6 repeats, 0.5 nm step, and 3 seconds per point. Control samples of silica, silane-coated silica and Tween-coated silica beads were obtained using the same parameters.

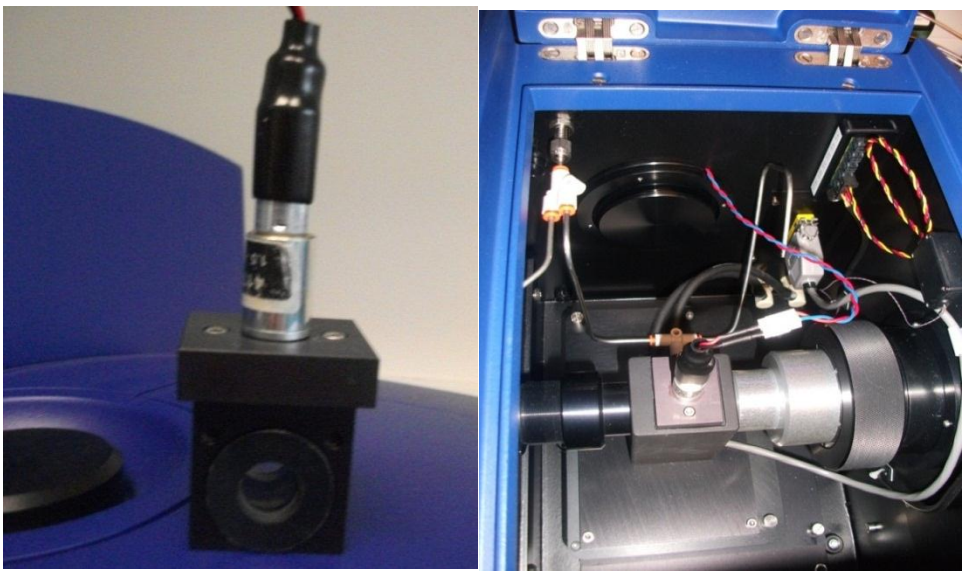

Figure 3-9. Image of the rotating cell and the rotating cell *in situ* in the peltier holder within the circular dichroism.

The same set of experiments were carried out for BSA adsorbed to the silane-coated silica beads (with the exception of OTS) to investigate the effect of surface energy on the secondary structure of an α-helical protein. This enabled a comparison to be made between the effects of surface energy on two different protein secondary structural motifs.

3.3.4.4 Empirical correction method

The CD spectra of the two proteins adsorbed to the silica, silane-coated silica and Tween coated beads were analysed using the empirical method to correct for absorption flattening developed by Ganesan et al., (2006). Absorption flattening occurs when a protein is adsorbed to a surface because the chromophores are tightly packed and so the cross-sectional area of the solution is less than if the protein was uniformly dispersed. The level of flattening is proportional to the absorbance at a given wavelength. To correct for this, the CD spectra are multiplied by an absorption

flattening coefficient (Q) which has been calculated based upon the difference between the CD spectra for the protein in solution and adsorbed to a solid surface. Using the correction factor it is possible to produce spectra comparable to that of a protein in solution (Ganesan et al., 2006).

3.3.4.5 Dichroweb Analysis

The online CD secondary structure analysis server Dichroweb was used to make a quantitative interpretation of the CD data obtained for mAb-1 and BSA in solution and adsorbed to silica beads (Whitmore and Wallace, 2004). The CONTIN algorithm (van Stokkum et al., 1990) with reference set SP175 (Lees et al., 2006) was used to reconstruct the data sets. The normalized root mean square deviation (nrmsd) with the experimental data was reported, with a value of ≤ 0.2 being within the acceptable range for this 'goodness of fit' parameter (Whitmore and Wallace, 2004).

3.4 Results

3.4.1 Contact angle and surface energies

It is generally accepted that a water contact angle which is above 90° indicates a hydrophobic surface, and one which is less than 90° is representative of a hydrophilic surface (Giovambattista et al., 2007, Feng et al., 2002). The images in Figure 3-10 are representative of a hydrophilic (left) and hydrophobic (right) surface. These values were used as an indicator of the hydrophobicity of the SAMs produced in this study.

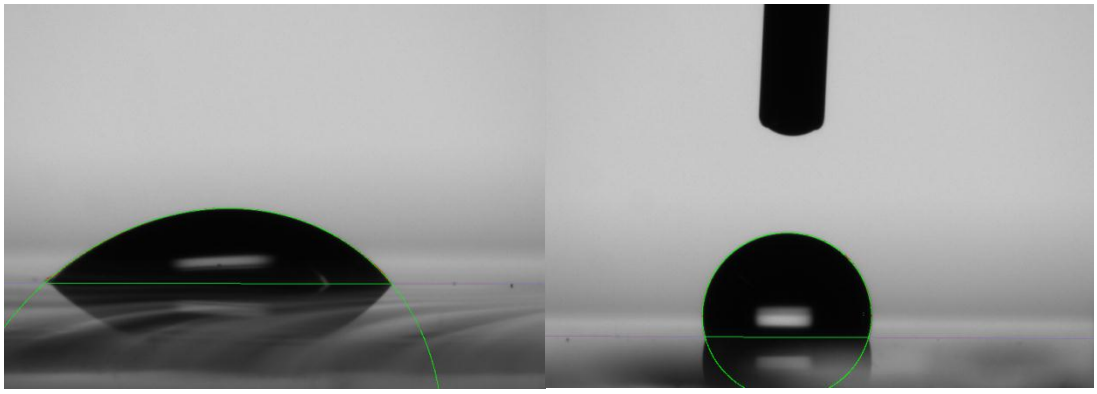

Figure 3-10. Contact angle images representative of a hydrophilic (left) and hydrophobic (right) surface with water contact angles of 46.3° and 104.7°.

The contact angle values of the silanised surfaces were reproducible (Table 3-3), as indicated by the standard deviations and were generally in good agreement with the values in the literature which suggested that the coating on the surface was homogeneous. This finding is consistent with the formation of covalently bound self-assembled monolayers (SAMs) as a result of the silanisation reaction. The SAMs can form a densely packed 'brush border' with the silane terminal group exposed to the liquid. The contact angle values of the solvents on the silica and silane-coated silica slides are related to the hydrophobicity and lipophilicity of the coating with the terminal group of the coating determining the wettability of the surface. The silica

control surface had the lowest water contact angle of 23.3 ± 10.6° which showed that it was the most hydrophilic of the surfaces studied. OTS was the most hydrophobic surface as shown by the water contact angle of 107.1 ± 3.3°. However, the standard deviations (SD) of the water contact angles for OTS (107.1 ± 3.3°) and PFTOS (105.6 ± 3.8°) indicated an overlap in the contact angle values associated with each surface. These two surfaces were therefore very similar in hydrophobicity. A range of water contact angles were obtained for the remaining silanes. The surfaces could be grouped into those which were hydrophilic (bare silica, mPEG-silane, APTMS, and GPTMS) and surfaces which were hydrophobic (TCMS, TCPS, TCOS, TCDS, PFTOS, and OTS) as shown in Table 3-3. The water contact angles obtained in this investigation are in good agreement with those in the literature.

Diiodomethane and ethylene glycol possess a different polarity to that of water (a polar molecule) and are used to probe the polarity, and lipophilicity, of the surface to enable determination of the surface energy. The contact angles for both diiodomethane and ethylene glycol are over a wide range with values going from 39.0 ± 2.0º to 83.0 ±14.5º and from 27.1 ± 8.4º to 88.1 ± 1.9º respectively.

Silane/surface	θ_A water	θ_A diiodomethane	θ_A ethylene glycol	value of θ_A for water from literature
Glass (control)	23.3 ± 10.6	51.2 ± 3.0	27.1 ± 8.4	29 ± 1[a]
mPEG-silane	42.6 ± 2.5	39.0 ± 2.0	30.3 ± 1.6	48 ± 2[b]
GPTMS	44.0 ± 10.9	45.6 ± 5.5	35.7 ± 3.4	44.3 ± 1.6[c]
APTMS	50.2 ± 6.2	43.1 ± 6.1	38.1 ± 5.3	54.5[d]
TCMS	97.5 ± 4.2	64.4 ± 3.0	72.3 ± 5.5	100[e]
TCPS	97.9 ± 2.4	63.8 ± 3.1	75.1 ± 3.0	87[f]
TCOS	100.9 ± 2.5	66.9 ± 0.8	88.1 ± 1.9	107[g]
TCDS	100.4 ± 4.2	69.2 ± 3.5	84.3 ± 2.7	-
OTS	107.1 ± 3.3	70.7 ± 2.2	87.3 ± 6.8	109[h]
PFTOS	105.6 ± 3.8	83.0 ± 14.5	83.5 ± 10.4	117 ± 2[i]

θ_A units °; values ± SD taken at room temperature; [a](Lamprou et al., 2010c); [b](Kang et al., 2007); [c](Lee et al., 2005); [d](Song et al., 2006); [e](Blackman and Harrop, 1968); [f](Felbel et al., 2004); [g](Cao et al., 2001); [h](Flinn et al., 1994); [i](Noel et al., 2004);-, no literature value found.

Table 3-3. Advancing contact angles (θ_A) of the probe liquids on silanised surfaces.

The value for the surface energy (γ) related to a hydrophilic or hydrophobic surface works conversely to the water contact angle, i.e. a high surface energy value signifies a hydrophilic surface (e.g. γ of 44 ± 3 for an –OH terminal group (Lamprou et al., 2010a)) and a low surface energy value indicates a hydrophobic surface (γ of 15 ± 2 for a -CF_3 terminated silane (Lamprou et al., 2010a). The SAM with the lowest surface energy and therefore the most hydrophobic was PFTOS with a γ value of 13.77 ± 1.9 mJ m^{-2} (Table 3-4). The SAM which was the most hydrophilic of those studied and consequently had the highest surface energy was mPEG-Silane, with a γ of 43.67 ± 0.6 mJ m^{-2}. The SAMs produced by mPEG-Silane, GPTMS and APTMS were all more hydrophilic in nature than the glass control. The remaining silanes

(excluding PFTOS) were hydrophobic with the surface energy differing by approximately 4 mJ m^{-2} between them (Table 3-4).

Silane/ surface	γ_s^{LW} (mJ m^{-2})	γ_s^+ (mJ m^{-2})	γ_s^- (mJ m^{-2})	γ_s (mJ m^{-2})	γ_s value from literature (mJ m^{-2})
Glass(control)	33.61 ± 1.0	0.21 ± 0.1	64.36 ± 2.7	40.78 ± 2.3	40.79[a]
mPEG-Silane	40.53 ± 1.6	4.88 ± 4.0	41.49 ± 4.2	43.67 ± 0.6	-
GPTMS	36.62 ± 3.0	1.11 ± 2.1	42.34 ± 17.3	41.52 ± 3.6	45.02[b]
APTMS	37.94 ± 3.2	2.75 ± 3.6	35.32 ± 10.2	42.06 ± 1.6	53[c]
TCMS	26.08 ± 1.7	1.46 ± 1.4	2.39 ± 1.0	26.70 ± 2.0	-
TCPS	26.38 ± 1.8	2.62 ± 3.4	2.13 ± 1.5	27.03 ± 1.6	-
TCOS	25.16 ± 1.3	4.12 ± 3.3	2.14 ± 1.5	25.26 ± 0.7	-
TCDS	23.31 ± 2.0	1.78 ± 2.3	3.24 ± 1.7	24.41 ± 2.7	18.5-19.1[d]
OTS	22.51 ± 0.3	1.09 ± 1.6	1.16 ± 1.2	23.20 ± 0.6	23e
PFTOS	12.5 ± 1.3	0.73 ± 0.5	3.08 ± 1.7	13.77 ± 1.9	21[f]

Values ± SD; other symbols in Methods; [a](Szymczyk and Janczuk, 2008); [b](Cortese et al., 2011); [c](Tormoen et al., 2004); [d](Miura et al., 1998); [e](Saha et al., 2011); [f](Noel et al., 2004); -, no literature value found.

Table 3-4. Surface energies (γ_s) calculated from the mean values of advancing contact angles on the silanised surfaces.

3.4.2 Atomic force microscopy (AFM)

3.4.2.1 Silane-coated glass surfaces

The dimensions of the AFM cantilever tips used were measured using a confocal microscope with a measuring function (DXR Raman, Confocal Microscope, Thermo Scientific, UK) for calculation of the accurate spring constant (Table 3-5). This is required for the determination of the force of adhesion (F_{ad}) between the functionalised tip with mAb-1 attached and the surfaces coated with silane, surfactant and HSA.

Tip	l / µm	w / µm	t / µm	k / N m^{-1}
SD	± 0.1	± 0.1	± 0.02	± 0.02
1	129.5	29.6	0.58	0.23
2	127.7	27.2	0.58	0.22
3	129.5	29.6	0.58	0.23
4	128.6	26.6	0.58	0.21
5	129.1	26.0	0.58	0.21

Table 3-5. Measured values of cantilever length l, width w and thickness t; and calculated values of k for each cantilever used.

F_{ad} values were obtained using a silicon nitride probe and J-scanner for the silanised, surfactant coated and HSA coated glass surfaces. Examples of force distance curves are shown in Figure 3-11 with (a) indicating a 'good' curve and (b) a 'bad' curve. A 'good' curve is one in which there is a straight line detachment with the point at which the interaction is broken being sharp and well defined. A 'bad' curve has more than one interaction between mAb-1 and the surface. As the cantilever is retracted from the surface one interaction will break but due to the presence of more than one interaction the cantilever is pulled back towards the surface before the interaction is broken. Each individual force versus distance curve was analysed with those which were determined to be 'bad' discarded from the F_{ad} calculation.

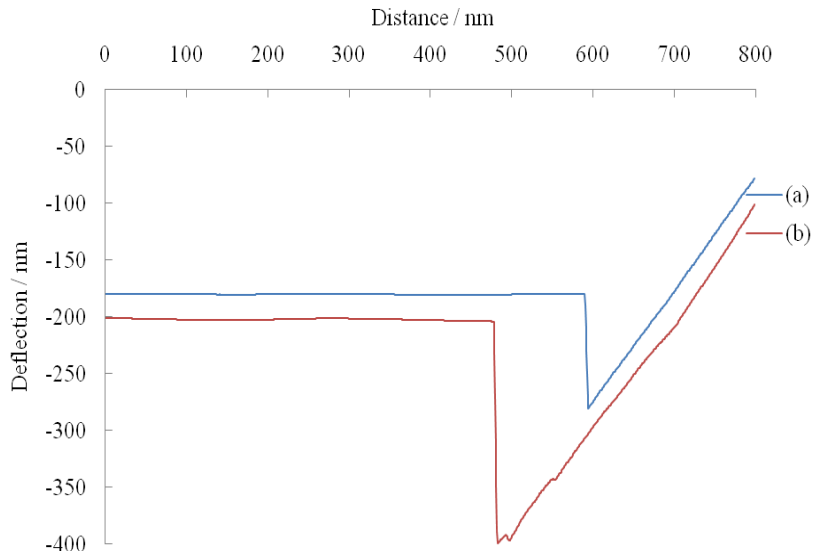

Figure 3-11. Typical examples of force-distance curves obtained; over 95% of the curves were of type (a) and could therefore be used in analysis of force of adhesion.

The F_{ad} values for mAb-1 to the silane-coated glass surfaces are separated into two clear groups (Figure). The F_{ad} was greater to the surfaces which were hydrophilic (glass, mPEG-Silane, GPTMS, APTMS) than to the surfaces which were hydrophobic (TCMS, TCPS, TCOS, TCDS, PFTOS, OTS). The F_{ad} of mAb-1 to the hydrophilic surfaces ranged from 36.28 for APTMS to 46.67 nN for glass and for the hydrophobic surfaces from 11.66 for TCOS to 18.38 for TCDS (Mean Adh/nN). These data show that mAb-1 is weakly attracted to a hydrophobic surface, and conversely it is attracted to a hydrophilic surface.

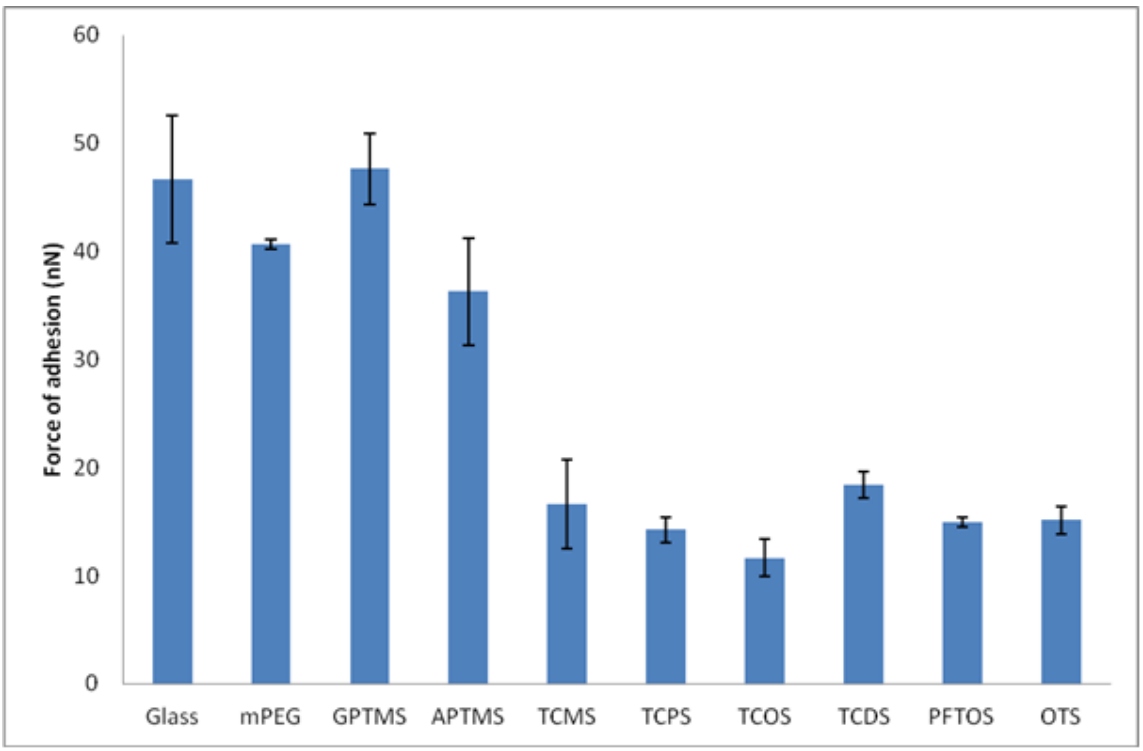

Figure 3-12. Force of adhesion (F_{ad}) values for the interaction between the oriented mAb-1 and the silanised glass surfaces. *n*=4 and the error bars represent the standard deviation (SD).

3.4.2.2 Tween coated glass surfaces

The contact angles of water, diiodomethane and ethylene glycol on Tween 20 and Tween 80 coated glass surfaces were determined with the results indicating that both surfactants produced a hydrophilic surface (Table 3-6). The contact angles for the three liquids on the surfaces which had been coated with Tween 20 below and above its CMC (section 2.3.2, Table 2-2) were highly similar to that for the control glass surface with the exception of ethylene glycol on a 1 mM Tween 20 coated surface. The Tween 80 coated surface at a concentration below its CMC was more hydrophobic than above the CMC or surfaces coated with Tween 20. The low concentration of Tween 80 used to obtain a concentration below the CMC may have

led to a different Tween surface arrangement, or incomplete surface coating. Tween 80 above the CMC produced, as for Tween 20, a hydrophilic surface.

Tween/surface	θ_A water	θ_A diiodomethane	θ_A ethylene glycol	θ_A value for water from literature
Glass (control)	23.3 ± 10.6	51.2 ± 3.0	27.1 ± 8.4	29 ± 1[a]
0.05 mM Tween 20	25.0 ± 3.9	48.1 ± 1.8	27.0 ± 4.8	-
1 mM Tween 20	28.3 ± 2.5	51.2 ± 3.1	19.3 ± 2.9	-
5 µM Tween 80	41.5 ± 10.1	49.2 ± 3.1	34.1 ± 4.4	-
1 mM Tween 80	36.6 ± 4.2	45.3 ± 2.4	22.6 ± 6.0	-

θ_A units °; values ± SD taken at room temperature; [a](Lamprou et al., 2010c)

Table 3-6. Advancing contact angles (θA) of the probe liquids on the Tween coated surfaces.

The contact angles obtained for the two Tween 20 concentrations were similar as also observed for Tween 80 concentrations. However, this was not found to be the case for surface energy (Table 3-7). Surfaces which had been coated with Tween 20 and 80 below their CMC had a surface energy value close to that of the glass control (which would suggest an incomplete surface coating): 39.96 ± 0.6 and 40.26 ± 1.0 mJ m^{-2} for Tween 20 and 80 respectively compared to 40.78 ± 2.3 mJ m^{-2} for glass. Above the CMC, the surface energy values for Tween 20 and 80 were virtually identical, 44.69 ± 0.6 and 44.74 ± 1.6 mJ m^{-2} respectively.

Tween/ surface	γ_s^{LW} (mJ m^{-2})	γ_s^+ (mJ m^{-2})	γ_s^- (mJ m^{-2})	γ_s (mJ m^{-2})	value of γ_s from literature (mJ m^{-2})
Glass (control)	33.61 ± 1.0	0.21 ± 0.1	64.36 ± 2.7	40.78 ± 2.3	40.79[a]
0.05 mM Tween 20	35.6 ± 0.8	2.99 ± 1.2	63.20 ± 1.9	39.96 ± 0.6	-
1 mM Tween 20	33.57 ± 0.8	0.56 ± 0.1	55.50 ± 0.8	44.69 ± 0.6	-
5 µM Tween 80	34.7 ± 1.2	3.14 ± 5.0	45.24 ± 12.7	40.26 ± 1.0	-
1 mM Tween 80	36.85 ± 0.8	0.36 ± 0.2	46.22 ± 1.8	44.74 ± 1.6	-

Values ± SD; other symbols in Methods; [a](Szymczyk and Janczuk, 2008);

Table 3-7. Surface energies (γ_s) calculated from the mean values of advancing contact angles on the Tween coated surfaces.

Surfactants like Tween are commonly used to prevent protein surface adsorption and it was therefore important to determine the level of attraction the Tween-coated surfaces had for mAb-1. The F_{ad} values for mAb-1 to a surface coated with Tween 20 below its CMC did not differ from that of the glass control, 45.25 ± 0.28 compared to 46.67 ± 5.9 nN respectively (Figure 3-13). MAb-1 adhesion to the 1 mM Tween 20-coated surface was marginally greater than to 0.05 mM Tween 20 with a F_{ad} of 52.2 ± 1.0 nN. MAb-1 was weakly attraced to surfaces coated with Tween 80 below its CMC (35.44 ± 0.26 nN), conversely, mAb-1 showed the highest level of adhesion to a surface coated with Tween 80 above its CMC (62.03 ± 0.30 nN).

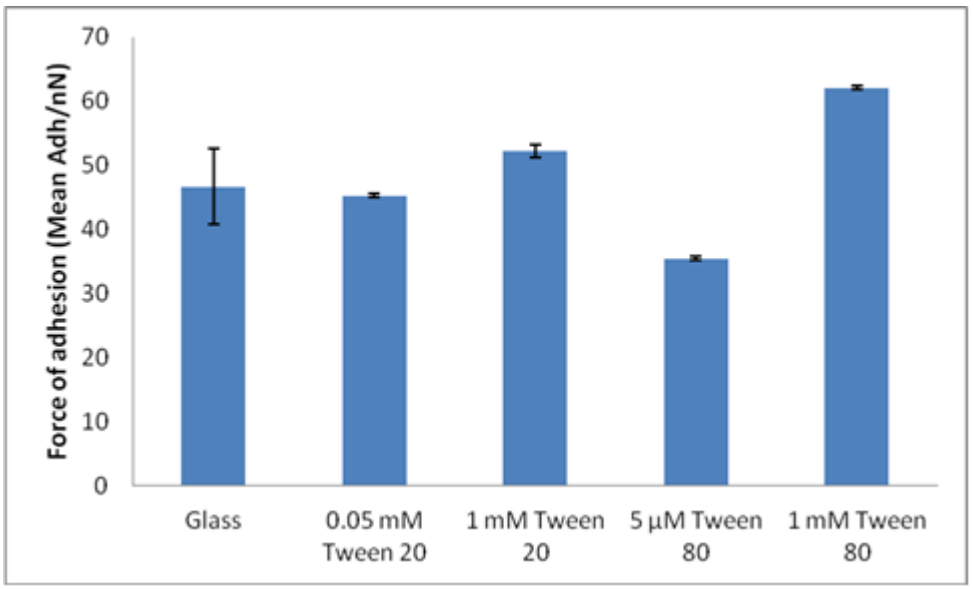

Figure 3-13. Force of adhesion (F_{ad}) values for the interaction between the oriented mAb-1 and the Tween coated glass surfaces. n=4 and the error bars represent the standard deviation.

3.4.2.3 Tween coated OTS glass surfaces

Investigation of mAb-1 adsorption to both hydrophilic and hydrophobic surfaces was carried out using TIRF (4.3.3.3). The surface energy of a silica surface coated with Tween was established (3.4.2.2) and so it was important to determine the surface energy of a hydrophobic surface coated with Tween. Additionally, plastic surfaces such as polystyrene are hydrophobic (3.4.2.6) and so by characterising the OTS surface coated with Tween (OTS was used in the TIRF experiments) would allow a greater understanding the effect Tween inclusion in formulations has on surface energy. This would allow conclusions to be made regarding the effect of surface energy on adsorption.

The surfaces which had first been coated with OTS prior to Tween remained hydrophobic (Table 3-8). Coating of the surface with 1 mM Tween 80 produced a more hydrophobic surface than OTS alone.

Tween/ surface	θ_A water	θ_A diiodomethane	θ_A ethylene glycol	value of θ_A for water from literature
Glass (control)	23.3 ± 10.6	51.2 ± 3.0	27.1 ± 8.4	29 ± 1[a]
OTS	107.1 ± 3.3	70.7 ± 2.2	87.3 ± 6.8	-
0.05 mM Tween 20	106.9 ± 4.2	69.6 ± 3.7	85.7 ± 4.2	-
1 mM Tween 20	102.9 ± 5.1	70.5 ± 2.8	79.9 ± 5.5	-
5 µM Tween 80	105.5 ± 3.6	69.8 ± 1.5	89.2 ± 1.2	-
1 mM Tween 80	110.3 ± 3.5	69.3 ± 2.6	83.1 ± 3.0	-

θ_A units °; values ± SD taken at room temperature; [a](Lamprou et al., 2010c)

Table 3-8. Advancing contact angles (θA) of the probe liquids on the Tween coated OTS surfaces.

The surface energy of the Tween coated OTS surfaces were very similar to that of OTS alone (Table 3-9). Coating of the OTS surface with Tween therefore had very little effect on the surface characteristics examined here.

Tween/ surface	γ_s^{LW} (mJ m^{-2})	γ_s^+ (mJ m^{-2})	γ_s^- (mJ m^{-2})	γ_s (mJ m^{-2})	Literature value of γ_s (mJ m^{-2})
Glass (control)	33.61 ± 1.0	0.21 ± 0.1	64.36 ± 2.7	40.78 ± 2.3	40.79[a]
OTS	22.51 ± 0.3	1.09 ± 1.6	1.16 ± 1.2	23.20 ± 0.6	-
0.05 mM Tween	23.13 ± 2.0	0.18 ± 0.1	1.10 ± 1.5	23.97 ± 2.6	-
1 mM Tween 20	22.59 ± 1.2	0.89 ± 1.3	1.24 ± 0.8	23.15 ± 1.5	-
5 µM Tween 80	22.99 ± 0.2	0.24 ± 0.1	1.88 ± 1.0	24.33 ± 0.6	-
1 mM Tween 80	23.28 ± 0.9	2.02 ± 1.1	4.44 ± 4.3	23.29 ± 0.9	-

Values ± SD; other symbols in Methods; [a](Szymczyk and Janczuk, 2008);

Table 3-9. Surface energies (γ_s) calculated from the mean values of advancing contact angles on the Tween coated OTS surfaces.

3.4.2.4 Pluronic coated glass surfaces

The coating of glass surfaces with the four Pluronic surfactants produced a wide range of water contact angles from 19.3 to 46.2° (Table 3-10). Surfaces which had been coated with Pluronic P103 or P123 were more hydrophilic than either Pluronic L43 or L61. A glass surface coated with Pluronic P123 at a concentration of 1 μM produced the most hydrophilic surface of those investigated, 19.3 ± 5.4°. Contact angles for diiodomethane varied by approximately 8° whereas a much wider variety was observed for ethylene glycol with angles ranging between ~17 and 56°.

Pluronic/surface	θ_A water	θ_A diiodomethane	θ_A ethylene glycol	Literature value of θ_A for water
Glass (control)	23.3 ± 10.6	51.2 ± 3.0	27.1 ± 8.4	29 ± 1[a]
5 μM P103	22.6 ± 6.6	48.5 ± 1.6	18.9 ± 5.2	-
1 mM P103	39.6 ± 12.8	48.9 ± 2.6	20.0 ± 3.5	-
1 μM P123	19.3 ± 5.4	50.1 ± 3.3	21.1 ± 4.6	-
0.1 mM P123	27.0 ± 5.5	48.5 ± 2.3	16.9 ± 3.1	-
1 mM L43	46.1 ± 3.4	54.9 ± 3.1	56.1 ± 20.5	-
5 mM L43	44.3 ± 4.5	55.9 ± 4.0	33.0 ± 5.7	-
0.05 L61	42.9 ± 5.0	52.7 ± 1.6	53.4 ± 8.5	-
0.5 L61	46.2 ± 4.4	55.0 ± 2.1	33.6 ± 11.6	-

θ_A units °; values ± SD taken at room temperature; [a](Lamprou et al., 2010c)

Table 3-10. Advancing contact angles (θA) of the probe liquids on the Pluronic coated surfaces.

The water contact angles demonstrated that the Pluronic coated glass surfaces had a wide range of wettability (Table 3-10). As found for Tween coated glass surfaces, the surface energy of the Pluronic surfaces did not differ greatly from the control (Table 3-11). Although the water contact angle for Pluronic L43 and L61 was higher

than that of the glass surface, the surface energy was not found to differ apart from for Pluronic L43 below its CAC. The Pluronic surfaces are all hydrophilic and so it would be expected that mAb-1 F_{ad} values to these surfaces would be high.

Pluronic/ surface	γ_s^{LW} (mJ m^{-2})	γ_s^+ (mJ m^{-2})	γ_s^- (mJ m^{-2})	γ_s (mJ m^{-2})	Literature value of γ_s (mJ m^{-2})
Glass (control)	33.61 ± 1.0	0.21 ± 0.1	64.36 ± 2.7	40.78 ± 2.3	40.79[a]
5 µM P103	35.11 ± 0.4	0.25 ± 0.1	67.36 ± 0.2	43.28 ± 0.1	-
1 mM P103	34.85 ± 1.2	0.79 ± 0.4	42.27 ± 17.2	45.40 ± 1.5	-
1 µM P123	33.9 ± 2.4	0.30 ± 0.1	64.69 ± 2.3	42.91 ± 0.8	-
0.1 mM P123	35.09 ± 0.5	0.44 ± 0.1	57.81 ± 1.1	45.2 ± 0.1	-
1 mM L43	31.50 ± 1.5	1.13 ± 1.2	51.41 ± 16.0	45.93 ± 11.2	-
5 mM L43	30.93 ± 1.9	0.58 ± 0.1	41.85 ± 2.7	40.69 ± 2.3	-
0.05 mM L61	32.78 ± 0.3	0.33 ± 0.1	58.86 ± 3.4	41.08 ± 1.8	-
0.5 mM L61	31.45 ± 0.8	0.64 ± 0.2	38.72 ± 2.3	41.31 ± 2.1	-

Values ± SD; other symbols in Methods; [a](Szymczyk and Janczuk, 2008);

Table 3-11. Surface energies (γ_s) calculated from the mean values of advancing contact angles on the Pluronic coated surfaces.

The level of adhesion exhibited by mAb-1 for the Pluronic surfaces was greater than that to the control glass surface. The Pluronic surfaces were in general more hydrophilic than bare silica (Table 3-11) and it was therefore expected they would exhibit stronger adhesion to mAb-1. Figure 3-14 shows that the F_{ad} of mAb-1 to the different Pluronic surfaces was similar with two exceptions, being below and above the average. The level of adhesion of mAb-1 to Pluronic P103 below its CAC was

the lowest value found (54.84 ± 6.8 nN) while the highest adhesion was exhibited between mAb-1 and the Pluronic L61 surface below its CAC (85.58 ± 0.36 nN). The F_{ad} for the remaining Pluronic surfaces was in the range from approximately 64 to 74 nN.

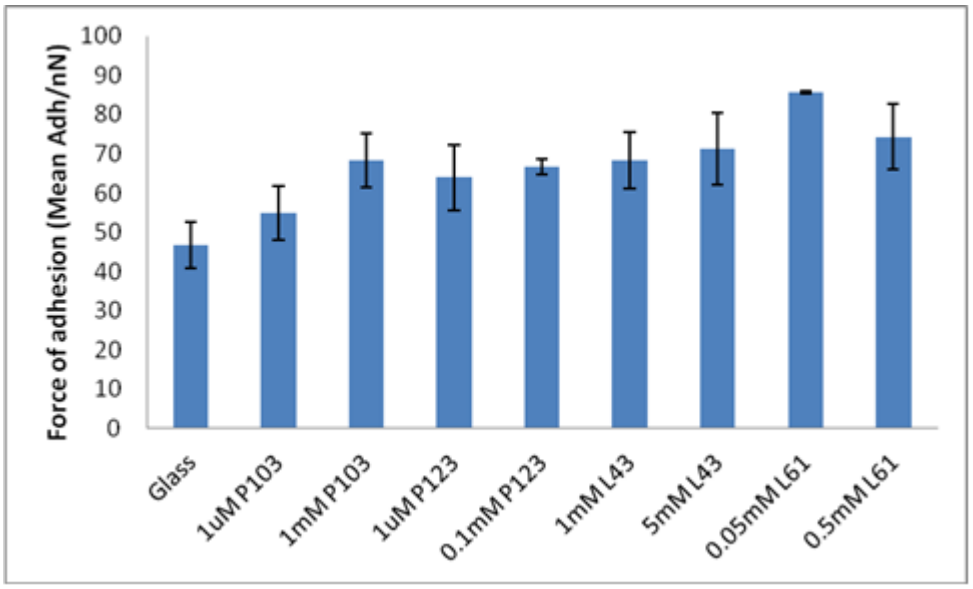

Figure 3-14. Force of adhesion (F_{ad}) values for the interaction between the oriented mAb-1 and the Pluronic coated glass surfaces. *n*=4 and the error bars represent the standard deviation.

3.4.2.5 Human serum albumin (HSA) coated glass surface

HSA has a number of uses within the pharmaceutical industry including fusion proteins (e.g. Albutropin™ (Chou et al., 2005)) and microspheres for drug targeting (Wunderlich et al., 2000), it was therefore informative to examine its effect on surface wettability and protein adhesion as an alternative to surfactant use for the reduction of protein adsorption. The water contact angles for a surface coated with HSA at 2.5 and 12.5 % (w/v) show a surface which is more hydrophobic than glass

(Table 3-12). The ethylene glycol contact angles were higher than for glass but the values for diiodomethane were very similar.

Human serum albumin/surface	θ_A water	θ_A diiodomethane	θ_A ethylene glycol	value of θ_A for water from literature
Glass (control)	23.3 ± 10.6	51.2 ± 3.0	27.1 ± 8.4	29 ± 1[a]
2.5 %	62.7 ± 4.4	49.9 ± 3.2	43.1 ± 7.6	63.5[b]
12.5 %	65.8 ± 6.1	49.1 ± 2.4	42.1 ± 3.8	63.5[b]

θ_A units °; values ± SD taken at room temperature; [a](Lamprou et al., 2010c), [b](Vanoss et al., 1986)

Table 3-12. Advancing contact angles (θA) of the probe liquids on the Human serum albumin (HSA) coated surfaces.

The surface energy values for HSA coated glass show a surface which is hydrophilic with a value similar to that of glass alone (Table 3-13). The concentration of HSA used to coat the surface did not affect the surface energy.

Human serum albumin/ surface	γ_s^{LW} (mJ m^{-2})	γ_s^+ (mJ m^{-2})	γ_s^- (mJ m^{-2})	γ_s (mJ m^{-2})	value of γ_s from literature (mJ m^{-2})
Glass (control)	33.61 ± 1.0	0.21 ± 0.1	64.36 ± 2.7	40.78 ± 2.3	40.79[a]
2.5 %	34.17 ± 1.4	2.72 ± 3.9	21.24 ± 3.6	38.98 ± 2.7	
12.5 %	34.8 ± 0.9	0.44 ± 0.2	16.68 ± 4.3	39.91 ± 0.3	

Values ± SD; other symbols in Methods; [a](Szymczyk and Janczuk, 2008);

Table 3-13. Surface energies (γ_s) calculated from the mean values of advancing contact angles on the Human serum albumin (HSA) coated surfaces.

MAb-1 was weakly attracted to surfaces which had been coated with HSA at 2.5 and 12.5 % (w/v) (Figure 3-15). As with surface energy, the concentration of HSA used to coat the surface did not affect the F_{ad} value obtained for mAb-1 as shown by the

F_{ad} values obtained being 17.76 ± 0.11 and 18.16 ± 0.15 nN for 2.5 and 12.5 % w/v HSA respectively. The surface energy of the bare silica and HSA coated surfaces is similar; however, the F_{ad} values are different. This shows that the nature of the surface coating, as opposed to the surface energy, determines the strength of mAb-1 adhesion.

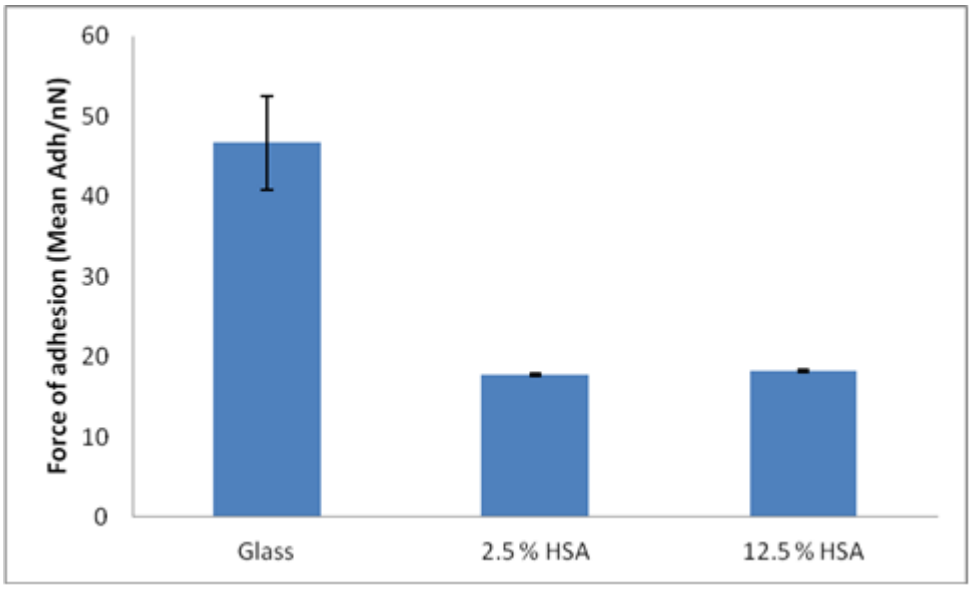

Figure 3-15. Force of adhesion (F_{ad}) values for the interaction between the oriented mAb-1 and the Human serum albumin (HSA) coated glass surfaces. *n*=4 and the error bars represent the standard deviation.

3.4.2.6 Polystyrene contact angle and surface energy

The contact angles of the three probe liquids on a polystyrene surface were measured in order to compare the values with those obtained for the silanised surfaces. The water contact angle measurements showed that the polystyrene surface was hydrophobic (Table 3-14) but the surface energy value did not differ significantly from that of the glass control (Table 3-15).

Surface	θ_A water	θ_A diiodomethane	θ_A ethylene glycol	value of θ_A for water from literature
Glass (control)	23.3 ± 10.6	51.2 ± 3.0	27.1 ± 8.4	29 ± 1[a]
Polystyrene	82.4 ± 5.5	46.6 ± 3.2	49.1 ± 4.6	

θ_A units °; values ± SD taken at room temperature; [a](Lamprou et al., 2010c)

Table 3-14. Advancing contact angles (θA) of the probe liquids on the polystyrene surface.

Surface	γ_s^{LW} (mJ m^{-2})	γ_s^+ (mJ m^{-2})	γ_s^- (mJ m^{-2})	γ_s (mJ m^{-2})	value of γ_s from literature (mJ m^{-2})
Glass (control)	33.61 ± 1.0	0.21 ± 0.1	64.36 ± 2.7	40.78 ± 2.3	40.79[a]
Polystyrene	36.13 ± 1.3	0.47 ± 0.1	3.7 ± 0.6	38.76 ± 1.2	

Values ± SD; other symbols in Methods; [a](Szymczyk and Janczuk, 2008);

Table 3-15. Surface energies (γs) calculated from the mean values of advancing contact angles on the polystyrene surfaces.

3.4.3 'Solid-state' circular dichroism (CD)

3.4.3.1 MAb-1 adsorption to silanised silica beads

The structure of mAb-1 adsorbed on the silane-coated silica beads was dependent upon surface energy (Figure 3-17 and Figure 3-18). The CD spectra show that the native β-sheet motif is maintained upon adsorption to silica and the silica beads which had been coated with GPTMS and mPEG-Silane. An example of the empirical correction is shown in Figure 3-16 with a value of 1.62 required to correct for absorption flattening at 220 nm.

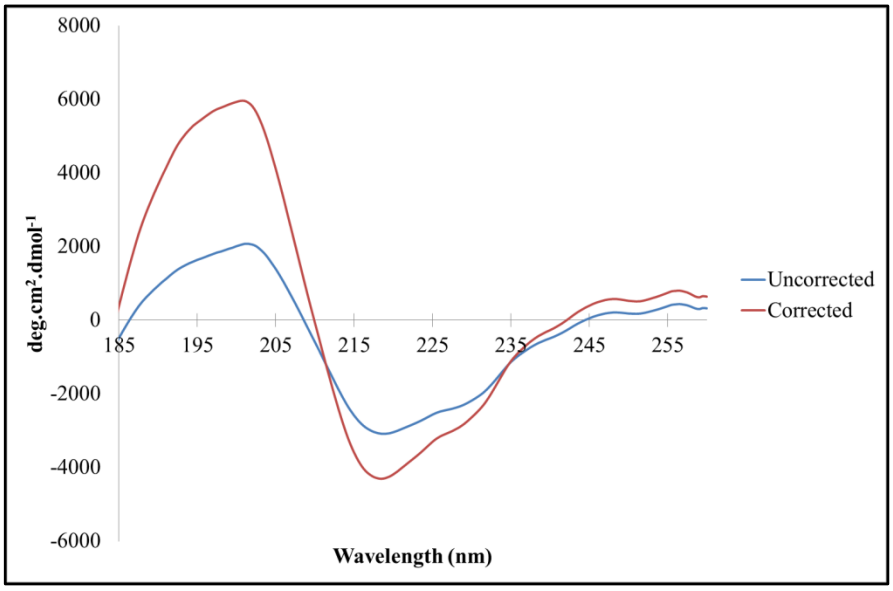

Figure 3-16. An example of the empirical correction of mAb-1 adsorbed to APTMS coated silica beads.

Of the hydrophilic surfaces, APTMS caused the largest degree of mAb-1 structural perturbation (Figure 3-17). The characteristic peak at ~195 nm and trough at 215 nm typical of a β-sheet containing protein were evident. The effect of a hydrophobic surface on the secondary structure of mAb-1 upon adsorption to the silane-coated silica beads was very different (Figure 3-18). A large loss of native mAb-1 secondary structure occurred as signified by a shift in the maxima peak at 195 nm and a flattening of the spectra. The loss of mAb-1 secondary structure was most pronounced upon adsorption to TCMS-coated silica beads. The spectrum was flat compared to the control, and spectra obtained for adsorption to the hydrophilic surfaces, which is suggestive of extensive unfolding of mAb-1. Although a degree of the native secondary structure was lost upon adsorption to the TCDS, TCOS, TCPS, OTS and PFTOS coated silica beads, the spectra is characteristic of a random coil and not complete unfolding.

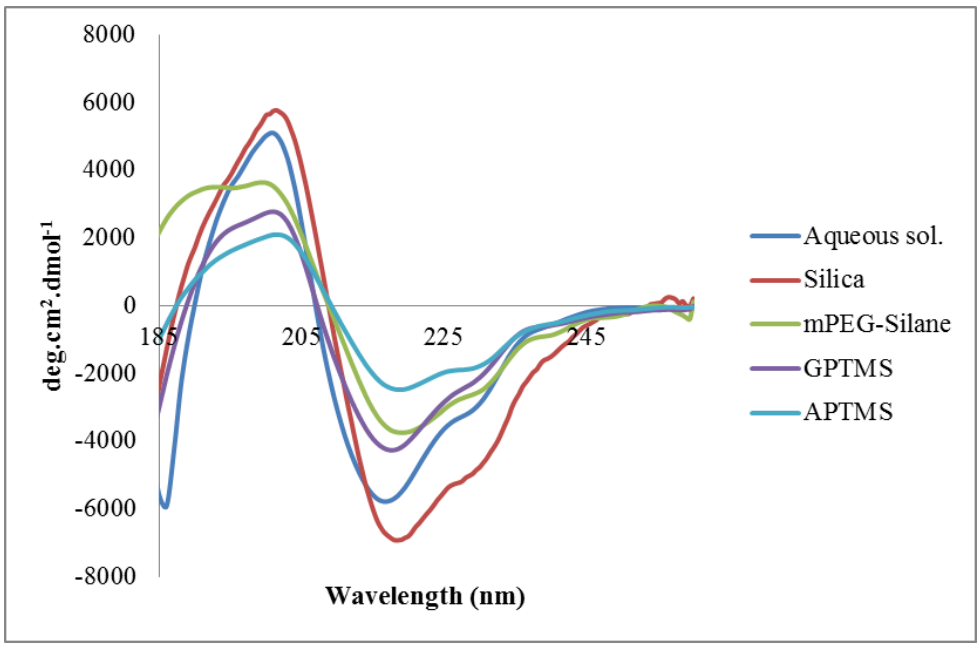

Figure 3-17. Effect of adsorption to hydrophilic surfaces on mAb-1 secondary structure.

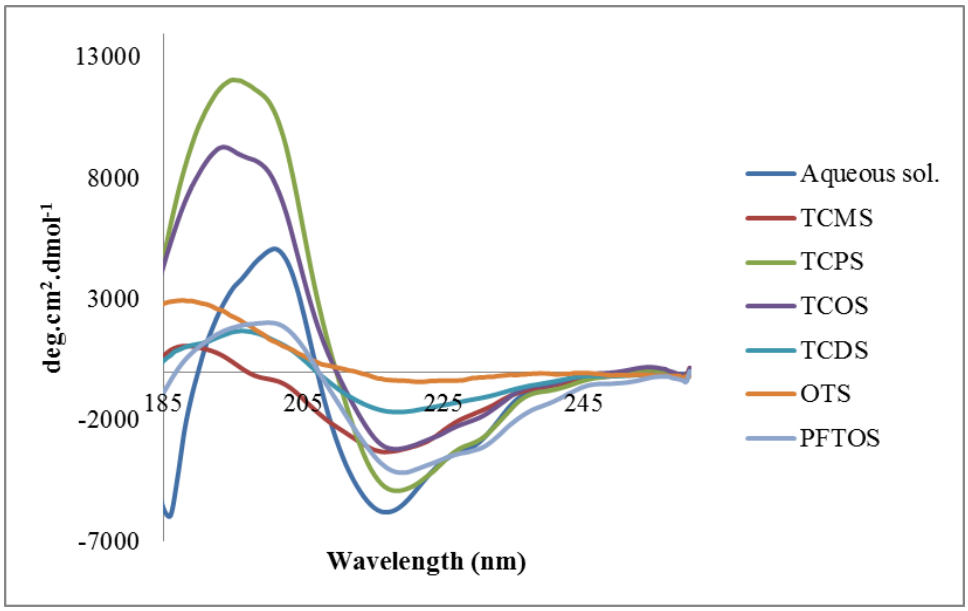

Figure 3-18. Effect of adsorption to a hydrophobic surface on mAb-1 secondary structure.

3.4.3.2 BSA adsorption to silanised silica beads

The adsorption of the α-helix containing BSA onto silane-coated silica surfaces resulted in a different outcome to that of mAb-1 (Figure 3-19). A large proportion of the native BSA α-helical structure (Figure 3-20) was lost upon adsorption to the hydrophilic GPTMS and mPEG-Silane surfaces. The native secondary structure was, however, retained when adsorbed to silica and APTMS which are both hydrophilic surfaces. The interaction between BSA and the silane terminal groups on the hydrophilic surfaces influenced the degree to which the native secondary structure was retained. This is less evident for BSA adsorption to hydrophobic surfaces with the native structure being retained when adsorbed to PFTOS only. The CD spectrum was slightly weaker than for silica and APTMS which may suggest a small level of unfolding. The CD spectra for BSA on the TCMS, TCPS, TCOS and TCDS surfaces exhibit a similar degree of structural loss which indicated unfolding of the protein.

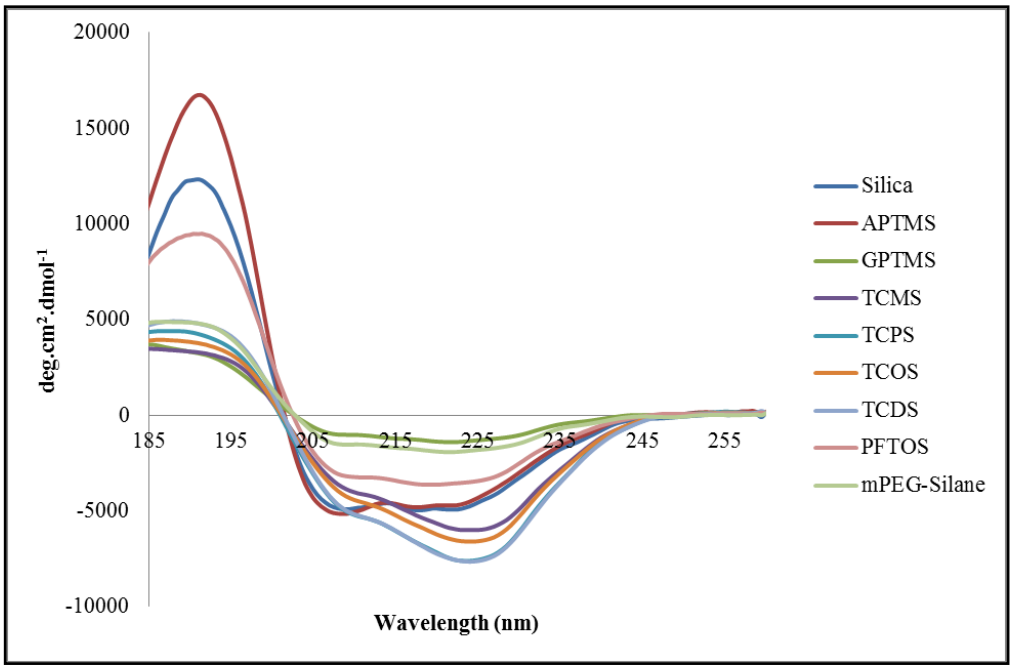

Figure 3-19. Bovine serum albumin (BSA) (spectra corrected for flattening) adsorbed to silica beads (control) and silane-coated silica beads with a range of surface hydrophobicities.

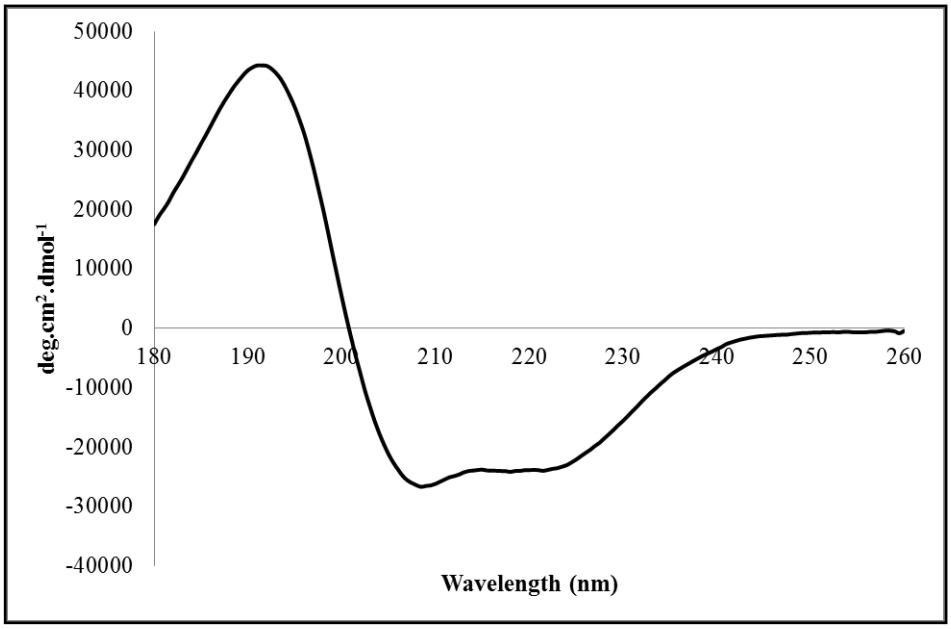

Figure 3-20. Bovine serum albumin secondary structure spectra generated by CD.

3.4.3.3 MAb-1 adsorbed to Tween coated silica beads

The Tween coated glass surfaces had been characterised in terms of their surface energy and the F_{ad} between the surface and mAb-1. The final step was to investigate adsorption of mAb-1 to these surfaces. The CD spectra obtained for mAb-1 adsorbed to the Tween coated silica beads showed that the native secondary structure was retained (Figure 3-21). The characteristic peak and trough associated with the β-sheet motif were present, maxima at ~195 nm and minima at ~215 nm. This finding correlates well with that of mAb-1 adsorption to the silane-coated silica surfaces in which the native structure was retained when adsorbed to a hydrophilic surface.

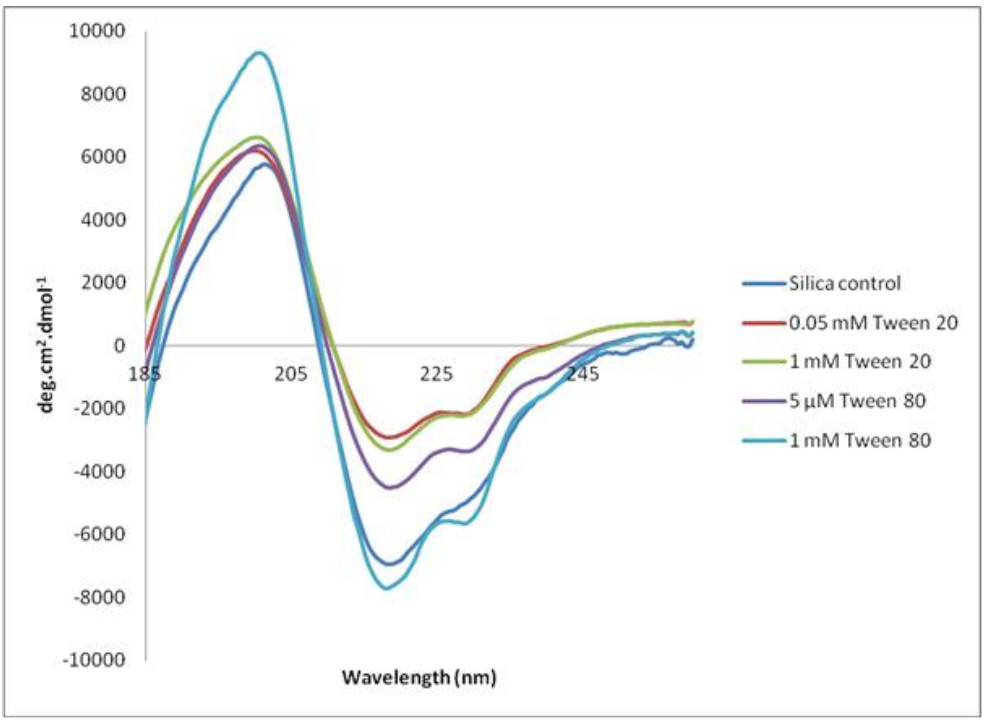

Figure 3-21. Secondary structure of mAb-1 adsorbed to Tween coated silica beads investigated using 'solid-state' circular dichroism.

3.4.4 Dichroweb analysis

3.4.4.1 MAb-1 secondary structure content on silanised beads

The Dichroweb analysis of mAb-1 in aqueous solution is consistent with a protein containing a high content of the β-sheet motif. The percentage of β-sheet is 51 % and the data showed that mAb-1 did not contain any α-helix (Table 3-16). The loss of native mAb-1 structure is indicated by an increase in the quantity of α-helix, β-turn and random coil with the consequent decrease in the percentage of β-sheet (Table 3-16). The nrmsd values, which indicate a good level of fit, were below 0.2 with the exception of TCMS and OTS surfaces. As the structure of immunoglobulins is mainly comprised of β-sheet, the change in the fraction of β-sheet calculated using the CONTIN algorithm in Dichroweb was used to quantify any changes in structure.

The largest loss of β-sheet fraction calculated by the CONTIN algorithm was for the hydrophobic surfaces (20-30 %) which correlates with the unfolding observed in the CD spectra. Correspondingly, the β-sheet fraction calculated for the hydrophilic surfaces showed a small level of native β-sheet loss (9-12 %). As an exception, despite the fact that TCOS, TCPS and OTS surfaces are hydrophobic the decrease in β-sheet fraction was less than or equivalent to that observed on the hydrophilic surfaces (Table 3-16). However, the nrmsd value generated for the OTS surface was above the value accepted to be representative of a good level of fit between the CD spectra and the secondary structure it is being compared with.

SAM surface	α-helix	β-sheet	β-turn	random coil	nrmsd
MAb-1 in aq. solution	0.00	0.51	0.10	0.37[a]	0.068
MAb-1 adsorbed to silica	0.06	0.42	0.12	0.39	0.061
MAb-1 adsorbed to mPEG-Silane	0.01	0.42	0.11	0.39	0.035
MAb-1 adsorbed to APTMS	0.04	0.39	0.12	0.45	0.122
MAb-1 adsorbed to GPTMS	0.06	0.39	0.12	0.40	0.084
MAb-1 adsorbed to TCMS	0.15	0.30	0.13	0.42	0.390[b]
MAb-1 adsorbed to TCPS	0.02	0.50	0.12	0.36	0.011
MAb-1 adsorbed to TCOS	0.01	0.47	0.12	0.38	0.008
MAb-1 adsorbed to TCDS	0.04	0.43	0.13	0.37	0.032
MAb-1 adsorbed to PFTOS	0.10	0.21	0.16	0.48	0.142
MAb-1 adsorbed to OTS	0.08	0.37	0.15	0.39	1.208[b]

[a], Dichroweb does not necessarily generate a total value of 1.0

[b], higher than the generally acceptable limit of < 0.2, using the Self Consistent Method.

Table 3-16. Fraction secondary structure elements for mAb-1 adsorbed to silane coated silica beads and in solution (control), calculated using the Dichroweb online server.

3.4.4.2 BSA structure on silane coated silica beads

Analysis of the CD spectra using Dichroweb showed that BSA was largely composed of α-helices with a low percentage of the β-sheet motif (Table 3-17). The Dichroweb analysis indicated that the BSA lost a large proportion of its native structure upon adsorption to both the hydrophilic and hydrophobic surfaces. The content of β-sheet increased for all surfaces as did the percentage of random coil. The

nrmsd values demonstrate that the fitting of the data to the reference set meets the 'goodness of fit' standard.

SAM surface	α-helix	β-sheet	β-turn	random coil	nrmsd
BSA in aq. solution	0.51	0.15	0.12	0.22	0.003
BSA adsorbed to bare silica	0.05	0.41	0.15	0.38	0.011
BSA adsorbed to APTMS	0.04	0.43	0.16	0.37	0.010
BSA adsorbed to GPTMS	0.02	0.55	0.10	0.31	0.089
BSA adsorbed to mPEG-silane	0.03	0.47	0.12	0.34	0.037
BSA adsorbed to TCMS	0.08	0.39	0.13	0.39	0.050
BSA adsorbed to TCPS	0.17	0.29	0.14	0.39	0.058
BSA adsorbed to TCOS	0.17	0.29	0.14	0.39	0.057
BSA adsorbed to TCDS	0.08	0.38	0.15	0.39	0.051
BSA adsorbed to PFTOS	0.04	0.43	0.14	0.37	0.016

Table 3-17. Percentage fraction of the secondary structure elements for bovine serum albumin (BSA) adsorbed to silane coated silica beads and in solution (control), calculated using the Dichroweb online server.

3.4.4.3 MAb-1 adsorption to Tween surfaces

The same Dichroweb algorithm and reference set were used to analyse mAb-1 adsorbed to the Tween coated silica beads. However, despite subtraction of the Tween control data from that of mAb-1, a high nrmsd value was generated for adsorption to Tween 20 and 80 surfaces below their CMC (Table 3-18). The α-

helical content for mAb-1 on all four Tween surfaces was approximately 10 % higher than the control with the corresponding β-sheet content being 10 % less. This would suggest that although the 'solid-state' CD spectra appear similar to the control, there is some loss of mAb-1 structure upon adsorption to the hydrophilic Tween surfaces.

Tween surface	α-helix	β-sheet	β-turn	random coil	nrmsd
MAb-1 in aq. solution	0.00	0.51	0.10	0.37[a]	0.068
MAb-1 adsorbed to silica	0.06	0.42	0.12	0.39	0.061
0.05 mM Tween 20	0.11	0.40	0.13	0.36	0.411[b]
1 mM Tween 20	0.10	0.41	0.12	0.36	0.151
5 μM Tween 80	0.10	0.40	0.12	0.39	0.355[b]
1 mM Tween 80	0.14	0.39	0.11	0.37	0.175

[a], Dichroweb does not necessarily generate a total value of 1.0

[b], higher than the generally acceptable limit of < 0.2, using the Self Consistent Method.

Table 3-18. Fraction secondary structure elements for mAb-1 adsorbed to Tween coated silica beads and in solution (control), calculated using the Dichroweb online server.

3.4.5 Correlation between water contact angle and mAb-1 structure

To investigate if a correlation existed between the water contact angle of the silane-coated silica surfaces and 'solid-state' CD spectra, water contact angle was plotted against the 'solid-state' CD peak and trough values at 195 and 218 nm (these values corresponded to the maxima and minima in the CD spectra respectively). The data

were grouped into two sets, although the data points within were quite dispersed, which could be assigned to surfaces which were hydrophilic and hydrophobic (Figure 3-22 and Figure 3-23). The data do not display evidence of a correlation between water contact angle and the degree of mAb-1 structural perturbation. The ratio of the mean residue molar ellipticity values at 195 and 218 nm were also plotted against water contact angle (Appendix B, Figure 8-7). As was the case when plotting mean residue molar ellipticity at a single wavelength, groups of data points were evident, three compared to two, but a correlation was not identified.

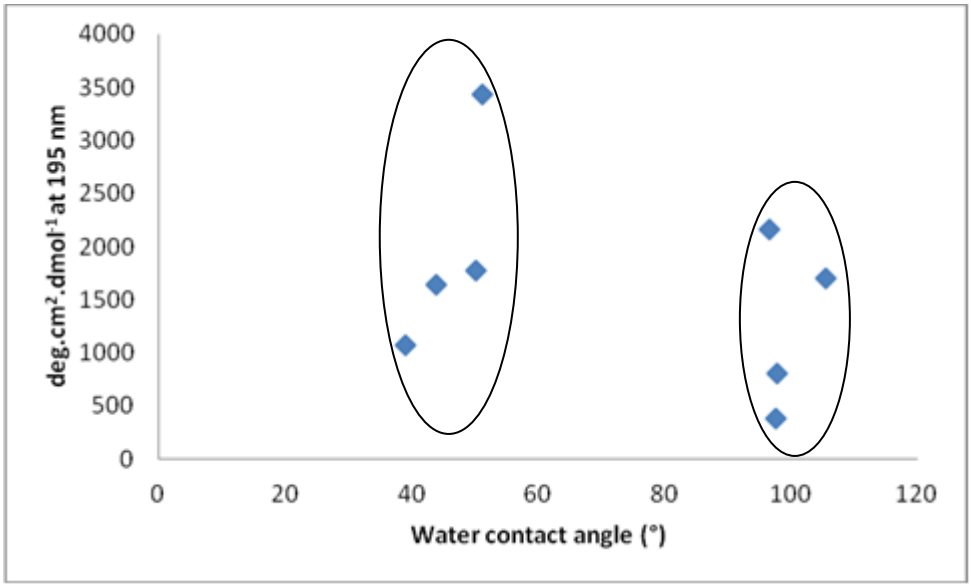

Figure 3-22. Water contact angle against 'solid-state' CD mAb-1 peak at 195 nm.

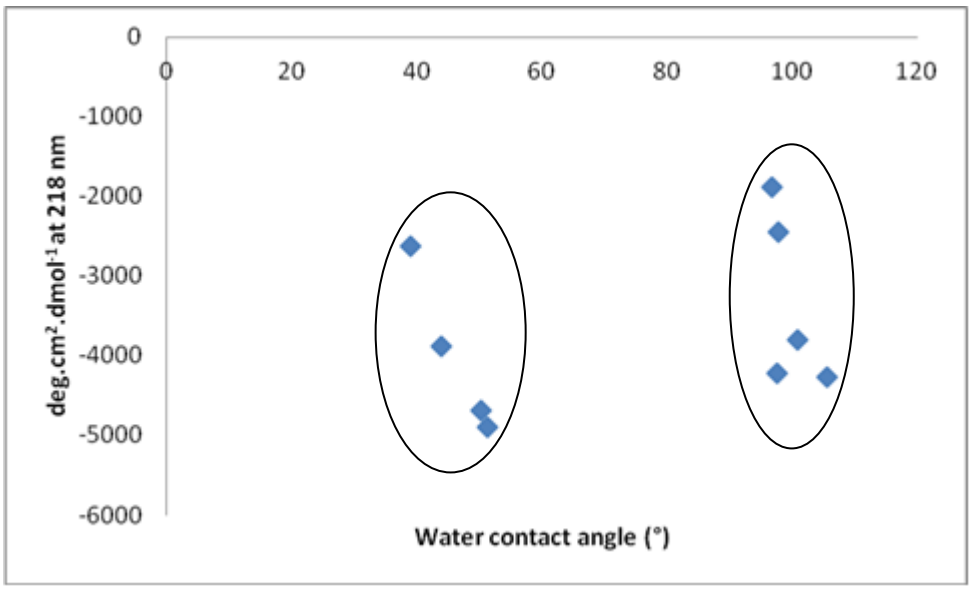

Figure 3-23. Water contact angle against mAb-1 trough in the 'solid-state' CD spectra at 218 nm.

3.4.5.1 Influence of surface energy on retention of mAb-1 structure

The mean residue molar ellipticity values at 195 and 218 nm when plotted against the surface energy for the silane-coated surfaces are approximately grouped into those corresponding to hydrophilic (γ ca. 40 mJ m^{-2}) and hydrophobic surfaces (γ ca. 25 mJ m^{-2}) (Figure 3-24 and Figure 3-25). From Figure 3-24 and Figure 3-25 it is concluded that a direct correlation between surface energy and mAb-1 secondary structure retention does not exist. The ratio between the maxima and minima peaks, at 195 and 218 nm respectively, was also plotted against surface energy but a correlation was not found to exist (Appendix B, Figure 8-8).

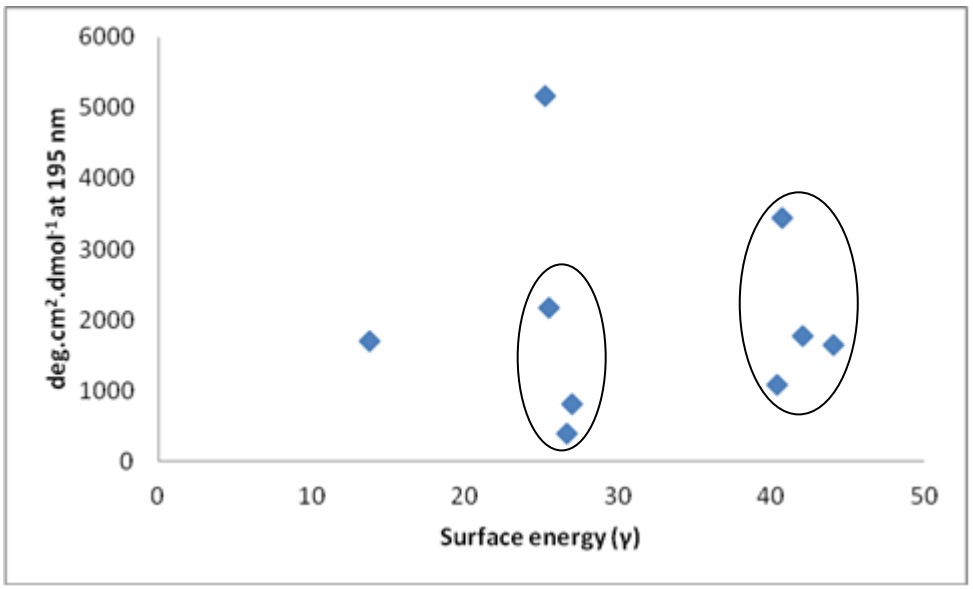

Figure 3-24. Surface energy against mAb-1 'solid-state' CD spectra peak at 195 nm.

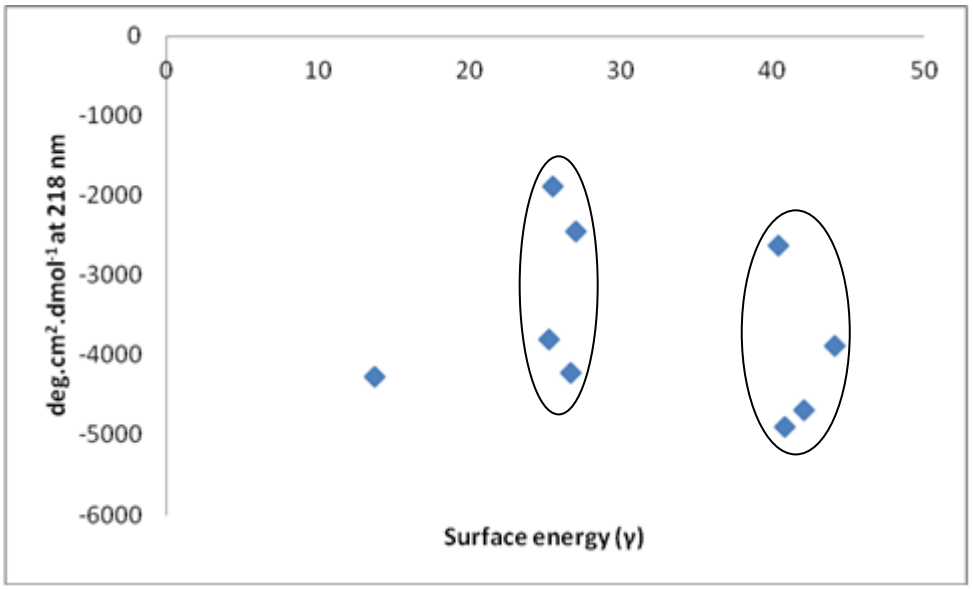

Figure 3-25. Surface energy against mAb-1 'solid-state' CD spectra trough at 218 nm.

3.4.5.2 Effect of surface wettability on mAb-1 force of adhesion

F_{ad} values for mAb-1 to the silane-coated surfaces when plotted against both water contact angle and surface energy did not show evidence of a correlation. As was the case with the 'solid-state' peak data, the F_{ad} values could be grouped into two clear

sets when plotted against water contact angle (Figure 3-26) corresponding to hydrophilic (values at ca. 40°) and hydrophobic surfaces (values at ca. 100°). The scenario for F_{ad} plotted against surface energy was similar with the exception of PFTOS (surface energy value of 13.77 ± 1.9 mJ m^{-2}) which did not fall into either the hydrophilic or hydrophobic surface groups (Figure 3-27).

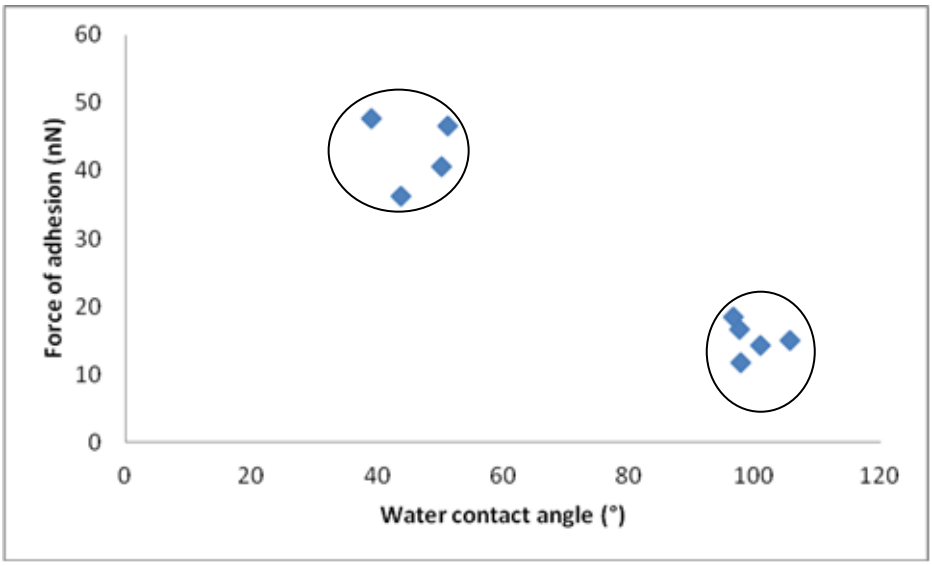

Figure 3-26. Water contact angle against the force of adhesion (nN) of mAb-1.

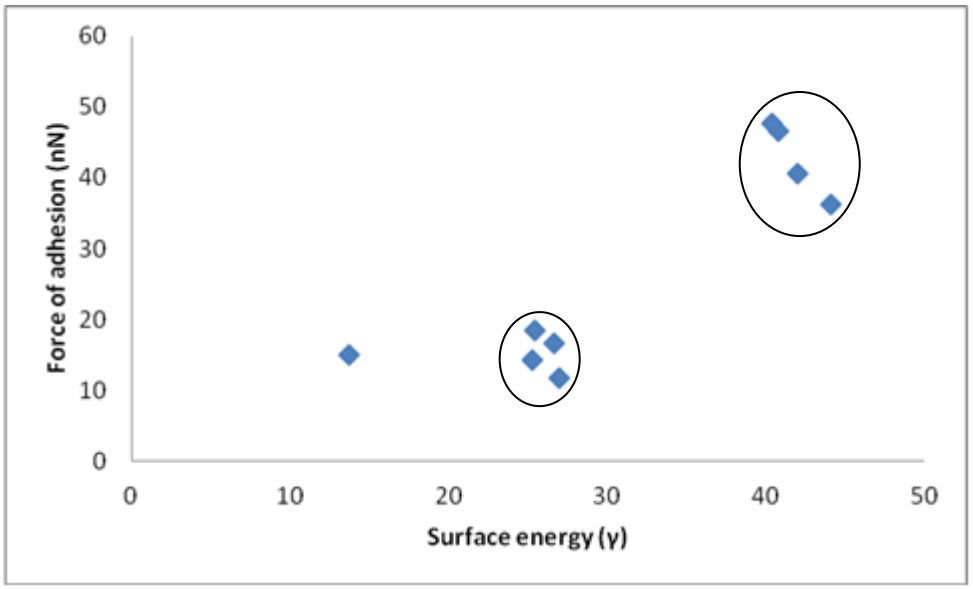

Figure 3-27. Surface energy against force of adhesion (nN) of mAb-1.

3.5 Discussion

3.5.1 Characterisation of silanised surfaces

The silanes were selected to mimic the surface characteristics of the materials a protein is likely to encounter during processing such as plastics and metal. It is not possible to use either of these two surfaces for secondary structure analysis using CD, thus the reason for the formation of SAMs on silica beads. A range of silanes were selected to coat the silica surfaces to investigate a possible a correlation between surface energy and mAb-1 native structure could be identified. The identification of a correlation was allow predictions to be made regarding the effect of different surfaces encountered during processing on protein structure and surface adsorption.

The water contact angle and surface energy values of the silanised surfaces were found to differ from the silica control which showed the silanisation reaction was successful and thus could be further analysed with respect to their effect on mAb-1 adhesion and structure. The hydrophobicity of the silanised surfaces were classified on the basis that a water contact angle above 90° indicated a hydrophobic surface and below this value a hydrophilic surface (Giovambattista et al., 2007, Feng et al., 2002). Comparison of the bare silica surface (control) with the silanised surfaces showed that the control was the most hydrophilic surface (Table 3-3) as indicated by the low water contact angle for this surface. The silane terminal groups which face the air/surface interface determine the wettability of the surface. The water contact angles showed that APTMS, GPTMS and mPEG-Silane all generated hydrophilic surfaces. The amine terminal group of APTMS, the cyclic ether terminal group of GPTMS and the methoxy terminal group of mPEG-silane were responsible for the

low water contact angles. These terminal groups have previously been shown to produce a hydrophilic surface, and therefore a low water contact angle (Kang et al., 2007, Lee et al., 2005, Song et al., 2006).

In contrast, the terminal groups of the trichlorosilanes produced a surface which was hydrophobic. The terminal methyl group of TCMS, the propyl group of TCPS, octyl of TCOS and the dodecyl group of TCDS all conferred hydrophobicity. The octadecyl group of OTS, which likewise terminates in a methyl group, also generated a hydrophobic surface with the terminal perfluorooctyl group of PFTOS producing a hydrophobic surface. The water contact angles and surface energy values of the silanised surfaces are similar to those previously reported in the literature (Table 3-3 and Table 3-4). Fluorinated alkanethiol SAMs have previously been shown to produce a surface with low wettability and therefore a high water contact angle with angles of 122 ± 2, 117 ± 1, 121 ± 2 and 113 ± 1° (Tamada et al., 1998). The structure on the surface produced by PFTOS is different to that produced by the trichlorosilanes. The structures of the trichlorosilanes are linear with hydrogen atoms being the side chain and the chain length being the differentiating factor between them (Figure 3-6). The hydrogen molecules of the trichlorosilanes and those available on the surface of mAb-1 will interact with each other. Fluorinated alkanethiol SAMs were found to form a distorted hexagonal or oblique lattice on a silica surface by AFM. The size of the lattice is increased relative to the simple alkanethiols due to the presence of the bulky perfluorocarbon chain (Tamada et al., 1998).

The SAMs were selected to mimic surfaces, such as polystyrene, which mAb-1 may encounter during processing. The water contact angle of the polystyrene surface was

high with the value being closer to that of the hydrophobic silanes (approximately 82° compared to 97°). However, the surface energy of the polystyrene surface investigated was closest to that of the silica surface. The effect of polystyrene on mAb-1 adhesion and structure is therefore likely to be between the hydrophilic and hydrophobic SAMs.

3.5.2 Characterisation of surfactant coated surfaces

Tween and Pluronic are commonly used surfactants in protein formulations to prevent surface adsorption and aggregation. It was important to determine the water contact angle and surface energy of surfaces coated with these surfactants to enable conclusions to be drawn regarding their effect on mAb-1 adhesion and surface adsorption studied using TIRF (4.4.4.6). Characterisation of surfactant coated surfaces may also aid in the selection of appropriate excipients to reduce adsorption and structural loss.

The silica surfaces which had been coated using Tween 20 and 80 at the two concentrations produced a hydrophilic surface as indicated by the low water contact angles (Table 3-6). The water contact angle of a silicon surface has previously been found to decrease when coated with Tween 20 (Zhang and Ferrari, 1997). In this study, the higher of the two Tween 20 concentrations (1 mM) had the lowest water contact angle of those investigated which is contrary to the findings of Zhang and Ferrari (1997) in which water contact angle was found to increase as the Tween concentration increased above 0.05 % v/v. At concentrations greater than the CMC, it was suggested by Zhang and Ferrari (1997) that the surfactant formed a bilayer or multi-layer, with hydrophobic ‘tails’ pointing into the media. The contact angle for Tween 20 was decreased compared to a concentration below the CMC so the

arrangement is likely to be different. It is possible that the Tween 80 molecules may orientate in the manner suggested by Zhang and Ferrari (1997) as the contact angle was found to be higher than that of the control surface. However, the structure of Tween 80 (Figure 1-6) shows the 'kink' in the (unsaturated) oleic acid tail which would prevent tight packing of the molecules.

The surfaces generated as a result of coating with the four Pluronic surfactants in this study, at concentrations below and above their CAC, were hydrophilic. Pluronic F108 has been shown to form a polymer brush layer on hydrophobic heptylamine and hexamethyldisiloxane surfaces (McLean et al., 2005). It is thought that Pluronic F108 adsorbs to a hydrophobic surface via the methyl groups on the hydrophobic PPO block forming a brush layer (Mclean et al., 2005). However, on a silica surface Pluronic F108 has been shown to form mushroom-like structures which are either isolated or do not interact (Efremova et al., 2000). The Pluronic F108 was expected to have a lower affinity for the silica surface and so form a less dense layer than on a hydrophobic surface which correlates with the repulsive forces found (McLean et al., 2005). The Pluronics used in this study are therefore also likely to have a lower affinity for the silica surface forming less dense layers. This correlates with the low water contact angles found during contact angle goniometry experiments.

3.5.3 Characterisation of HSA coated silica surfaces

Through the determination of the characteristics of a surface coated with HSA and force of adhesion analysis, the hydrophilicity of a protein surface which could form a protein repellent surface was identified. The glass surface coated with HSA produced a relatively hydrophobic surface as indicated by the water contact angles of 62.7° (± 4.4) and 65.8° (± 6.1) for a 2.5% and 12.5% w/v HSA solution respectively. During

interpretation of the water contact angle data for the HSA coated surface, it must be taken into consideration the requirement for the surface to be dry in order to carry out the measurements. Dehydration of proteins can lead to a loss of native structure due to the absence of the hydration (water) shell surrounding the protein (Dong and Shannon, 2000). Although contact angle goniometry will provide information on the hydrophobicity of the surface generated, it is entirely plausible that the structure of the HSA on the surface is different from that adopted when the protein is adsorbed to a surface in a hydrated state. This is demonstrated by the difference in the diameter of an IgG when in a hydrated state (10 nm (Silverton et al., 1977)) compared to dehydrated (52.4 nm (Dong and Shannon, 2000)).

3.5.4 MAb-1 force of adhesion

Functionalization of the AFM probe was performed in this study (attachment of mAb-1 in a specific orientation) for measurement of the F_{ad} between mAb-1 and the coated surfaces which will differ in surface structure as a result of the functionality of the coating. It was a requirement for consistent F_{ad} measurements that non-specific adsorption and adsorption-induced unfolding of mAb-1 on the probe surface were avoided. This required the generation of a mAb-1 monolayer of uniformly orientated mAb-1 molecules on the cantilever tip which was generated as described in 3.3.3.1. The F_{ad} values for an IgG physically and covalently bound to an APTES-mica surface have been shown not to differ and thus the method of mAb-1 attachment was not expected to affect the measured values (You and Lowe, 1996). Non-specific adsorption of the anti-F_c antibody to the amino-functionalised probe was allowed; however, this was not considered to be a problem as free F_c domain binding sites on the primary antibody for mAb-1 would still exist. The silanised

surfaces in this study were shown to be homogeneous and therefore the contribution of non-specific interactions to the force of adhesion would be minimal. In addition, mAb-1 was oriented in a specific manner and therefore interactions which did not involve the F_{ab} domain would be reduced and thus have had a negligible impact.

3.5.5 Force of adhesion (F_{ad}) to silanised surfaces

The F_{ad} between mAb-1 and the silanised surfaces could be separated into two categories, those with a high (ca. 36-47 nN) and a low (ca. 11-16 nN) F_{ad} value. The two groups reflect the terminal groups of the silanes, the hydrophilic surfaces (bare silica and silica coated with mPEG-Silane, GPTMS and APTMS) which interact strongly with mAb-1 and the silanes with a hydrophobic functionality (TCMS, TCPS, TCOS, TCDS, OTS and PFTOS coated silica) which interacted weakly.

The strong F_{ad} observed between mAb-1 and the mPEG-Silane functionalised surface may at first be unexpected. However, it was expected that the mPEG polymer (1000 MW) investigated in this study would produce a well hydrated SAM, as shown by the low water contact angle measurement (Table 3-3), which did not necessarily repel proteins. A PEG of a similar size (2000 MW) to the mPEG studied, has been shown to facilitate protein adsorption as a result of structural rearrangements in the PEG backbone. This was particularly the case when a high compressive protein load was placed on the brush border (Sheth and Leckband, 1997b) which would take place during the AFM F_{ad} measurements. It has been suggested that in situations where a high compressive force is involved, the protein interacts with the ethylene oxide units within the brush border which are exposed due to rearrangement of the PEG backbone. Brush borders which are comprised of short chain tri(ethylene glycol) molecules and are dense in nature have been found to repel proteins (Skoda

et al., 2009) which is in contrast to those with an increased chain length which have been identified as facilitating protein adsorption (Efremova et al., 2001).

A weak interaction was observed between mAb-1 and the alkyl surfaces generated by TCMS, TCPS, TCOS and TCDS. This was also found to be the case for the alkyl SAM produced by OTS. The number of exposed hydrophobic patches on globular proteins such as immunoglobulins in their native state is low which is consistent with the weak F_{ad} values and a restricted capability for interactions to form through dipole-dipole (London dispersion) forces. The F_{ad} between mAb-1 and the perfluorinated (PFTOS) surface was comparable to the values for the alkyl surfaces (

Figure 3-12).

Fluorine is a highly electronegative molecule and possesses a low polarisability (Siegemund et al., 2000). These features of fluorine would be expected to lead to minimal interactions with mAb-1 attached to the AFM probe through dipole-dipole forces. Additionally, the PFTOS surface was both hydrophobic (as shown by the high water contact angle and low surface energy value) and lipophobic (as indicated by the high contact angle for diiodomethane compared to the alkyl surfaces) (Table 3-3). Transient dehydration (due to movement of the water molecules on the surface of the protein or loss of water followed by rehydration) of the mAb-1 molecule, based on the assumption that mAb-1 retained a hydration (water) shell when attached to the AFM probe, when coming into contact with the PFTOS surface may have contributed to the F_{ad} value obtained.

3.5.6 MAb-1 force of adhesion to surfactant coated surfaces

The water contact angle and surface energy data showed the surfactant coated silica surfaces to be hydrophilic (Table 3-6 and Table 3-7). Based on the F_{ad} values for the silanised surfaces, high F_{ad} values between mAb-1 and the surfactant coated surfaces were expected due to the hydrophobicity of the surface. Indeed, this was found to be the case for Tween surfaces with F_{ad} values of approximately 35 to 62 nN. The interaction between mAb-1 and Pluronic coated surfaces was stronger than that for Tween with F_{ad} values from 54 to 85 nN. This finding is similar to the high adhesion force observed at short distances between collagen and Pluronic PE6800 (De Cupere et al., 2003).

MAb-1 F_{ad} values for the Pluronic surfaces are higher than that for glass alone which suggests that there is an interaction between the two. Pluronic F108 has been shown to form a polymer brush layer on hydrophobic heptylamine and hexamethyldisiloxane surfaces (McLean et al., 2005). The repulsive force between Pluronic F108 layers (on the cantilever tip and silica surface) when adsorbed to a hydrophilic silica surface was found to be weak with a range of 6 nm. The Pluronic F108 was expected to have a lower affinity for the silica surface and so form a less dense layer than on a hydrophobic surface which correlates with the repulsive forces found by Mclean et al., (2005). The Pluronics used in this study are therefore also likely to have a lower affinity for the silica surface forming less dense layers. This correlates with the F_{ad} values found between mAb-1 and Pluronic coated surfaces. The adhesion was higher to Pluronic surfaces than the glass control. McLean et al. (2005) explained the attractive force which was found to exist within the silica and Pluronic F108 system to be due to Van der Waals interactions. The same experiment

was carried out for Pluronic F108 on the hydrophobic surfaces but no weak interactions were identified (McLean et al., 2005). AFM force of adhesion measurements determine the direct force and so weak attractive Van der Waals interactions could be dominated by the stronger steric repulsion of two Pluronic layers (McLean et al., 2005). The contact angle and F_{ad} data obtained for the Pluronic surfactants used in this study showed that the PPO block is likely to be facing the surface with the PEO block at the interface with air (dry) or aqueous (wetted). This is shown by determination of the Pluronic surfaces to be hydrophilic which correlates with the hydrophilic PEO group facing away from the silica. The F_{ad} measurements for mAb-1 to the Pluronic coated surfaces were high which correlates with the surface being hydrophilic. Pluronics have previously been found to form a hydrophilic polymer brush border on a surface which is in agreement with the surface energy and F_{ad} data in this study (Alexandridis et al., 1994) and also with the findings for the silane-coated surfaces in this study. It has been found that the length of the PEO block influences protein repulsion with longer PEO blocks conferring a greater degree of steric repulsion undergone by a protein when coming into contact with the surface (McGurk et al., 1999). The highest F_{ad} value was observed for Pluronic L61 which had the shortest PEO block in this study supporting the finding of McGurk et al., (1999) (the length of the PEO blocks of the Pluronics selected in this study are shown in Table 2-1). Pluronic P103 was shown to have the lowest F_{ad} but the PEO block was shorter than for Pluronic P123 by 3 monomers which may indicate an influence of PPO block length on adhesion.

In this study, F_{ad} measurements were not carried out with BSA attached to the probe but they have previously been determined for selected surfaces using an AFM

cantilever functionalised with BSA. A non-specific interaction between BSA and a glass surface was identified which was prevented when the surface had been coated with BSA or a PEG (mPEG(2K)-Maleimide) (Celik and Moy, 2012). Petri dishes which were coated with Pluronic F 180NF also prevented a non-specific interaction with the BSA (Celik and Moy, 2012). Pluronic has also been shown to inhibit adhesion of albumin to a polystyrene surface by coating the surface with 0.1 % (w/v) Pluronic F127 and reduced from 7.0 ± 0.7 nN to 2.8 and 1 nN by 0.1 % (w/v) Pluronic L35 and 61 respectively (McGurk et al., 1999). This is in contrast to the F_{ad} values observed between mAb-1 and Pluronic coated glass surfaces found in this work.

3.5.7 MAb-1 force of adhesion to HSA coated silica surfaces

The F_{ad} between mAb-1 and surfaces coated with HSA at two concentrations (2.5 and 12.5 % w/v) were 17.76 ± 0.11 and 18.16 ± 0.15 nN respectively. The F_{ad} values for the HSA coated surfaces are significantly less than the 47.67 nN found for glass. This variation does not result from differences in the calculated surface energy values as they were very similar as indicated by the values of 38.98 ± 2.7 and 39.91 ± 0.3 mJ m^{-2} for HSA compared to 40.78 ± 2.3 mJ m^{-2} for silica. This may, however, be explained by the water contact angle of the HSA surfaces being greater than that of the silica control (Table 3-12). The HSA coated surface weakly attracted mAb-1 to a similar extent to the silanised surfaces (Figure 3-12 and Figure 3-15). An advantage of HSA use over the silanes is that it is a non-toxic molecule as demonstrated by a clinical trial showing that neither HSA nor recombinant HSA caused an immunogenic response (Bosse et al., 2005).

Clear binding forces (between 0.2 and 1.8 nN) have been observed between human IgG attached to a functionalised AFM cantilever and rat anti-human IgG immobilised on a surface. The interaction was not observed when a tip which had not been functionalised was used and only a small binding interaction detected when the human IgG coated tip was blocked demonstrating the interaction was largely due to specific binding (Lv et al., 2010). The adhesion force between anti-ovalbumin IgG and its antigen (ovalbumin), which is a specific interaction, is affected by approach time. A sufficient time period is required for the IgG to adopt the correct orientation to interact with the antigen. The pull-off force was generally larger when the IgG was in a specific orientation compared to when non-specifically attached (Brogan et al., 2004). The adhesion force between the IgG and ovalbumin or BSA was almost equal demonstrating the influence of non-specific interactions. The force of unbinding of an antigen from an orientated antibody single-chain Fv fragment (scFv) has been found to be from 40 ± 3 to 50 ± 4 pN depending on the mutation of the scFv (Ros et al., 1998). The force of unbinding of an antibody (polyclonal anti-HSA antibody) covalently linked to an AFM tip via an 8 nm long PEG derivative and HSA was 244 ± 22 pN (Hinterdorfer et al., 1996). This value is 4 times that observed by Ros et al., (1998) which may be due to differences in the strength of the interaction or additional binding with a greater number of domains of the intact antibody.

3.5.8 MAb-1 secondary structure analysis by 'solid-state' CD

The surface chosen for the storage vessel and use in the delivery method can have an effect upon the immunoglobulin structure within a formulation. A loss of native structure can lead to the formation of aggregates in solution and consequently a loss of function and an immunogenic response. A substantial change in subtilisin

Carlsberg secondary structure upon adsorption to a solid surface has been identified using 'solid-state' CD (Ganesan et al., 2006). The authors developed an empirical correction method to adjust for absorption flattening experienced by proteins adsorbed to surfaces. This technique was used to correct the spectra for both mAb-1 and BSA adsorbed to surfaces in this study. A different method to correct for absorption flattening has recently been developed using the chiral tris(ethylenediamide)Co(III) complex (Gerdova et al., 2011). This method corrects for the distribution of particles within a suspension as they are unlikely to be homogeneously distributed throughout the cell. The number of particles the light will pass through has the potential to vary from zero upwards. Using different distributions of tris(ethylenediamide)Co(III) within a sephadex bead suspension, the authors found that the absorption flattening of the CD spectra could be corrected accurately using the correct theoretical model (Gerdova et al., 2011).

3.5.8.1 MAb-1 structural changes on hydrophilic silanised surfaces

The far UV spectrum of mAb-1 in solution (Figure 2-16) showed a protein containing a large proportion of the β-sheet motif, which was expected based on knowledge of mAb-1 structure. Structural changes in mAb-1 adsorbed to hydrophilic and hydrophobic surfaces were evaluated based on the reference spectrum obtained for mAb-1 in solution. The CD spectra for mAb-1 adsorbed to the bare silica surface showed that the native β-sheet structure was largely retained (Figure 3-17). The positive elliptical maxima at 202 nm (approximately 5000 $deg.cm^2.dmol^{-1}$) and the trough representing the minima negative ellipticity at 218 nm (-6000 $deg.cm^2.dmol^{-1}$) observed in solution were also seen in the spectrum of mAb-1 on bare silica. A shoulder in the CD spectrum of mAb-1 on the bare silica is evident at 230 nm which

is known to arise in proteins as a result of the aromatic amino acid contribution in the far UV region (Krittanai and Johnson, 1997). The contribution of the aromatic residues to the ellipticity can be either negative, as was the case in this study, or positive (Khan et al., 1989). The native β-sheet secondary structure was also largely maintained when adsorbed to the hydrophilic mPEG-Silane and GPTMS surfaces with a reduction in the positive and negative maxima and minima. An IgG has previously been shown to retain its native structure upon adsorption to hydrophilic silica beads which correlates well with the data in this study (Giacomelli et al., 1999).

The positively charged APTMS beads caused the most noteworthy loss of mAb-1 secondary structure of the hydrophilic surfaces. In the buffers in this study which were near neutral, aminosilanisation (undertaken in this study using APTMS) has previously been shown to transform the net negative charge on the surface of bare silica into a net positive charge (Metwalli et al., 2006). Adsorption of mAb-1 to the silanised beads was carried out in pH 7.4 buffer in this study; at this pH mAb-1 will have a net positive charge as its pI is 8.99. Despite the similar charge of APTMS-coated beads and the protein, mAb-1 was not anticipated to be repelled by the APTMS surface, as charge distribution on protein surfaces is not uniform. The shoulder at 230 nm observed in mAb-1 spectra in solution and on the other hydrophilic surfaces was more prominent on the APTMS surface (this could not be correlated to surface characteristics or the measured F_{ad}). The shoulder is representative of the local environment surrounding the aromatic residues and so the increased strength of the shoulder is likely to be due to an increase in the rigidity of the residues as a result of surface adsorption (Pereira et al., 2008). The findings for

mAb-1 structural changes are consistent with previous investigations into the structure of an immunoglobulin-like domain pair adsorbed to a hydrophilic and hydrophobic surface (Pereira et al., 2008). Changes were observed in the spectra for both the secondary structure and the aromatic environment, which is indicative of tertiary structure (Pereira et al., 2008).

The tertiary structure of mAb-1 on the silanised surfaces was not investigated here as a sufficient concentration for analysis of the near UV could not be achieved (mAb-1 surface concentration on the beads was approximately 100-150 µg/mL). The contribution to the spectrum of the aromatic residues and disulphide bonds is weak and so the concentration required is higher than that for investigation of the secondary structure. It has been suggested that the orientation of an IgG on a surface is the main factor influencing the adsorbed concentration (Buijs et al., 1995). 'Solid state' CD is not able to determine the orientation of mAb-1 on the surfaces studied, although it does provide information on the folded state of the protein. The orientation of mAb-1 on a silicon and an OTS-coated silicon substrate have been investigated using neutron reflectometry (4.5.9).

3.5.8.2 MAb-1 structural changes induced by a hydrophobic surface

The CD spectra of mAb-1 adsorbed to the hydrophobic silanised beads (TCMS, TCOS, TCPS, TCDS, PFTOS and OTS) displayed a varying level of structural loss (Figure 3-17). The degree of denaturation was not consistent across the hydrophobic surfaces despite the surface energy of TCMS, TCPS, TCOS and TCDS being found not to differ (Table 3-4). The degree of mAb-1 unfolding on PFTOS was similar to that for the alkyl silanes although the surface energy is approximately half the value, 13.77 compared to ca. 25.85 mJ m^{-2}, for the alkyl silanes. Adsorption to silica beads

coated with OTS also resulted in structural loss due to unfolding but to a level which did not differ to the other silanes studied. A correlation was not found between surface energy or water contact angle and the degree of mAb-1 denaturation on the silanised surfaces (Figure 3-22 to Figure 3-25). The silanised beads prepared using TCMS, and which had a methyl terminal group, displayed the greatest quantity of mAb-1 unfolding. The CD spectrum represented an increase in the quantity of random coil with a subsequent decrease in β-sheet. The spectrum was no longer characteristic of a β-sheet as evidenced by the positive ellipticity at 202 nm having diminished, a shift in the minima to 216 nm and a loss of the shoulder at 230 nm.

A hydrophobic surface was also found to differently affect the secondary structure and stability of F_{ab} and F_c fragments of an IgG after adsorption as studied by DSC and CD (Vermeer et al., 2001). It has been found that adsorption results in denaturation of the F_{ab} fragment with the F_c fragment retaining its structure, which is due to the higher hydrophobicity of the F_{ab} fragment (Vermeer et al., 2001). This feature may become relevant during the production of chimeric and humanised antibodies. A study into the binding of an IgG to hydrophobic surfaces found that binding occurred between the hinge region and the C_H2 domain of the F_c fragment through the use of a reactant adsorptive membrane bioreactor separator (RAMBS) system (Yu and Ghosh, 2010). The finding was confirmed through digestion of adsorbed immunoglobulin using papain and pepsin and analysis of the digested immunoglobulin fragments (Yu and Ghosh, 2010). RAMBS utilises a stack of adsorptive membranes held in a temperature controlled atmosphere which the IgG binds to with any remaining proteins flowing through the system. The bound IgG is then digested using enzymes to determine the regions involved in surface adsorption.

As shown by the CD spectra in this study (Figure 3-17) and the findings of Vermeer et al., (2001) and Yu and Ghosh (2010), the material selected for the storage vessel can have an effect upon immunoglobulin structure and binding characteristics. This in turn may influence the aggregation potential and the eventual adverse immunogenic effect of the protein.

As the surface produced by the HSA is hydrophobic, based on the data produced in this study and from the literature it would be expected that mAb-1 would lose a degree of its native secondary structure. However, as the surface coating is a protein it would be expected to be different to that generated by the SAMs and its effect on mAb-1 structure may vary. It was not possible using the 'solid-state' CD technique to investigate mAb-1 adsorption on HSA coated beads. CD spectra are produced through an averaging of the left and right circularly polarised light (Kelly and Price, 2000, Kelly et al., 2005) and so HSA itself would produce a CD spectrum which would combine with that of mAb-1. This would lead to a combined spectrum not representative of the structure of either of the proteins alone.

3.5.8.3 Effect of surface adsorption on BSA secondary structure

The α-helical structure of the BSA when adsorbed to the silane-coated is affected differently to that of the β-sheet containing mAb-1. The 'solid-state' CD spectra show that the BSA loses a degree of its native structure upon adsorption to all the SAM surfaces studied (both hydrophilic and hydrophobic) apart from silica and APTMS. A smaller quantity of native structural loss was identified for adsorption to the hydrophobic PFTOS surface. A previous study, using FTIR reflection spectra, has also shown the secondary structure of BSA upon adsorption to a hydrophilic surface (Germanium hydroxide, GeOH) to be perturbed (Jeyachandran et al., 2010).

The adsorption of human fibrinogen and albumin to SAMs with the terminal groups CH_3, OH, NH_2, COOH and CF_3 on gold surfaces has been studied (Sivaraman et al., 2009). The surface chemistry of the SAM was the mitigating factor in the degree of conformational changes to the fibrinogen and albumin secondary structures. The loss of α-helix increased with surface hydrophobicity for both fibrinogen and albumin (Sivaraman et al., 2009). This was also observed for BSA adsorbed to the SAM surfaces in this study. The β-sheet content of fibrinogen, albumin (Sivaraman et al., 2009) and BSA (in this investigation) increased with the loss of α-helix and so the change in conformation would be better classified as refolding than denaturation. The loss of the percentage of α-helix in the native structure of albumin has been found to increase over a period of 6 months when adsorbed to both a hydrophilic SAM (OH terminal group) and a hydrophobic SAM (CH_3 terminal group) (Sivaraman and Latour, 2012). The decrease in α-helix motif is greater on the hydrophobic surface, from approximately 65 to 25 %, compared to a loss of 30% observed for the hydrophilic surface. In this study, the reduction in the percentage of α-helix motif in BSA in this study was greater on the hydrophilic APTMS, GPTMS and mPEG-Silane surfaces than on the hydrophobic surfaces terminating with a CH_3 group, which is contrary to the observations of Sivaraman et al. (2012). These differences in structural loss (between BSA, fibrinogen and albumin) show that proteins which are composed mainly of the same secondary structure motif (α-helix) are affected to a different degree by surface chemistry although a loss of native structure was observed when adsorbed to hydrophobic surfaces.

3.5.8.4 MAb-1 adsorption to Tween coated silica surfaces

The water contact angle and surface energy data for Tween 20 and Tween 80 showed that they generated a hydrophilic surface when used to coat silica (Table 3-8 and Table 3-9) and mAb-1 was strongly attracted to the surfaces as demonstrated by high F_{ad} values (Figure 3-13). MAb-1 retained its secondary structure on the hydrophilic Tween surfaces as for the hydrophilic silanised surfaces (Figure 3-17 and Figure 3-21). There is a large volume of literature available on the effect of Tween inclusion on stability and structure in solution. However, there is a lack of knowledge of the effect adsorption to a Tween coated surface has on mAb-1 structure and this is the first study investigating this using 'solid-state' CD.

3.5.9 Analysis of conformation loss using Dichroweb curve reconstruction

The conformational changes in mAb-1 and BSA structures when adsorbed to the bead surfaces were quantified using Dichroweb. The CD spectrum for mAb-1 in solution had no α-helix calculated as would be expected. The data generated by Dichroweb for mAb-1 adsorbed to the bead surfaces using the CONTIN algorithm correlated well with the CD spectra. A reduction in the fraction of β-sheet in the Dichroweb analysis coincided with unfolding observed in the CD spectra. In general, a hydrophobic surface caused the calculated β-sheet fraction to decrease by a greater degree than a hydrophilic surface (Table 3-16). Dichroweb analysis of the hydrophobic surfaces generated by silanisation with TCOS and TCPS showed the native structure to be largely retained (Table 3-16) which supported the CD spectra showing a mainly β-sheet containing protein (Figure 3-17). This was in contrast to the loss of β-sheet fraction for the other hydrophobic surfaces investigated.

The calculated α-helical fraction for BSA was below the percentage which would have been anticipated based on the crystal structure (Protein Data Bank ID: 3V03). The helix fraction was calculated to be 51 % from the CD spectrum in solution compared to the 74 % helix expected from the crystal structure although the contribution of the α-helix appeared to be very strong in the CD spectrum of BSA (Figure 3-19). The calculated helical contribution to the CD spectra of BSA adsorbed to the beads was subsequently low (less than 10 % with the exception of TCPS and TCDS, Table 3-17) despite the spectra showing a strong helical influence. Nevertheless, the combination of the CD spectra and the quantification using Dichroweb together enabled interpretation of the data.

Interpretation of the data generated by the CONTIN algorithm showed that mAb-1 and BSA when partially unfolded on the silanised surfaces did not form 'molten globules'. The formation of 'molten globules' was first proposed for α-lactalbumin and cytochrome-c (Dolgikh et al., 1981, Ohgushi and Wada, 1983) in which the proteins maintain a native-like secondary structure but instead of the tertiary structure being relatively rigid, it fluctuates. In this study, unfolding of mAb-1 and BSA resulted in the formation of intermediate conformations as the secondary structure altered between helix, sheet, turn and random coil. The conformational intermediates of mAb-1 and BSA adsorbed to the silica and functionalized silica in an irreversible manner as they were not desorbed despite repeated buffer washes.

Desorption of the partially folded intermediates observed in the 'solid-state' CD spectra by surfactant presence (e.g. Tween) in formulations could result in a soluble but misfolded protein species being present in solution. This in turn could,

potentially lead to the initialisation of aggregation and ultimately the formation of visible precipitates which could cause an immunogenic response.

In this study, Dichroweb analysis of mAb-1 adsorbed to Tween coated silica surfaces (using the same parameters as for the silanised surfaces), showed that the native β-sheet structure was largely retained with a decrease in the calculated fraction of 10 %. This was similar to that observed for the hydrophilic silane surfaces (Table 3-18 and Table 3-16). Although Tweens are included to minimise protein surface adsorption, the CD spectra and data generated using the CONTIN algorithm of Dichroweb show that adsorption does take place eventually, even though the native structure is retained. Therefore, desorption from the surfaces which had been coated with the Tween surfactants would not result in misfolded protein intermediates becoming present in solution, avoiding the triggering of aggregation and eventual undesirable immunogenic responses.

3.6 Conclusions

The F_{ad} data showed that mAb-1 was strongly attracted to hydrophilic surfaces compared to the weak attraction observed for hydrophobic surfaces. The high F_{ad} values detected for mAb-1 interaction with mPEG and Tween brush borders is consistent with a high compression force facilitating non-covalent interaction between mAb-1 and buried ethylene oxide units (Sheth and Leckband, 1997a). MAb-1 native structure was largely retained when adsorbed to hydrophilic surfaces compared to a loss upon adsorption to a hydrophobic surface. MAb-1 was weakly attracted by the hydrophobic TCOS and TCPS surfaces but the native structure was retained. These two silanes could potentially reduce protein surface adsorption without causing a loss of structure. The loss of mAb-1 structure on the APTMS surface which possessed the same net positive charge as mAb-1 at pH 7.4 supports the interpretation that adsorption of mAb-1 to the surfaces was driven entropically due to surface dehydration and in combination with electrostatic interactions taking place via net positive/negative surface patches. Moreover, CD data do not support the hypothesis stating that adsorbed mAb-1 or BSA are in a molten globule state on the surface. Instead, data in this study correlates well with the formation of distinct partially folded intermediate conformations. The presence of a relationship between mAb-1 secondary structural loss and surface characteristics was not identified.

The effect of surface hydrophobicity and surfactant on mAb-1 surface adsorption was subsequently investigated using total internal reflection fluorescence (TIRF) and complimented with neutron reflectivity (NR) data to characterise the adsorption process at the molecular level.

Chapter 4. Adsorption behaviour of mAb-1 at hydrophilic and hydrophobic surfaces under flow conditions

4.1 Introduction

MAb-1 adsorption at the solid/liquid interface to hydrophilic and hydrophobic surfaces was investigated initially using total internal reflection fluorescence (TIRF). The influence of pH, excipient inclusion and injection scenario on mAb-1 adsorption was also studied. The interaction of mAb-1 in the bulk solution with Tween and the effect of surface adsorption on structure are detailed in 2.5.1 and 3.5.8. The TIRF data was complemented with surface adsorption data gathered using neutron reflectometry (NR) to describe the difference in adsorption/desorption of mAb-1 under the different conditions.

4.1.1 Total Internal Reflection Fluorescence (TIRF)

Total internal reflection fluorescence (TIRF) is an extremely sensitive surface technique which was used in this study to investigate surface adsorption/desorption of mAb-1. TIRF has previously been used to study the adsorption/desorption of two different proteins to that studied here, fibrinogen and albumin, to a hydrophobic surface (Wertz and Santore, 1999, Wertz and Santore, 2002). In TIRF, a fluorescent label which has been attached to a protein is excited by an evanescent wave. According to Snell's Law (Equation 4-1) an evanescent wave is formed at the interface between two media, or between a medium and a surface, with different refractive indices. Snell's law (Equation 4-1) states that the ratio of the sines of the angles of incidence and refraction is equivalent to the ratio of velocities of the two media or the opposite ratio of the indices of refraction (Figure 4-1A).

$$\frac{Sin\theta_1}{Sin\theta_2} = \frac{v_1}{v_2} = \frac{n_1}{n_2}$$ **Equation 4-1**

θ is the angle measured from the interface, ν is the velocity of light in the medium (meters per second, m/s) and *n* is the reflective index of the medium (unitless).

An evanescent wave only forms at the point of total internal reflection, the strength of which decays exponentially with distance from the surface and thus only flurophores within 100 nm of the surface will be excited (Figure 4-1B). Molecules with the fluorophore attached and which are adsorbed to the surface are likely to dominate the signal as they will be present at the point at which the evanescent wave is strongest. The raw fluorescent data can be converted to a quantitative measure of protein mass per unit area using the Leveque equation (Equation 4-7) providing that adsorption is transport limited (Lok et al., 1983a). The transport limited kinetics necessary for the conversion of fluorescence data using the Leveque equation have been shown to only be maintained for low protein concentrations and shear rate (Wertz and Santore, 1999, Lok et al., 1983a).

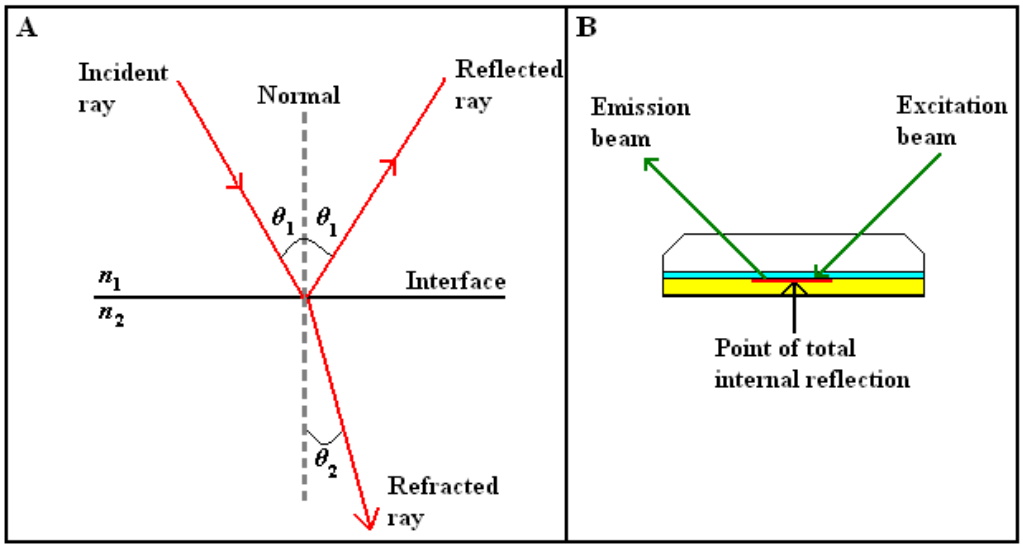

Figure 4-1. (A) Diagrammatic representation of Snell's law; **(B)** Point of total internal reflection fluorescence.

In this way, Pereira et al. (2008) identified a two phase adsorption of an IgG-like domain pair onto silica from within a bulk solution using TIRF. A rapid initial phase, when the protein concentration used was above 1 mg/mL, was followed by a second phase during which the quantity of protein which adsorbed to the silica was very small (Pereira et al., 2008). The data produced by TIRF does not provide information on the adsorbed protein layer at the molecular level and thus, the orientation of the protein and build-up of layers cannot be determined using this technique. To investigate adsorption at this level, NR was selected as a complimentary technique.

4.1.2 Neutron Reflectometry (NR)

Neutron reflectometry (NR) is a high resolution technique used to investigate the structure of thin films on surfaces. In biology, for example, it can differentiate between the orientations a protein may adopt on a surface and provide information on how molecules are distributed at a surface in terms of packing and layer number formation (Lakey, 2009). In addition, NR can generate information on aggregation and polymer and surfactant adsorption. Neutrons interact weakly with samples and so are able to penetrate into a sample without causing damage in the process.

A beam of neutrons is shone onto an extremely flat surface and the intensity of the reflected neutrons is then measured as a function of the angle or the neutron wavelength (Figure 4-2). The ratio of the reflected beam intensity to that of the incident beam intensity is used to measure the neutron reflectivity. The distribution profiles of interfacial components and their scattering lengths will determine the intensity of the reflected beam (Lu et al., 1999). The scattering length density (SLD) is calculated from the sum of the scattering lengths of each element (e.g. carbon, hydrogen, oxygen, nitrogen) which composes a molecule. The SLD differs between molecules and so multiple reflectivity profiles can be measured at once. An example of this is the determination of the layer thickness of each component of a protein array – composed of an immobilised protein on the surface, a bound antibody and an antigen interacting with the bound antibody (Le Brun et al., 2011).

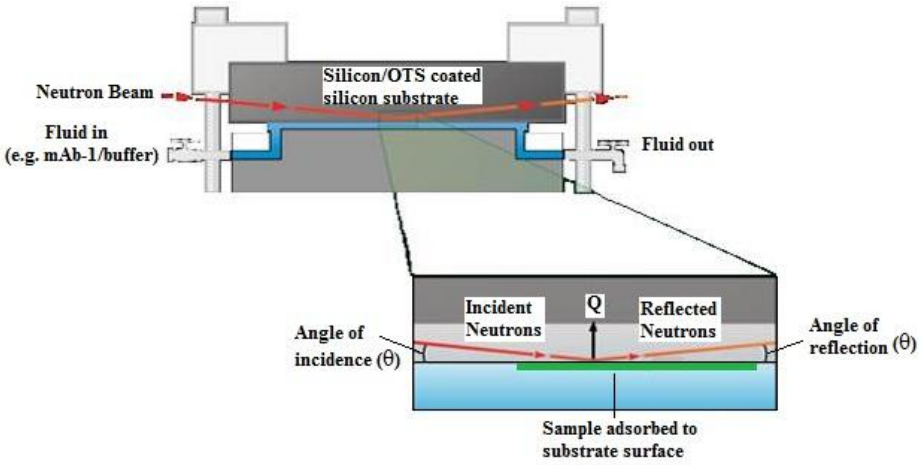

Figure 4-2. Neutron reflectivity set-up (Adapted from http://www.lanl.gov/science/1663/august2011/story3full.shtml, accessed 09/2012).

The orientation of a mouse mAb to the β unit of human chorionic gonadotrophin (anti-β-hCG) was identified as being "flat-on" by NR when adsorbed to a silicon oxide-water interface. The surface fraction and number of layers increased with concentration (Xu et al., 2006b). An earlier investigation by the same authors also found anti-β-hCG adsorbed to the surface to have a thickness of 41 Å, suggesting the value corresponded to a "flat-on" orientation based on IgG dimensions (Deisenhofer, 1981). The dimensions of the IgG would result in a layer thickness of 85 Å or 142 Å (Deisenhofer, 1981), therefore the 40 Å suggests a "flat-on" orientation. Adsorption of anti-β-hCG is dependent upon pH and ionic strength, using PBS at an ionic strength of 200 mM anti-β-hCG was reduced compared to 20 mM with a decrease at both ionic strengths with increasing pH (Xu et al., 2006a). The pH chosen for NR studies has been shown to cause differences in the adsorption of an IgG to both a hydrophilic silica surface and a hydrophobic methylated silica surface (Buijs et al., 1996). The highest surface adsorption was detected at pH 6, the IgG has a pI of 5.8

(Buijs et al., 1996). These investigations show that NR can be used to study immunoglobulin surface adsorption and is capable of identifying layer thickness.

4.2 Materials

Tween 20, Tween 80, concentrated sulphuric acid, toluene, *N*,*N*-dimethylformamide, octadecyltrichlorosilane (OTS), dimethyl sulfoxide (DMSO), potassium dichromate, sodium chloride, potassium chloride, sodium phosphate monobasic, potassium phosphate monobasic, sodium hydroxide, fluorescein isothiocyanate I (FITC), L-histidine, L-histidine monohydrochloride, sodium acetate, acetic acid, diiodomethane, 1,2-ethanediol (ethylene glycol) and deuterium were obtained from Sigma Aldrich (UK). Water was purified to > 14 MΩ.cm with a BioSelect, Purite, UK. Alexa Fluor® 488 5-SDP ester (Alexa Fluor 488 sulfodichlorophenol ester) was purchased from Life Technologies Ltd (Invitrogen), UK. The immunoglobulin (mAb-1) was kindly provided by MedImmune Ltd, Cambridge (UK).

4.3 Methods

4.3.1 MAb-1 fluorescent labelling

MAb-1 was labelled using fluorescein isothiocyanate I (FITC) for experiments undertaken at pH 7.4 and Alexa Fluor® 488 5-SDP ester (Alexa Fluor 488 sulfodichlorophenol ester) for those carried out at pH 5.5.

For labelling of mAb-1 using FITC, the manufacturer's protocol was followed with minor alterations. FITC was dissolved in DMSO at 1 mg/ml and 100 µl slowly added under stirring to 3 mL of mAb-1 solution at a concentration of 20 mg/mL in phosphate buffered saline pH 7.4 (PBS - 10 mM sodium phosphate monobasic, 2 mM potassium phosphate monobasic, 137 mM sodium chloride, 2.7 mM potassium chloride), and left stirring in the dark for 2 h at room temperature. The mAb-1-FITC solution was dialysed using a snakeskin dialysis membrane (10,000 Dalton MWCO) (Pierce, Thermo Scientific, UK) with three buffer changes to remove unbound FITC. The mAb-1 to label ratio and mAb-1 concentration were calculated using Equation **4-2** and Equation 4-3 respectively:

$$Molar\ \frac{F}{P} = \frac{2.77\ x\ A_{495}}{A_{280} - (0.35\ x\ A_{495})} \qquad \textbf{Equation 4-2}$$

$$Immunoglobulin\ (mg/mL) = \frac{[A_{280} - (0.35\ x\ A_{495})]}{1.4} \qquad \textbf{Equation 4-3}$$

where, A_{280} and A_{495} are the absorbance values of the solution at each given wavelength, and 0.35 is the correction factor for FITC absorbance at 280 nm.

Fluorescein is pH sensitive, and consequently at pHs which are slightly acidic its quantum yield is reduced (Rebar and Santore, 1996). For this reason, mAb-1 was labelled with Alexa Fluor® 488 5-SDP ester for the experiments undertaken at pH 5.5. A 50 mg/mL mAb-1 solution in PBS pH 7.4, with a volume of 1.5 mL, was added to 1 mg Alexa Fluor® 488 5-SDP ester label and rotated at room temperature for 1 hour to ensure thorough mixing. The mAb-1-Alexa Fluor® 488 5-SDP ester solution was dialysed against L-histidine pH 5.5 (30 mM L-histidine, 30 mM L-histidine monohydrochloride) at 4 °C in the dark to remove unbound Alexa Fluor® 488 5-SDP ester. MAb-1 concentration and the number of moles of label per mole of mAb-1 were calculated using the following equations:

$$\boldsymbol{Protein\ concentration\ (M)} = \frac{[A_{280} - (A_{494}\ x\ 0.11)]\ x\ dilution\ factor}{molar\ extinction\ coefficient} \qquad \textbf{Equation 4-4}$$

$$\boldsymbol{Moles\ dye\ per\ mole\ protein} = \frac{A_{494}\ x\ dilution\ factor}{71{,}000\ x\ protein\ concentration\ (M)} \qquad \textbf{Equation 4-5}$$

where, A_{280} and A_{494} are the absorbance values obtained at these wavelengths, 0.11 is a correction factor to account for absorbance by the dye at 280 nm, and 71,000 cm^{-1} M^{-1} is the molar extinction coefficient of the dye at 494 nm.

4.3.2 Calculation of the diffusion coefficient of mAb-1

Using dynamic light scattering (nanoZS, Malvern, UK) the hydrodynamic diameter of mAb-1 at a concentration of 1 mg/mL in PBS was determined. The hydrodynamic

diameter of mAb-1 was subsequently used to calculate the diffusion coefficient using the Stokes-Einstein equation:

$$D = \frac{kT}{6\pi rn} \qquad \textbf{Equation 4-6}$$

D = diffusion coefficient (cm^2/s); k = Boltzmann constant (1.3806503 x 10^{-23} m^2 kg s^{-2} K^{-1}); T = absolute temperature (Kelvin); r = hydrodynamic diameter (nm) and; η = viscosity of water at 25°C (0.89 centipoise).

4.3.3 Total Internal Reflection Fluorescence (TIRF)

Quartz (silica) slides were cleaned through immersion in chromic acid (80 g $K_2Cr_2O_7$ per litre 96-98% sulphuric acid) for 1 hour followed by thorough rinsing with deionised water. Slides were left in deionised water overnight and dried (Pereira et al., 2008).

The width of the flow chamber (1.6 cm) and the gasket thickness (0.01 cm) of the TIRF cell were maintained throughout (TIRF Flow System, TIRF Technologies Inc., Harrisburg, USA), and fluorescence was measured with a Varian Cary Eclipse spectrofluorometer (Agilent Technologies, Berkshire, UK). The fluidic block was set up as shown in Figure 4-3. Blank runs of FITC and unlabelled protein in PBS pH 7.4 and Alexa Fluor® 488 5-SDP in L-histidine pH 5.5 were carried out to confirm their contribution to the fluorescent signal was negligible.

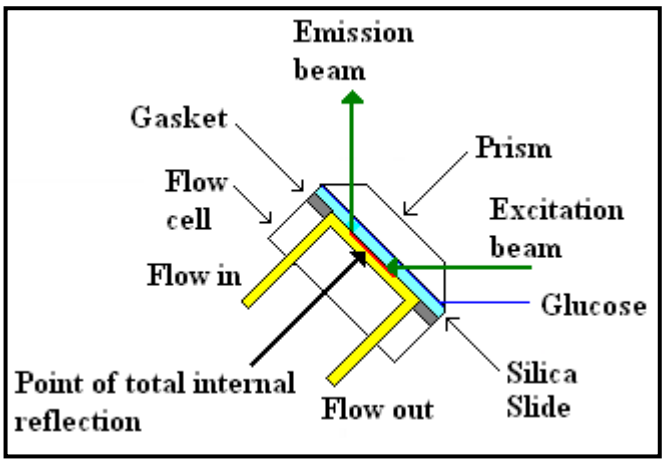

Figure 4-3. Fluidic block set up (adapted from Tirf technologies).

4.3.3.1 Confirmation of transport limited adsorption

MAb-1 surface adsorption must be transport limited to satisfy the Leveque equation (Equation 4-7) for the conversion of fluorescence data to mAb-1 surface coverage.

$$\frac{d\Gamma}{dt} = 0.538\ x\ (\frac{\gamma}{L})^{\frac{1}{3}}\ x\ D^{\frac{2}{3}}\ x\ C \qquad \textbf{Equation 4-7}$$

dΓ/dt – rate of surface adsorption; L – distance from point of entry to measurement point (cm); D – mAb-1 diffusion coefficient (calculated using the Stokes-Einstein equation, (Equation 4-6) and; C – concentration (mg/mL).

The transport limited nature of mAb-1 surface adsorption was confirmed through alteration of shear rate (s^{-1}) (Equation 4-8) and mAb-1 concentration while measuring the change in fluorescence (λ excitation 450 nm/emission 520 nm). To investigate the effect of shear rate, a mAb-1 concentration of 0.01 mg/mL was used with the shear rate varied from 6 s^{-1} to 84 s^{-1}, which was controlled using a syringe

pump driver (KDS Scientific, UK). The effect of mAb-1 concentration on surface adsorption was studied using a shear rate of 6 s^{-1} and a mAb-1 concentration range from 5 µg/mL to 0.5 mg/mL.

$$\gamma = \frac{6V}{wb^2} \qquad \textbf{Equation 4-8}$$

γ – shear rate (s^{-1}); V – flow rate (mL/h); w – width of flow chamber (mm); b = gasket thickness (mm) (Lok et al., 1983a).

PBS (pH 7.4) or L-histidine buffer (pH 5.5) was injected for 180 seconds prior to sample injection to ensure a smooth baseline was obtained. Sample time for all TIRF experiments was 3600 seconds (1 hour) with *n*=5.

A shear rate of $6s^{-1}$ was found to produce reproducible adsorption profiles for mAb-1 at a range of concentrations from 5 µg/mL to 0.5 mg/mL in PBS pH 7.4 and so it was selected for all future TIRF experiments. Calibration of the raw fluorescence data generated by the TIRF experiments is discussed in 4.5.2.

4.3.3.2 Effect of pH on mAb-1 surface adsorption

The pH of a solution can affect the charge present on the surface of a protein and also the surface to which it is adsorbing (Behrens and Grier, 2001, Mathes and Friess, 2011). Surface adsorption of mAb-1 was investigated at pH 5.5 in L-histidine buffer

(labelled using Alexa Fluor® 488 5-SDP) and at pH 7.4 in PBS (labelled using FITC) at a concentration of 0.01 mg/mL. A hydrophilic surface was used at both pH values for comparison.

4.3.3.3 Effect of surface energy on mAb-1 adsorption

As shown in section 3.4.3.1 Figure 3-18 mAb-1 loses a degree of its native secondary structure upon adsorption to hydrophobic surfaces. Silica slides were coated with OTS to produce a hydrophobic surface and mimic adsorption to plastic surfaces. The slides were prepared by immersion in a solution of 0.14 g OTS in 180 mL of n-hexadecane for 2 h under stirring at room temperature, as described by Pereira et al (2008). The hydrophobic OTS-coated silica surface and a hydrophilic silica surface were then used to investigate the effect of surface energy on mAb-1 surface adsorption. TIRF experiments were carried out in L-histidine buffer pH 5.5 with the remaining parameters as for studies at neutral pH.

The surface characteristics of both the silica and OTS-coated silica surfaces have been determined previously in 3.4.1.

4.3.3.4 Effect of Tween 20 and Tween 80 injection time on mAb-1 surface adsorption

The effect of Tween on mAb-1 surface adsorption to silica was investigated using a shear rate of $6s^{-1}$ and a concentration of 0.01 mg/mL. The investigation was carried

out at pH 5.5 (using Alexa Fluor® 488 5-SDP λex/em 495/519 nm) and pH 7.4 (using FITC λex/em 450/520 nm). Tween 20 and Tween 80 concentrations below and above their CMC were used: 0.05 and 1 mM for Tween 20; and 5 µM and 1 mM for Tween 80. These are the same concentrations as those which were used to study the effect of Tween on mAb-1 stability, structure and force of adhesion in section 2.4.2, 3.4.2.2 and 3.4.3.3. The effect of Tween on mAb-1 surface adsorption was investigated under three conditions:

1- co-dissolved with mAb-1;

2- injection into the flow chamber (over 1800 s) prior to mAb-1 injection (over 3600 s);

3- injection into the flow chamber (over 1800 s) after injection of mAb-1 (over 1800 s).

The same set of experiments was undertaken at pH 5.5 in L-histidine buffer using an OTS-coated silica surface to investigate the effect of Tween on mAb-1 surface adsorption to a hydrophobic surface.

4.3.3.5 Effect of storage in pre-filled syringes on mAb-1 surface adsorption

Therapeutic proteins for subcutaneous injection are commonly distributed in pre-filled syringes. The formulations would most likely be stored for a period of time prior to administration. For this reason, mAb-1 labelled with FITC at a concentration of 28 mg/mL was stored at 4°C for 2 months in a CZ staked syringe, a BD syringe shown in Figure 4-4 (both kindly provided by MedImmune, Cambridge, UK) and in

a glass vial to investigate the effect of storage on mAb-1 surface adsorption to silica. A shear rate of $6s^{-1}$ and a concentration of 0.01 mg/mL were used during as for the previous TIRF experiments.

Figure 4-4. Image of (left) a CZ staked syringe and (right) a BD syringe.

4.3.4 Neutron reflectometry – surface adsorption at the molecular level

Silicon <1 1 1> substrates 10 cm in diameter and with a thickness of 1 cm were washed with Decon 90 (Decon Laboratories Limited, Hove, UK), thoroughly rinsed with deionised water and dried using nitrogen. The hydrophobic silicon wafer was prepared by immersion in OTS in *n*-hexadecane for 1 h to allow self-assembly of the silane monolayer (Lu et al., 1998). The surface was rinsed with dichloromethane, ethanol and water sequentially. The cleaned substrate (either silicone or OTS-coated silicone) was then clamped to a silicon trough which had a void volume of approximately 3 mL. The experiments were carried out at mAb-1 concentrations from 50 to 5000 mg/L in acetate buffer pH 5.5 and phosphate buffer 7.4 for the silicon surface, and in acetate buffer pH 5.5 for the OTS-coated silicon surface. The neutron reflectometry experiments were performed using the INTER instrument at

ISIS (Didcot, UK) with assistance from Dr Max Skoda (ISIS). The sample was analysed at fixed incident angles of 0.7 and 2.3° to achieve a reduced data set producing a single reflectivity profile with Q values (momentum transfer; which is the change in momentum of the neutron after reflection) of up to 0.3 $Å^{-1}$. The neutrons used had a wavelength range from 1.0 to 15.0 Å. A flat background, which was determined by extrapolation to high values of momentum transfer Q ($Q = 4\pi\sin\theta/\lambda$, where θ is the glancing angle of incidence and λ the wavelength) was subtracted. All the experiments were carried out at 25 °C. Blank silicon-acetate buffer (pH 5.5), silicon-phosphate buffer (pH 7.4) and OTS silicon-acetate buffer were undertaken in order to characterise the substrate.

MAb-1 was injected into the trough at a controlled rate (2 mL/h at 50 mg/L) using a high performance liquid chromatography (HPLC) pump. MAb-1 was allowed to adsorb to the surface for 30 minutes after injection into the sample chamber before commencement of the NR experiment to allow an equilibrium between the surface and the bulk solution to form. Solutions containing mAb-1 at increasing concentration were subsequently injected. The reflectivity profile at each concentration was generated using a time of 30 seconds per period (a period is the duration of time the neutron beam is shone onto the surface) and a total of 120 periods. The sample was analysed at fixed incident angles of 0.7 and 2.3° to achieve a reduced data set producing a single reflectivity profile with Q values of up to 0.3 $Å^{-1}$.

To investigate if mAb-1 adsorption to the substrate surfaces was reversible and to determine if Tween could desorb mAb-1 the following experiments were carried out. After the final mAb-1 sample (5000 mg/L), the surface was rinsed with five volumes

of D_2O to remove the mAb-1 bulk solution prior to injection of buffer or Tween. Post mAb-1 adsorption to the silicon substrate at pH 5.5, acetate buffer was injected followed by a 1 mM Tween 20 solution. Due to time constraints only 0.05 mM Tween 20 was injected into the trough after adsorption of the final mAb-1 sample (5000 mg/L) to the silicon substrate at pH 7.4 and to the OTS-coated silicon substrate at pH 5.5. NR data were fitted using a Global MOTOFIT analysis (Nelson, 2006) described in section 4.3.6.

4.3.5 MAb-1 adsorption kinetics studied using NR

NR produces data on the molecular nature of layers formed on a surface which would improve the understanding of the adsorption/desorption of mAb-1 under the three Tween injection scenarios. Adsorption of mAb-1 (at a concentration of 0.1 mg/mL) in the presence of Tween (at a concentration of 0.05 mM) to a SiO_2 surface at pH 7.4 was investigated. MAb-1 was injected at a flow rate of 2.0 mL/h (to achieve a shear rate equivalent to that used in the TIRF experiments), with 30 seconds per period and a total of 120 periods. A short period duration was used in order to investigate the transient adsorption which was rapid in the TIRF experiments. All other parameters were the same as for investigation of layer formation.

For investigation of Tween injection after adsorption of mAb-1 to the SiO_2 surface, a concentration of 0.5 mg/mL and a Tween 20 concentration of 0.05 mM were selected. The time per period was increased to 60 seconds with a subsequent reduction in the number of periods to 40 as the TIRF data showed desorption did not take place as rapidly as the transient profile observed.

4.3.6 NR Data Fitting

A theoretical calculation of the SLD of mAb-1 in H_2O pH 7 was required to fit the experimental data. A spreadsheet method developed by Dr R. May, Institut Laue-Langevin, was used which involved summing the scattering lengths for each amino acid. For the calculation of the SLD of mAb-1 in D_2O, it was necessary to make an assumption of the fraction exchange of the non-hydrogen bonded N-H protons. A 70 % fraction exchange was assumed based on data for lysozyme adsorbed to silica particles (Larsericsdotter et al., 2004). A calculation of hydrogen-deuterium exchange could not be made based on a known hydrogen bonding pattern as the 3-dimensional structure of mAb-1 has not been determined. The protein fraction of the layer covering a surface (a) from the fitted SLD (ρ) made up from contributions of the protein and subphase (D_2O) was calculated using Equation 4-9.

$$\rho_{fitted} = (1 - a).\rho_{\mathrm{D2O}} + a.\rho_{calc} \qquad \textbf{Equation 4-9}$$

NR data were fitted at the university (by myself) using a Global MOTOFIT analysis (Nelson, 2006). The parameters fitted to the NR data were SLD, layer thickness and interfacial roughness. For each silicon substrate (SiO_2) used and the OTS-coated silicon substrate, the parameters were first fitted for the bare surface in D_2O. These parameters were then kept fixed during fitting of the reflectivity profiles for the adsorbed mAb-1 layers from buffer prepared using D_2O. Maintaining the values for the bare surface throughout the subsequent fitting process for the adsorbed proteins layers ensures that any changes which took place were as a result of the protein layer(s) alone. The SLD value of the silicon substrate was constrained to 2.07 x 10^{-6} $Å^{-2}$. The SLD values for H_2O and D_2O used during MOTOFIT analysis were -0.56 and 6.36 (x 10^{-6} $Å^{-2}$) respectively with a deviation of 5 % from this value allowed.

The value for the parameters investigated for the bare substrates in buffer alone are shown in Table 4-1.

Substrate	Background value ($Å^{-2}$)	SiO_2 layer thickness (Å)	SLD ($Å^{-2}$)
Silicon	5.0-6.0 x 10^{-6}	3	3.47 x 10^{-6}
OTS-coated silicon	3.0 x 10^{-6}	7	3.47 x 10^{-6}

Table 4-1. Parameter values for the bare substrates in buffer which were used in the neutron reflectivity experiments.

The SiO_2 layer of the OTS coated substrate was found to be 17 Å thick and had a SLD of 3.55 x 10^{-6} $Å^{-2}$. The SiO_2 layer which formed on the surface of the substrate was more porous on the OTS coated surface than the bare silicon and the layer was thicker. The surface roughness of the silicon and SiO_2 layers ranged from 2 to 11 Å. The higher roughness values were fitted for the layers which had an interface with a protein layer; these were in the range of 4 to 7 Å.

To assess the strength of the models used to fit the NR data, analysis using the N-sigma (Nσ) qualifier was undertaken (Equation 4-10) (Ihringer 1995). The χ^2 value for each model generated from the NR data was weighted against the number of data points and parameters studied. For two models which could reasonably have a different number of layers fitted to the data this analysis is of particular importance. The parameters for the Silicon/SiO_2 layers of two models when being analysed were fixed resulting in the number of degrees of freedom being three for a model with a single layer and six for a two layer model.

$$N\sigma = \frac{\chi^2 - \nu}{\sqrt{2\nu}} \qquad \textbf{Equation 4-10}$$

where, χ^2 is the error-weighted least-squares sum and $\nu = n - p$ is the effective number of degrees of freedom, n is the number of data points used in the fit and p is the number of fitting parameters. A small $N\sigma$ value is illustrative of a high probability that the assumed model is correct.

4.4 Results

4.4.1 MAb-1 labelling

MAb-1 concentration and mAb-1 to label ratio for FITC and Alexa Fluor® 488 5-SDP were calculated using Equation 4-2 to Equation 4-5. The final concentration of labelled mAb-1 was dependent on the initial concentration used but ranged from 20 to 30 mg/mL. The labelling ratio of label to mAb-1 was approximately 1:1 for FITC and 3:1 for Alexa Fluor® 488 5-SDP.

4.4.2 Confirmation of transport limited adsorption

The surface adsorption of mAb-1 must be transport limited for the conversion of fluorescence intensity (a.u.) data to mAb-1 surface adsorption (mg/m^2) using the Leveque equation (Equation 4-7). Therefore, the transport limited nature of the surface adsorption had to first be confirmed to allow the above conversion of raw data. Two parameters of the Leveque equation can be altered, shear rate (γ) and concentration (C), while the additional parameters remain constant. Therefore, in order to confirm the transport limited nature of the adsorption the effect of shear rate and concentration were investigated. The change in fluorescence over time was plotted against concentration, and shear rate to the power of 1/3 (as the Leveque equation states that for transport limited adsorption the initial rate of adsorption will be proportional to shear rate to the 1/3 power). A linear fitting with an R^2 value close to the unit will indicate transport limited adsorption.

It was important to establish that the transport of mAb-1 to the surface was not driven by the fluorophore and that intrinsic fluorescence from the protein did not contribute to the signal. The fluorescent signal detected upon injection of FITC or

Alexa Fluor 488 5-SDP was not above the background of the buffer alone as was the case with unlabelled mAb-1.

The effect of mAb-1 concentration on surface adsorption was investigated using a shear rate of $6s^{-1}$ (flow rate 0.6 mL/h) and a concentration range from 5 µg/mL to 0.5 mg/mL. In Figure 4-5 a linear increase in fluorescence intensity for mAb-1 concentrations from 5 µg/mL to 0.25 mg/mL at a shear rate of $6s^{-1}$ is evident. Adsorption above 0.25 mg/mL is no longer transport limited as demonstrated by the deviation from linearity at a concentration of 0.5 mg/mL. The raw fluorescence data from which the values were obtained is shown in Figure 4-6.

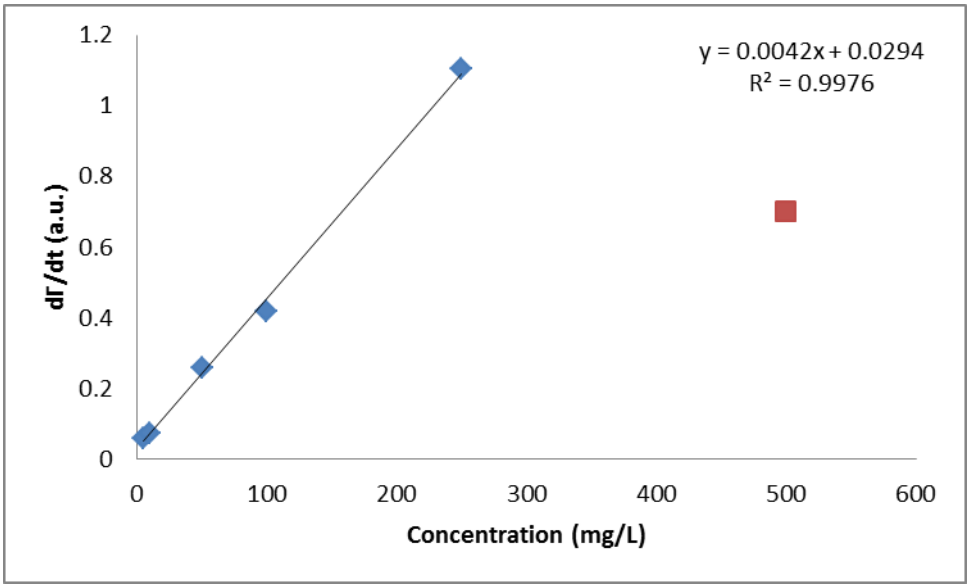

Figure 4-5. MAb-1 surface adsorption is transport limited up to a concentration of 0.25 mg/mL at pH 7.4, FITC label: blue diamond (◆) – 5 to 250 mg/L; red square (■) – 500 mg/L.

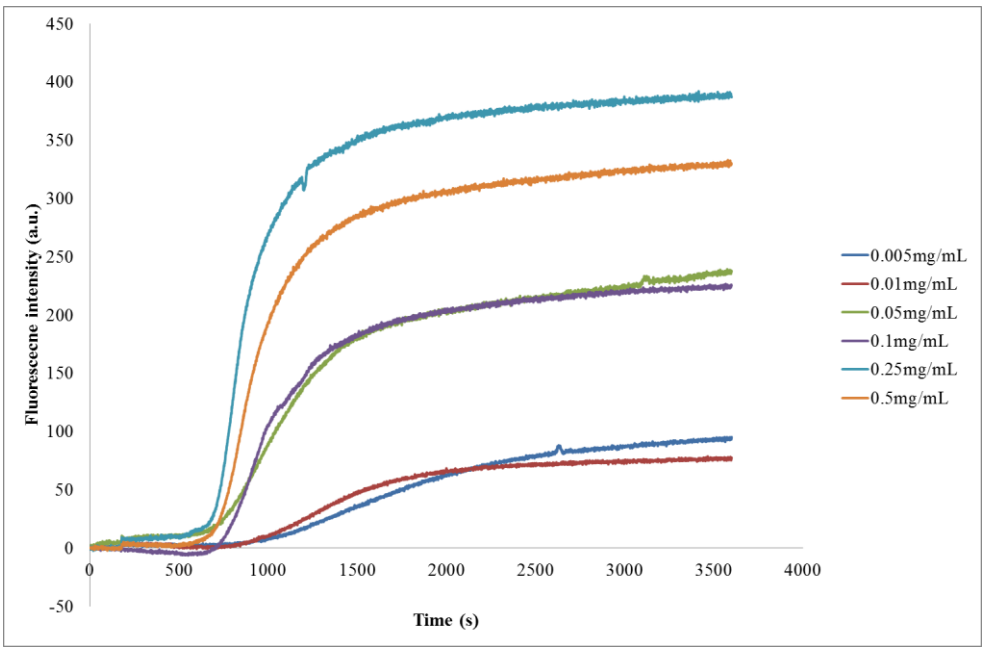

Figure 4-6. Raw fluorescence data showing the effect of mAb-1 concentration on surface adsorption using a shear rate of $6s^{-1}$ (flow rate 0.6 mL/h).

Analysis of the effect of shear rate showed that mAb-1 adsorption (at a concentration of 0.01 mg/mL) was transport limited for shear rates of 42 s^{-1} and below (Figure 4-7). The increase in fluorescence intensity observed at a shear rate of 84 s^{-1} demonstrated that surface adsorption was no longer transport limited as shown by the shift from linearity. (The raw fluorescence intensity values from which the data was plotted is shown in Figure 4-8.)

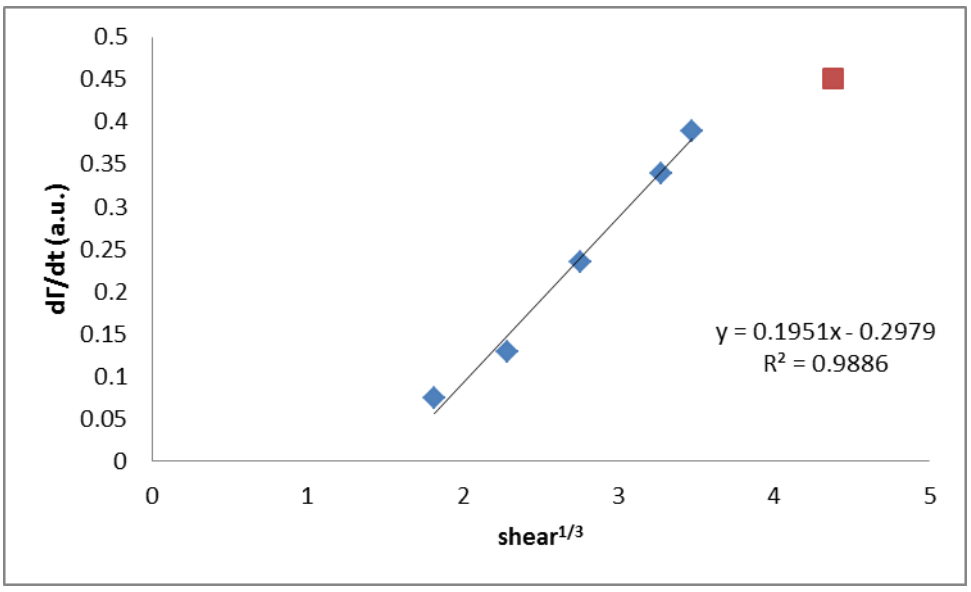

Figure 4-7. MAb-1 surface adsorption is transport limited up to a shear rate of 42s^{-1}, pH 7.4, FITC label: blue diamond ( ) – 6 to 42 s^{-1}; red square ( ) 84 s^{-1}.

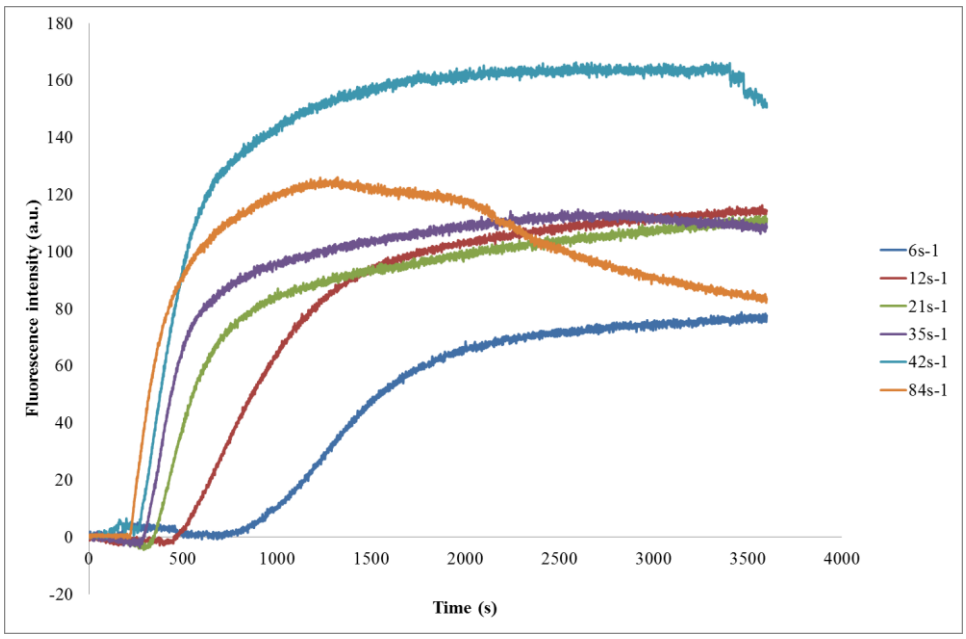

Figure 4-8. Raw fluorescence intensity data showing the effect of shear rate on mAb-1 surface adsorption using a concentration of 0.01 mg/mL.

MAb-1 surface adsorption is transport limited at concentrations up to 0.25 mg/mL when a shear rate of 42 s^{-1} or below is used. The conversion of fluorescence intensity data to surface adsorption using the Leveque equation is therefore valid providing these parameters are adhered to; the converted data is shown in Figure 4-9 and Figure 4-10. The raw fluorescence data was calibrated through previously acquired data for an immunoglobulin domain pair which was known to adsorb in an almost irreversible manner to bare silica at surface saturation (Pereira et al., 2008) and which was characterised against neutron reflectivity data for the same protein (Kreiner et al., 2009) (discussed in section 4.5.2). A mAb-1 concentration of 0.01 mg/mL and shear rate of $6s^{-1}$ were selected to investigate the effect of pH, surface and surfactant on mAb-1 surface adsorption.

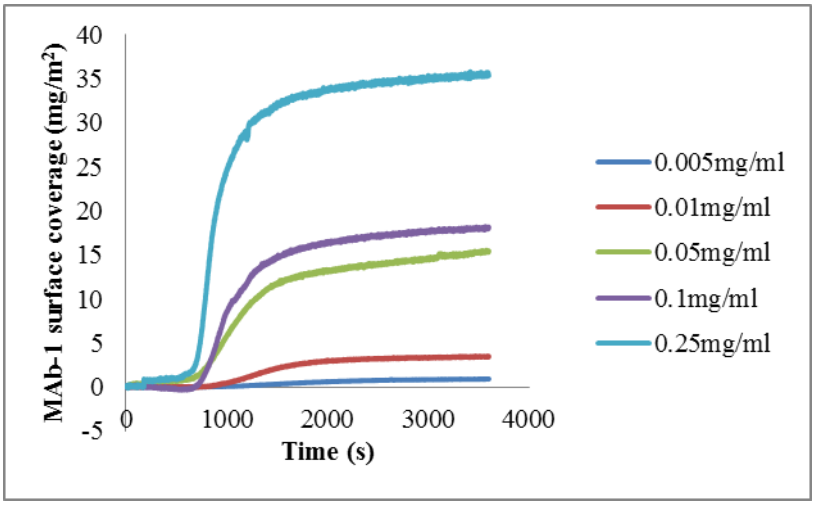

Figure 4-9. Effect of mAb-1 concentration on surface adsorption using a shear rate of $6s^{-1}$ (flow rate 0.6 mL/h).

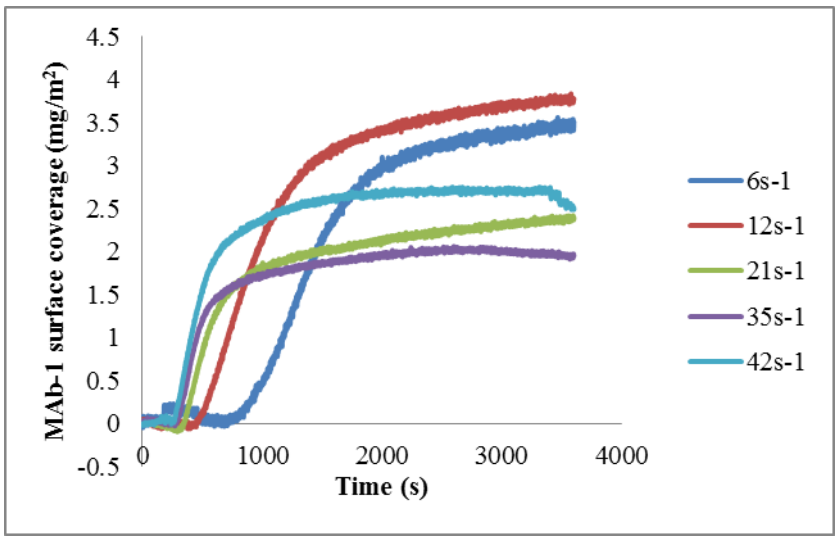

Figure 4-10. Effect of shear rate on mAb-1 surface adsorption using a concentration of 0.01 mg/mL.

4.4.3 Effect of pH on MAb-1 surface adsorption

Adsorption of mAb-1 at pH 7.4 was approximately 3 times that observed at pH 5.5: 11.72 mg/m^2 at pH 7.4 compared to 4.28 mg/m^2 at pH 5.5 (Figure 4-11). The electrostatic interaction between a protein (mAb-1) and the surface (in this case silica) which is known to play a key role in adsorption (Mathes and Friess, 2011) will differ depending upon the pH. The charge on the surface of mAb-1 would be expected to be positive at both pH 5.5 and 7.4, as the pI of mAb-1 is given as 8.99. This would facilitate the formation of electrostatic interactions with the net negatively charged silica surface. The difference in mAb-1 surface adsorption at the two pH values may be due to small local changes in the charged state of the amino acid residues.

The useable pH range of Alexa Fluor 488 5-SDP stated by the manufacturer is pH 6.5-8.5 although it is stable from pH 4 to 10. The pH used in this study is therefore not within the stated manufacurer's useable range and therefore the acid sensitivity

of the dye cannot be discounted as a cause of the difference in fluorescence intensity detected.

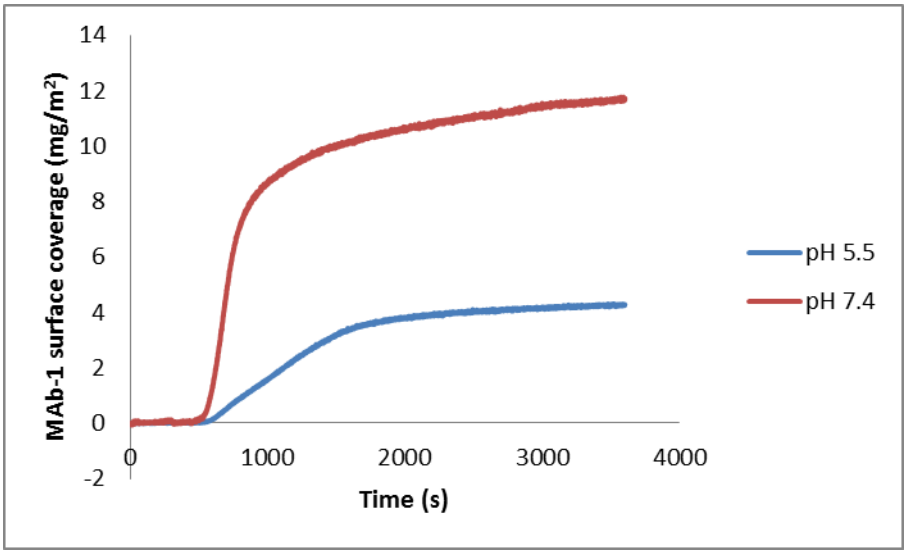

Figure 4-11. Adsorption of mAb-1 to a silica surface at a concentration of 0.01 mg/mL using a shear rate of $6s^{-1}$ was found to be affected by solution pH.

4.4.4 Effect of Tween on mAb-1 surface adsorption

Prior to investigation of the effect of Tween on mAb-1 surface adsorption it was necessary to determine if an interaction took place between them. The ITC data in section 2.4.1.1 showed that an interaction did not take place between either Tween 20 or 80 and mAb-1. This allowed the conclusion that surface adsorption was driven by mAb-1 alone and not by a specific interaction with Tween. DSC and CD data showed that Tween inclusion did not affect the structure of mAb-1 and therefore perturbations in secondary structure were assumed not to be a cause of differences observed (section 2.4, Table 2-4, Figure 2-20 and Figure 2-21). This led to the assumption that the surface adsorption investigated using TIRF would take place with mAb-1 in its native state.

4.4.4.1 Injection condition 1 - Effect of co-dissolved Tween on mAb-1 surface adsorption

MAb-1 surface adsorption in the presence of Tween 20 or Tween 80 was strongly dependent on concentration at both pH 5.5 and 7.4. At a concentration of Tween above its CMC, it was expected that mAb-1 surface adsorption would be minimally affected as Tween would be present as micelles in solution and so energy would be required to disrupt these and drive the individual Tween molecules onto the surface. However, this was not found to be the case when co-dissolved with mAb-1 at pH 5.5. The co-dissolved Tween 20 and 80 above their CMC reduced surface adsorption by > 50 % – 2.16 and 2.42 mg/m^2 compared to 5.46 mg/m^2 for the control (Figure 4-12). Relatively noisy TIRF signals were observed for mAb-1 co-dissolved with Tween 20/80 above their respective CMC values. This may be due to large changes in the quantity of mAb-1 entering into the range in which the evanescent wave will excite before leaving this region. In addition, the mAb-1 layer is not assumed to be static and so there will be a constant fluctuation with competition for the surface between the surfactant and mAb-1. Below the CMC, Tween 20/80 would exist in solution as individual molecules which is thermodynamically less favourable and so the monomers would be driven towards surface adsorption. The adsorption data showed that both Tweens studied initially drove mAb-1 onto the surface before causing desorption. Tween 80 below its CMC (5 µM) demonstrated a small transient curve which proceeded to decrease resulting in mAb-1 surface adsorption being the lowest of four formulations investigated at pH 5.5 (Table 4-2). The most notable adsorption curve was for co-dissolved Tween 20 below its CMC. In this scenario, a large transient curve was observed in which mAb-1 adsorption was more rapid and

extensive than the control before it decreased to a level similar to that of Tween above its CMC (2.24 mg/m^2).

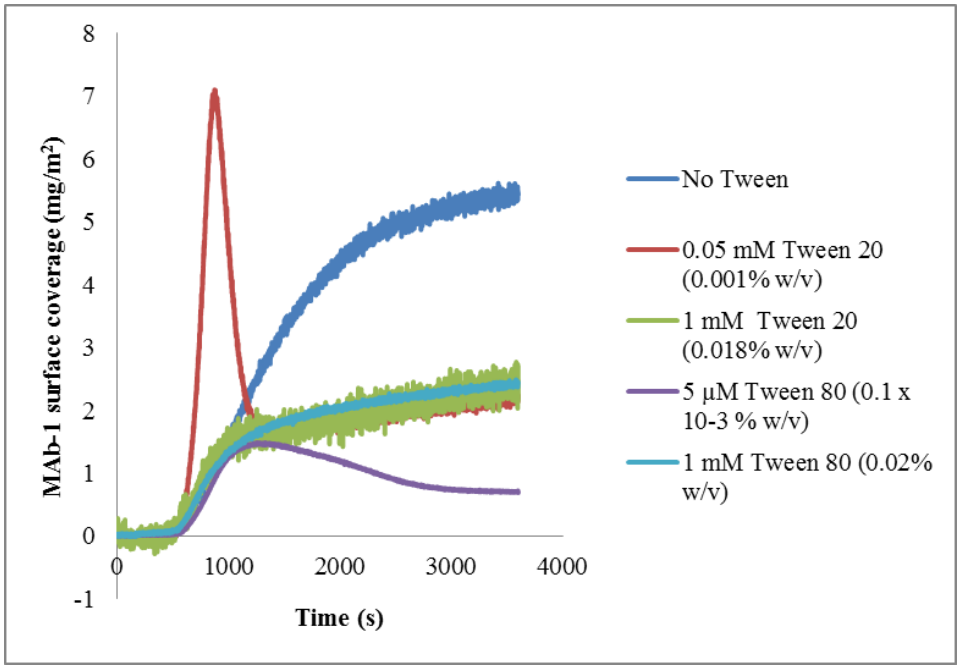

Figure 4-12. Effect of co-dissolved Tween on mAb-1 surface adsorption to a silica surface at pH 5.5.

In contrast to pH 5.5, co-dissolved Tween 20 or 80 above their CMC at pH 7.4 increased mAb-1 surface adsorption to ~25-30 mg/m^2 compared to ~12 mg/m^2 (Figure 4-13 and Table 4-2) although the initial rate of surface adsorption did not differ. As observed in the TIRF profiles at pH 5.5, the signals were noisy which could be due to the reasons discussed previously.

Similar to pH 5.5, mAb-1 surface adsorption was decreased by both Tween 20 and 80 below their CMC. A clear switch from increased to decreased mAb-1 surface adsorption is caused by differences in Tween concentration. The differences in the effect of Tween concentration suggests that non-specific binding sites on mAb-1

become saturated with Tween, and adsorption caused by the Tween under the circumstances investigated are important in understanding the switch observed. The transient curve was larger in the case of Tween 80 than Tween 20 which is most likely to be due to the 10-fold difference in concentration, or it could be due to the Tween 80 affinity for silica being reduced compared to Tween 20.

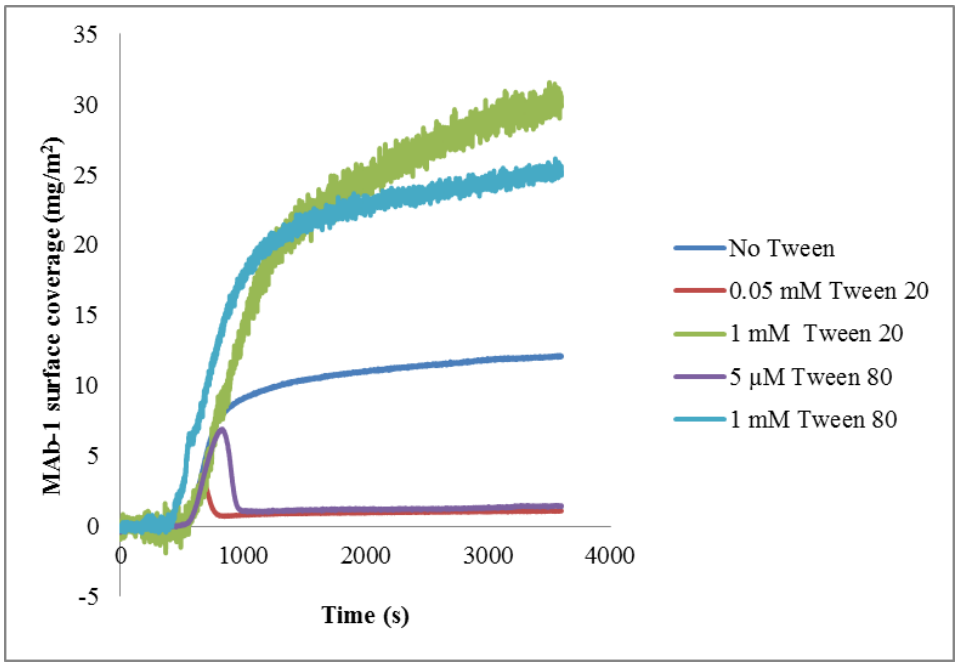

Figure 4-13. Effect of co-dissolved Tween on mAb-1 surface adsorption to a silica surface at pH 7.4.

Formulation	MAb-1 adsorption at pH 5.5 (mg/m^2)	MAb-1 adsorption at pH 7.4 (mg/m^2)
Control (No Tween)	5.46	12.12
0.05 mM Tween 20	2.24	1.08
1 mM Tween 20	2.16	29.84
5 µM Tween 80	0.69	1.48
1 mM Tween 80	2.42	24.95

Table 4-2. MAb-1 surface adsorption to a hydrophilic silica surface at pH 5.5 and pH 7.4 when co-dissolved with Tween 20 and 80 at concentrations below and above their CMC.

4.4.4.2 Injection condition 2 - Effect of pre-coating silica with Tween on mAb-1 surface adsorption

To investigate the apparent competition for the silica surface between mAb-1 and Tween the effect of pre-injected Tween 20 and 80 on adsorption was investigated. The level of surface saturation was dependent on the affinity of the Tween for the silica surface. The pre-coated Tween surfaces were established to be hydrophilic (section 3.4.2.2, Table 3-6). MAb-1 adhesion to the 1 mM Tween 80 surface was the highest (of the Tween surfaces) and found to be lowest for 5 µM Tween 80. It was anticipated that mAb-1 adsorption to a 1 mM Tween 80 surface would be the highest of those investigated and lowest when 5 µM Tween 80 was analysed.

The surfactants were injected at a constant rate over a period of time to achieve saturation with the remaining bulk solution washed out upon injection of mAb-1. The data show that a surface pre-coated with Tween reduced mAb-1 surface adsorption (Figure 4-14). MAb-1 does not displace Tween 20 or 80 from the silica surface; if this had been the case the profiles would have been the same as that for silica (Figure 4-14). The concentration of Tween 20 did not affect the quantity of mAb-1 adsorbed while for Tween 80 at concentrations below and above its CMC only a small difference was observed (Table 4-3). Therefore a surface which had first been exposed to Tween at pH 5.5 was effective at preventing adsorption.

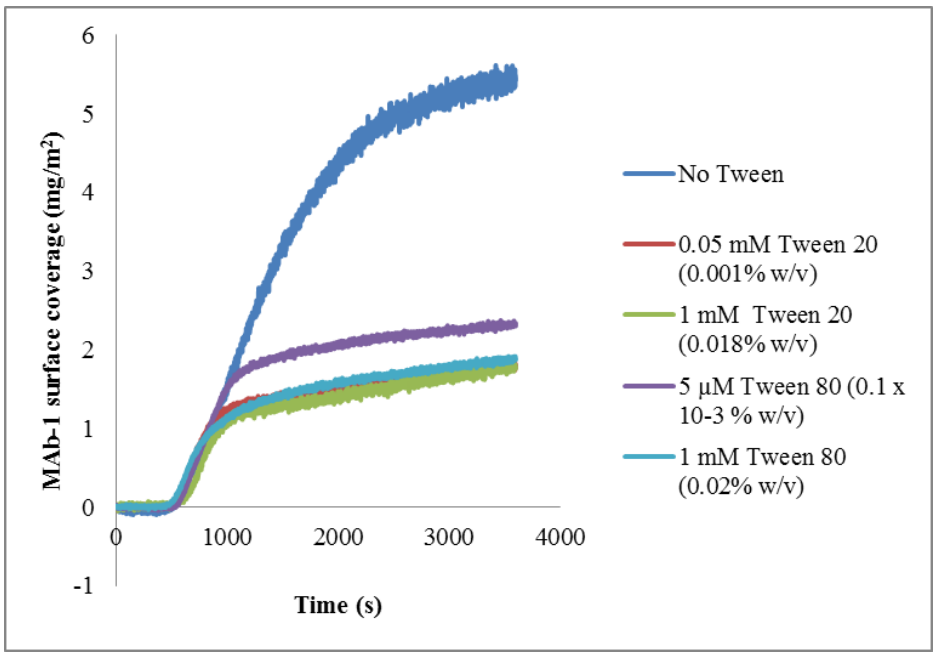

Figure 4-14. Effect of injecting Tween before mAb-1 on surface adsorption at pH 5.5.

A surface pre-coated with Tween at pH 7.4 had a very different effect on mAb-1 adsorption than observed at pH 5.5 (Table 4-3). MAb-1 adsorption to a pre-coated Tween 80 surface was almost equivalent at near plateau to bare silica (approximately 12-14 mg/m^2) (Figure 4-15). The profiles for Tween 80 suggest the surfactant is largely displaced by mAb-1. This was in stark contrast to the effect of Tween 20 which led to an increase in mAb-1 adsorption from ca. 12 mg/m^2 to 20-22 mg/m^2 (Figure 4-15). These data suggest that Tween 80 adsorbs weakly to the silica surface compared to Tween 20 which has a higher affinity, which is consistent to those of co-dissolved Tween.

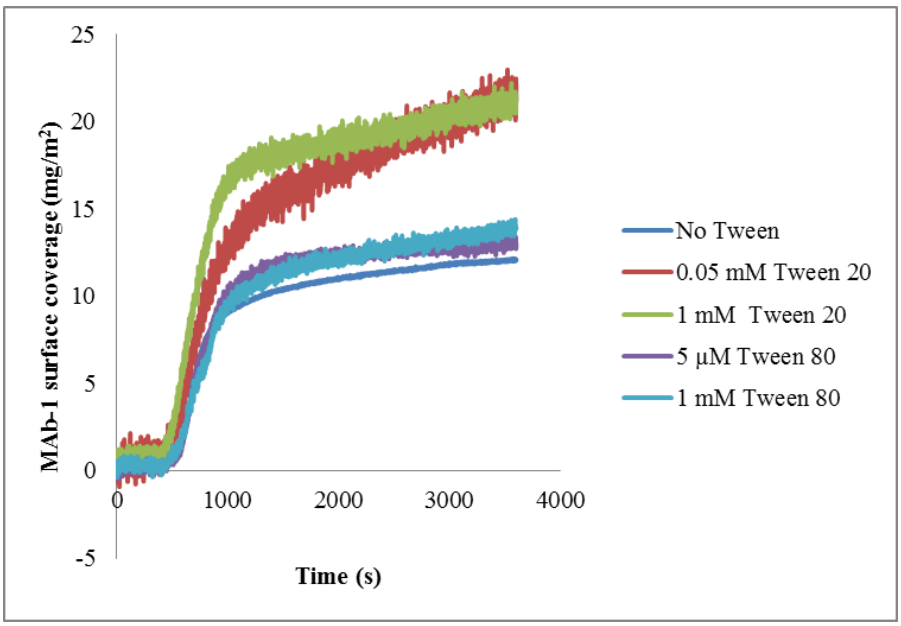

Figure 4-15. Effect of injecting Tween before mAb-1 on surface adsorption at pH 7.4.

Formulation	MAb-1 adsorption at pH 5.5 (mg/m^2)	MAb-1 adsorption at pH 7.4 (mg/m^2)
Control (No Tween)	5.46	12.12
0.05 mM Tween 20	1.80	21.15
1 mM Tween 20	1.79	21.51
5 µM Tween 80	2.32	13.05
1 mM Tween 80	1.89	13.97

Table 4-3. MAb-1 surface adsorption to a hydrophilic silica surface at pH 5.5 and pH 7.4 which had been pre-coated with Tween 20 and 80 at concentrations below and above their CMC.

4.4.4.3 Injection condition 3 - Effect of Tween injection after adsorption of mAb-1

The third Tween injection scenario investigated was injection of Tween after mAb-1 had been allowed to flow through the TIRF cell for 1800 s (30 minutes). The surface adsorption of the control and the curves for the 4 different Tween solution injections

were expected to overlap until 1800 s when Tween was injected. However, as Figure 4-16 shows, this was not the case when adsorption took place at pH 5.5. Nevertheless, overlapping of the curves was observed at pH 7.4 (Figure 4-17). Possible explanations for this discrepancy at pH 5.5 are discussed in section 4.5.6. The effect of Tween injection on adsorption will be discussed in terms of the individual profiles obtained for each Tween solution.

The injection of Tween after mAb-1 had adsorbed to the surface resulted in mAb-1 desorption and a decrease in the final mAb-1 surface adsorption value (Figure 4-16 and Table 4-4). Tween 20 at 0.05 mM (0.001 % w/v) and 1 mM Tween 80 (0.02 % w/v) were more effective at desorbing mAb-1 with surface adsorption levels returning to near baseline (Figure 4-16); desorption was rapid in both these cases. Desorption of mAb-1 by Tween 80 below its CMC (5 µM) caused a steady decrease in mAb-1 adsorption with desorption still taking place at the termination of the run.

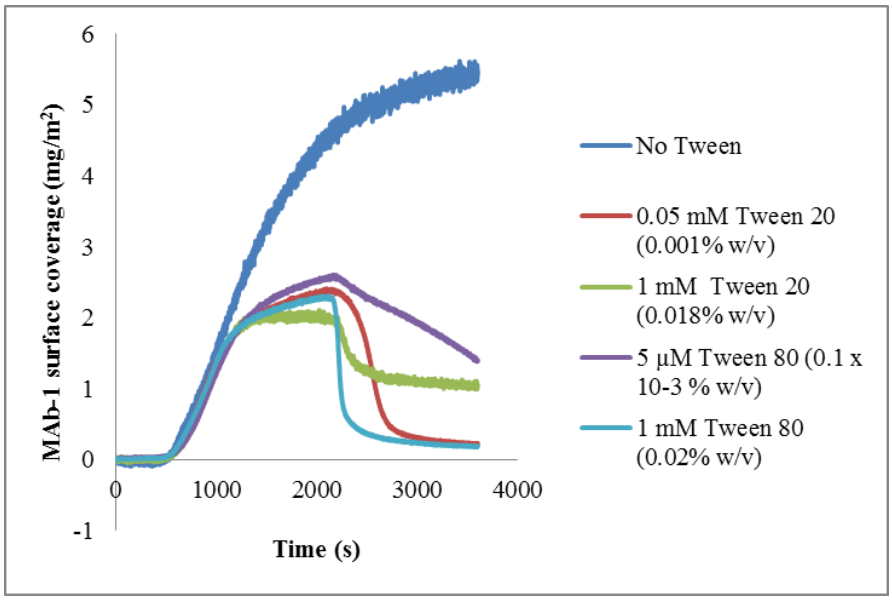

Figure 4-16. Effect of injecting Tween after mAb-1 on surface adsorption to a silica surface at pH 5.5.

The TIRF technique shows good reproducibility in measuring mAb-1 behaviour at the surface at pH 7.4 as demonstrated by overlap of the profiles which represent the adsorption phase, up to the point at which Tween was injected (Figure 4-17). The exception to this was the profile for 1 mM Tween 80 which was displaced upward by approximately 1 mg/m^2. Rapid desorption of mAb-1 from the silica surface was observed apart from Tween 80 below its CMC (Figure 4-17). MAb-1 displacement by Tween 20 was almost complete for both below and above the CMC as demonstrated by approximately 1 mg/m^2 mAb-1 remaining compared to ~12 mg/m^2 for bare silica at the plateau (Table 4-4). The quantity of mAb-1 desorbed by Tween 80 was less with adsorption values of 7 and 2 mg/m^2 for below and above the CMC respectively. These data show that with respect to mAb-1 desorption, Tween 20 affinity for the silica surface was greater than that of Tween 80.

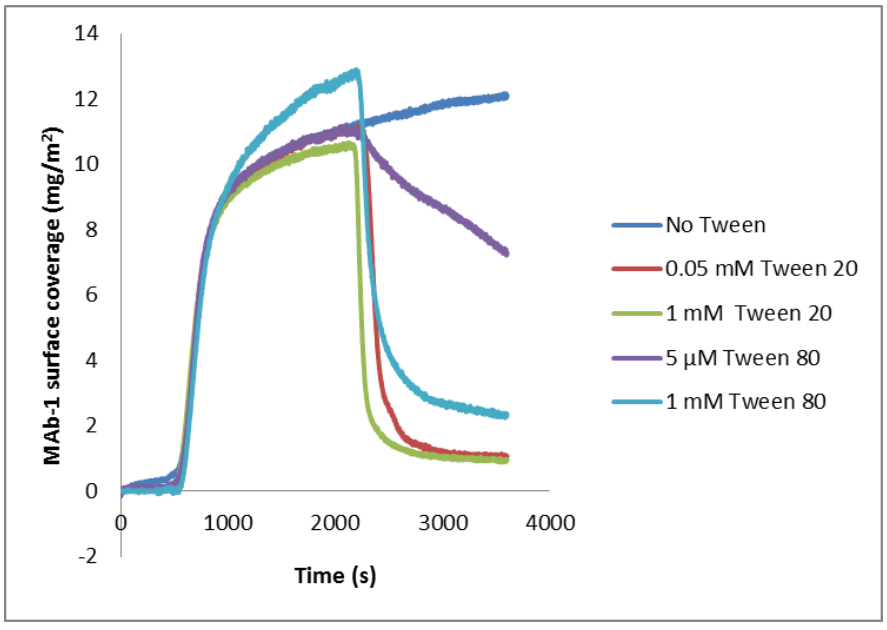

Figure 4-17. Effect of injecting Tween after mAb-1 on surface adsorption to a silica surface at pH 7.4.

Formulation	MAb-1 adsorption at pH 5.5 (mg/m^2)	MAb-1 adsorption at pH 7.4 (mg/m^2)
Control (No Tween)	5.46	12.12
0.05 mM Tween 20	0.23	1.07
1 mM Tween 20	1.05	0.94
5 μM Tween 80	1.39	7.24
1 mM Tween 80	0.19	2.32

Table 4-4. The effect of injecting Tween 20 and 80 at concentrations below and above their CMC on mAb-1 surface adsorption to a hydrophilic silica surface at pH 5.5 and pH 7.4.

4.4.4.4 Investigation of mAb-1 adsorption to a hydrophobic surface

In order to mimic immunoglobulin adsorption to hydrophobic plastic surfaces, silica was silanised with OTS from n-hexane to produce an octadecyl monolayer (McGovern et al., 1994). The kinetics of mAb-1 adsorption were investigated at pH 5.5 with adsorption observed on the silica surface to be approximately double that on the OTS-coated silica surface (ca. 4 mg/m^2 compared to ca. 2mg/m^2) (Figure 4-18). This suggests a reduced number of mAb-1 molecules per unit area which would result in a decreased fluorescent signal. TIRF does not provide layer formation data which was investigated using NR. The 'solid-state' CD and AFM data showed that mAb-1 secondary structure was lost on an OTS surface and had a low level of adhesion (section 3.4, Figure 3-12 and Figure 3-18) which corroborates the reduced adsorption determined from the TIRF data. MAb-1 retained its native state on silica (section 3.4.3.1, Figure 3-17) and therefore would be able to pack tighter resulting in the observed increase in fluorescent signal.

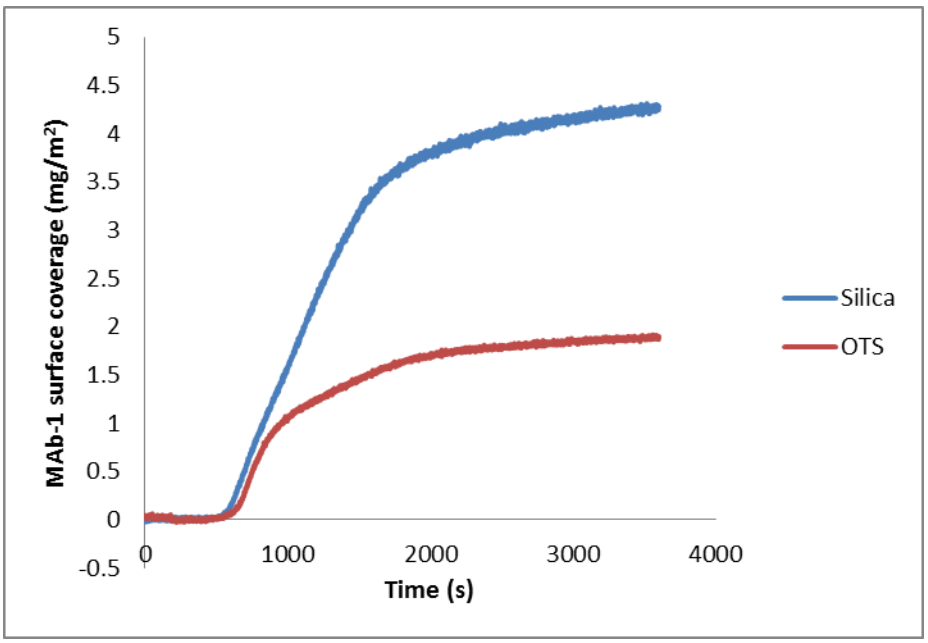

Figure 4-18. MAb-1 surface adsorption (at a concentration of 0.01 mg/mL and a shear rate of $6s^{-1}$) from a buffer at pH 5.5 was found to be influenced by surface energy.

4.4.4.5 Injection condition 1 – Effect of co-dissolved Tween on mAb-1 adsorption to a hydrophobic surface

The presence of co-dissolved Tween on mAb-1 adsorption to a simulated plastic surface was investigated. Tween 80 had a minimal effect on mAb-1 surface adsorption with no difference in concentration observed (Figure 4-19). This is in contrast to the effect observed for Tween 20, for which concentration had a clear influence on the extent of mAb-1 surface adsorption. Below the CMC of Tween 20, mAb-1 surface adsorption increased from the point at which adsorption to bare silica was beginning to plateau. The increase in adsorption was approximately linear with no plateau being reached in the duration of the experiment. On the other hand, Tween 20 above its CMC decreased adsorption by ~ 0.5 mg/m^2 compared to the control.

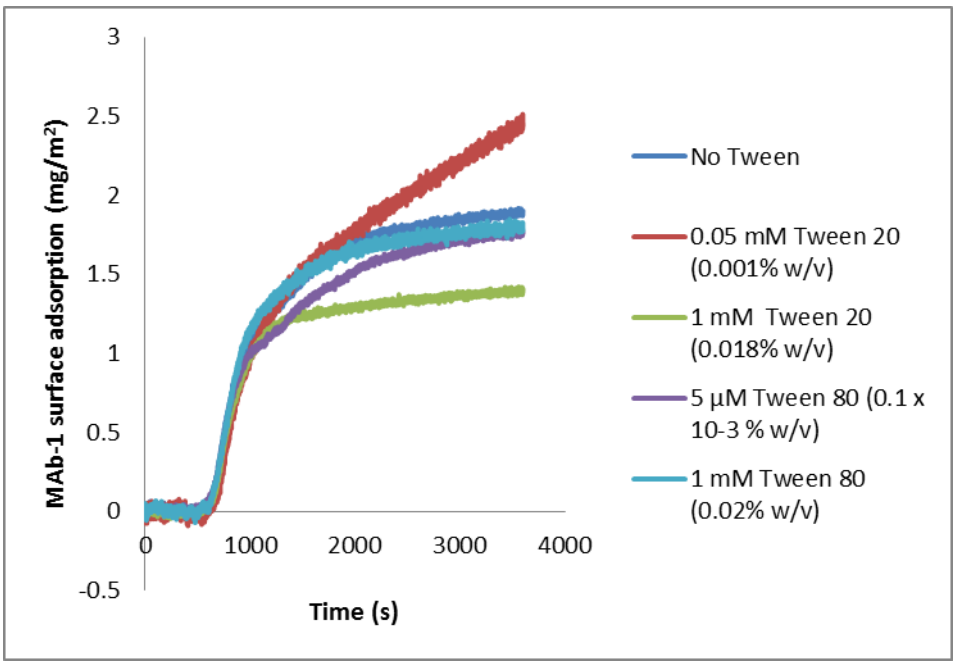

Figure 4-19. Co-dissolved Tween affects mAb-1 surface adsorption, at a concentration of 0.01 mg/mL, to an OTS-coated silica surface at pH 5.5 using a shear rate of $6s^{-1}$. Surface adsorption values were: No Tween (control) - 1.90 mg/m^2; 0.05 mM Tween 20 – 2.43 mg/m^2; 1 mM Tween 20 – 1.41 mg/m^2; 5 µM Tween 80 – 1.76 mg/m^2; and 1 mM Tween 80 – 1.77 mg/m^2.

4.4.4.6 Injection condition 2 – Effect of Tween injection prior to mAb-1 on surface adsorption to a hydrophobic surface

MAb-1 adsorption to the hydrophobic OTS surface was dependent on the concentration of Tween used during the pre-coating step. Above the CMC, both Tween 20 and 80 pre-coated surfaces reduced mAb-1 adsorption compared to the control by approximately 50 % (Figure 4-20). Adsorption had reached a near steady state as for the control to the OTS surface pre-coated with Tween 20/80 above their CMC. The opposite was the case for Tween 20/80 below their CMC, which increased mAb-1 adsorption by 1-2 mg/m^2 although adsorption had not ceased increasing (Figure 4-20). However, as with adsorption under the two alternative

Tween injection scenarios, the absolute change in mAb-1 adsorption was small compared to that observed for the silica surface. This is discussed further in section 4.5.7.

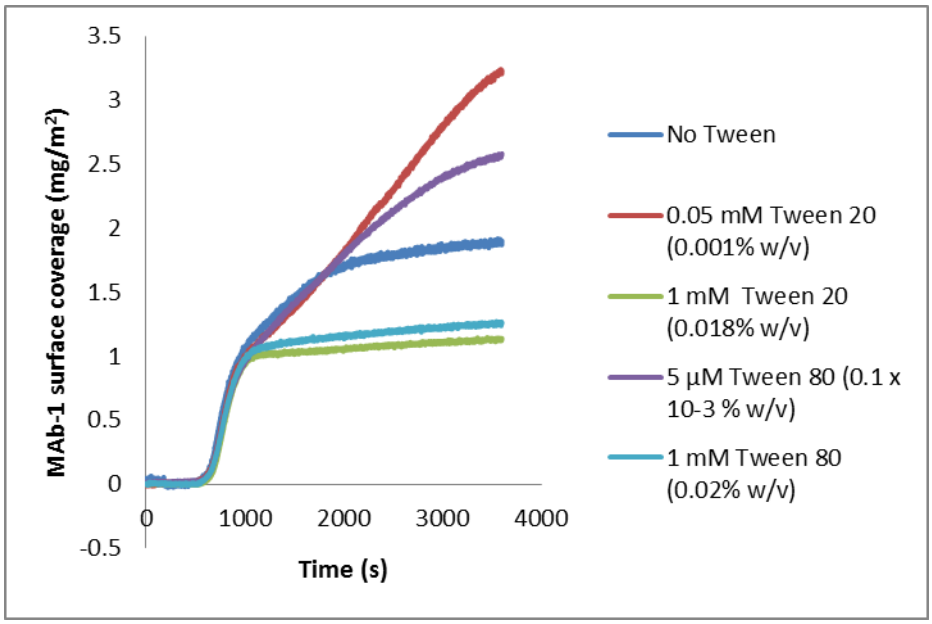

Figure 4-20. The concentration of Tween used to pre-coat an OTS-coated silica surface has a large influence on immunoglobulin surface adsorption at pH 5.5. Surface adsorption values were: No Tween (control) - 1.90 mg/m^2; 0.05 mM Tween 20 – 3.23 mg/m^2; 1 mM Tween 20 – 1.14 mg/m^2; 5 µM Tween 80 – 2.58 mg/m^2; and 1 mM Tween 80 – 1.26 mg/m^2.

4.4.4.7 Injection condition 3 – Effect of Tween injection after mAb-1 adsorption to a hydrophobic surface

Injection of Tween through the TIRF flow cell at a constant rate after mAb-1 resulted in antibody desorption from the surface, the degree of which was dependent on surfactant concentration (Figure 4-21). In contrast to desorption from the silica surface (Figure 4-16), Tween 80 below its CMC rapidly desorbed mAb-1 before reaching a near steady state of ca. 0.5 mg/m^2. Above the CMC, rapid desorption by Tween 80 was also observed however, the final adsorption level was less than that

seen below the CMC. At the end of the data collection period, desorption by Tween 20 was not complete as shown by the adsorption values still decreasing. These findings are in contrast to those observed for desorption of mAb-1 from the silica surface, where Tween 20 desorption was more rapid and to a greater extent than Tween 80. Desorption of mAb-1 from the surface is determined by the affinity of the two Tween surfactants for the specific surface which supports the explanation made for the silica surface data.

The TIRF profiles for adsorption of mAb-1 prior to Tween injection showed a large variability (Figure 4-21). The surface of the octadecyl monolayer is likely to be less consistent than bare, cleaned silica slides despite the formation of the self-assembled monolayer overnight which aids the formation of a homogenous layer. The scale of the y-axis for mAb-1 adsorption to the OTS-coated surface is over a smaller range than for silica. Thus any minor deficiency in the OTS layer may result in larger observed changes in the fluorescence profile despite the numerical difference being small. The profile of Tween 20 below its CMC was the most similar to the control during the adsorption phase compared to the remaining 3 solution profiles which were displaced downward.

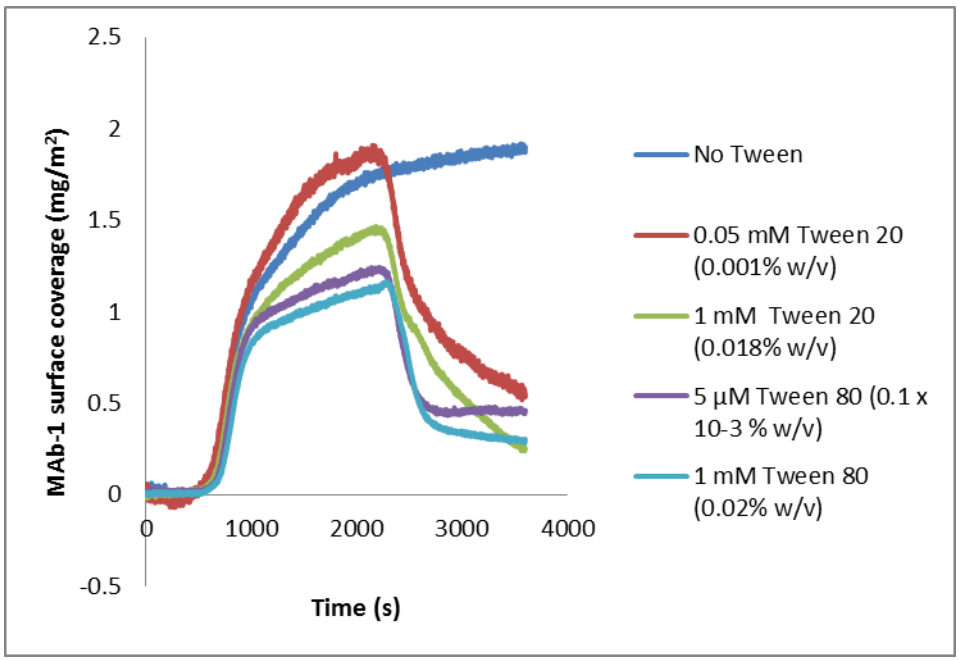

Figure 4-21. Injection of Tween after mAb-1 led to desorption from an octadecyltrichlorosilane (OTS)-coated silica surface at pH 5.5. Surface adsorption values were: No Tween (control) - 1.90 mg/m^2; 0.05 mM Tween 20 – 0.53 mg/m^2; 1 mM Tween 20 – 0.25 mg/m^2; 5 µM Tween 80 – 0.46 mg/m^2; and 1 mM Tween 80 – 0.30 mg/m^2.

4.4.4.8 Effect of storage in a pre-filled syringe on mAb-1 surface adsorption

Formulations for subcutaneous injection are typically stored in pre-filled syringes for ease of delivery. The effect of storage at 4 °C for 2 months was investigated using 2 types of syringe, CZ staked syringe and a BD syringe, and a glass vial (control). MAb-1 was stored at a concentration of 28 mg/mL in pH 7.4 buffer then diluted to a concentration of 0.01 mg/mL which satisfied the Leveque equation. Figure 4-22 shows that storage of mAb-1 at a concentration of 28 mg/mL in a CZ staked syringe or a BD syringe had no effect upon immunoglobulin surface adsorption. Although the data may indicate that mAb-1 is stable during storage in the syringes, the concentration used in the study was below that used for subcutaneous injection and so it may not be fully representative of the effect on a formulation. Due to the sample

volume and concentration required for TIRF analysis (as required for maintenance of the transport-limited model), it was not possible to use a high concentration as is typical in protein formulations.

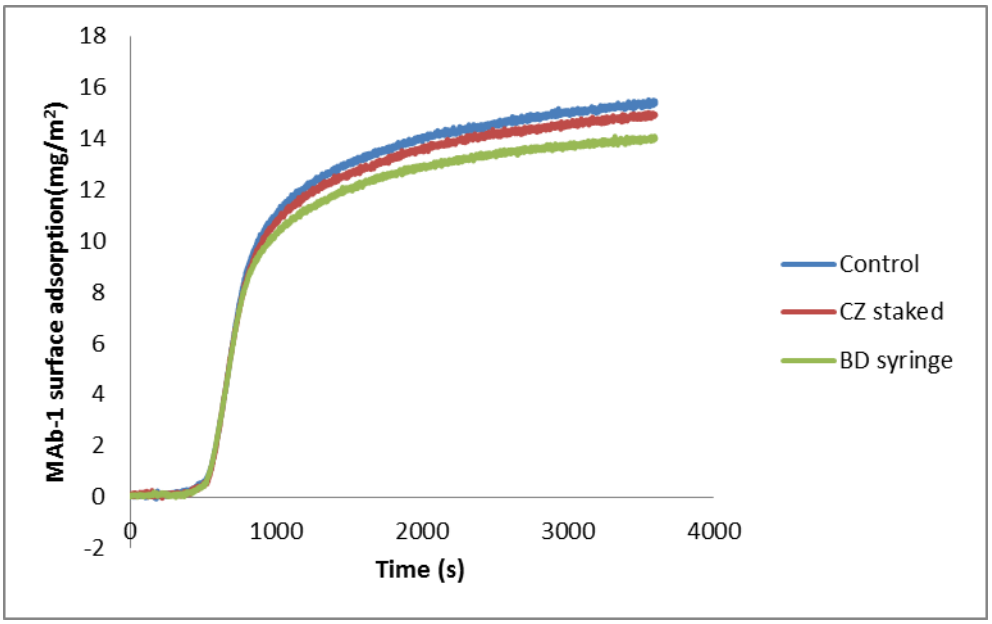

Figure 4-22. Effect of mAb-1 storage at a concentration of 28 mg/mL in CZ staked syringe or BD syringe on surface coverage.

4.4.5 Characterisation of mAb-1 surface fraction and orientation using neutron reflectivity (NR)

In order to gain a better understanding of the nature of the mAb-1 layer(s) adsorbed to the silica and OTS-coated silica surfaces during the TIRF experiments, and therefore improve interpretation, NR was used. Reflectivity profiles produced by the NR experiments allow possible models of how mAb-1 adsorbed to the silica and OTS surfaces as a result of a change in mAb-1 concentration and pH. In general, a theoretical SLD value of a protein is calculated for an assumed H/D exchange of 70 %. However, for the mAb-1 layer in D_2O the theoretical SLD value calculated for

H/D exchange of 70 % had to be changed to be able to fit the data to the parameters and obtain the best agreement (as determined by the χ^2 value). Using a 70 % H/D exchange, the surface fraction for the mAb-1 layer was greater than 1.0 which is not possible. Fitting of the NR data suggested that the mAb-1 layer was saturated (the surface fraction was 1.0), and so from the data fitting a theoretical SLD value was calculated using an H/D exchange of 50 %. Using this exchange rate, a theoretical SLD of 2.57 x 10^{-6} $Å^{-2}$ was generated which was used to calculate the surface fraction for all subsequent protein layers. Although the SLD value for mAb-1 has been calculated using a lower H/D exchange than is usual, a reduced H/D exchange has been found for lysozyme adsorbed to a silica surface compared to in bulk solution (Larsericsdotter et al., 2004). In a saturated layer, mAb-1 would be tightly packed thus reducing exposure to the solvent phase and the subsequent H/D exchange.

In contrast to the requirements for the TIRF experiments in which low concentrations had to be used to satisfy the Leveque equation, NR did not have this constraint. Concentrations which could realistically be used in protein formulations could be studied (50 to 150 mg/mL), however, due to sample concentration and volume restrictions the concentration was limited to a maximum of 5 mg/mL.

Over the range of mAb-1 concentrations investigated, a distinct difference in adsorption to the hydrophilic (SiO_2 which is the equivalent of the bare silica in the TIRF experiments) and hydrophobic (OTS-coated SiO_2) surfaces was apparent.

A clear fringe at a Q value of 0.09 $Å^{-1}$ was evident in the reflectivity profiles for mAb-1 adsorbed to the SiO_2 substrate from pH 5.5 buffer (Figure 4-23). Two

additional fringes could also be seen, one at a Q value higher and one lower than the main fringe. The same features were observed for all mAb-1 concentrations investigated. A similar result was found in the profiles for adsorption from buffer at pH 7.4 (Figure 4-24). In fitting of the reflectivity data for the bare SiO_2 substrate in D_2O, a very thin layer was included with a thickness of 1.5 to 3.5 Å and an SLD of 0.35 to 0.61 × 10^{-6} $Å^{-2}$ as this improved the fitting process in terms of the χ^2 values. This layer suggested the presence of a sporadic hydrogenous layer which was assumed to have been left as a result of the cleaning process (using Piranha solution) (Marsh et al., 1999, Kreiner et al., 2009).

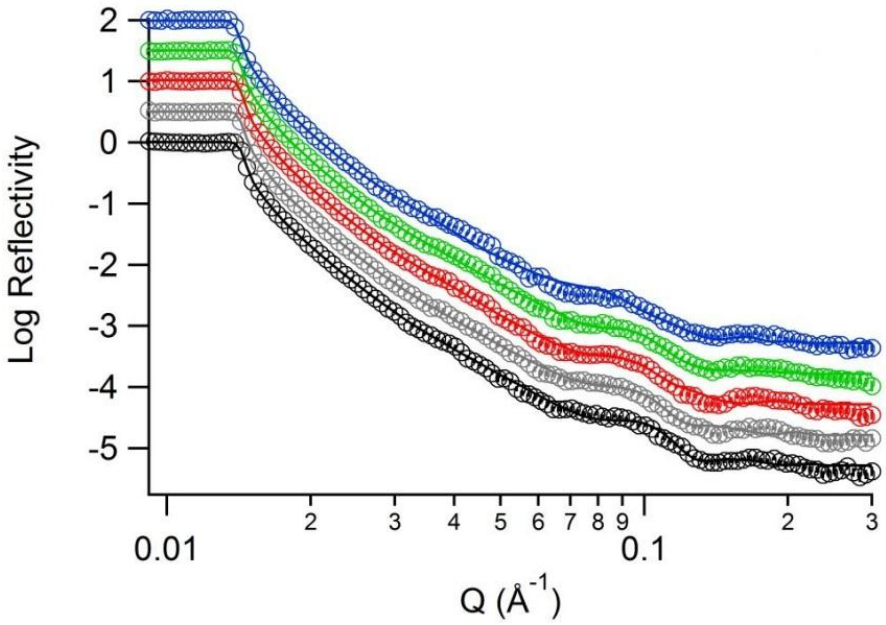

Figure 4-23. Reflectivity profile for MAb-1 adsorbed to a SiO_2 surface at bulk concentrations of 50 (black), 200 (grey), 500 (red), 2000 (green) and 5000 (blue) mg/mL in acetate buffer pH 5.5 (prepared using D_2O). Data points are shown as empty circles, with the fitted reflectivity profiles shown as solid lines in the same colour. For clarity, reflectivity profiles for increasing bulk concentrations are sequentially offset in the ordinate by a factor of $\log_{10}0.5$.

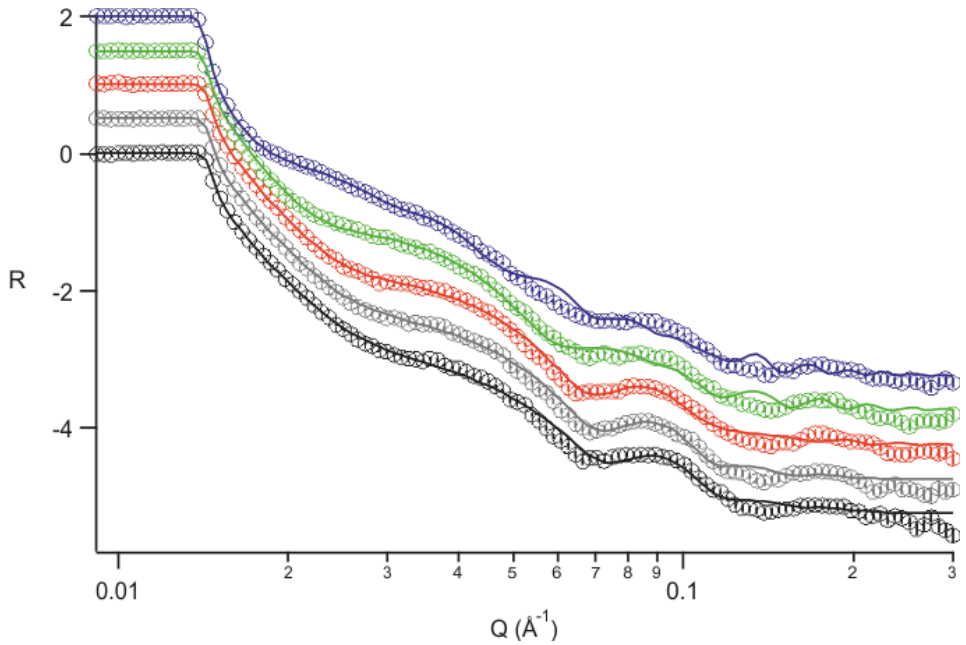

Figure 4-24. Reflectivity profile for MAb-1 adsorbed to a SiO_2 surface at bulk concentrations of 50 (black), 200 (grey), 500 (red), 2000 (green) and 5000 (blue) mg/mL in acetate buffer pH 7.4 (prepared using D_2O). Data points are shown as empty circles, with the fitted reflectivity profiles shown as solid lines in the same colour. For clarity, reflectivity profiles for increasing bulk concentrations are sequentially offset in the ordinate by a factor of $\log_{10}0.5$.

At both pH 5.5 and 7.4, the SLD profiles showed a bilayer model up to a concentration of 2000 mg/L (Figure 4-28). N-sigma analysis for bilayer and trilayer models was statistically in favour of bilayer formation for both pH values studied (Table 4-5 and Table 4-6).

[mAb] mg/L	1 layer χ^2	Degrees of freedom	N_sigma 1 layer	2 layer χ^2	Degrees of freedom	N_sigma 2 layers	Additional layer
50	7.46	3	51.51	1.98	6	8.27	Yes
200	6.95	3	47.42	1.87	6	7.37	Yes
500	10.50	3	75.66	2.47	6	12.21	Yes
2000	8.85	3	62.51	2.15	6	9.66	Yes
5000	11.86	3	86.41	5.51	6	36.67	Yes

Table 4-5. N_sigma analysis of mAb-1 adsorption to a SiO_2 substrate at pH 5.5.

[mAb] mg/L	1 layer χ^2	Degrees of freedom	N_sigma 1 layer	2 layer χ^2	Degrees of freedom	N_sigma 2 layers	Additional layer
50	8.39	3	58.86	3.67	6	21.89	Yes
200	7.24	3	49.70	3.28	6	18.70	Yes
500	9.36	3	66.57	3.08	6	17.11	Yes
2000	9.94	3	71.17	6.82	6	47.20	Yes
5000	12.64	3	92.62	5.70	6	38.16	Yes

Table 4-6. N_sigma analysis of mAb-1 adsorption to a SiO_2 substrate at pH 7.4.

The pH of the buffer from which mAb-1 was adsorbing to the surface and the solution concentration was shown from the SLD profiles to determine both orientation and surface fraction (Figure 4-23 and Figure 4-24; Table 4-7 and Table 4-8). At pH 5.5, the protein fraction of the layer in direct contact with the SiO_2 surface (the inner layer) was approximately 1.0 compared to the calculated fraction at pH 7.4 which ranged from 0.82 to 0.94. The layer thickness was greater at pH 7.4 which shows that the orientation of mAb-1 is different at the two pH values studied. The crystal structure of mAb-1 used here is not known, however, based on the

dimensions determined for an immunoglobulin by Silverton et al., (1977) and Harris et al., (1998) it is likely that at pH 5.5 mAb-1 adsorbed in a side-on manner when present at a low concentration which underwent a transition to end on upon an increase in concentration (Figure 4-25). The thickness of the layer was 95 Å at 50 mg/L which became 130 Å at 5000 mg/L which approximately correspond to the length and width dimensions of a mAb.

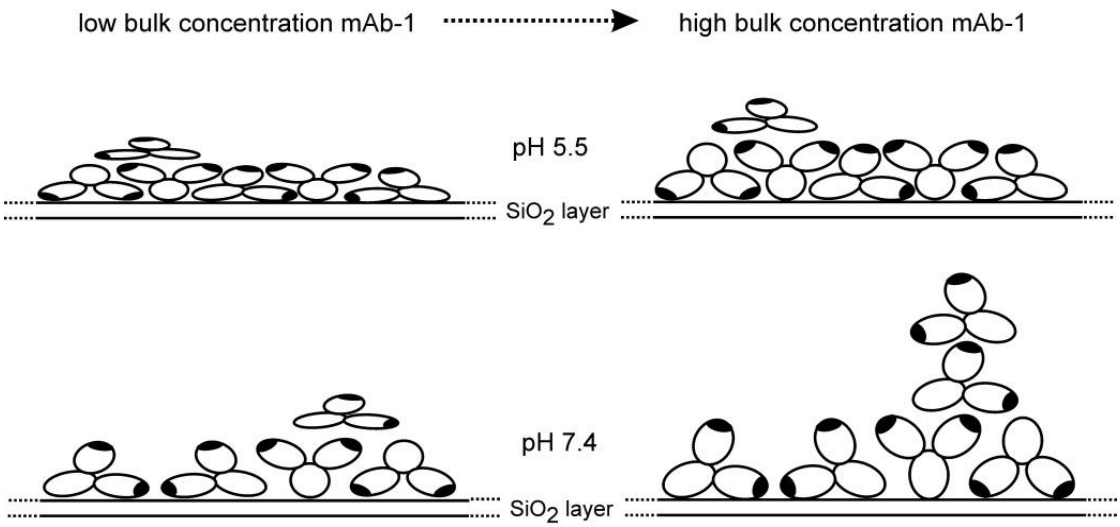

Figure 4-25. Cartoon depicting mAb-1 orientation on the SiO_2 surface at pH 5.5 and pH 7.4 and the change in orientation with the increase in bulk solution concentration.

The protein surface fraction of mAb-1 adsorbed at pH 5.5 was higher than at pH 7.4 with no increase observed as the concentration increased. The thickness of the inner mAb-1 layer when adsorbed from buffer at pH 7.4 increased from 130 to 207 Å as the solution concentration increased (Table 4-8). At pH 5.5, the outer layer remained in a side on orientation up to the highest concentration studied with the protein fraction indicating the layer to be sparse (Table 4-7). The most notable re-orientation of the mAb-1 layers took place at pH 7.4 when the highest concentration of 5000

mg/L was investigated. Up to this concentration, the inner layer was adsorbed in an end on orientation and the outer layer in a side on manner. At 5000 mg/L a sparse third layer formed on the SiO_2 surface with all three layers becoming oriented in an end-on manner (depicted in Figure 4-25). The protein surface fraction at pH 7.4 is reduced compared to pH 5.5 which would be expected for mAb-1 adsorbed end-on as the footprint would be less. The fraction increased with mAb-1 concentration from 2000 to 5000 mg/L which indicated that additional molecules adsorbed during the bilayer to trilayer transition.

[mAb] mg/L	Layer 1 thickness (Å)	Layer 2 thickness (Å)	Layer 1 protein fraction	Layer 2 protein fraction
50	95	60	0.99	0.22
200	102	62	1.00	0.24
500	115	63	1.00	0.27
2000	117	66	1.01	0.29
5000	130	70	1.01	0.31

Table 4-7. MAb-1 layer thickness and protein fraction when adsorbed to SiO_2 from buffer at pH 5.5 prepared using D_2O.

[mAb] mg/L	Layer 1 thickness (Å)	Layer 2 thickness (Å)	Layer 3 thickness (Å)	Layer 1 protein fraction	Layer 2 protein fraction	Layer 3 protein fraction
50	131	68	-	0.90	0.17	-
200	133	68	-	0.88	0.26	-
500	141	67	-	0.85	0.15	-
2000	160	69	-	0.82	0.14	-
5000	207	145	178	0.94	0.25	0.15

Table 4-8. MAb-1 layer thickness and protein fraction when adsorbed to SiO_2 from buffer at pH 7.4 prepared using D_2O.

The reflectivity profile for mAb-1 adsorbed to the OTS-coated SiO_2 surface showed a single fringe at Q of 0.1 $Å^{-1}$ (Figure 4-26 and Figure 4-28). The OTS layer was found to be 17 Å thick with a negative SLD of ~0.76 × 10^{-6} $Å^{-2}$ which is similar to previously fitted data for an OTS substrate (thickness of 16 Å and SLD -0.5 ± 0.3 × 10^{-6} $Å^{-2}$ (Lu et al., 1998)).

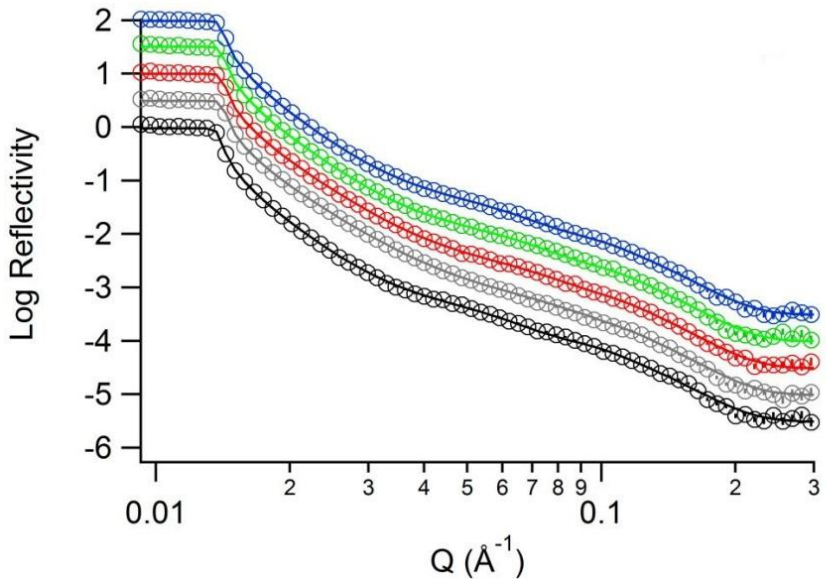

Figure 4-26. Reflectivity profile for MAb-1 adsorbed to OTS-coated SiO_2 surface at bulk concentrations of 50 (black), 200 (grey), 500 (red), 2000 (green) and 5000 (blue) mg/mL in acetate buffer pH 5.5 (prepared using D_2O). Data points are shown as empty circles, with the fitted reflectivity profiles shown as solid lines in the same colour. For clarity, reflectivity profiles for increasing bulk concentrations are sequentially offset in the ordinate by a factor of $\log_{10}0.5$.

The surface fraction and layer thickness increased upon the transition from low to high mAb-1 concentration (Table 4-9). These data suggest reorientation of mAb-1 on the OTS surface (Figure 4-27). Analysis of 1-layer and 2-layer protein models at the OTS-coated surface using N-sigma was statistically in favour of a mAb-1 monolayer as shown by smaller χ^2 values (Table 4-10).

[mAb] mg/L	Layer 1 thickness (Å)	Layer 1 protein fraction
50	99	0.12
200	107	0.15
500	113	0.19
2000	119	0.21
5000	125	0.23

Table 4-9. Layer thickness and protein fraction of mAb-1 adsorbed to an OTS-coated SiO_2 substrate from buffer at pH 5.5 prepared with D_2O.

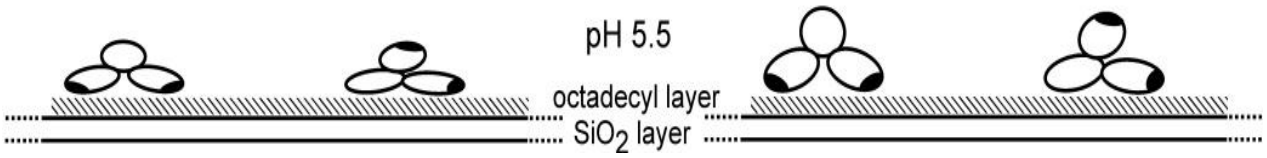

Figure 4-27. Cartoon depicting mAb-1 orientation on the OTS-coated SiO_2 surface at pH 5.5 and the change in orientation as a result of the concentration increase in bulk solution.

[mAb] mg/L	1 layer $\chi 2$	Degrees of freedom	N_sigma 1 layer	2 layer $\chi 2$	Degrees of freedom	N_sigma 2 layers	Additional layer
50	506.82	3	3161.63	2.34	6	9.08	Yes
200	501.91	3	3130.94	1.66	6	4.71	Yes
500	535.64	3	3341.76	3.58	6	19.98	Yes
2000	529.41	3	3302.82	1.95	6	6.54	Yes
5000	500.67	3	3123.18	3.86	6	18.76	Yes

Table 4-10. N_sigma analysis of mAb-1 adsorption to an OTS-coated SiO_2 substrate at pH 5.5.

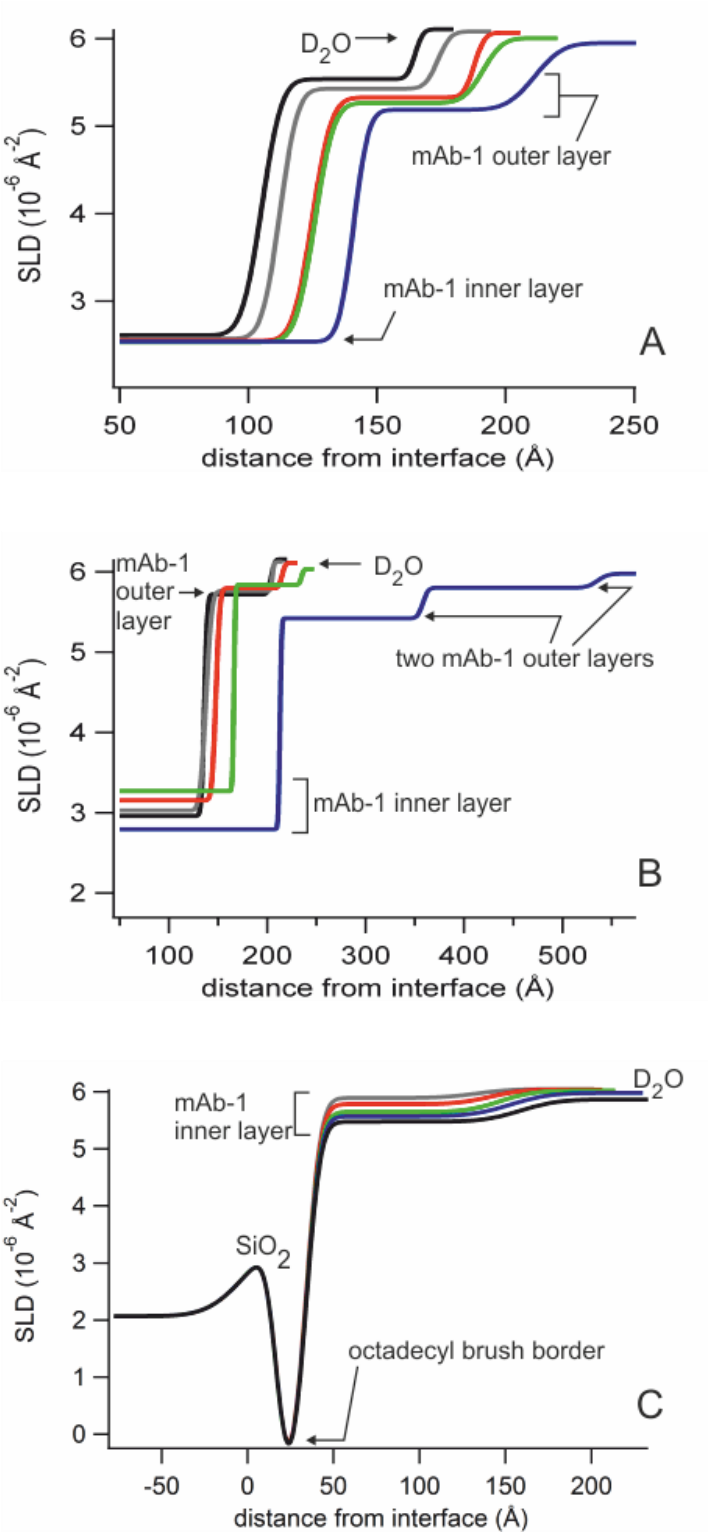

Figure 4-28. Fitted SLD profiles for reflectivity data for mAb-1 adsorbed to SiO_2 from solutions in acetate pH 5.5 (A) or PBS pH 7.4 (B), and to OTS-coated SiO_2 from solutions in acetate pH 5.5 (C) prepared with D_2O. Profiles are shown as the distance from the silicon-SiO_2 interface and labels are used as a guide for the SLD of each layer.

4.5 Discussion

4.5.1 Fluorescent labelling and contribution to the signal intensity

The ratio of FITC label to mAb-1 in these studies was approximately 1:1 with a minimal difference in the precise ratio being calculated between each labelled protein batch. However, this was not of great concern as different labelling densities have been shown to produce the same protein surface adsorption kinetics (Wertz and Santore, 1999). Fluorescein undergoes self-quenching due to Forster resonance energy transfer between nearby fluorescein molecules and it has been reported that due to this process an increase in labelling ratio does not correspond to an increase in fluorescence (Lakowicz et al., 2003). Adsorption of a labelled IgG-like domain pair with FITC has been observed to occur with no bleaching of the fluorophores (Pereira et al., 2008) and thus bleaching was not expected to take place in this study. The Alexa Fluor 488 5-SDP label has previously been used to label three proteins (IgG, HSA, and fibrinogen) for the investigation of adsorption using TIRF (Ding and Hlady, 2011) demonstrating its suitability in this study.

The FITC and Alexa Fluor 488 5-SDP labels were not found to adsorb to the silica surface which is similar to a previous study of adsorption of FITC to a hexadecyltrichlorosilane self-assembled monolayer (Wertz and Santore, 1999). The presence of a label was therefore assumed not to influence the kinetics of mAb-1 adsorption as has been shown previously for proteins labelled with FITC (Malmsten et al., 1997). The contribution of labelled protein in the bulk solution was found to be minimal as a sharp drop off in signal was not observed when labelled mAb-1 was removed from the flow channel (Figure 4-8).

Relaxation of labelled protein at the surface could also influence the fluorescent signal. At near steady state fluorescence, a drift in the signal would signify relaxation of the protein and changes in the fluorescence. The TIRF profile of mAb-1 at near steady state in the absence of surfactant (Figure 4-6) did not demonstrate a drift in the fluorescent signal. This suggests that over the duration of the run, any relaxation of the adsorbed mAb-1 layer does not affect the fluorescent signal. This is supported by the relaxation of albumin and fibrinogen at the surface also having been found not to alter the fluorescent signal (Wertz and Santore, 1999). The 'solid-state' CD data in section 3.4.3 showed mAb-1 to largely retain its native structure upon adsorption to a silica surface, and it was therefore assumed that adsorption during the TIRF experiments would take place with mAb-1 in its native state.

4.5.2 Calibration of raw fluorescence data

The calibration of raw fluorescence data to allow the conversion from arbitrary units (AU) into a quantitative adsorption unit would ideally be undertaken by obtaining radioactive measurements of the amount of adsorbed radio labelled protein. This method has previously been used for BSA labelled with FITC and tritium to quantify the adsorption observed in the TIRF experiments. It was found that a linear increase in fluorescence intensity of a labelled protein adsorbed to a surface corresponded to a linear increase in the protein concentration on the surface (Lok et al., 1983a, Lok et al., 1983b). However, this method was not used in this study for a number of reasons: (1) it would be required for each slide surface tested; (2) a standard curve would be required to relate radioactivity to protein quantity and decay would have to be taken into account; (3) it would require a suitable non-denaturing radio labelling procedure and; (4) radioactivity is avoided if at all possible due to safety concerns.

To avoid the use of a radioactive label, a secondary technique such as Brewster angle microscopy can be used to calibrate a TIRF system. For example, the increase in the fluorescent signal of a labelled polymer investigated using TIRF has been found to be linear and proportional to the quantity of adsorbed polymer (Fu and Santore, 1998). The TIRF data produced in the experiment by Fu and Santore (1998) was externally calibrated using a near Brewster internal reflection optical reflectometer. This calibration data was then used in further experiments by the authors. It was found that the fluorescence intensity produced as a result of adsorption of albumin and fibrinogen to a surface could be converted to a quantitative measure of protein adsorption providing the diffusion coefficient was known. The quantity of the two proteins determined to be adsorbed to the surface were consistent with previous findings supporting the validity of conversion of fluorescence data to protein surface adsorption using the Leveque equation (Lok et al., 1983a, Nygren and Stenberg, 1988).

An alternative TIRF calibration method has been used for the proteins lysozyme and chymotrypsin A. Through initial measurement of fluorescence under conditions during which adsorption was not expected to occur, any subsequent increase in fluorescence detected upon addition of protein solution was inferred to be due to adsorption to the surface. It was found that a linear increase in fluorescence corresponded to a linear increase in lysozyme surface adsorption, a similar result was also observed for chymotrypsin A (Shibata and Lenhoff, 1992b). A further study by the same authors identified transport limited adsorption for lysozyme and chymotrypsin A using TIRF (Shibata and Lenhoff, 1992a). Thus, by knowing the protein concentration and diffusion coefficient, the quantity of protein adsorbed to

the surface can be derived from the rate change of fluorescence intensity using the Leveque equation. This holds under the condition that the increase in fluorescence intensity detected using TIRF is transport limited, shown by a linear increase in fluorescence with increasing protein concentration.

Calibration of the raw fluorescence data using the TIRF set-up in this study had been accomplished in a previous investigation which compared TIRF data for an immunoglobulin domain pair known to adsorb to bare silica in an irreversible manner at surface saturation (Pereira et al., 2008) to neutron reflectivity data for the same protein (Kreiner et al., 2009). A range of bulk concentrations of the immunoglobulin domain pair were injected into the TIRF cell and the fluorescence signal measured. The signal at the point a steady state had been reached following protein adsorption and rinsing with a buffer was then calibrated against the neutron reflectivity data which had been fitted for the domain pair adsorbed to the surface over the same concentration range and following a buffer rinse. As the same TIRF set-up was used in these experiments, which meant that calibration of the raw fluorescence data had been carried out, the fluorescence units (AU) were converted to surface coverage for the non-identical but related immunoglobulin protein.

4.5.3 Confirmation of transport limited adsorption

For mAb-1, surface adsorption was transport limited (which is necessary to satisfy the Leveque equation) up to a concentration of 0.25 mg/mL (Figure 4-5). The requirement of transport limited adsorption is necessary to ensure laminar flow of mAb-1 to the surface and not a turbulent flow. Consequently, TIRF is not a suitable technique for the investigation of concentrations typically used in protein formulations. In addition to this, the maximum shear rate which could be selected

was 42 s^{-1} (4.0 mL/h) and thus the concentration of mAb-1 and shear rate used during the TIRF experiments was restricted. Similar to the findings for mAb-1, adsorption of BSA and fibrinogen has been shown to no longer be transport limited at high concentration (> 100 mg/L) or shear rate (above 41 s^{-1}) (Wertz and Santore, 1999, Lok et al., 1983a).

At high shear strain rates, aggregation and precipitation of an IgG4 (Biddlecombe et al., 2007) and recombinant human growth hormone (Maa and Hsu, 1997) have been shown to occur, however, at the low shear rate used in this study aggregation and precipitation of mAb-1 due to shear is not expected. In the absence of an air/liquid interface, two factors were identified as being important in the formation of large soluble IgG4 aggregates: pH and nanometer-scale surface roughness (Biddlecombe et al., 2009). The TIRF system used in this study was closed and therefore aggregation induced by exposure to an air-liquid interface is unlikely to be a factor in mAb-1 surface adsorption.

4.5.4 MAb-1 adsorption is affected by co-dissolved Tween

Adsorption of mAb-1 in the presence of Tween 20 and 80 was found to be strongly dependent on both Tween concentration and pH. Above the CMC, Tween 20 and 80 presence reduced mAb-1 surface adsorption to silica at pH 5.5 (Figure 4-12) which was in contrast to the increased adsorption observed at pH 7.4 (Figure 4-13). The increase in adsorption at pH 7.4 was unforeseen as the higher concentration of Tween would be expected to compete with mAb-1 for surface binding sites. However, it is likely that the co-dissolved Tween above its CMC saturated the silica surface and non-specific binding sites on mAb-1. MAb-1 will remain in its native state in this scenario, as shown by the CD data (section 2.4.3, Figure 2-21), although

in a non-specific complex with the Tween. The retention of native structure is predicted from calorimetry data in this study for Tween interaction with mAb-1 and previously calorimetry data for a recombinant human IgG (Hoffmann et al., 2009a). In this situation the mAb-1-Tween complex would approach the silica surface which is also saturated with Tween. It would therefore be possible for self-assembly of Tween chains at the silica and mAb-1 surfaces to occur thus driving the observed increase in mAb-1 surface coverage at pH 7.4. This increase could result from a change in protein packing and/or the formation of multiple mAb-1 layers which would both be demonstrated in the TIRF profiles simply as an increase in the quantity of protein adsorbed. The length of the alkyl chain of the Tween molecules (section 1.5.4, Figure 1-6) was anticipated to affect affinity for the silica surface. The shorter C12 alkyl chain of Tween 20 was expected to show an increased affinity for the silica surface compared to the C18 alkyl chain of Tween 80, the opposite being the case for the OTS-coated surface. However, the TIRF profiles showed their effect in reducing mAb-1 adsorption on the silica surface to be similar at pH 5.5.

At a concentration above the CMC (1 mM in this study), Tween would be in the form of micelles and expected to remain so when present in the TIRF cell. In this scenario there will also be monomers which will likely fill the non-specific binding sites on mAb-1 and adsorb to the surfaces investigated. An increase in the entropy of the system would be required for the micelles to dis-assemble and drive them onto the silica surface which would be thermodynamically unfavourable. However, Tween 80 micelles are known to be highly dynamic and readily dis-assemble (Amani et al., 2011). Individual Tween monomers would therefore become present in the

solution, and thus be free to compete with mAb-1 for surface binding sites which would account for the decreased adsorption observed at pH 5.5 (Figure 4-12).

Co-dissolved Tween below the CMC decreased mAb-1 surface adsorption at both pH 5.5 and 7.4 (Figure 4-12 and Figure 4-13). The data suggest that the affinity of the Tween molecules for the silica surface is greater than that for the mAb-1 surface which led to a reduction in protein adsorption. The greater affinity for the silica surface may be as a result of the interaction of the silica surface hydroxyl groups with the polyethylene glycol (PEG) head groups of the Tween. The TIRF adsorption profiles were characterised by a transient peak upon co-injection. Initial adsorption of mAb-1 at pH 5.5 when co-dissolved with 0.05 mM Tween 20 increased to a level greater than that of the control (~7 mg/m^2 compared to ca. 5.5 mg/m^2); however, adsorption was of a similar level to that observed for co-dissolved Tween 80 below its CMC at pH 7.4 (~7.3 mg/m^2). The transient peak is indicative of competition between free mAb-1 and Tween molecules in solution with the latter competing with mAb-1 for surface sites. It is most probable that this is due to the difference in the diffusion coefficients, the value for Tween 80 is five-orders of magnitude smaller than that of mAb-1: 1.8×10^{-6} cm^2/s compared to 1.99×10^{-11} cm^2/s calculated using the Stokes-Einstein equation as described in 4.3.2. Inclusion of 0.01 % (w/v) Tween 80 has been found to reduce IgG1 surface adsorption to nylon (from ~1920 to ca. 170 μg/17 cm^2 filter surface) and cellulose acetate surfaces by approximately 76 μg/17 cm^2 filter surface (from 90 to 12 μg/17 cm^2 filter surface) (Mahler et al., 2010). The finding in this study and that by Mahler et al., (2010) are in contrast to findings for lysozyme, in which Tween 80 co-dissolved with lysozyme at 80 ppm did not affect lysozyme adsorption (Joshi and McGuire, 2009).

A kinetic experiment using NR was undertaken using co-dissolved Tween 20 (at a concentration of 0.05 mM) in order to attempt to gain a better understanding of the processes taking place during the transient adsorption phase. However, transient immunoglobulin adsorption was not observed and due to time constraints no further kinetic experiments with co-dissolved Tween were carried out.

4.5.5 MAb-1 adsorption to pre-coated Tween surfaces

The second injection scenario was the flow of Tween through the TIRF cell prior to injection of mAb-1 to investigate adsorption to pre-coated Tween surfaces. Pre-coating of the silica surface with Tween was expected to change the functional group present on the surface to which mAb-1 would be exposed (from –OH (Zhuravlev, 1993) to a PEG group). Characterisation of the Tween surfaces demonstrated a change from the silica control surface with data showing the surface to be more hydrophilic and have a greater level of adhesion for mAb-1 (section 3.4, Table 3-6 and Figure 3-13). As discussed in 3.5.2 Tween 20/80 were not expected to form a densely packed ordered 'brush border' on the surface in this study which is in contrast to tri(ethylene glycol) which has been shown to form a brush border which repels proteins (Skoda et al., 2009). The Tween surfaces were therefore assumed not to be protein repellent, which was found to be the case in this study as demonstrated by the increased mAb-1 adsorption observed on a hydrophilic surface at pH 7.4 (Figure 4-15) and to a hydrophobic surface coated with Tween below its CMC (Figure 4-20). The observed mAb-1 adsorption to the Tween coated surfaces is consistent with findings in the literature which showed a PEG surface facilitated protein adsorption (Sheth and Leckband, 1997a, Efremova et al., 2001). It has been suggested that protein adsorption to PEG surfaces is due to rearrangement of the

PEG backbone and interaction with the ethylene oxide unit (Sheth and Leckband, 1997a, Efremova et al., 2001). This explanation could similarly be correlated with the data obtained in this study which showed mAb-1 adsorption to the Tween coated surfaces.

The 'solid-state' CD spectra showed the native structure of mAb-1 to be retained upon adsorption to Tween coated silica beads (3.4.3.3, Figure 3-21), however, Dichroweb analysis showed that the quantity of β-sheet loss and increase in α-helical content in mAb-1 was greater on the Tween coated surfaces than on silica. These data demonstrate that structural changes in mAb-1 are highly likely upon adsorption to the Tween coated surfaces in the TIRF experiments here, but extensive unfolding is unlikely. Tween 20 was found to generate a more hydrophilic surface than Tween 80 (3.4.2.2, Table 3-6), and therefore would better maintain adsorbed mAb-1 in its native state thus permit tighter packing on the surface. As a result of tighter packing there would be an increase in the number of mAb-1 molecules per unit area and consequently an increase in the fluorescent signal detected during the TIRF experiments. The hydrophilicity of the Tween 80 coated surface increased to a lesser extent (3.4.2.2, Table 3-6) and correspondingly the signal was expected to increase by a smaller degree (compared to silica control).

However, the hydrophilicity of the Tween coated surfaces was not found to determine mAb-1 adsorption at pH 5.5 as shown by decreased mAb-1 adsorption to all four pre-coated Tween surfaces (Figure 4-14). The differences in adsorption data at pH 5.5 corresponded to the increased loss of mAb-1 structure on the pre-coated surfaces with Tween above its CMC as suggested by Dichroweb analysis (section 3.4.4.3, Table 3-18). The nrmsd value was high for surfaces coated with Tween

below the CMC and so the calculated percentages of mAb-1 secondary structure may not be accurate (section 3.4.4.3, Table 3-18). The reduced mAb-1 adsorption to the Tween coated surfaces at pH 5.5 (Figure 4-14) is similar to findings for a surfactant coated silica surface which likewise did not inhibit protein adsorption but led to a reduction in the quantity adsorbed (Lichtenbelt et al., 1993).

In contrast to mAb-1 adsorption at pH 5.5 (Figure 4-14), the hydrophilicity of the Tween coated surfaces influenced mAb-1 adsorption at pH 7.4 (Figure 4-15). The water contact angle of a Tween 20 coated surface was approximately 10° less than that of a Tween 80 coated surface. The TIRF data showed that the level of mAb-1 adsorption was greater on Tween 20 coated surfaces than on surfaces which had been coated with Tween 80. Therefore, the TIRF data obtained for adsorption of mAb-1 to the silica surface coated with Tween at pH 7.4 agrees with the Dichroweb data.

It has been suggested that PEG chains exist either in a protein repellent or a protein attractive state (Efremova et al., 2001). The TIRF profiles for mAb-1 adsorption to the Tween surfaces in this study at pH 7.4 agree with this suggestion, as adsorption was increased by the presence of Tween 20 on a surface compared to Tween 80 which caused a decrease in mAb-1 adsorption (Figure 4-15). The ability of a Tween coated surface to repel mAb-1 will be also be affected by packing of the surfactant molecules and therefore access to non-specific binding sites. Tighter packing of Tween 20 than Tween 80 at the air-liquid interface has been found with the difference attributed to the difference in their structures (Ruiz-Pena et al., 2010) (Tween structures are shown in section 1.5.4, Figure 1-6).

The interaction between a hydrophilic surface and Tween has previously been found to be weaker than that with a hydrophobic surface owing to the lack of hydrophobic interactions (Joshi and McGuire, 2009). In the investigation by Joshi and McGuire (2009) injection of the protein lysozyme onto a surface which had been pre-coated with Tween 80 (similar to the experiment in this study) desorbed the Tween from the surface. Lysozyme was subsequently found to adsorb to the surface to a similar extent to that observed on bare silica (Joshi and McGuire, 2009). In the study here, mAb-1 adsorption at pH 7.4 on surfaces which had been pre-coated with Tween 80 was similar to that of bare silica which corroborates the findings by Joshi and McGuire (2009). However, this was not found to be the case in this study for Tween 20 coated surfaces at pH 7.4 (on which mAb-1 adsorption increased) or pre-coated Tween surfaces at pH 5.5 (to which mAb-1 adsorption decreased).

4.5.6 Tween desorption of mAb-1 from a hydrophilic surface

The third and final Tween injection condition investigated was injection of mAb-1 followed by Tween. MAb-1 was desorbed from the silica surface by injection of both Tween 20 and 80 at concentrations below and above their CMC at the two pHs (pH 5.5 and 7.4) investigated (Figure 4-16 and Figure 4-17). The extent of mAb-1 desorption was dependent on the type of Tween and concentration injected. The kinetics of Tween adsorption and displacement of mAb-1 must be rapid as desorption of mAb-1 by Tween took place almost immediately upon injection. MAb-1 desorption was only slow for Tween 80 below its CMC, which could be a result of the concentration being 10-fold less than that for Tween 20 (this was necessary to achieve concentrations below the CMCs of Tween and 20 and 80). Under the flow conditions, continuous ‘arrival’ of Tween molecules at the surface can be envisioned.

It consequently appears that the absolute concentration of Tween is of more relevance than concentration with regard to the CMC. The concentration of Tween 20 in a wash solution has been shown to affect the degree of protein adsorption, as evidenced by a concentration of 0.5 % w/v being more effective than 0.005 % w/v (Feng et al., 1995). This was also found to be the case in this study, with 5 µM Tween 80 being the least effective at desorbing mAb-1 from the silica surface. The process of mAb-1 desorption from the surface most likely takes place via the phenomenon termed orogenic displacement. Orogenic displacement is a three step mechanism: **(1)** adsorption of the surfactant to defects in the protein layer on the surface; **(2)** expansion of the surfactant sites and compression of the protein film which increases in thickness and; **(3)** displacement of the protein from the surface (Mackie et al., 1999, Mackie et al., 2000b). This process of protein displacement by surfactants has been shown for the globular proteins β-casein and β-lactoglobulin from the air/water and oil/water interface by various surfactants including Tween and sodium dodecyl sulphate (SDS) (Mackie et al., 1999, Mackie et al., 2000a, Gunning et al., 2004).

Nevertheless, mAb-1 was not desorbed fully by Tween 20/80 below or above their CMC as the initial baseline value did not return to that prior to mAb-1 injection into the cell upon completion of the run. This finding suggested that the adsorbed protein population was heterogeneous. A similar result has been observed with residual adsorbed antibody detected on a hydrophilic (You and Lowe, 1996) and hydrophobic surface (Oom et al., 2012) post desorption by surfactant. The finding indicates that mAb in direct contact with the surface adsorbs irreversibly and the subsequent layers are reversibly bound. In contrast to these studies, only a small decrease in the layer

thickness of a mAb on a silica surface has been observed after injection of Tween 20 (Lichtenbelt et al., 1993). Similar to the study by Lichtenbelt et al., (1993) desorption of the protein lysozyme from a silica surface was largely unaffected by Tween 80 injection (Joshi and McGuire, 2009).

4.5.7 MAb-1 adsorption to a hydrophobic surface and the effect of Tween

Comparison of mAb-1 adsorption to the silica and OTS-coated silica surface was proposed as a means of mimicking adsorption to plastics such as polypropylene/polystyrene which may be encountered during processing. MAb-1 adsorption to the hydrophobic OTS surface was reduced compared to that on the hydrophilic (silica) surface to ~2 mg/m^2 compared to ~5.5 to 12 mg/m^2 (Figure 4-18 and Figure 4-11). This result is consistent with that of previous data showing reduced antibody adsorption to surfaces with a range of wettabilities (Zangmeister, 2012). The mAb-1 surface loading of ~2 mg/m^2 determined from the TIRF profile is similar to that observed for lysozyme on a hydrophobic surface, although there will be differences in the size and architecture of the two proteins (Joshi and McGuire, 2009). The lower mAb-1 surface loading on the OTS-coated silica following surface adsorption can be explained by protein relaxation. Surface relaxation of a protein has been suggested to occur via a two-step process: first, an interaction takes place between the protein surface and the interface which has rapid kinetics (seconds) and; secondly, the hydrophobic core of the protein becomes exposed to the interface the kinetics of which are slower and dependent on both the interface and protein (Xu and Siedlecki, 2007a). In the scenario where there is extensive protein relaxation and a large loss of protein tertiary structure, the layer formed will be much thinner thus reducing surface loading as a result of the protein footprint being increased.

The extent of mAb-1 adsorption to a hydrophobic surface from a co-dissolved Tween solution was dependent on the Tween. Adsorption in the presence of Tween 80 did not differ from the control which was the opposite of that observed for Tween 20 (Figure 4-19). The percentage decrease in mAb-1 adsorption to the hydrophobic OTS surface was, in general, less than that observed from the hydrophilic surface (silica) when co-dissolved with Tween (a reduction of ~25 % compared to circa. 55-85 %). In contrast to the findings in this study for mAb-1 adsorption to a hydrophobic surface in the presence of Tween 80, adsorption of lysozyme to a hydrophobic silanised surface in the presence of the same surfactant was reduced, with an increasing Tween 80 concentration causing a greater decrease. The adsorption kinetics of lysozyme-Tween 80 at the highest Tween concentration (80 ppm) was similar to that of Tween 80 alone which suggested Tween was the dominant force when present at high concentration (Joshi and McGuire, 2009). The adsorption of a hydrophilic and hydrophobic mAb has been shown to have surface loadings very similar to the results obtained in this study: surface loading of ~ 5 and 10 mg/m^2 to bare silica, and ~ 2 mg/m^2 and negligible in the presence of Tween 80, for the hydrophilic and hydrophobic mAb respectively (Oom et al., 2012).

The surface energy of the Tween coated OTS surfaces was found not to differ significantly from that of OTS alone (section 3.4.2.3, Table 3-8) and it was therefore anticipated that mAb-1 adsorption to the different surfaces would be similar. The TIRF data showed that mAb-1 adsorption was decreased when surfaces were coated with a Tween concentration above the CMC; on the other hand, mAb-1 adsorption to OTS surfaces coated with Tween below the CMC increased (Figure 4-20). The reduced mAb-1 adsorption indicates the binding interaction with surface coated with

Tween above its CMC is not as favourable. This finding in agreement with that of adsorption of the protein lysozyme to a hydrophobic surface pre-coated with Tween 80 which occurred but was reduced compared to a bare hydrophobic surface (Joshi and McGuire, 2009). The increase in mAb-1 adsorption on the Tween coated surfaces (below their CMC) suggested an decrease in the hydrophobicity of the surface which is consistent with data for a polysorbate-coated octadecyl monolayer (section 3.4.2.3, Table 3-8). The observed differences in the effect of Tween concentration on mAb-1 adsorption are consistent with data in the literature which found that the concentration of Tween 20 used to coat a modified silicon surface determined the reduction in protein adsorption (Boxshall et al., 2006).

Surfactant molecules adsorbed at a hydrophobic solid/liquid interface have been shown to partially orientate themselves with the ethylene glycol groups towards the aqueous solution (Fragneto et al., 1996). This finding by Fragneto et al., (1996) together with those of Sheth and Leckband (1997) and Efremova et al., (2001), which show protein interaction with a PEG surface, could account for the increased mAb-1 adsorption to the Tween coated OTS, and silica, surfaces in this study.

MAb-1 was largely desorbed from the hydrophobic OTS surface as a result of Tween injection (Figure 4-21). Over the duration of the mAb-1 injection phase, irreversible binding to the surface was low as demonstrated by desorption as a result of Tween injection. This is in contrast to the minor desorption by Tween 20 of a mAb from a polystyrene latex surface (Lichtenbelt et al., 1993). The concentration of Tween 80 injected has also been found to determine the extent of desorption of a different protein, lysozyme, from a hydrophobic surface. At 20 ppm, Tween 80 did not desorb lysozyme but at 80 ppm the adsorption values were comparable to that of Tween

alone which suggested the adsorbed protein had been replaced by Tween molecules (Joshi and McGuire, 2009). The effect of Tween 80 concentration on mAb-1 desorption in this study was less dramatic as the quantity of mAb-1 adsorbed to the surface at run completion was similar for both concentrations (Figure 4-21). A small difference in the degree of mAb-1 desorption between the two Tween 20 concentrations was observed, however, it must be noted that a steady state plateau had not been reached at the end of the run duration.

4.5.8 MAb-1 surface adsorption after storage in pre-filled syringes

MAb formulations for subcutaneous injection are frequently distributed in pre-filled syringes. These syringes are coated with silicon oil as a lubricant for ease of injection, however, silicon oil has been implicated in the aggregation of antibodies (Jones et al., 2005). To establish if storage in pre-filled syringes affected adsorption of mAb-1 two syringe types were investigated along with a control glass vial. MAb-1 surface adsorption after storage in the two syringe types did not differ from that of the (control) glass vial (Figure 4-22).

Adsorption of mAbs to silicone oil has been identified previously with aggregation being found to occur only if the sample is agitated (Thirumangalathu et al., 2009). The mAb-1 storage samples (in CZ staked and BD syringes) in this study were static and so the findings are in agreement with those of Thirumangalathu et al., (2009).

Proteins are known to adsorb to the surfaces of pharmaceutical containers (Burke et al., 1992) and also at the silicone oil/water interface with adsorption found to be largely irreversible (Dixit et al., 2012). In the present study it is therefore possible that mAb-1 adsorbed to the syringe irreversibly and only antibody free in solution

was investigated in the TIRF experiments. MAb adsorption to glass particles, which was largely irreversible, has been identified (Bee et al., 2010) in addition to adsorption to stainless steel needles of pre-filled syringes (Bee et al., 2010). These findings support the suggestion that the TIRF experiments were most likely carried out using mAb-1 which was free in solution and thus did not investigate the real effect of adsorption to the syringe surfaces on subsequent surface adsorption to silica.

TIRF is not able to investigate adsorption of mAb-1 to the syringe and needle surface *in situ*. A method does exist which is able to investigate adsorption of therapeutic proteins to container surfaces which makes use of the binding capacity of gold nanoparticles to proteins (Eu et al., 2011). Adsorption of a therapeutic protein (150 kDa) was found to preferentially take place on non-siliconised glass syringe surfaces as shown by staining with gold nanoparticles. On the siliconised syringe surface, a complete lack of gold nanoparticle staining was detected which showed the protein did not adsorb to the siliconised surface. A hydrophobic plastic and hydrophilic glass vial surface were also investigated. As for the siliconised syringe, adsorption of the protein to the hydrophobic plastic surface was not detected compared to gold staining over the entire surface of the glass vial indicating a large degree of protein adsorption (Eu et al., 2011).

4.5.9 MAb-1 adsorption at the molecular level

Surface adsorption of mAb-1 was investigated at two pH values, 5.5 and 7.4, and as shown by the TIRF profiles, adsorption to the silica at pH 5.5 was less than at pH 7.4 by approximately 5.5 mg/m^2 (Figure 4-11). The pH of the solution therefore has a clear effect on mAb-1 adsorption. The proximity of the buffer pH to the pI of a protein has been previously shown to affect the degree of surface adsorption, with

the adsorption of selected IgGs reported to be higher at a pH close to their pI (Buijs et al., 1996, Wang et al., 2008b). This was also the case for mAb-1 in this study (with a pI of 8.9) as adsorption was found to be greater at pH 7.4. A monoclonal IgG with a pI of 5.8 adsorbed to silica and methylated silica surfaces to a greater extent at pH 4 and 6 than at pH 8 (Buijs et al., 1996). Adsorption of a mAb (type IgG1) with a pI of 6 to a silica surface at pH 6 was higher than at either pH 4 or 8; > 3 mg/m^2 at pH 6 compared to ~2.5 and < 1 mg/m^2 at pH 4 and 8 respectively (Wang et al., 2008b).

The net surface charge on silica is known to alter with pH (Behrens and Grier, 2001), although the difference in the zeta potential is small as shown by the range over pH 7 to 12 being between -60 and -70 mV (Mathes and Friess, 2011). A decrease in pH to the mildly acidic conditions at pH 5.5 reduced the negative potential of the silica surface to approximately -50 mV (Mathes and Friess, 2011). At pH 5.5 and 7.4 mAb-1 is expected to have a net positive charge, and therefore electrostatic interactions will be the dominant force in the surface interactions (Mathes and Friess, 2011). The adsorption plateau of two IgGs and their F_{ab} fragments is dependent on electrostatic interactions, when the net charge on the protein increased the quantity adsorbed to the surface decreased (Buijs et al., 1995). In addition to electrostatic interactions, the charges present on the surface and the protein can reduce adsorption through electrostatic repulsion between individual molecules and between surface and protein (Wang et al., 2008b, Buijs et al., 1996). These findings show that solution pH affects the extent of protein surface adsorption. The structure of three mAbs (two IgG4, one type IgG1) has been shown to not be affected at pH 6, which is nearer to the pH used in this study (Ejima et al., 2007). The pH of the buffer is therefore not expected to affect the conformational stability of mAb-1 in this study.

From the calculated surface loading for mAb-1 at pH 7.4, it is likely that adsorption has taken place in the form of multiple layers. This is based on a theoretical calculation of a packed antibody monolayer which would have a surface loading range of 1.3-2.7 mg/m^2 for dimensions of 146 x 135 x 69 Å (Harris et al., 1998), to 3.9 mg/m^2 for a sphere of 80 Å (Oom et al., 2012). The values expected from these two models are both less than the surface loading of approximately 10 mg/m^2 obtained here for mAb-1 adsorbed to bare silica. It is therefore expected that mAb-1 adsorption took the form of at least a bilayer. Through interpretation of the neutron reflectivity data the suitability of this model for adsorbed mAb-1 is discussed.

The reflectivity profiles generated by the NR experiments suggested that adsorption of mAb-1 to the SiO_2 surfaces at pH 5.5 and 7.4 is a complex process dependent upon pH and protein concentration. A mAb-1 bilayer was fitted to the NR data at concentrations up to 2000 mg/L at both pH 5.5 and 7.4 (Table 4-7 and Table 4-8). The inner and outer mAb-1 layers adsorbed to the SiO_2 surface at pH 7.4 were thicker than at pH 5.5 but the surface fractions were marginally less. The differences in layer thickness and SLD can be explained by modelling the NR profiles of the adsorbed mAb-1 to different orientations at pH 5.5 and 7.4. The crystal structure of mAb-1 is not known, however, the dimensions of mAbs has been suggested to be between 142 × 85 × 38 Å (Silverton et al., 1977) and 146 × 135 × 69 Å (Harris et al., 1998). At pH 5.5 mAb-1 adsorbed in an orientation between ‘side-on’ and ‘end-on’ at 50 mg/L as indicated by the layer thickness of 95 Å. The surface fraction of mAb-1 was near saturation at 50 mg/L, and so in order for additional molecules to adsorb to the surface mAb-1 tilted into an ‘end-on’ orientation. The orientation of the inner mAb-1 layer adsorbed to the SiO_2 surface from pH 7.4 buffer was ‘end-on’ from 50

to 2000 mg/L (Table 4-8). Adsorption in the 'end-on' orientation may be due to the charge on the silica surface repelling regions of mAb-1 which have a high number of acidic amino acid residues. As the pH of the buffer increased it would have become further away from the pK_a of the side chains of Aspartic acid and Glutamic acid (pK_a 3.9-4.3). The negative potential of these regions would increase thereby creating electrostatic repulsion from the silica surface. The pKa of the basic residues Lysine and Arginine side chains is 11.1 to 12.0 and so it would not be likely that the charge present would differ significantly between pH 5.5 and 7.4.

The thickness of the outer layer at pH 5.5 for all concentrations studied and at pH 7.4 up to 2000 mg/L suggested that mAb-1 adsorbed in a 'flat-on' orientation based on the crystal structure of a mAb (Harris et al., 1998). The thickness and protein fraction increased with concentration but the protein surface fraction calculated from the SLD values implied that the outer layer was sparse (Table 4-7 and Table 4-8). The most dramatic change in mAb-1 orientation and layer thickness took place at 5000 mg/L when adsorbed from a buffer at pH 7.4. In addition to the re-orientation of the outer layer to an 'end-on' position (thickness of 145 Å), a second outer layer formed in which mAb-1 was also in the 'end-on' orientation. The dimension of the inner layer increased to 207 Å which was greater than the dimension which should be possible from the values established for the crystal structure of mAbs (Harris et al., 1998, Silverton et al., 1977). It is unlikely that mAb-1 unfolded on the surface upon the increase in bulk concentration to 5000 mg/L as the thickness of the layer suggests mAb-1 was in an 'end-on' orientation. Unfolded protein would form a thin layer on the surface which would be spread out as was found to be the case for lysozyme on a hydrophobic surface (Lu et al., 1998). Adsorption of a murine mAb to a silica surface

has been shown using AFM to form heterogeneous surface aggregates and NR profiles demonstrated a three-layer model at higher concentrations which is in agreement with the findings in this study (Xu et al., 2006b). Fitting of the NR data, led to a model being suggested in which adsorption of mAb-1 to the surface took place in the form of oligomers (soluble aggregates) which has previously been shown for mAbs at high concentration (Kukrer et al., 2010). However, the N-sigma analysis of the reflectivity profile of mAb-1 adsorbed to SiO_2 at a concentration of 5000 mg/L (from buffer at pH 7.4) fitted to a three layer model compared to a two layer model indicated a lower degree of confidence in the model being correct (Table 4-6).

There is a precedent for protein re-orientation upon an increase in concentration. An IgG-like domain pair adsorbed to a SiO_2 surface as a monolayer oriented in a side-on manner at low concentration, which re-orientated to become end-on with the formation of an outer layer at high concentration (Kreiner et al., 2009). The process of IgG-like domain adsorption was comparable to the surface pressure area isotherm of surfactants (Harvey et al., 2004). At low surfactant concentration at an air-liquid interface the surfactant tail can adopt a wide range of conformations and there is little interaction between neighbouring molecules. As the concentration is increased, the area available to each molecule decreases resulting in the surfactant tails adopting a vertical arrangement and interacting with the adjacent molecules. Adsorption of mAb-1 to the SiO_2 surface in this study differed from this process as the protein surface fraction was close to 1.0 at the lowest concentrations studied and therefore indicated close packing regardless of the protein concentration used in this study.

The NR data demonstrated that mAb-1 formed a sparse monolayer adsorbed to the OTS-coated SiO_2 surface in a side-on orientation at low concentration which moved

toward end-on with increasing concentration (Table 4-9). These data argue against unfolding of mAb-1, despite the 'solid-state' CD data showing it to take place on an OTS-coated silica surface (3.4.3.1, Figure 3-18) and lysozyme being found to unfold on an OTS-coated surface (Lu et al., 1998). Monolayer formation of a monoclonal human IgG1 on a hydrophobic self-assembled monolayer has been identified previously using quartz crystal microbalance. At a low concentration the mAb was oriented in a flat-on position with a low surface fraction, as the concentration was increased the mAb bound to the surface in an end-on orientation and the surface fraction increased (Wiseman and Frank, 2012). The authors suggested that as the concentration was increased, the mAb adsorbed to available surface binding sites in an end-on orientation or desorbed the mAb present on the surface in a flat-on position replacing them with molecules in a side-on or end-on orientation. As for mAb-1 in this study, the orientation of tropoelastin has been shown to be affected by surface hydrophobicity. Tropoelastin formed a dense heterogeneous monolayer on silica in an end-on manner compared to a hydrophobic OTS on which adsorption took place along the length of tropoelastin (Le Brun et al., 2012).

4.6 Conclusions

Through the use of TIRF and NR, adsorption of mAb-1 to hydrophilic silica from buffer at pH 5.5 and 7.4 and to hydrophobic OTS-coated silica from pH 5.5 was studied with changes in surface loading, layer number and antibody orientation determined through data interpretation.

The affinity of Tween 20 and 80 for the surface, hydrophilic silica or hydrophobic OTS, was responsible for the extent to which mAb-1 was desorbed. The concentration of Tween and injection point was important in determining the extent of mAb-1 adsorption. MAb-1 injected simultaneously (injection condition **1**) or to a silica surface pre-coated with Tween above its CMC (injection condition **2**) did not attenuate subsequent adsorption. A fraction of mAb-1 remained irreversibly adsorbed to the surface after injection of Tween 20/80 (injection condition **3**) which suggests a multilayer system with irreversibly and reversibly adsorbed layers. Despite the principle reason for polysorbate inclusion in protein formulation being to prevent aggregation, the data in this study demonstrated a secondary effect of their inclusion was the control of surface adsorption.

Adsorption of mAb-1 to hydrophobic surfaces was clearly reduced compared to that observed for hydrophilic surfaces with no evidence of unfolding over the duration of the TIRF or NR experiments. It was observed in the TIRF profile that mAb-1 adsorption to silica at pH 5.5 (away from the pI of 8.99) was reduced. The NR data suggested the molecular arrangement at the surface at this pH (pH 5.5) was more complex than simply electrostatic forces reducing adsorption. MAb-1 formed a bilayer when adsorbed to a silicon substrate at pH 5.5 with a transition in its orientation from side-on to end-on as the concentration increased. A change in buffer

pH resulted in extensive reorientation of the mAb-1 layer in direct contact with the silica surface. An end-on orientation was favoured at pH 7.4 with adsorption taking place in the form of soluble oligomers at the highest concentration and forming a non-uniform triple layer.

Chapter 5. Overall Summary

In this study the interaction between mAb-1 and polysorbates in the bulk solution and at solid/liquid interfaces has been investigated. It was shown that a specific binding interaction does not take place between mAb-1 and Tween 20/80 or the Pluronic triblock copolymers. This does not however exclude the possibility that a transient non-specific interaction does take place. The native secondary structure was minimally affected by surfactant presence with the exception of Pluronic L61. In addition to this, surfactant inclusion did not affect mAb-1 thermal transition temperatures. MAb-1 solution stability is therefore not influenced by a direct antibody-surfactant interaction or an increase in thermal stability. The characterisation of the interaction in bulk solution was necessary for the investigation of mAb-1 surface adsorption in the presence of surfactant. It was determined that mAb-1 adsorption was due to the antibody interacting with the surface and was not driven by an interaction with surfactant adsorbed to the surface.

MAb-1 was attracted to hydrophilic surfaces and weakly attracted to hydrophobic surfaces as shown by AFM force of adhesion data. This suggested that selection of a hydrophobic surface could reduce the degree of antibody loss from solution due to surface adsorption. However, 'solid-state' CD spectra the data showed that in general, mAb-1 secondary structure was maintained on a hydrophilic surface with a varying degree of loss upon adsorption to a hydrophobic surface A correlation does not exist between surface characteristics or force of adhesion and the loss of mAb-1 native secondary structure.

A hydrophobic surface is effective at reducing mAb-1 adsorption as demonstrated by both the TIRF data and neutron reflectivity profiles which showed a monolayer formed on a hydrophobic surface compared to a bilayer or trilayer on a hydrophilic surface. Re-orientation of the mAb-1 layers on the silicon surface occurred with increasing bulk concentration. MAb-1 adsorption was greater at pH 7.4 than pH 5.5 which can be accounted for by the formation of a trilayer at pH 7.4. The concentration of Tween and time of injection with respect to mAb-1 influenced the degree of antibody adsorption. A proportion of mAb-1 remained adsorbed to the surface which suggests that both reversible and irreversible adsorption took place.

The findings in this thesis add to the knowledge base in the area of protein pharmaceutics. The interaction of a monoclonal antibody with the commonly used polysorbate surfactants has been characterised in the bulk solution and at solid/liquid interfaces with the effect of their presence on antibody adsorption being found to differ. It has been shown that the choice of surfactant, concentration and the time of injection with respect to the protein all influence the degree to which adsorption is attenuated. This study has also shown that TIRF and 'solid-state' CD are bench top techniques which could easily be incorporated into the formulation process. A drawback of TIRF is the inability to investigate surface adsorption of a protein at a pharmaceutically relevant concentration. 'Solid-state' CD is able to investigate the effect surface hydrophobicity on protein structure and could therefore be utilised during processing for the selection of surface materials which prevent or reduce the loss of native structure and the potential for immunogenicity due to aggregate formation.

Chapter 6. Future work

The surface energy and water contact angles of the silanised surfaces in this study could approximately be arranged into two groups based on the values obtained; those which were hydrophilic (water contact angle ca. 45° and γ of ca. 42) and those which were hydrophobic (water contact angle ca. 100° and γ of ca. 25). It would therefore be informative to study surfaces which have a hydrophilicity between those of the two groups identified in this study to further investigate the effect of surface on both protein adhesion and structure. Additionally, the structure of mAb-1 on surfaces which had been coated with TCPS and TCOS was comparable to that of the native structure in solution and thus could potentially reduce surface adsorption without causing protein unfolding. A more detailed characterisation of these two surfaces through the use of techniques such as AFM, ellipsometry, Raman spectroscopy, and NR could provide information on the thickness and homogeneity of the layer. Analysis using both TIRF and NR as in this study to investigate mAb-1 adsorption to these surfaces would increase the understanding of how these surfaces repel mAb-1 but do not affect structure. These findings would determine if the surfaces could indeed be utilised during processing and storage to reduce protein adsorption.

As shown in this study TIRF cannot be used to investigate protein adsorption at concentrations typically used in therapeutic formulations. However, further investigation of adsorption using this technique could be undertaken with the additional excipients used in formulations (e.g. non-reducing sugars such as trehalose and sucrose) to more closely mimic the anticipated adsorption which would take

place. This would enable conclusions on potential loss of protein concentration from formulations to be made.

The transient adsorption curve observed in the TIRF profiles for mAb-1 adsorption when co-dissolved with Tween 20 and 80 below their CMC requires further investigation to establish the nature of this finding. This transient adsorption was not detected during the NR experiments, however, this technique could provide a greater understanding of this process through optimisation of the parameters such as protein and surfactant concentrations and the time frame of each data collection period. Ellipsometry could also be used to investigate this process as it would provide information on the layer thickness during the adsorption and desorption phases (Wang et al., 2008b). AFM has been used previously to investigate protein desorption by surfactant via orogenic displacement using Langmuir-Blodgett films (Mackie et al., 1999, Mackie et al., 2000a). It would be possible to image the surface as the co-dissolved mAb-1-Tween solution flowed over the surface which would generate images of the adsorption/desorption process.

As each isotype and subclass of immunoglobulin differs it would not be possible from the data produced in this study to draw conclusions on the effect of surfactant on surface adsorption of different immunoglobulins. By investigating the surface adsorption of an immunoglobulin in each isotype it would provide information on any differences in adsorption between isotypes and act as a guide as to potential adsorption which could be expected from formulations. In addition to this, analysis of immunoglobulin fragment surface adsorption in the presence/absence of surfactant would also be of benefit to the pharmaceutical industry as this type of therapeutic protein is now available on the market (Elvin et al., 2013).

A number of mAb fragment are available to treat conditions such as ischaemia/angina and wet age-related macular degeneration (Elvin et al., 2013). The effect of hydrophobicity on F_{ab} and F_c structure has been shown to differ (Vermeer et al., 2001) and so it would be informative to separate mAb-1 into its individual domains and investigate the effect adsorption on the structure and stability of each individual domain. The F_{ab} fragments are known to differ between immunoglobulins (Tetin et al., 2003) and thus surface hydrophobicity may affect the Fab fragment of mAb-1 differently. Additionally, as mAb-1 is of one immunoglobulin isotype it would be of interest to investigate the effect of adsorption of a member of the four other immunoglobulin isotypes to the silanised surfaces. The hydrophobicity of the surface may affect the immunoglobulins to a different extent as a result of the differences in monomer number and structure between the isotypes.

Chapter 7. Bibliography

AHRER, K., BUCHACHER, A., IBERER, G. & JUNGBAUER, A. 2006. Thermodynamic stability and formation of aggregates of human immunoglobulin G characterised by differential scanning calorimetry and dynamic light scattering. *Journal of Biochemical and Biophysical Methods,* 66, 73-86.

ALEXANDRIDIS, P., HOLZWARTH, J. F. & HATTON, T. A. 1994. MICELLIZATION OF POLY(ETHYLENE OXIDE)-POLY(PROPYLENE OXIDE)-POLY(ETHYLENE OXIDE) TRIBLOCK COPOLYMERS IN AQUEOUS-SOLUTIONS - THERMODYNAMICS OF COPOLYMER ASSOCIATION. *Macromolecules,* 27, 2414-2425.

AMANI, A., YORK, P., DE WAARD, H. & ANWAR, J. 2011. Molecular dynamics simulation of a polysorbate 80 micelle in water. *Soft Matter,* 7, 2900-2908.

AMIJI, M. & PARK, K. 1992. PREVENTION OF PROTEIN ADSORPTION AND PLATELET-ADHESION ON SURFACES BY PEO PPO PEO TRIBLOCK COPOLYMERS. *Biomaterials,* 13, 682-692.

ANDERSEN, C. B., MANNO, M., RISCHEL, C., THOROLFSSON, M. & MARTORANA, V. 2010. Aggregation of a multidomain protein: A coagulation mechanism governs aggregation of a model IgG1 antibody under weak thermal stress. *Protein Science,* 19, 279-290.

ANDYA, J. D., MAA, Y. F., COSTANTINO, H. R., NGUYEN, P. A., DASOVICH, N., SWEENEY, T. D., HSU, C. C. & SHIRE, S. J. 1999. The effect of formulation excipients on protein stability and aerosol performance of spray-dried powders of a recombinant humanized anti-IgE monoclonal antibody. *Pharmaceutical Research,* 16, 350-358.

BAM, N. B., CLELAND, J. L., YANG, J., MANNING, M. C., CARPENTER, J. F., KELLEY, R. F. & RANDOLPH, J. W. 1998. Tween protects recombinant human growth hormone against agitation-induced damage via hydrophobic interactions. *Journal of Pharmaceutical Sciences,* 87, 1554-1559.

BAM, N. B., RANDOLPH, T. W. & CLELAND, J. L. 1995. STABILITY OF PROTEIN FORMULATIONS - INVESTIGATION OF SURFACTANT EFFECTS BY A NOVEL EPR SPECTROSCOPIC TECHNIQUE. *Pharmaceutical Research,* 12, 2-11.

BARREIRO-IGLESIAS, R., ALVAREZ-LORENZO, C. & CONCHEIRO, A. 2003. Poly(acrylic acid) microgels (carbopol (R) 934)/surfactant interactions in aqueous media Part I: Nonionic surfactants. *International Journal of Pharmaceutics,* 258, 165-177.

BARUAH, G. L., NAYAK, A., WINKELMAN, E. & BELFORT, G. 2006. Purification of monoclonal antibodies derived from transgenic goat milk by ultrafiltration. *Biotechnology and Bioengineering,* 93, 747-754.

BASZKIN, A., BOISSONNADE, M. M., KAMYSHNY, A. & MAGDASSI, S. 2001. Native and hydrophobically modified human immunoglobulin G at the air/water interface - Sequential and competitive adsorption. *Journal of Colloid and Interface Science,* 239, 1-9.

BEE, J. S., CHIU, D., SAWICKI, S., STEVENSON, J. L., CHATTERJEE, K., FREUND, E., CARPENTER, J. F. & RANDOLPH, T. W. 2009. Monoclonal Antibody Interactions With Micro- and Nanoparticles: Adsorption, Aggregation, and Accelerated Stress Studies. *Journal of Pharmaceutical Sciences,* 98, 3218-3238.

BEE, J. S., DAVIS, M., FREUND, E., CARPENTER, J. F. & RANDOLPH, T. W. 2010. Aggregation of a Monoclonal Antibody Induced by Adsorption to Stainless Steel. *Biotechnology and Bioengineering,* 105, 121-129.

BEE, J. S., GOLETZ, T. J. & RAGHEB, J. A. 2012. The future of protein particle characterization and understanding its potential to diminish the immunogenicity of biopharmaceuticals: A shared perspective. *Journal of Pharmaceutical Sciences,* 101, 3580-3585.

BEHRENS, S. H. & GRIER, D. G. 2001. The charge of glass and silica surfaces. *Journal of Chemical Physics,* 115, 6716-6721.

BENVENUTO, E., ORDAS, R. J., TAVAZZA, R., ANCORA, G., BIOCCA, S., CATTANEO, A. & GALEFFI, P. 1991. PHYTOANTIBODIES - A GENERAL VECTOR FOR THE EXPRESSION OF IMMUNOGLOBULIN DOMAINS IN TRANSGENIC PLANTS. *Plant Molecular Biology,* 17, 865-874.

BIDDLECOMBE, J. G., CRAIG, A. V., ZHANG, H., UDDIN, S., MULOT, S., FISH, B. C. & BRACEWELL, D. G. 2007. Determining antibody stability: Creation of solid-liquid interfacial effects within a high shear environment. *Biotechnology Progress,* 23, 1218-1222.

BIDDLECOMBE, J. G., SMITH, G., UDDIN, S., MULOT, S., SPENCER, D., GEE, C., FISH, B. C. & BRACEWELL, D. G. 2009. Factors Influencing Antibody Stability at Solid-Liquid Interfaces in a High Shear Environment. *Biotechnology Progress,* 25, 1499-1507.

BLACKMAN, L. C. & HARROP, R. 1968. HYDROPHILATION OF GLASS SURFACES .I. INVESTIGATION OF POSSIBLE PROMOTERS OF FILMWISE CONDENSATION. *Journal of Applied Chemistry of the Ussr,* 18, 37-&.

BOSSE, D., PRAUS, M., KIESSLING, P., NYMAN, L., ANDRESEN, C., WATERS, J. & SCHINDEL, F. 2005. Phase I comparability of recombinant human albumin and human serum albumin. *Journal of Clinical Pharmacology,* 45, 57-67.

BOUCHEMAL, K., AGNELY, F., KOFFI, A. & PONCHEL, G. 2009. A concise analysis of the effect of temperature and propanediol-1, 2 on Pluronic F127 micellization using isothermal titration microcalorimetry. *Journal of Colloid and Interface Science,* 338, 169-176.

BOXSHALL, K., WU, M. H., CUI, Z., CUI, Z. F., WATTS, J. F. & BAKER, M. A. 2006. Simple surface treatments to modify protein adsorption and cell attachment properties within a poly(dimethylsiloxane) micro-bioreactor. *Surface and Interface Analysis,* 38, 198-201.

BROGAN, K. L., SHIN, J. H. & SCHOENFISCH, M. H. 2004. Influence of surfactants and antibody immobilization strategy on reducing nonspecific protein interactions for molecular recognition force microscopy. *Langmuir,* 20, 9729-9735.

BRYCH, S. R., GOKARN, Y. R., HULTGEN, H., STEVENSON, R. J., RAJAN, R. & MATSUMURA, M. 2010. Characterization of Antibody Aggregation: Role of Buried, Unpaired Cysteines in Particle Formation. *Journal of Pharmaceutical Sciences,* 99, 764-781.

BUIJS, J., LICHTENBELT, J. W. T., NORDE, W. & LYKLEMA, J. 1995. ADSORPTION OF MONOCLONAL IGGS AND THEIR F(AB')(2) FRAGMENTS ONTO POLYMERIC SURFACES. *Colloids and Surfaces B-Biointerfaces,* 5, 11-23.

BUIJS, J., VANDENBERG, P. A. W., LICHTENBELT, J. W. T., NORDE, W. & LYKLEMA, J. 1996. Adsorption dynamics of IgG and its F(ab')(2) and Fc fragments studied by reflectometry. *Journal of Colloid and Interface Science,* 178, 594-605.

BURKE, C. J., STEADMAN, B. L., VOLKIN, D. B., TSAI, P. K., BRUNER, M. W. & MIDDAUGH, C. R. 1992. THE ADSORPTION OF PROTEINS TO PHARMACEUTICAL CONTAINER SURFACES. *International Journal of Pharmaceutics,* 86, 89-93.

CAO, C. T., FADEEV, A. Y. & MCCARTHY, T. J. 2001. Reactions of organosilanes with silica surfaces in carbon dioxide. *Langmuir,* 17, 757-761.

CAPPELLA, B. & DIETLER, G. 1999. Force-distance curves by atomic force microscopy. *Surface Science Reports,* 34, 1-+.

CELIK, E. & MOY, V. T. 2012. Nonspecific interactions in AFM force spectroscopy measurements. *Journal of Molecular Recognition,* 25, 53-56.

CHANG, B. S., KENDRICK, B. S. & CARPENTER, J. F. 1996. Surface-induced denaturation of proteins during freezing and its inhibition by surfactants. *Journal of Pharmaceutical Sciences,* 85, 1325-1330.

CHEN, C. Y., EVEN, M. A. & CHEN, Z. 2003. Detecting molecular-level chemical structure and group orientation of amphiphilic PEO-PPO-PEO copolymers at solution/air and solid/solution interfaces by SFG vibrational spectroscopy. *Macromolecules,* 36, 4478-4484.

CHOU, D. K., KRISHNAMURTHY, R., RANDOLPH, T. W., CARPENTER, J. F. & MANNING, M. C. 2005. Effects of Tween 20 (R) and Tween 80 (R) on the stability of albutropin during agitation. *Journal of Pharmaceutical Sciences,* 94, 1368-1381.

CHUNG, C. H., MIRAKHUR, B., CHAN, E., LE, Q., BERLIN, J., MORSE, M., MURPHY, B. A., SATINOVER, S. M., HOSEN, J., MAURO, D., SLEBOS, R. J., ZHOU, Q. W., GOLD, D., HATLEY, T.,

HICKLIN, D. J. & PLATTS-MILLS, T. A. E. 2008. Cetuximab-induced anaphylaxis and IgE specific for galactose-alpha-1,3-galactose. *New England Journal of Medicine,* 358, 1109-1117.

COOPER, A., JOHNSON, C. M., LAKEY, J. H. & NOLLMANN, M. 2001. Heat does not come in different colours: entropy-enthalpy compensation, free energy windows, quantum confinement, pressure perturbation calorimetry, solvation and the multiple causes of heat capacity effects in biomolecular interactions. *Biophysical Chemistry,* 93, 215-230.

COOPER, A., MCALPINE, A. & STOCKLEY, P. G. 1994. CALORIMETRIC STUDIES OF THE ENERGETICS OF PROTEIN-DNA INTERACTIONS IN THE ESCHERICHIA-COLI METHIONINE REPRESSOR (METJ) SYSTEM. *Febs Letters,* 348, 41-45.

COOPER, A., NUTLEY, M. A. & CAMILLERI, P. 1998. Microcalorimetry of chiral surfactant-cyclodextrin interactions. *Analytical Chemistry,* 70, 5024-5028.

CORTESE, B., MOWLEM, M. C. & MORGAN, H. 2011. Characterisation of an irreversible bonding process for COC-COC and COC-PDMS-COC sandwich structures and application to microvalves. *Sensors and Actuators B-Chemical,* 160, 1473-1480.

CROWE, J. H., CROWE, L. M., WOLKERS, W. F., OLIVER, A. E., MA, X. C., AUH, J. H., TANG, M. K., ZHU, S. J., NORRIS, J. & TABLIN, F. 2005. Stabilization of dry mammalian cells: Lessons from nature. *Integrative and Comparative Biology,* 45, 810-820.

CROWE, L. M., REID, D. S. & CROWE, J. H. 1996. Is trehalose special for preserving dry biomaterials? *Biophysical Journal,* 71, 2087-2093.

CROY, S. R. & KWON, G. S. 2004. The effects of Pluronic block copolymers on the aggregation state of nystatin. *Journal of Controlled Release,* 95, 161-171.

DA SILVA, A. J., DA COSTA IEMMA, M. R., LUPERNI HORTA, A. C., SARGO, C. R., DE LIMA CAMARGO GIORDANO, R., DE CAMPOS GIORDANO, R., ZANGIROLAMI, T. C. & MARQUES NOVO, M. T. 2012. Cloning, Auto-induction Expression, and Purification of rSpaA Swine Erysipelas Antigen. *Current microbiology,* 65, 369-74.

DAERON, M. 1997. Fc receptor biology. *Annual Review of Immunology,* 15, 203-234.

DAI, W. G., DONG, L. C., LI, S. & DENG, Z. Y. 2008. Combination of Pluronic/Vitamin E TPGS as a potential inhibitor of drug precipitation. *International Journal of Pharmaceutics,* 355, 31-37.

DANI, B., PLATZ, R. & TZANNIS, S. T. 2007. High concentration formulation feasibility of human immunoglubulin G for subcutaneous administration. *Journal of Pharmaceutical Sciences,* 96, 1504-1517.

DE CUPERE, V. M., VAN WETTER, J. & ROUXHET, P. G. 2003. Nanoscale organization of collagen and mixed collagen-pluronic adsorbed layers. *Langmuir,* 19, 6957-6967.

DE WILDT, R. M. T., MUNDY, C. R., GORICK, B. D. & TOMLINSON, I. M. 2000. Antibody arrays for high-throughput screening of antibody-antigen interactions. *Nature Biotechnology,* 18, 989-994.

DEISENHOFER, J. 1981. CRYSTALLOGRAPHIC REFINEMENT AND ATOMIC MODELS OF A HUMAN FC FRAGMENT AND ITS COMPLEX WITH FRAGMENT-B OF PROTEIN-A FROM STAPHYLOCOCCUS-AUREUS AT 2.9-A AND 2.8-A RESOLUTION. *Biochemistry,* 20, 2361-2370.

DEWEZ, J. L., BERGER, V., SCHNEIDER, Y. J. & ROUXHET, P. G. 1997. Influence of substrate hydrophobicity on the adsorption of collagen in the presence of pluronic F68, albumin, or calf serum. *Journal of Colloid and Interface Science,* 191, 1-10.

DING, Y. X. & HLADY, V. 2011. Competitive Adsorption of Three Human Plasma Proteins onto Sulfhydryl-to-sulfonate Gradient Surfaces. *Croatica Chemica Acta,* 84, 193-202.

DIXIT, N., MALONEY, K. M. & KALONIA, D. S. 2012. The effect of Tween (R) 20 on silicone oil-fusion protein interactions. *International Journal of Pharmaceutics,* 429, 158-167.

DOLGIKH, D. A., GILMANSHIN, R. I., BRAZHNIKOV, E. V., BYCHKOVA, V. E., SEMISOTNOV, G. V., VENYAMINOV, S. Y. & PTITSYN, O. B. 1981. ALPHA-LACTALBUMIN - COMPACT STATE WITH FLUCTUATING TERTIARY STRUCTURE. *Febs Letters,* 136, 311-315.

DONG, Y. Z. & SHANNON, C. 2000. Heterogeneous immunosensing using antigen and antibody monolayers on gold surfaces with electrochemical and scanning probe detection. *Analytical Chemistry,* 72, 2371-2376.

DORAN, P. M. 2006. Loss of secreted antibody from transgenic plant tissue cultures due to surface adsorption. *Journal of Biotechnology,* 122, 39-54.

DRABER, P., DRABEROVA, E. & NOVAKOVA, M. 1995. STABILITY OF MONOCLONAL IGM ANTIBODIES FREEZE-DRIED IN THE PRESENCE OF TREHALOSE. *Journal of Immunological Methods,* 181, 37-43.

EFREMOVA, N. V., BONDURANT, B., O'BRIEN, D. F. & LECKBAND, D. E. 2000. Measurements of interbilayer forces and protein adsorption on uncharged lipid bilayers displaying poly(ethylene glycol) chains. *Biochemistry,* 39, 3441-3451.

EFREMOVA, N. V., SHETH, S. R. & LECKBAND, D. E. 2001. Protein-induced changes in poly(ethylene glycol) brushes: Molecular weight and temperature dependence. *Langmuir,* 17, 7628-7636.

EJIMA, D., TSUMOTO, K., FUKADA, H., YUMIOKA, R., NAGASE, K., ARAKAWA, T. & PHILO, J. S. 2007. Effects of acid exposure on the conformation, stability, and aggregation of monoclonal antibodies. *Proteins-Structure Function and Bioinformatics,* 66, 954-962.

ELVIN, J. G., COUSTON, R. G. & VAN DER WALLE, C. F. 2013. Therapeutic antibodies: Market considerations, disease targets and bioprocessing. *International Journal of Pharmaceutics,* 440, 83-98.

EU, B., CAIRNS, A., DING, G., CAO, X. L. & WEN, Z. Q. 2011. Direct Visualization of Protein Adsorption to Primary Containers by Gold Nanoparticles. *Journal of Pharmaceutical Sciences,* 100, 1663-1670.

FELBEL, J., BIEBER, I., PIPPER, J. & KOHLER, J. M. 2004. Investigations on the compatibility of chemically oxidized silicon (SiOx)-surfaces for applications towards chip-based polymerase chain reaction. *Chemical Engineering Journal,* 101, 333-338.

FENG, L., LI, S. H., LI, Y. S., LI, H. J., ZHANG, L. J., ZHAI, J., SONG, Y. L., LIU, B. Q., JIANG, L. & ZHU, D. B. 2002. Super-hydrophobic surfaces: From natural to artificial. *Advanced Materials,* 14, 1857-1860.

FENG, M. H., MORALES, A. B., POOT, A., BEUGELING, T. & BANTJES, A. 1995. EFFECTS OF TWEEN-20 ON THE DESORPTION OF PROTEINS FROM POLYMER SURFACES. *Journal of Biomaterials Science-Polymer Edition,* 7, 415-424.

FIELDS, G. B., ALONSO, D. O. V., STIGTER, D. & DILL, K. A. 1992. THEORY FOR THE AGGREGATION OF PROTEINS AND COPOLYMERS. *Journal of Physical Chemistry,* 96, 3974-3981.

FLINN, D. H., GUZONAS, D. A. & YOON, R. H. 1994. CHARACTERIZATION OF SILICA SURFACES HYDROPHOBIZED BY OCTADECYLTRICHLOROSILANE. *Colloids and Surfaces a-Physicochemical and Engineering Aspects,* 87, 163-176.

FRAGNETO, G., LI, Z. X., THOMAS, R. K., RENNIE, A. R. & PENFOLD, J. 1996. A neutron reflectivity study of the adsorption of aerosol-OT on self-assembled monolayers on silicon. *Journal of Colloid and Interface Science,* 178, 531-537.

FU, Z. G. & SANTORE, M. M. 1998. Poly(ethylene oxide) adsorption onto chemically etched silicates by Brewster angle reflectivity. *Colloids and Surfaces a-Physicochemical and Engineering Aspects,* 135, 63-75.

GANESAN, A., PRICE, N. C., KELLY, S. M., PETRY, I., MOORE, B. D. & HALLING, P. J. 2006. Circular dichroism studies of subtilisin Carlsberg immobilised on micron sized silica particles. *Biochimica Et Biophysica Acta-Proteins and Proteomics,* 1764, 1119-1125.

GARBER, E. & DEMAREST, S. J. 2007. A broad range of Fab stabilities within a host of therapeutic IgGs. *Biochemical and Biophysical Research Communications,* 355, 751-757.

GARIDEL, P., HOFFMANN, C. & BLUME, A. 2009. A thermodynamic analysis of the binding interaction between polysorbate 20 and 80 with human serum albumins and immunoglobulins: A contribution to understand colloidal protein stabilisation. *Biophysical Chemistry,* 143, 70-78.

GERDOVA, A., KELLY, S. M. & HALLING, P. 2011. Experimental Test of Absorption Flattening Correction for Circular Dichroism of Particle Suspensions. *Chirality,* 23, 574-579.

GIACOMELLI, C. E., BREMER, M. & NORDE, W. 1999. ATR-FTIR study of IgG adsorbed on different silica surfaces. *Journal of Colloid and Interface Science,* 220, 13-23.

GIOVAMBATTISTA, N., DEBENEDETTI, P. G. & ROSSKY, P. J. 2007. Effect of surface polarity on water contact angle and interfacial hydration structure. *Journal of Physical Chemistry B,* 111, 9581-9587.

GRAMER, M. J., ECKBLAD, J. J., DONAHUE, R., BROWN, J., SHULTZ, C., VICKERMAN, K., PRIEM, P., VAN DEN BREMER, E. T. J., GERRITSEN, J. & VAN BERKEL, P. H. C. 2011. Modulation of Antibody Galactosylation Through Feeding of Uridine, Manganese Chloride, and Galactose. *Biotechnology and Bioengineering,* 108, 1591-1602.

GUNNING, P. A., MACKIE, A. R., GUNNING, A. P., WOODWARD, N. C., WILDE, P. J. & MORRIS, V. J. 2004. Effect of surfactant type on surfactant-protein interactions at the air-water interface. *Biomacromolecules,* 5, 984-991.

HA, E., WANG, W. & WANG, Y. J. 2002. Peroxide formation in polysorbate 80 and protein stability. *Journal of Pharmaceutical Sciences,* 91, 2252-2264.

HARRIS, L. J., SKALETSKY, E. & MCPHERSON, A. 1998. Crystallographic structure of an intact IgG1 monoclonal antibody. *Journal of Molecular Biology,* 275, 861-872.

HARVEY, R. D., HEENAN, R. K., BARLOW, D. J. & LAWRENCE, M. J. 2004. Effect of cholesterol and phospholipid on the behavior of dialkyl polyoxyethylene ether surfactant (2C(18)E(12)) monolayers and bilayers. *Langmuir,* 20, 9282-9290.

HAZEL, J. L. & TSUKRUK, V. V. 1999. Spring constants of composite ceramic/gold cantilevers for scanning probe microscopy. *Thin Solid Films,* 339, 249-257.

HE, F., HOGAN, S., LATYPOV, R. F., NARHI, L. O. & RAZINKOV, V. I. 2010. High Throughput Thermostability Screening of Monoclonal Antibody Formulations. *Journal of Pharmaceutical Sciences,* 99, 1707-1720.

HERMELING, S., CROMMELIN, D. J. A., SCHELLEKENS, H. & JISKOOT, W. 2004. Structure-immunogenicity relationships of therapeutic proteins. *Pharmaceutical Research,* 21, 897-903.

HIGASHIYAMA, T. 2002. Novel functions and applications of trehalose. *Pure and Applied Chemistry,* 74, 1263-1269.

HILLGREN, A., LINDGREN, J. & ALDEN, M. 2002. Protection mechanism of Tween 80 during freeze-thawing of a model protein, LDH. *International Journal of Pharmaceutics,* 237, 57-69.

HINTERDORFER, P., BAUMGARTNER, W., GRUBER, H. J., SCHILCHER, K. & SCHINDLER, H. 1996. Detection and localization of individual antibody-antigen recognition events by

atomic force microscopy. *Proceedings of the National Academy of Sciences of the United States of America,* 93, 3477-3481.

HOBER, S., NORD, K. & LINHULT, M. 2007. Protein A chromatography for antibody purification. *Journal of Chromatography B-Analytical Technologies in the Biomedical and Life Sciences,* 848, 40-47.

HOEHNE, M., SAMUEL, F., DONG, A., WURTH, C., MAHLER, H. C., CARPENTER, J. F. & RANDOLPH, T. W. 2011. Adsorption of Monoclonal Antibodies to Glass Microparticles. *Journal of Pharmaceutical Sciences,* 100, 123-132.

HOFFMANN, C., BLUME, A., MILLER, I. & GARIDEL, P. 2009a. Insights into protein-polysorbate interactions analysed by means of isothermal titration and differential scanning calorimetry. *European Biophysics Journal,* 38, 557-568.

HOFFMANN, C., BLUME, A., MILLER, I. & GARIDEL, P. 2009b. Insights into protein-polysorbate interactions analysed by means of isothermal titration and differential scanning calorimetry. *European Biophysics Journal with Biophysics Letters,* 38, 557-568.

HU, H. Y., LI, Q., CHENG, H. C. & DU, H. N. 2001. beta-sheet structure formation of proteins in solid state as revealed by circular dichroism spectroscopy. *Biopolymers,* 62, 15-21.

HUANG, K., LEE, B. P., INGRAM, D. R. & MESSERSMITH, P. B. 2002. Synthesis and characterization of self-assembling block copolymers containing bioadhesive end groups. *Biomacromolecules,* 3, 397-406.

HWANG, W. Y. K. & FOOTE, J. 2005. Immunogenicity of engineered antibodies. *Methods,* 36, 3-10.

IONESCU, R. M., VLASAK, J., PRICE, C. & KIRCHMEIER, M. 2008. Contribution of variable domains to the stability of humanized IgG1 monoclonal antibodies. *Journal of Pharmaceutical Sciences,* 97, 1414-1426.

JAIN, N. K. & ROY, I. 2008. Role of trehalose in moisture-induced aggregation of bovine serum albumin. *European Journal of Pharmaceutics and Biopharmaceutics,* 69, 824-834.

JANCZUK, B., BIALOPIOTROWICZ, T. & ZDZIENNICKA, A. 1999. Some remarks on the components of the liquid surface free energy. *Journal of Colloid and Interface Science,* 211, 96-103.

JANDA, A. & CASADEVALL, A. 2010. Circular Dichroism reveals evidence of coupling between immunoglobulin constant and variable region secondary structure. *Molecular Immunology,* 47, 1421-1425.

JENKINS, N. 2007. Modifications of therapeutic proteins: challenges and prospects. *Cytotechnology,* 53, 121-125.

JEYACHANDRAN, Y. L., MIELCZARSKI, J. A., MIELCZARSKI, E. & RAI, B. 2010. Efficiency of blocking of non-specific interaction of different proteins by BSA adsorbed on hydrophobic and hydrophilic surfaces. *Journal of Colloid and Interface Science,* 341, 136-142.

JIA, L. W., GUO, C., XIANG, J. F., WANG, N., YANG, L. R., TANG, Y. L. & LIU, H. Z. 2012. Interaction between PEO-PPO-PEO Copolymers and a Hexapeptide in Aqueous Solutions. *Langmuir,* 28, 1725-1732.

JOHNSON, R. & JISKOOT, W. 2012. Models for evaluation of relative immunogenic potential of protein particles in biopharmaceutical protein formulations. *Journal of Pharmaceutical Sciences,* 101, 3586-3592.

JONES, L. S., KAUFMANN, A. & MIDDAUGH, C. R. 2005. Silicone oil induced aggregation of proteins. *Journal of Pharmaceutical Sciences,* 94, 918-927.

JOSHI, O. & MCGUIRE, J. 2009. Adsorption Behavior of Lysozyme and Tween 80 at Hydrophilic and Hydrophobic Silica-Water Interfaces. *Applied Biochemistry and Biotechnology,* 152, 235-248.

JOSHI, O., MCGUIRE, J. & WANG, D. Q. 2008. Adsorption and Function of Recombinant Factor VIII at Solid-Water Interfaces in the Presence of Tween-80. *Journal of Pharmaceutical Sciences,* 97, 4741-4755.

KABANOV, A. V., BATRAKOVA, E. V. & ALAKHOV, V. Y. 2002. Pluronic (R) block copolymers as novel polymer therapeutics for drug and gene delivery. *Journal of Controlled Release,* 82, 189-212.

KANG, E., PARK, J. W., MCCLELLAN, S. J., KIM, J. M., HOLLAND, D. P., LEE, G. U., FRANSES, E. I., PARK, K. & THOMPSON, D. H. 2007. Specific adsorption of histidine-tagged proteins on silica surfaces modified with Ni2+/NTA-derivatized poly(ethylene glycol). *Langmuir,* 23, 6281-6288.

KAYE, G. W. C. & LABY, T. H. 1995. *Table of Physical and Chemical Constants,* Harlow, Longman Scientific and Technical.

KELLY, S. M., JESS, T. J. & PRICE, N. C. 2005. How to study proteins by circular dichroism. *Biochimica Et Biophysica Acta-Proteins and Proteomics,* 1751, 119-139.

KELLY, S. M. & PRICE, N. C. 2000. The use of circular dichroism in the investigation of protein structure and function. *Current Protein and Peptide Science,* 1, 349-384.

KENDRICK, B. S., CHANG, B. S., ARAKAWA, T., PETERSON, B., RANDOLPH, T. W., MANNING, M. C. & CARPENTER, J. F. 1997. Preferential exclusion of sucrose from recombinant interleukin-1 receptor antagonist: Role in restricted conformational mobility and compaction of native state. *Proceedings of the National Academy of Sciences of the United States of America,* 94, 11917-11922.

KERWIN, B. A. 2008. Polysorbates 20 and 80 used in the formulation of protein biotherapeutics: Structure and degradation pathways. *Journal of Pharmaceutical Sciences,* 97, 2924-2935.

KHAN, M. Y., VILLANUEVA, G. & NEWMAN, S. A. 1989. ON THE ORIGIN OF THE POSITIVE BAND IN THE FAR-ULTRAVIOLET CIRCULAR DICHROIC SPECTRUM OF FIBRONECTIN. *Journal of Biological Chemistry,* 264, 2139-2142.

KIRDAR, A. O., GREEN, K. D. & RATHORE, A. S. 2008. Application of multivariate data analysis for identification and successful resolution of a root cause for a bioprocessing application. *Biotechnology Progress,* 24, 720-726.

KISHORE, R. S. K., KIESE, S., FISCHER, S., PAPPENBERGER, A., GRAUSCHOPF, U. & MAHLER, H. C. 2011a. The Degradation of Polysorbates 20 and 80 and its Potential Impact on the Stability of Biotherapeutics. *Pharmaceutical Research,* 28, 1194-1210.

KISHORE, R. S. K., PAPPENBERGER, A., DAUPHIN, I. B., ROSS, A., BUERGI, B., STAEMPFLI, A. & MAHLER, H. C. 2011b. Degradation of Polysorbates 20 and 80: Studies on Thermal Autoxidation and Hydrolysis. *Journal of Pharmaceutical Sciences,* 100, 721-731.

KISS, E., DRAVETZKY, K., HILL, K., KUTNYANSZKY, E. & VARGA, A. 2008. Protein interaction with a Pluronic-modified poly(lactic acid) Langmuir monolayer. *Journal of Colloid and Interface Science,* 325, 337-345.

KNEVELMAN, C., DAVIES, J., ALLEN, L. & TITCHENER-HOOKER, N. J. 2010. High-Throughput Screening Techniques for Rapid PEG-Based Precipitation of IgG(4) mAb from Clarified Cell Culture Supernatant. *Biotechnology Progress,* 26, 697-705.

KREILGAARD, L., JONES, L. S., RANDOLPH, T. W., FROKJAER, S., FLINK, J. M., MANNING, M. C. & CARPENTER, J. F. 1998. Effect of Tween 20 on freeze-thawing- and agitation-induced aggregation of recombinant, human factor XIII. *Journal of Pharmaceutical Sciences,* 87, 1597-1603.

KREINER, M., CHILLAKURI, C. R., PEREIRA, P., FAIRHEAD, M., LI, Z. H., MARDON, H. J., HOLT, S. A. & VAN DER WALLE, C. F. 2009. Orientation and surface coverage of adsorbed fibronectin cell binding domains and bound integrin alpha 5 beta 1 receptors. *Soft Matter,* 5, 3954-3962.

KRITTANAI, C. & JOHNSON, W. C. 1997. Correcting the circular dichroism spectra of peptides for contributions of absorbing side chains. *Analytical Biochemistry,* 253, 57-64.

KUELTZO, L. A., WANG, W., RANDOLPH, T. W. & CARPENTER, J. F. 2008. Effects of solution conditions, processing parameters, and container materials on aggregation of a monoclonal antibody during freeze-thawing. *Journal of Pharmaceutical Sciences,* 97, 1801-1812.

KUKRER, B., FILIPE, V., VAN DUIJN, E., KASPER, P. T., VREEKEN, R. J., HECK, A. J. R. & JISKOOT, W. 2010. Mass Spectrometric Analysis of Intact Human Monoclonal Antibody

Aggregates Fractionated by Size-Exclusion Chromatography. *Pharmaceutical Research,* 27, 2197-2204.

KUMAR, V., DIXIT, N., ZHOU, L. Q. & FRAUNHOFER, W. 2011. Impact of short range hydrophobic interactions and long range electrostatic forces on the aggregation kinetics of a monoclonal antibody and a dual-variable domain immunoglobulin at low and high concentrations. *International Journal of Pharmaceutics,* 421, 82-93.

LAKEY, J. H. 2009. Neutrons for biologists: a beginner's guide, or why you should consider using neutrons. *Journal of the Royal Society Interface,* 6, S567-S573.

LAKOWICZ, J. R., MALICKA, J., GRYCZYNSKI, I., GRYCZYNSKI, Z. & GEDDES, C. D. 2003. Radiative decay engineering: the role of photonic mode density in biotechnology. *Journal of Physics D-Applied Physics,* 36, R240-R249.

LAMPROU, D. A., SMITH, J. R., NEVELL, T. G., BARBU, E., STONE, C., WILLIS, C. R. & TSIBOUKLIS, J. 2010a. A comparative study of surface energy data from atomic force microscopy and from contact angle goniometry. *Applied Surface Science,* 256, 5082-5087.

LAMPROU, D. A., SMITH, J. R., NEVELL, T. G., BARBU, E., WILLIS, C. R. & TSIBOUKLIS, J. 2010b. Self-assembled structures of alkanethiols on gold-coated cantilever tips and substrates for atomic force microscopy: Molecular organisation and conditions for reproducible deposition. *Applied Surface Science,* 256, 1961-1968.

LAMPROU, D. A., SMITH, J. R., NEVELL, T. G., BARBU, E., WILLIS, C. R. & TSIBOUKLIS, J. 2010c. Towards the Determination of Surface Energy at the Nanoscale: A Further Assessment of the AFM-Based Approach. *Journal of advanced microscopy research,* 5, 138-142.

LARSERICSDOTTER, H., OSCARSSON, S. & BUIJS, J. 2004. Thermodynamic analysis of lysozyme adsorbed to silica. *Journal of Colloid and Interface Science,* 276, 261-268.

LE BRUN, A. P., CHOW, J., BAX, D. V., NELSON, A., WEISS, A. S. & JAMES, M. 2012. Molecular Orientation of Tropoelastin is Determined by Surface Hydrophobicity. *Biomacromolecules,* 13, 379-386.

LE BRUN, A. P., HOLT, S. A., SHAH, D. S. H., MAJKRZAK, C. F. & LAKEY, J. H. 2011. The structural orientation of antibody layers bound to engineered biosensor surfaces. *Biomaterials,* 32, 3303-3311.

LEE, M. H., BRASS, D. A., MORRIS, R., COMPOSTO, R. J. & DUCHEYNE, P. 2005. The effect of non-specific interactions on cellular adhesion using model surfaces. *Biomaterials,* 26, 1721-1730.

LEE, R. C., RIVER, L. P., PAN, F. S., JI, L. & WOLLMANN, R. L. 1992. SURFACTANT-INDUCED SEALING OF ELECTROPERMEABILIZED SKELETAL-MUSCLE MEMBRANES INVIVO. *Proceedings of the National Academy of Sciences of the United States of America,* 89, 4524-4528.

LEE, S., ITEN, R., MULLER, M. & SPENCER, N. D. 2004. Influence of molecular architecture on the adsorption of poly(ethylene oxide)-poly(propylene oxide)-poly(ethylene oxide) on PDMS surfaces and implications for aqueous lubrication. *Macromolecules,* 37, 8349-8356.

LEES, J. G., MILES, A. J., WIEN, F. & WALLACE, B. A. 2006. A reference database for circular dichroism spectroscopy covering fold and secondary structure space. *Bioinformatics,* 22, 1955-62.

LEGMANN, R., SCHREYER, H. B., COMBS, R. G., MCCORMICK, E. L., RUSSO, A. P. & RODGERS, S. T. 2009. A Predictive High-Throughput Scale-Down Model of Monoclonal Antibody Production in CHO Cells. *Biotechnology and Bioengineering,* 104, 1107-1120.

LI, J. T. & CALDWELL, K. D. 1996. Plasma protein interactions with Pluronic(TM)-treated colloids. *Colloids and Surfaces B-Biointerfaces,* 7, 9-22.

LI, L. Y., CHEN, S. F., OH, S. J. & JIANG, S. Y. 2002. In situ single-molecule detection of antibody-antigen binding by tapping-mode atomic force microscopy. *Analytical Chemistry,* 74, 6017-6022.

LICHTENBELT, J. W. T., HEUVELSLAND, W. J. M., OLDENZEEL, M. E. & ZSOM, R. L. J. 1993. ADSORPTION AND IMMUNOREACTIVITY OF PROTEINS ON POLYSTYRENE AND ON SILICA - COMPETITION WITH SURFACTANTS. *Colloids and Surfaces B-Biointerfaces,* 1, 75-82.

LO, Y. S., ZHU, Y. J. & BEEBE, T. P. 2001. Loading-rate dependence of individual ligand-receptor bond-rupture forces studied by atomic force microscopy. *Langmuir,* 17, 3741-3748.

LOK, B. K., CHENG, Y. L. & ROBERTSON, C. R. 1983a. PROTEIN ADSORPTION ON CROSSLINKED POLYDIMETHYLSILOXANE USING TOTAL INTERNAL-REFLECTION FLUORESCENCE. *Journal of Colloid and Interface Science,* 91, 104-116.

LOK, B. K., CHENG, Y. L. & ROBERTSON, C. R. 1983b. TOTAL INTERNAL-REFLECTION FLUORESCENCE - A TECHNIQUE FOR EXAMINING INTERACTIONS OF MACROMOLECULES WITH SOLID-SURFACES. *Journal of Colloid and Interface Science,* 91, 87-103.

LONG, J., HYDER, M. N., HUANG, R. Y. M. & CHEN, P. 2005. Thermodynamic modeling of contact angles on rough, heterogeneous surfaces. *Advances in Colloid and Interface Science,* 118, 173-190.

LU, J. R., SU, T. J. & PENFOLD, J. 1999. Adsorption of serum albumins at the air/water interface. *Langmuir,* 15, 6975-6983.

LU, J. R., SU, T. J., THIRTLE, P. N., THOMAS, R. K., RENNIE, A. R. & CUBITT, R. 1998. The denaturation of lysozyme layers adsorbed at the hydrophobic solid/lquid surface studied by neutron reflection. *Journal of Colloid and Interface Science,* 206, 212-223.

LV, Z. J., WANG, J. H., CHEN, G. P. & DENG, L. H. 2010. Probing Specific Interaction Forces Between Human IgG and Rat Anti-Human IgG by Self-Assembled Monolayer and Atomic Force Microscopy. *Nanoscale Research Letters,* 5, 1032-1038.

MAA, Y. F. & HSU, C. C. 1997. Protein denaturation by combined effect of shear and air-liquid interface. *Biotechnology and Bioengineering,* 54, 503-512.

MACKIE, A. R., GUNNING, A. P., WILDE, P. J. & MORRIS, V. J. 1999. Orogenic displacement of protein from the air/water interface by competitive adsorption. *Journal of Colloid and Interface Science,* 210, 157-166.

MACKIE, A. R., GUNNING, A. P., WILDE, P. J. & MORRIS, V. J. 2000a. Competitive displacement of beta-lactoglobulin from the air/water interface by sodium dodecyl sulfate. *Langmuir,* 16, 8176-8181.

MACKIE, A. R., GUNNING, A. P., WILDE, P. J. & MORRIS, V. J. 2000b. Orogenic displacement of protein from the oil/water interface. *Langmuir,* 16, 2242-2247.

MAHLER, H. C., HUBER, F., KISHORE, R. S. K., REINDL, J., RUCKERT, P. & MULLER, R. 2010. Adsorption Behavior of a Surfactant and a Monoclonal Antibody to Sterilizing-Grade Filters. *Journal of Pharmaceutical Sciences,* 99, 2620-2627.

MAHLER, H. C., MULLER, R., FRIESS, W., DELILLE, A. & MATHEUS, S. 2005. Induction and analysis of aggregates in a liquid IgG1-antibody formulation. *European Journal of Pharmaceutics and Biopharmaceutics,* 59, 407-417.

MAITY, H., O'DELL, C., SRIVASTAVA, A. & GOLDSTEIN, J. 2009. Effects of Arginine on Photostability and Thermal Stability of IgG1 Monoclonal Antibodies. *Current Pharmaceutical Biotechnology,* 10, 761-766.

MALMSTEN, M., MULLER, D. & LASSEN, B. 1997. Sequential adsorption of human serum albumin (HSA), immunoglobulin G (IgG), and fibrinogen (Fgn) at HMDSO plasma polymer surfaces. *Journal of Colloid and Interface Science,* 193, 88-95.

MARKS, J. D., PAN, C.-Y., BUSHELL, T., CROMIE, W. & LEE, R. C. 2001. Amphiphilic, tri-block copolymers provide potent membrane-targeted neuroprotection. *FASEB Journal,* 15, 1107-1109.

MARSH, R. J., JONES, R. A. L., SFERRAZZA, M. & PENFOLD, J. 1999. Neutron reflectivity study of the adsorption of beta-lactoglobulin at a hydrophilic solid/liquid interface. *Journal of Colloid and Interface Science,* 218, 347-349.

MARTIN, A. N., SINKO, P. J. & SINGH, Y. 2011. *Martin's physical pharmacy and pharmaceutical sciences : physical chemical and biopharmaceutical principles in the pharmaceutical sciences.,* Baltimore, MD, Lippincott Williams & Wilkins.

MATHES, J. & FRIESS, W. 2011. Influence of pH and ionic strength on IgG adsorption to vials. *European Journal of Pharmaceutics and Biopharmaceutics,* 78, 239-247.

MCGOVERN, M. E., KALLURY, K. M. R. & THOMPSON, M. 1994. ROLE OF SOLVENT ON THE SILANIZATION OF GLASS WITH OCTADECYLTRICHLOROSILANE. *Langmuir,* 10, 3607-3614.

MCGURK, S. L., GREEN, R. J., SANDERS, G. H. W., DAVIES, M. C., ROBERTS, C. J., TENDLER, S. J. B. & WILLIAMS, P. M. 1999. Molecular interactions of biomolecules with surface-engineered interfaces using atomic force microscopy and surface plasmon resonance. *Langmuir,* 15, 5136-5140.

MCLEAN, S. C., LIOE, H., MEAGHER, L., CRAIG, V. S. J. & GEE, M. L. 2005. Atomic force microscopy study of the interaction between adsorbed poly(ethylene oxide) layers: Effects of surface modification and approach velocity. *Langmuir,* 21, 2199-2208.

MCLEOD, A. G., WALKER, I. R., ZHENG, S. & HAYWARD, C. P. M. 2000. Loss of factor VIII activity during storage in PVC containers due to adsorption. *Haemophilia,* 6, 89-92.

METWALLI, E., HAINES, D., BECKER, O., CONZONE, S. & PANTANO, C. G. 2006. Surface characterizations of mono-, di-, and tri-aminosilane treated glass substrates. *Journal of Colloid and Interface Science,* 298, 825-831.

MIURA, Y. F., TAKENAGA, M., KOINI, T., GRAUPE, M., GARG, N., GRAHAM, R. L. & LEE, T. R. 1998. Wettabilities of self-assembled monolayers generated from CF3-terminated alkanethiols on gold. *Langmuir,* 14, 5821-5825.

MUKHERJEE, S., PONDAVEN, S. P. & JARONIEC, C. P. 2011. Conformational Flexibility of a Human Immunoglobulin Light Chain Variable Domain by Relaxation Dispersion Nuclear Magnetic Resonance Spectroscopy: Implications for Protein Misfolding and Amyloid Assembly. *Biochemistry,* 50, 5845-5857.

MUSTAFI, D., SMITH, C. M., MAKINEN, M. W. & LEE, R. C. 2008. Multi-block poloxamer surfactants suppress aggregation of denatured proteins. *Biochimica Et Biophysica Acta-General Subjects,* 1780, 7-15.

NELSON, A. 2006. Co-refinement of multiple-contrast neutron/X-ray reflectivity data using MOTOFIT. *Journal of Applied Crystallography,* 39, 273-276.

NOEL, O., BROGLY, M., CASTELEIN, G. & SCHULTZ, J. 2004. In situ determination of the thermodynamic surface properties of chemically modified surfaces on a local scale: an attempt with the atomic force microscope. *Langmuir,* 20, 2707-12.

NORDE, W., MACRITCHIE, F., NOWICKA, G. & LYKLEMA, J. 1986. PROTEIN ADSORPTION AT SOLID LIQUID INTERFACES - REVERSIBILITY AND CONFORMATION ASPECTS. *Journal of Colloid and Interface Science,* 112, 447-456.

NYGREN, H. & STENBERG, M. 1988. MOLECULAR AND SUPRAMOLECULAR STRUCTURE OF ADSORBED FIBRINOGEN AND ADSORPTION-ISOTHERMS OF FIBRINOGEN AT QUARTZ SURFACES. *Journal of Biomedical Materials Research,* 22, 1-11.

OFFORD, D. A., JOHN, C. M. & GRIFFIN, J. H. 1994. CONTACT-ANGLE GONIOMETRY, ELLIPSOMETRY, XPS, AND TOF-SIMS ANALYSIS OF GOLD-SUPPORTED, MIXED SELF-ASSEMBLED MONOLAYERS FORMED FROM MIXED DIALKYL DISULFIDES. *Langmuir,* 10, 761-766.

OHGUSHI, M. & WADA, A. 1983. MOLTEN-GLOBULE STATE - A COMPACT FORM OF GLOBULAR-PROTEINS WITH MOBILE SIDE-CHAINS. *Febs Letters,* 164, 21-24.

OOM, A., POGGI, M., WIKSTROM, J. & SUKUMAR, M. 2012. Surface interactions of monoclonal antibodies characterized by quartz crystal microbalance with dissipation: Impact of hydrophobicity and protein self-interactions. *Journal of Pharmaceutical Sciences,* 101, 519-529.

ORFORD, P. D., PARKER, R. & RING, S. G. 1990. ASPECTS OF THE GLASS-TRANSITION BEHAVIOR OF MIXTURES OF CARBOHYDRATES OF LOW-MOLECULAR-WEIGHT. *Carbohydrate Research,* 196, 11-18.

OTZEN, D. E., SEHGAL, P. & WESTH, P. 2009. alpha-Lactalbumin is unfolded by all classes of surfactants but by different mechanisms. *Journal of Colloid and Interface Science,* 329, 273-283.

PAGANO, B., VIRNO, A., MATTIA, C. A., MAYOL, L., RANDAZZO, A. & GIANCOLA, C. 2008. Targeting DNA quadruplexes with distamycin A and its derivatives: An ITC and NMR study. *Biochimie,* 90, 1224-1232.

PANYUKOV, Y. V., NEMYKH, M. A., DOBROV, E. N. & DRACHEV, V. A. 2008. Surfactant-induced amorphous aggregation of tobacco mosaic virus coat protein: A physical methods approach. *Macromolecular Bioscience,* 8, 199-209.

PAVLOU, A. K. & BELSEY, M. J. 2005. The therapeutic antibodies market to 2008. *European Journal of Pharmaceutics and Biopharmaceutics,* 59, 389-396.

PEREIRA, P., KELLY, S. M., GELLERT, P. R. & VAN DER WALLE, C. F. 2008. Interdomain mobility and conformational stability of type III fibronectin domain pairs control surface adsorption, desorption and unfolding. *Colloids and Surfaces B-Biointerfaces,* 64, 1-9.

PIERCE, M. M., RAMAN, C. S. & NALL, B. T. 1999. Isothermal titration calorimetry of protein-protein interactions. *Methods-a Companion to Methods in Enzymology,* 19, 213-221.

PINHOLT, C., HARTVIG, R. A., MEDLICOTT, N. J. & JORGENSEN, L. 2011. The importance of interfaces in protein drug delivery - why is protein adsorption of interest in pharmaceutical formulations? *Expert Opinion on Drug Delivery,* 8, 949-964.

QUAN, J. M., TIDDENS, H., SY, J. P., MCKENZIE, S. G., MONTGOMERY, M. D., ROBINSON, P. J., WOHL, M. E. B., KONSTAN, M. W. & PULMOZYME EARLY INTERVENTION, T. 2001. A two-year randomized, placebo-controlled trial of dornase alfa in young patients with cystic fibrosis with mild lung function abnormalities. *Journal of Pediatrics,* 139, 813-820.

REBAR, V. A. & SANTORE, M. M. 1996. A total internal reflectance fluorescence nanoscale probe of interfacial potential and ion screening in polyethylene oxide layers adsorbed onto silica. *Journal of Colloid and Interface Science,* 178, 29-41.

RIPPLE, D. C. & DIMITROVA, M. N. 2012. Protein particles: What we know and what we do not know. *Journal of Pharmaceutical Sciences,* 101, 3568-3579.

ROQUES, C., BOUCHEMAL, K., PONCHEL, G., FROMES, Y. & FATTAL, E. 2009. Parameters affecting organization and transfection efficiency of amphiphilic copolymers/DNA carriers. *Journal of Controlled Release,* 138, 71-77.

ROS, R., SCHWESINGER, F., ANSELMETTI, D., KUBON, M., SCHAFER, R., PLUCKTHUN, A. & TIEFENAUER, L. 1998. Antigen binding forces of individually addressed single-chain Fv antibody molecules. *Proceedings of the National Academy of Sciences of the United States of America,* 95, 7402-7405.

RUIZ-PENA, M., OROPESA-NUNEZ, R., PONS, T., LOURO, S. R. W. & PEREZ-GRAMATGES, A. 2010. Physico-chemical studies of molecular interactions between non-ionic surfactants and bovine serum albumin. *Colloids and Surfaces B-Biointerfaces,* 75, 282-289.

SAHA, B., TOR, S. B., LIU, E., HARDT, D. E. & CHUN, J. H. 2011. Hot-embossing performance of silicon micromold coated with self-assembled n-octadecyltrichlorosilane. *Sensors and Actuators B-Chemical,* 160, 207-214.

SAHU, A., KASOJU, N., GOSWAMI, P. & BORA, U. 2011. Encapsulation of Curcumin in Pluronic Block Copolymer Micelles for Drug Delivery Applications. *Journal of Biomaterials Applications,* 25, 619-639.

SALEH, O. A. & SOHN, L. L. 2003. Direct detection of antibody-antigen binding using an on-chip artificial pore. *Proceedings of the National Academy of Sciences of the United States of America,* 100, 820-824.

SAPHIRE, E. O., STANFIELD, R. L., CRISPIN, M. D. M., PARREN, P., RUDD, P. M., DWEK, R. A., BURTON, D. R. & WILSON, I. A. 2002. Contrasting IgG structures reveal extreme asymmetry and flexibility. *Journal of Molecular Biology,* 319, 9-18.

SARCIAUX, J. M., MANSOUR, S., HAGEMAN, M. J. & NAIL, S. L. 1999. Effects of buffer composition and processing conditions on aggregation of bovine IgG during freeze-drying. *Journal of Pharmaceutical Sciences,* 88, 1354-1361.

SCHMITT, H., BADIA, A., DICKINSON, L., REVEN, L. & LENNOX, R. B. 1998. The effect of terminal hydrogen bonding on the structure and dynamics of nanoparticle self-assembled monolayers (SAMs): An NMR dynamics study. *Advanced Materials,* 10, 475-+.

SEK, L., BOYD, B. J., CHARMAN, W. N. & PORTER, C. J. H. 2006. Examination of the impact of a range of pluronic surfactants on the in-vitro solubilisation behaviour and oral bioavailability of lipiclic formulations of atovaquone. *Journal of Pharmacy and Pharmacology,* 58, 809-820.

SENGUPTA, I., NADAUD, P. S., HELMUS, J. J., SCHWIETERS, C. D. & JARONIEC, C. P. 2012. Protein fold determined by paramagnetic magic-angle spinning solid-state NMR spectroscopy. *Nature Chemistry,* 4, 410-417.

SHETH, S. R. & LECKBAND, D. 1997a. Measurements of attractive forces between proteins and end-grafted poly(ethylene glycol) chains. *Proceedings of the National Academy of Sciences of the United States of America,* 94, 8399-8404.

SHETH, S. R. & LECKBAND, D. 1997b. Measurements of attractive forces between proteins and end-grafted poly(ethylene glycol) chains. *Proc. Natl. Acad. Sci. USA,* 94, 8399-404.

SHIBATA, C. T. & LENHOFF, A. M. 1992a. TIRF OF SALT AND SURFACE EFFECTS ON PROTEIN ADSORPTION. *Journal of Colloid and Interface Science,* 148, 485-507.

SHIBATA, C. T. & LENHOFF, A. M. 1992b. TIRF OF SALT AND SURFACE EFFECTS ON PROTEIN ADSORPTION .1. EQUILIBRIUM. *Journal of Colloid and Interface Science,* 148, 469-484.

SIEGEMUND, G., SCHWERTFEGER, W., FEIRING, A., SMART, B., BEHR, F., VOGEL, H. & MCKUSICK, B. 2000. Fluorine Compounds, Organic. *In:* ELVERS, B. (ed.) *Ullmann's Encyclopedia of Industrial Chemistry.* Wiley VCH.

SILVERTON, E. W., NAVIA, M. A. & DAVIES, D. R. 1977. 3-DIMENSIONAL STRUCTURE OF AN INTACT HUMAN IMMUNOGLOBULIN. *Proceedings of the National Academy of Sciences of the United States of America,* 74, 5140-5144.

SIMPERLER, A., KORNHERR, A., CHOPRA, R., JONES, W., MOTHERWELL, W. D. S. & ZIFFERER, G. 2007. The glass transition temperatures of amorphous trehalose-water mixtures and the mobility of water: an experimental and in silico study. *Carbohydrate Research,* 342, 1470-1479.

SINGH, S. K. 2011. Impact of Product-Related Factors on Immunogenicity of Biotherapeutics. *Journal of Pharmaceutical Sciences,* 100, 354-387.

SIVARAMAN, B., FEARS, K. P. & LATOUR, R. A. 2009. Investigation of the Effects of Surface Chemistry and Solution Concentration on the Conformation of Adsorbed Proteins Using an Improved Circular Dichroism Method. *Langmuir,* 25, 3050-3056.

SIVARAMAN, B. & LATOUR, R. A. 2012. Time-Dependent Conformational Changes in Adsorbed Albumin and Its Effect on Platelet Adhesion. *Langmuir,* 28, 2745-2752.

SKODA, M. W. A., SCHREIBER, F., JACOBS, R. A. J., WEBSTER, J. R. P., WOLFF, M., DAHINT, R., SCHWENDEL, D. & GRUNZE, M. 2009. Protein Density Profile at the Interface of Water with Oligo(ethylene glycol) Self-Assembled Monolayers. *Langmuir,* 25, 4056-4064.

SONG, X. Y., ZHAI, J., WANG, Y. L. & JIANG, L. 2006. Self-assembly of amino-functionalized monolayers on silicon surfaces and preparation of superhydrophobic surfaces based on alkanoic acid dual layers and surface roughening. *Journal of Colloid and Interface Science,* 298, 267-273.

STEEN, J., UHLEN, M., HOBER, S. & OTTOSSON, J. 2006. High-throughput protein purification using an automated set-up for high-yield affinity chromatography. *Protein Expression and Purification,* 46, 173-178.

SUGIN, Z., YUKSEL, N. & BAYKARA, T. 2006. Preparation and characterization of polymeric micelles for solubilization of poorly soluble anticancer drugs. *European Journal of Pharmaceutics and Biopharmaceutics,* 64, 261-268.

SUN, W. Q. & DAVIDSON, P. 1998. Protein inactivation in amorphous sucrose and trehalose matrices: effects of phase separation and crystallization. *Biochimica Et Biophysica Acta-General Subjects,* 1425, 235-244.

SZYMCZYK, K. & JANCZUK, B. 2008. Wettability of a glass surface in the presence of two nonionic surfactant mixtures. *Langmuir,* 24, 7755-7760.

TALUJA, A. & BAE, Y. H. 2007. Role of a novel excipient poly(ethylene Glycol)-b-poly(L-histidine) in retention of physical stability of insulin in aqueous solutions. *Pharmaceutical Research,* 24, 1517-1526.

TAMADA, K., NAGASAWA, J., NAKANISHI, F., ABE, K., HARA, M., KNOLL, W., ISHIDA, T., FUKUSHIMA, H., MIYASHITA, S., USUI, T., KOINI, T. & LEE, T. R. 1998. Structure of SAMs generated from functionalized thiols on gold. *Thin Solid Films,* 327, 150-155.

TETIN, S. Y., PRENDERGAST, F. G. & VENYAMINOV, S. Y. 2003. Accuracy of protein secondary structure determination from circular dichroism spectra based on immunoglobulin examples. *Analytical Biochemistry,* 321, 183-187.

THIRUMANGALATHU, R., KRISHNAN, S., RICCI, M. S., BREMS, D. N., RANDOLPH, T. W. & CARPENTER, J. F. 2009. Silicone Oil- and Agitation-Induced Aggregation of a Monoclonal Antibody in Aqueous Solution. *Journal of Pharmaceutical Sciences,* 98, 3167-3181.

TORCELLO-GOMEZ, A., SANTANDER-ORTEGA, M. J., MANUEL PEULA-GARCIA, J., MALDONADO-VALDERRAMA, J., JOSE GALVEZ-RUIZ, M., LUIS ORTEGA-VINUESA, J. & MARTIN-RODRIGUEZ, A. 2011. Adsorption of antibody onto Pluronic F68-covered nanoparticles: link with surface properties. *Soft Matter,* 7, 8450-8461.

TORMOEN, G. W., DRELICH, J. & BEACH, E. R. 2004. Analysis of atomic force microscope pull-off forces for gold surfaces portraying nanoscale roughness and specific chemical functionality. *Journal of Adhesion Science and Technology,* 18, 1-17.

TREUHEIT, M. J., KOSKY, A. A. & BREMS, D. N. 2002. Inverse relationship of protein concentration and aggregation. *Pharmaceutical Research,* 19, 511-516.

TSAI, C. J., LIN, S. L., WOLFSON, H. J. & NUSSINOV, R. 1997. Studies of protein-protein interfaces: A statistical analysis of the hydrophobic effect. *Protein Science,* 6, 53-64.

VAN BEERS, M. M. C., GILLI, F., SCHELLEKENS, H., RANDOLPH, T. W. & JISKOOT, W. 2012. Immunogenicity of recombinant human interferon beta interacting with particles of glass, metal, and polystyrene. *Journal of Pharmaceutical Sciences,* 101, 187-199.

VAN BUREN, N., REHDER, D., GADGIL, H., MATSUMURA, M. & JACOB, J. 2009. Elucidation of Two Major Aggregation Pathways in an IgG2 Antibody. *Journal of Pharmaceutical Sciences,* 98, 3013-3030.

VAN STOKKUM, I. H., SPOELDER, H. J., BLOEMENDAL, M., VAN GRONDELLE, R. & GROEN, F. C. 1990. Estimation of protein secondary structure and error analysis from circular dichroism spectra. *Anal Biochem,* 191, 110-8.

VANOSS, C. J., GOOD, R. J. & CHAUDHURY, M. K. 1986. SOLUBILITY OF PROTEINS. *Journal of Protein Chemistry,* 5, 385-405.

VERMEER, A. W. P., BREMER, M. & NORDE, W. 1998. Structural changes of IgG induced by heat treatment and by adsorption onto a hydrophobic Teflon surface studied by circular dichroism spectroscopy. *Biochimica Et Biophysica Acta-General Subjects,* 1425, 1-12.

VERMEER, A. W. P., GIACOMELLI, C. E. & NORDE, W. 2001. Adsorption of IgG onto hydrophobic teflon. Differences between the F-ab and F-c domains. *Biochimica Et Biophysica Acta-General Subjects,* 1526, 61-69.

VERMEER, A. W. P. & NORDE, W. 2000. The thermal stability of immunoglobulin: Unfolding and aggregation of a multi-domain protein. *Biophysical Journal,* 78, 394-404.

VERMEER, A. W. P., NORDE, W. & VAN AMERONGEN, A. 2000. The unfolding/denaturation of immunogammaglobulin of isotype 2b and its F-ab and F-c fragments. *Biophysical Journal,* 79, 2150-2154.

VINE, N. D., DRAKE, P., HIATT, A. & MA, J. K. C. 2001. Assembly and plasma membrane targeting of recombinant immunoglobulin chains in plants with a murine immunoglobulin transmembrane sequence. *Plant Molecular Biology,* 45, 159-167.

WANG, P. L. & JOHNSTON, T. P. 1993. THERMAL-INDUCED DENATURATION OF 2 MODEL PROTEINS - EFFECT OF POLOXAMER-407 ON SOLUTION STABILITY. *International Journal of Pharmaceutics,* 96, 41-49.

WANG, W., WANG, Y. J. & WANG, D. Q. 2008a. Dual effects of Tween 80 on protein stability. *International Journal of Pharmaceutics,* 347, 31-38.

WANG, X. Q., WANG, Y. N., XU, H., SHAN, H. H. & LUB, J. R. 2008b. Dynamic adsorption of monoclonal antibody layers on hydrophilic silica surface: A combined study by spectroscopic ellipsometry and AFM. *Journal of Colloid and Interface Science,* 323, 18-25.

WEI, Y. & LATOUR, R. A. 2010. Correlation between Desorption Force Measured by Atomic Force Microscopy and Adsorption Free Energy Measured by Surface Plasmon Resonance Spectroscopy for Peptide-Surface Interactions. *Langmuir,* 26, 18852-18861.

WERTZ, C. F. & SANTORE, M. M. 1999. Adsorption and relaxation kinetics of albumin and fibrinogen on hydrophobic surfaces: Single-species and competitive behavior. *Langmuir,* 15, 8884-8894.

WERTZ, C. F. & SANTORE, M. M. 2002. Adsorption and reorientation kinetics of lysozyme on hydrophobic surfaces. *Langmuir,* 18, 1190-1199.

WHITMORE, L. & WALLACE, B. A. 2004. DICHROWEB, an online server for protein secondary structure analyses from circular dichroism spectroscopic data. *Nucleic Acids Res,* 32, W668-73.

WISEMAN, M. E. & FRANK, C. W. 2012. Antibody Adsorption and Orientation on Hydrophobic Surfaces. *Langmuir,* 28, 1765-1774.

WUNDERLICH, G., PINKERT, J., ANDREEFF, M., STINTZ, M., KNAPP, F. F., KROPP, J. & FRANKE, W. G. 2000. Preparation and biodistribution of rhenium-188 labeled albumin microspheres B 20: a promising new agent for radiotherapy. *Applied Radiation and Isotopes,* 52, 63-68.

XIONG, W., LUO, Y. H., ZHANG, C. X., TAN, D. Y. & ZUO, S. Y. 2012. Expression, Purification of Recombinant Human Mitochondrial Transcription Termination Factor 3 (hMTERF3) and Preparation of Polyclonal Antibody Against hMTERF3. *Applied Biochemistry and Biotechnology,* 167, 2318-2329.

XU, H., LU, J. R. & WILLIAMS, D. E. 2006a. Effect of surface packing density of interfacially adsorbed monoclonal antibody on the binding of hormonal antigen human chorionic gonadotrophin. *Journal of Physical Chemistry B,* 110, 1907-1914.

XU, H., ZHAO, X. B., GRANT, C., LU, J. R., WILLIAMS, D. E. & PENFOLD, J. 2006b. Orientation of a monoclonal antibody adsorbed at the solid/solution interface: A combined study using atomic force microscopy and neutron reflectivity. *Langmuir,* 22, 6313-6320.

XU, L. C. & SIEDLECKI, C. A. 2007a. Effects of surface wettability and contact time on protein adhesion to biomaterial surfaces. *Biomaterials,* 28, 3273-3283.

XU, L. C. & SIEDLECKI, C. A. 2007b. Effects of surface wettability and contact time on protein adhesion to biomaterial surfaces. *Biomaterials,* 28, 3273-83.

YANG, S. Q., WANG, T., BOHON, J., GAGNE, M. E. L., BOLDUC, M., LECLERC, D. & LI, H. L. 2012. Crystal Structure of the Coat Protein of the Flexible Filamentous Papaya Mosaic Virus. *Journal of Molecular Biology,* 422, 263-273.

YOU, H. X. & LOWE, C. R. 1996. AFM studies of protein adsorption .2. Characterization of immunoglobulin G adsorption by detergent washing. *Journal of Colloid and Interface Science,* 182, 586-601.

YU, D. Q. & GHOSH, R. 2010. Method for Studying Immunoglobulin G Binding on Hydrophobic Surfaces. *Langmuir,* 26, 924-929.

ZANGMEISTER, R. A. 2012. Application of x-ray photoelectron spectroscopic analysis to protein adsorption on materials relevant to biomanufacturing. *Journal of Pharmaceutical Sciences,* 101, 1639-1644.

ZHANG, M. Q. & FERRARI, M. 1997. Reduction of albumin adsorption onto silicon surfaces by Tween 20. *Biotechnology and Bioengineering,* 56, 618-625.

ZHOU, J. X., QIU, J. S., JIANG, G., ZHOU, C., BINGHAM, N., YEUNG, H., DRANSART, B., WADHWA, M. V. & TRESSEL, T. 2008. Non-specific binding and saturation of Polysorbate-20 with aseptic filter membranes for drug substance and drug product during mAb production. *Journal of Membrane Science,* 325, 735-741.

ZHURAVLEV, L. T. 1993. CHARACTERIZATION OF AMORPHOUS SILICA SURFACE. *Reaction Kinetics and Catalysis Letters,* 50, 15-25.

ZISMAN, WILLIAM & ALBERT 1964. Relation of the Equilibrium Contact Angle to Liquid and Solid Constitution. *In:* FOWKES, F. M. (ed.) *Contact Angle, Wettability, and Adhesion.*

Chapter 8. Appendices

8.1 Appendix A – Differential scanning calorimetry (DSC) thermograms

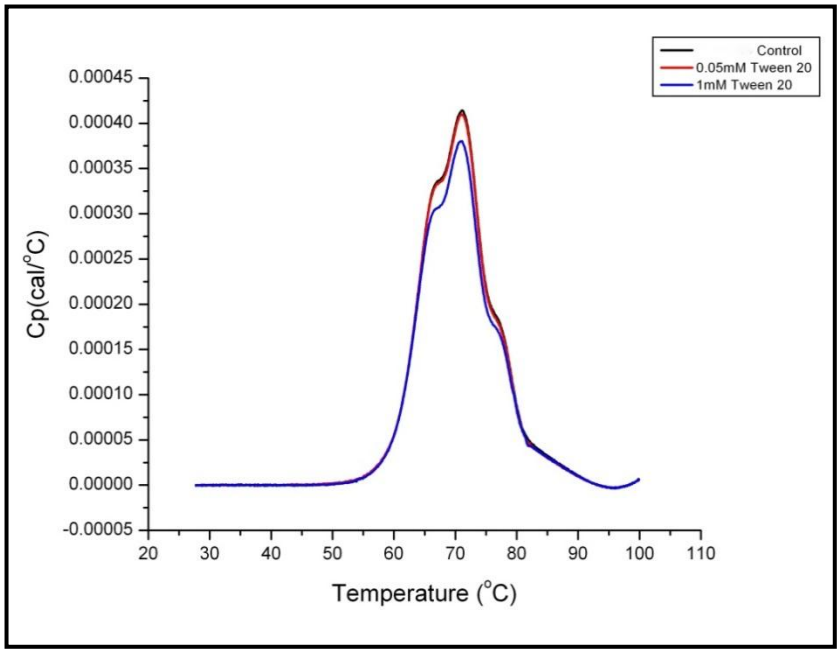

Figure 8-1. The differential scanning calorimetry (DSC) thermogram illustrating the effect of Tween 20 inclusion on mAb-1 thermal stability.

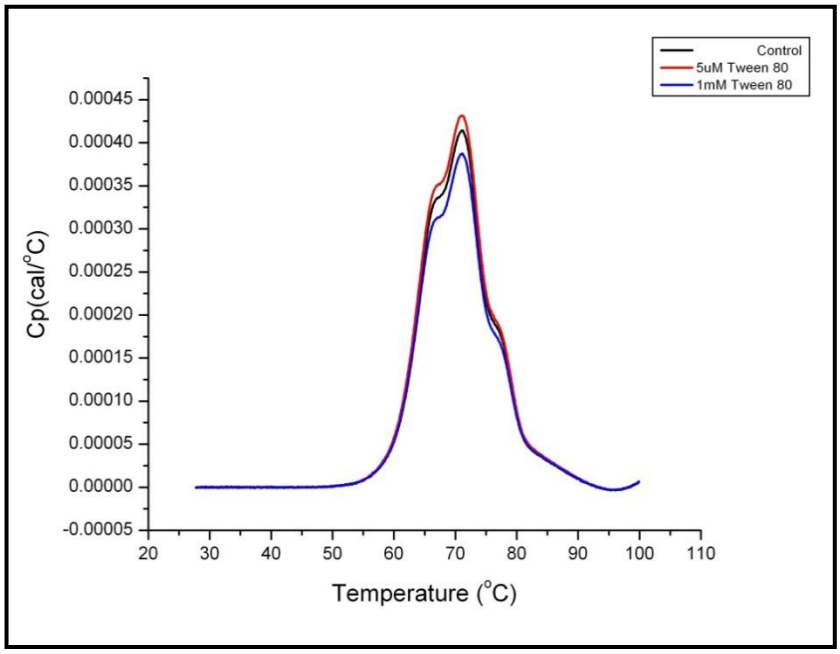

Figure 8-2. The differential scanning calorimetry (DSC) thermogram illustrating the effect of Tween 80 inclusion on mAb-1 thermal stability.

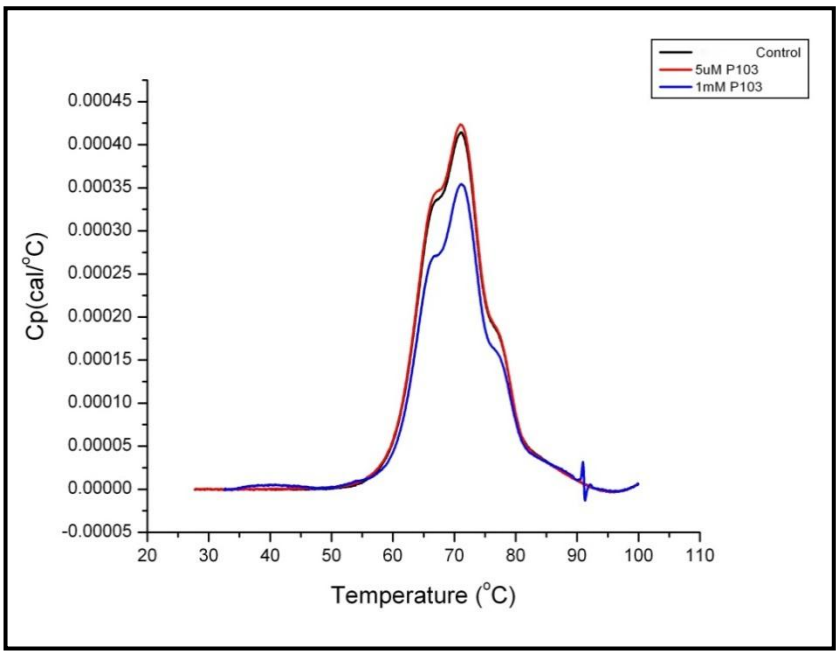

Figure 8-3. The differential scanning calorimetry (DSC) thermogram illustrating the effect of Pluronic P103 inclusion on mAb-1 thermal stability.

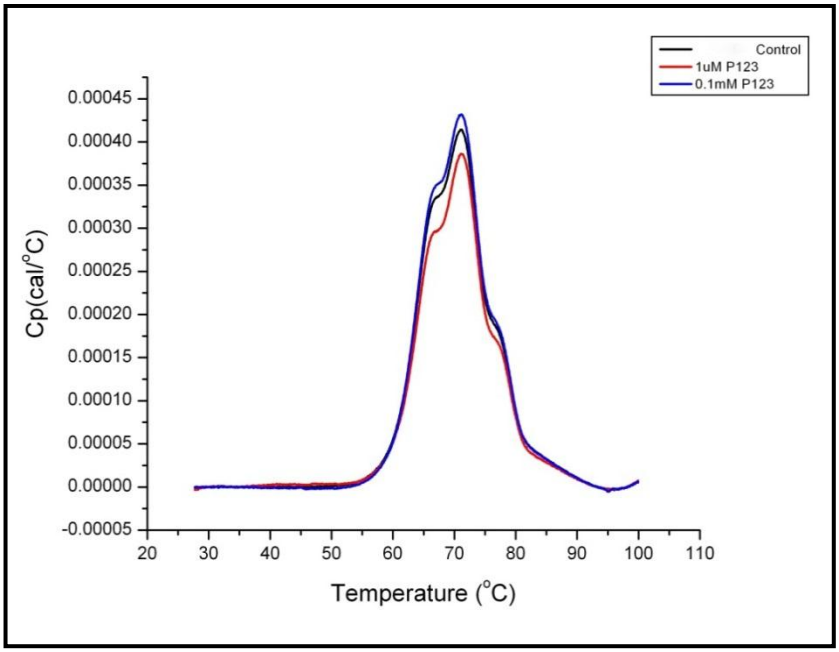

Figure 8-4. The differential scanning calorimetry (DSC) thermogram illustrating the effect of Pluronic P123 inclusion on mAb-1 thermal stability.

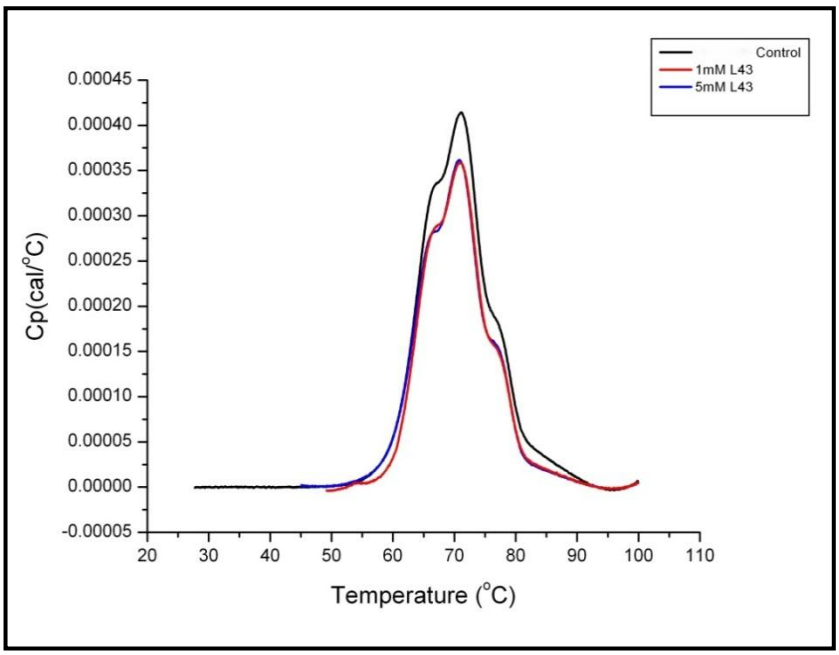

Figure 8-5. The differential scanning calorimetry (DSC) thermogram illustrating the effect of Pluronic L43 inclusion on mAb-1 thermal stability.

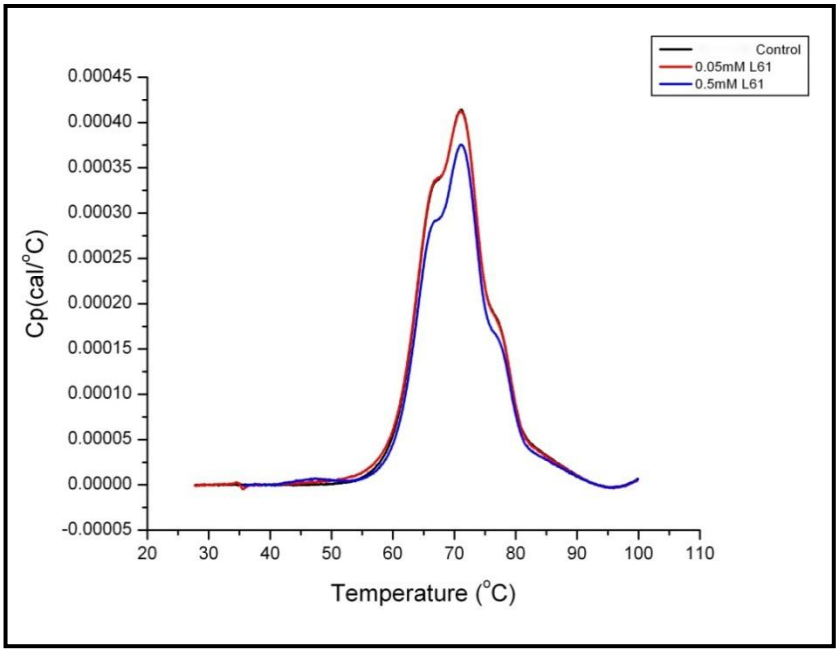

Figure 8-6. The differential scanning calorimetry (DSC) thermogram illustrating the effect of Pluronic L61 inclusion on mAb-1 thermal stability.

8.2 Appendix B – Plots of circular dichroism peak ratio against water contact angle and surface energy

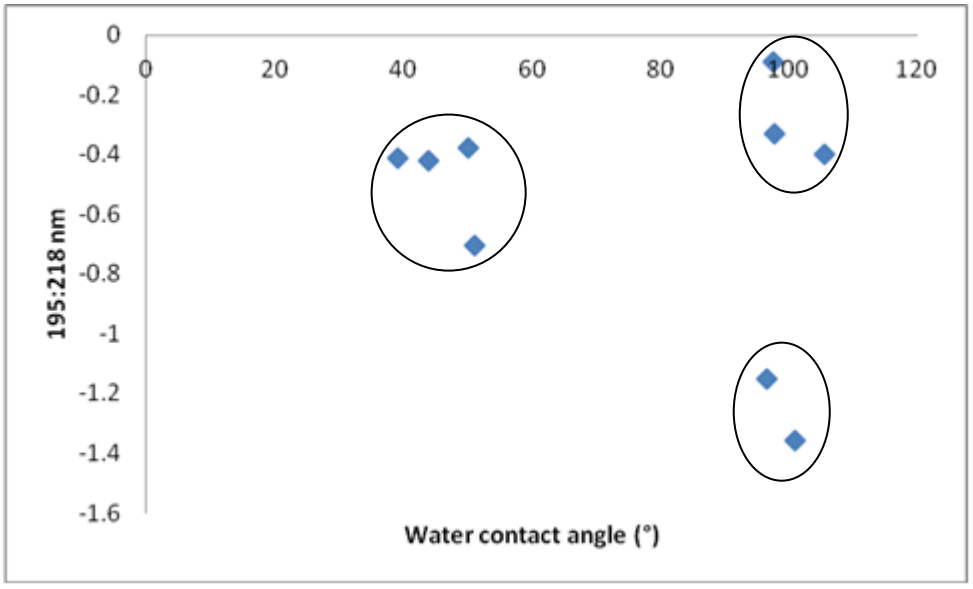

Figure 8-7. Water contact angle against 'solid-state' CD peak ratio (195:218 nm) for mAb-1.

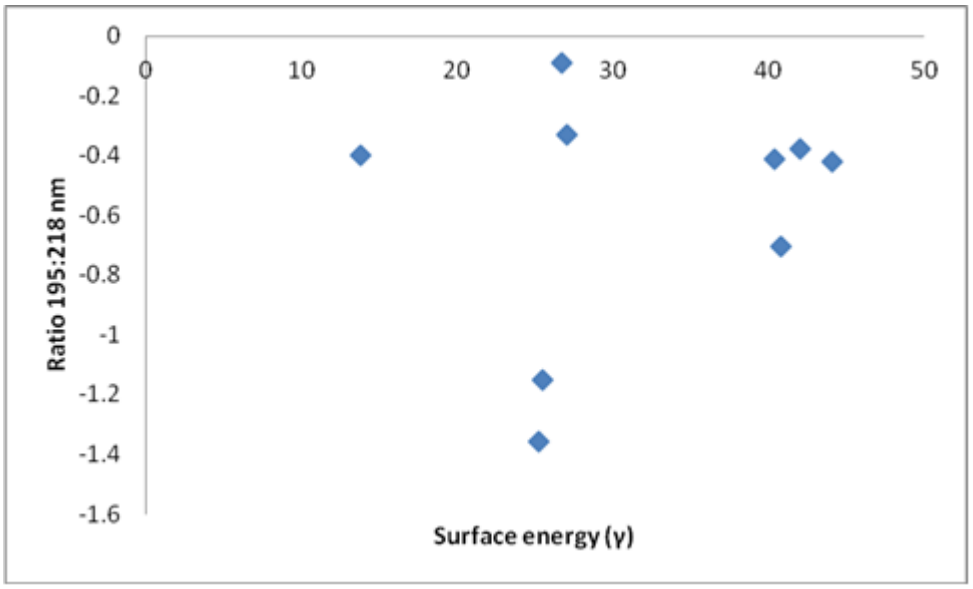

Figure 8-8. Surface energy against the 'solid-state' CD peak ratio (195:218 nm) for mAb-1.